Modelling of subsidence induced damage to masonry buildings

Influence of soil heterogeneity on settlement and development of fragility curves

Prosperi, A.

DOI
10.4233/uuid:798679cf-f2a3-46fb-be53-93e07968e7a6

Publication date
2025

Document Version
Final published version

Citation (APA)
Prosperi, A. (2025). *Modelling of subsidence induced damage to masonry buildings: Influence of soil heterogeneity on settlement and development of fragility curves*. [Dissertation (TU Delft), Delft University of Technology]. https://doi.org/10.4233/uuid:798679cf-f2a3-46fb-be53-93e07968e7a6

Important note
To cite this publication, please use the final published version (if applicable).
Please check the document version above.

MODELLING OF SUBSIDENCE INDUCED DAMAGE TO MASONRY BUILDINGS

INFLUENCE OF SOIL HETEROGENEITY ON SETTLEMENT AND DEVELOPMENT OF FRAGILITY CURVES

MODELLING OF SUBSIDENCE INDUCED DAMAGE TO MASONRY BUILDINGS

INFLUENCE OF SOIL HETEROGENEITY ON SETTLEMENT AND DEVELOPMENT OF FRAGILITY CURVES

Dissertation

for the purpose of obtaining the degree of doctor
at Delft University of Technology
by the authority of the Rector Magnificus Prof.dr.ir. T.H.J.J. van der Hagen
chair of the Board for Doctorates
to be defended publicly on
14 February 2025 at 10.00 o'clock

by

Alfonso PROSPERI

Master of Science in Civil Engineering,
University of Salerno, Italy

born in Nocera Inferiore, Italy

This dissertation has been approved by the promotors:

Prof. dr. ir. J. G. Rots
Dr. ir. M. Korff

Composition of the doctoral committee:

Rector Magnificus	Chairperson
Prof. dr. ir. J. G. Rots	Promotor, Delft University of Technology, NL
Dr. ir. M. Korff	Copromotor, Delft University of Technology, NL

Independent members:

Prof. dr. ir. F. C. Vossepoel	Delft University of Technology, NL
Prof. dr. E. Stouthamer	Utrecht University, NL
Dr. B. Ghiassi	University of Birmingham, UK
Dr. G. Giardina	Delft University of Technology, NL

Non-independent member:

Dr. ir. P. A. Korswagen	Delft University of Technology, NL

Reserve member:

Prof. dr. ir. L. J. Sluijs	Delft University of Technology, NL

Dr. ir. P. A. Korswagen has made significant contributions to the realization of this thesis.

The research presented in this dissertation is part of the project Living on Soft Soils: Subsidence and Society (grantnr.: NWA.1160.18.259). This project is funded through the Dutch Research Council (NWO-NWA-ORC), Utrecht University, Wageningen University, Delft University of Technology, Ministry of Infrastructure & Water Management, Ministry of the Interior & Kingdom Relations, Deltares, Wageningen Environmental Research, TNO-Geological Survey of The Netherlands, STOWA, Water Authority: Hoogheemraadschap de Stichtse Rijnlanden, Water Authority: Drents Overijsselse Delta, Province of Utrecht, Province of Zuid-Holland, Municipality of Gouda, Platform Soft Soil, Sweco, Tauw BV, NAM.

Keywords: Subsidence, Masonry, Damage, Fragility curves, Soil heterogeneity

Printed by: Ipskamp Printing

Cover design: Alfonso Prosperi

ISBN 978-94-6473-706-6

An electronic version of this dissertation is available at
http://repository.tudelft.nl/

Bisognerebbe avere
almeno tre vite
dici
la prima per gli errori necessari
la seconda per non sbagliare mai
la terza infine
per sbagliare nuovamente
ed essere felici.[1]

Francesco Carofiglio - Poesie del tempo stretto

[1] Translation into English by the author of this thesis.

One should have
at least three lives
you say:
the first for the necessary mistakes,
the second to never make mistakes,
and the third, finally,
to make mistakes again
and be happy.

Propositions

accompanying the dissertation

MODELLING OF SUBSIDENCE INDUCED DAMAGE TO MASONRY BUILDINGS

INFLUENCE OF SOIL HETEROGENEITY ON SETTLEMENT AND DEVELOPMENT OF FRAGILITY CURVES

by

Alfonso PROSPERI

1. When the angular distortion measured on walls reaches 2.00 ‰(1/500), the threshold recommended by international standards, one in two buildings will develop cracks up to 5 millimetres wide. (*)
2. Differential settlements at the scale of structures can result from heterogeneous soil thicknesses and may lead to building damage. (*)
3. Settlements measured on walls due to subsidence can take the shape of a Gaussian distribution, similar to settlements due to tunnelling, mining and excavations. (*)
4. Shape matters: assessing damage to structures should account not only for the building's shape but also the shape of the ground settlements. This includes both symmetric and asymmetric sagging and hogging shapes. (*)
5. Discrepancies between numerical models and observations of existing structures are expected if time effects, including material degradation, viscoelasticity, and time-dependent settlements, are not considered in the analyses.
6. Researchers should have access to open data on existing buildings, including information about foundation systems and construction materials.
7. While some would rather abandon a subsiding city than preserve its architectural heritage, investing in preservation is essential for maintaining cultural identity, supporting the economy, and protecting historic landmarks.
8. Damage assessment for existing buildings shares similarities with preventive medicine. The goal of both is to prevent a pathology before symptoms start.
9. University staff should be able to choose one or more roles, such as teaching, research, and funding acquisition, without being required to excel in all of them.
10. When facing life's challenges, finite element analyses can inspire: problems can be broken down into smaller and more manageable parts and subsequently assembled and solved.

(*) *These propositions pertain to this dissertation.*

These propositions are regarded as opposable and defendable, and have been approved as such by the promotor **Prof. dr. ir. J. G. Rots**, and copromotor **Dr. ir. M. Korff**.

SUMMARY

Land subsidence is a well-known phenomenon that describes the progressive sinking of the ground surface relative to the sea level. Subsidence affects many densely populated areas in North America, Asia and Europe. In the Netherlands, the western and northern areas have undergone subsidence for centuries, due to the peat and clay rich subsurface, and a combination of natural processes and human activities. The ongoing process of land subsidence requires careful planning and significant investment to maintain current land use, as it continues to affect buildings and infrastructure. Furthermore, the rates of land subsidence are evolving due to climate change, which alters patterns of precipitation, groundwater levels, and soil moisture content. These environmental shifts exacerbate the subsidence process, leading to more unpredictable and accelerated rates of ground settlements in affected areas.

The evident outcomes of land subsidence include social unease and economic loss. In this context, individuals and public organizations are increasingly concerned with how subsidence impacts the built heritage.

Dutch cities are renowned worldwide for their masonry buildings, characterized by fired-clay brick veneers, a tradition that continues in modern architecture. Masonry, however, is a quasi-brittle material with limited tensile strength, and it is thus vulnerable to differential settlements that induce visible cracks in walls, which may affect the aesthetics, functionality and/or safety of buildings. Old masonry buildings with unreinforced shallow foundations are particularly susceptible to subsidence movements.

Subsidence at the scale of single structures can be triggered by different processes, including urban development and groundwater changes, in combination with the spatially heterogeneous nature of compressible organic soil strata in the subsurface. Moreover, land subsidence is aggravated by the increasing frequency and intensity of droughts due to climate changes. The simultaneous presence of various triggering factors can lead to spatially variable ground deformations, known as *differential settlements*, which in turn affect how structures respond. Conversely, the effects of subsidence on different structures emerge at different times, as some buildings are better able to withstand ground deformation than others, due to the wide variability of the structural features of the built stock. Subsidence may progress slowly and remain almost unnoticed, but over time, it can reach a point where the effects become intolerable for structures in a specific area, thereby impacting entire communities.

This thesis evaluates the relationship between subsidence and damage to existing masonry structures to support risk assessment analyses, mitigation and adaptation efforts.

RESEARCH FRAMEWORK AND OBJECTIVES

This PhD research integrates information from literature, measurements of existing structures, numerical modelling, and engineering judgement to achieve a better understanding

of how subsidence processes impact structures.

The project targets two research areas: examining how soil heterogeneity affects settlements at the scale of structures and developing statistical tools to estimate the probability of damage to masonry structures experiencing settlements. For the soil heterogeneity aspect, an area in the Netherlands with available in-situ measurements is selected for analysis. These observations serve as input for numerical analyses designed to assess how variations in soil layer thickness might trigger or exacerbate spatially variable subsidence. The research emphasizes the spatial variability of soil as a potential driver of settlements that can affect structures.

Regarding the probability of damage to masonry structures, the research incorporates both empirical and numerical data. First, damage surveys conducted on existing masonry structures in the Netherlands are collected. The collected information includes technical reports, photographs of the damage, and measurements of the buildings' displacements caused by ground settlements. Analyses are carried out to retrieve probabilistic relationships between the intensity of the settlements and the probability of damage to structures.

The empirical insight is complemented by numerical analyses. Non-linear numerical models are built to simulate the response of masonry structures to settlements. Initially, these simulations evaluate how various geotechnical and structural factors influence the vulnerability of buildings to settlements. Subsequently, additional numerical analyses are conducted to establish the probabilistic relationship between ground settlement intensity and structural damage probability, following a similar approach to the analyses based on empirical information.

Ultimately, the results of the analyses are compared and validated against the scientific literature and the current standards for structures affected by ground settlements.

THE INFLUENCE OF THE SOIL HETEROGENEITY ON THE SETTLEMENT OCCURRENCE

Variations in soil stratigraphy, particularly in strata thickness, can cause differential settlements at the scale of individual structures, exacerbating those caused by regional subsidence.

The effect of soil heterogeneity is investigated through the use of closely spaced in-situ cone penetration tests (typically spaced from approximately 1.25 m to 5.0 m apart) across a particular study area. This approach allows for a detailed characterization of soil strata and their variations.

One-dimensional (1D), two-dimensional (2D), and three-dimensional (3D) numerical analyses are employed to calculate settlements across the study area under a uniform load. This approach is used to assess the impact of soil heterogeneity on settlement occurrence.

The "correlation length", a metric used to describe the distance over which observations remain significantly correlated, is employed to quantify the spatial variability (the

variation of a given property across different locations within a selected domain) of the material thickness of each soil layer and the computed settlements.

The results indicate that the values of the correlation length of the computed settlements for each soil strata, derived via numerical modelling, match the values of the correlation length of the soil thickness. Furthermore, the spatial variability of the computed settlements is quantified by a correlation length ranging from approximately 1 to 10 meters, corresponding to the scale of typical structures. This match between the scale of soil fluctuation and the building scale highlights how spatial variations in soil layer distribution can lead to uneven settlement patterns in existing structures, potentially increasing the risk of structural damage.

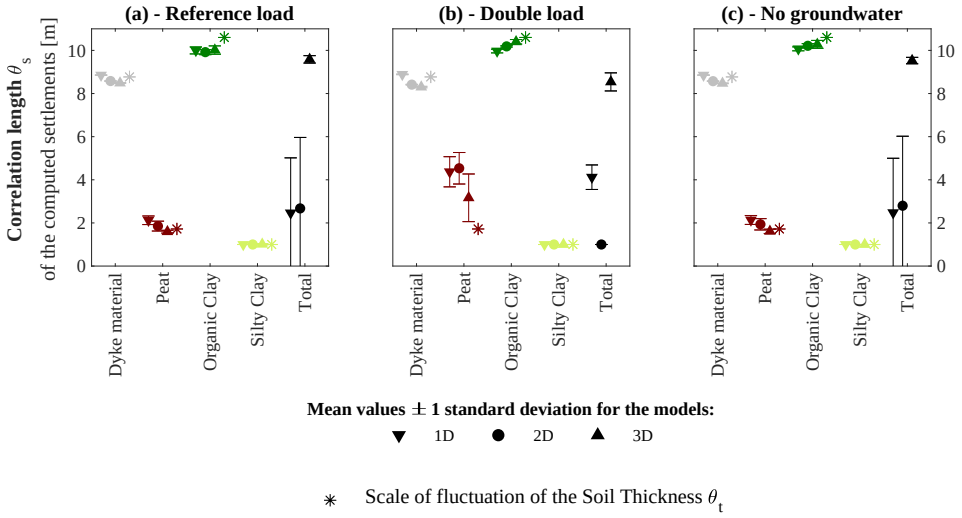

Figure 1: Relationship between soil strata variability and computed settlements, quantified by correlation length. The results reveal a link between soil variability and superficial settlements at the structural scale.

Further numerical analyses are conducted using a country-scale model to discretize the subsurface study area. The results of these additional analyses show a good agreement with those of the in-situ resolution models, supporting the upscaling and the integration of soil heterogeneity effects in regional risk assessment studies.

EMPIRICAL INSIGHT OF STRUCTURES EXPOSED TO SUBSIDENCE-RELATED SETTLEMENTS

Empirical observations of actual structures affected by ground settlements are essential for enhancing our understanding of their response to subsidence. A desk collection of the information on 386 surveyed masonry buildings, 122 on shallow foundations and 264 on piled foundations, is carried out. The collected information includes manual levelling measurements and recorded damage for buildings experiencing subsidence from non-registered causes.

With bed-joint levelling measurements available for each building, settlement intensity

parameters are computed, including *differential settlement*, *rotation*, *angular distortion* and *deflection ratio*. It is thus possible to identify the most effective settlement intensity metric for predicting building damage. The analyses confirm that building distortion, measured through the two parameters *rotation* or *angular distortion*, serves as a reliable predictor of building damage.

With the availability of levelling measurements, it is possible to investigate whether the wall deformations are associated with recurring shapes. Consequently, it is observed that building deformations due to land subsidence conform to a Gaussian distribution, similar to what has been observed in settlements induced by tunnelling, mining, and excavation.

Finally, empirical probabilistic relationships linking the probability of damage to the intensity of settlements have been established.

FINITE ELEMENT MODELS TO EXPLORE THE DAMAGE TO BUILDINGS EXPOSED TO SUBSIDENCE

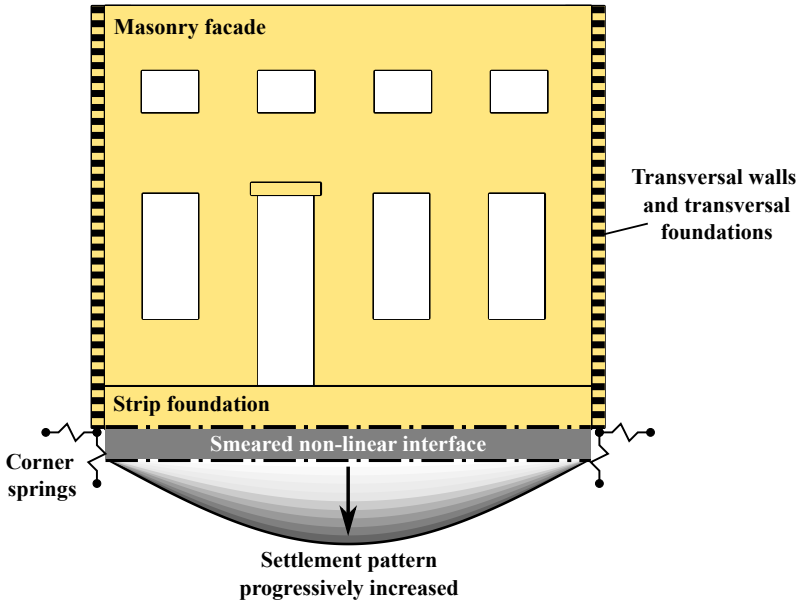

Figure 2: Schematic illustration of a 2D non-linear finite element model of a masonry facade on strip foundations subjected to ground settlements, applied progressively at the bottom of the model. Interfaces simulate the contact interaction with the soil. The model includes the effect of transversal walls and foundations, supported by springs.

Non-linear finite element analyses are often employed to investigate the response of structures subjected to various actions. In the context of buildings exposed to settlements, the state-of-the-art typically focuses on ground movements triggered by human activities such as tunnelling, mining or excavations. Consequently, there is a need for models that specifically target structures affected by subsidence.

Therefore, a comparison of existing modelling approaches is carried out to select the optimum modelling strategy for building damage caused by subsidence-related settlements.

Accordingly, an ad-hoc 2D modelling approach further refines existing models and it is selected for the analyses. The model is able to simulate the response of the structure including the relevant structural features of old masonry buildings located in the Netherlands, such as the effect of lateral house-to-house separation walls.

Both 2D and 3D non-linear numerical analyses are conducted and compared with the proposed 2D model. All selected models employ the smeared crack approach to simulate crack initiation and propagation in the masonry material. The analyses primarily focused on the in-plane behaviour of the facade subjected to settlements, though out-of-plane effects were also assessed in the selected 3D models.

The deformations, stresses, and cracking damage of the proposed two-dimensional model agree with those of the more complex three-dimensional models. Additionally, the proposed 2D modelling approach has lower complexity than 3D models and is 9 to 40 times faster in terms of computational time, meaning each simulation runs significantly quicker. This enables a parametric study to investigate the probability of damage.

AN OBJECTIVE ASSESSMENT OF THE CRACKING DAMAGE

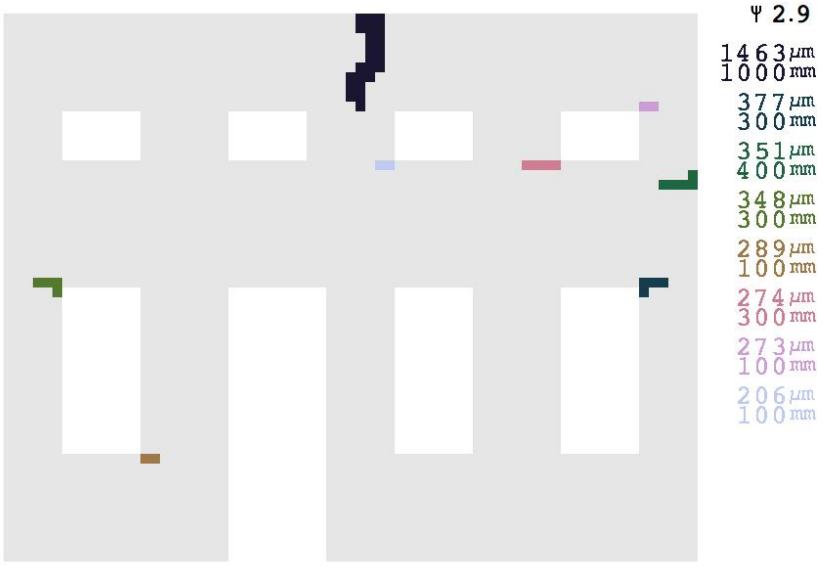

Figure 3: An example of the automatic identification of cracks and calculation of Ψ from the results of a facade model subjected to a symmetric hogging settlement. In the legend, the crack width is expressed in μm whereas the crack length is in mm.

Cracking is commonly considered to assess the damage to structures affected by settlements. Measurements of cracks' width are often used to provide direct insights into the severity and extent of damage to buildings. Nevertheless, cracks can occur in inaccessible

parts of buildings, or be difficult to detect by inexperienced observers. In the Netherlands, damage to masonry structures caused by subsidence-related settlements generally results in minor rather than significant structural concerns. Typically, this damage is characterized as "*light*", which might be hard to detect and measure objectively. Moreover, the number of cracks and their length, in addition to their width, offer further valuable insights into the extent of the damage, which should not be overlooked.

A continuous damage parameter Ψ, tuned against existing damage scales, is used to objectively quantify the damage of the numerical analyses. Moreover, the parameter Ψ offers direct insight into both undetectable (crack width smaller than 0.1 mm) and visible damage. This damage parameter, formulated in other studies and used in this thesis, provides an effective way to observe the initiation of the damage and its accumulation during the progression of the settlement.

THE EFFECT OF BUILDING FEATURES AND SOIL ON DAMAGE

Exploratory numerical analyses are carried out to evaluate the influence of different structural and geotechnical aspects, such as construction material, structural layout (geometry and openings), foundation system, and soil. Key observations are described next:

The response of the building model strongly depends on the shape of the ground settlements they are exposed to.

The flexibility of the buildings is influenced by the degree of damage: as settlement progresses, the damage to the building accumulates and the structure becomes, in turn, more flexible.

Careful consideration should be given to differentiating between soil displacements and deformation of buildings, as these can vary significantly depending on the interaction between the soil and the structure.

In agreement with the state-of-the-art, the relationship between the length and height of the building strongly influences the response of the structure exposed to settlements.

Facades with openings are more vulnerable than blind walls.

The response of the structure is governed by the soil on which they rest: buildings on softer soil (clay) require larger displacements to reach the same level of damage as the ones on stiffer soil (sand). In fact, the building behaves more rigidly on softer soil and more flexibly on stiffer soil. However, larger soil displacements are likely to occur in softer soils, while smaller displacements are expected in stiffer soils.

Reinforced concrete strip foundations are found to increase the building's stiffness relative to the soil compared to unreinforced masonry foundations. This results in buildings with reinforced concrete strip foundations generally experiencing less damage. The effect is most significant under symmetric sagging conditions, where tensile stresses concentrate at the bottom of the building. In such scenarios, the reinforcement bars in the concrete foundations can counteract these tensile stresses, thus opposing damage. However, this beneficial effect is reduced in hogging scenarios, where tensile stresses develop at the top of the building.

NUMERICALLY-BASED FRAGILITY CURVES

Fragility functions represent statistical tools which express the probability that an event will occur as a function of a hazard metric. In the context of damage to buildings, fragility curves retrieve the relationship between (the intensity of) the ground settlement and the probability of having or exceeding a specific damage state.

Fragility curves are developed by means of numerical analyses focusing on old masonry buildings exposed to subsidence-induced settlements on strip foundations as a function of the angular distortion. The curves are developed considering realistic scenarios and variations of the soil and buildings' features in the non-linear numerical models, including 8 geometries, 3 masonry materials, 2 shallow foundation systems, and 2 soil typologies. Moreover, the models considered 72 variations of possible symmetric and asymmetric settlement deformations. A total of 6912 analyses are carried out.

Two sets of curves are proposed, distinguishing the functions in terms of the soil distortions, and the ones in terms of the distortions measured on buildings.

The curves in terms of distortions measured on buildings, accounting for all selected variations of the considered structural and geotechnical features, reveal that 1 out of 2 buildings could exhibit cracks up to 5 mm for an angular distortion equal to 1/500 (or 2 ‰), a threshold recommended by international and national standards as an acceptable limit for structures.

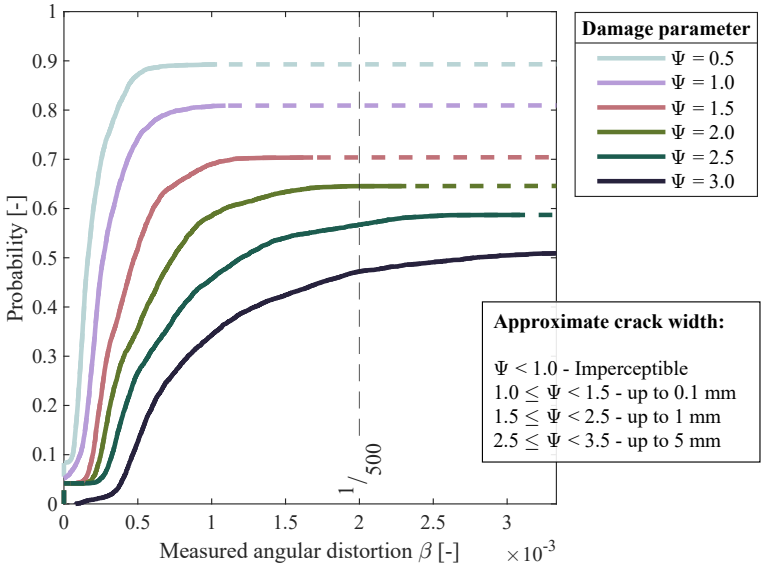

Figure 4: Fragility curves in terms of measured angular distortions. The curves reveal a probability of cracks up to 5mm (corresponding to Ψ = 3.0) equal to about 47% for an angular distortion measured on the building equal to 2 ‰(or 1/500).

The proposed fragility functions are expected to provide insights into the behaviour of old Dutch masonry structures on shallow foundations and will serve as inputs for integration into damage and risk assessment frameworks.

LIMITATIONS AND RECOMMENDATIONS

A comparison of the proposed empirical and numerical fragility curves is conducted to investigate their differences. The results indicate that numerical fragility curves provide more conservative estimates of the probability of damage than the empirical curves for a given settlement intensity.

Although the adopted numerical analyses have been set up using engineering properties derived from experimental campaigns and modelling approaches from previous studies on building damage caused by other types of load, the observed discrepancies between the empirical and the numerical results highlight the need for integrating more detailed empirical, experimental and monitoring data to calibrate the numerical analyses of masonry structures exposed to settlements. Considering the slow development of subsidence, monitoring existing structures over an extensive time frame represents a complex and expensive task that does not guarantee that: i) damage due to settlement will occur and accumulate; ii) damage will occur only due to settlements, disentangling other causes. These constraints highlight the need to establish experimental benchmarks.

Other limitations of the analyses must be highlighted:

Currently, there is limited understanding of how the spatial variability of soil impacts settlement occurrence across different scales. The preliminary results suggest a correlation between various scales. It remains unclear how common it is for soil layers to exhibit significant spatial variations that can influence the response of individual structures. Furthermore, the relationship between soil spatial variability and ground settlement requires further investigation in future research.

In this research, facades are used to represent the behaviour of entire structures. In reality, the 3D effects of structures provide an additional source of complexity and must be further studied. Similarly, the ground settlements might present a 3D spatial distribution, which is herein disregarded. It is known that significant horizontal strains have been measured for certain settlement drivers like tunnelling, mining, and excavation, and their effects on damage are recognized. Currently, there is no evidence suggesting that similar horizontal strains could occur for land subsidence.

Another source of uncertainties lies in the engineering properties and constitutive relationships adopted in the numerical analyses. The properties reported in standards and guidelines are often derived from measurements on small experimental samples in research. Consequently, discrepancies might arise between the engineering properties of masonry samples, such as cores, couplets and triplets, window banks, or walls, and existing structures due to scale effects. In terms of the constitutive relationship, a smeared cracking approach is employed to represent the masonry material as an equivalent continuum. However, since masonry is a composite material, the model may not fully capture the complex interactions between its individual components. Additionally, the model does not account for long-term effects: viscoelastic effects may occur in existing structures exposed to slow settlements, further increasing the differences from models.

The information regarding the construction material, foundation systems, and geometrical features such as the distribution of windows and doors of walls are examples of key

information which are typically unavailable except in certain municipalities or areas. The availability of data on existing structures poses a challenge for any attempt at damage assessment over wide areas. Preliminary analyses, however, can be carried out by deriving such information through correlations with available data.

SOCIETAL RELEVANCE

Land subsidence is an ongoing irreversible phenomenon. This geohazard is exacerbated by increasingly frequent and intense weather events due to climate change. The impacts of subsidence present challenges to urban expansion and land development. In this context, understanding the impact on existing structures is crucial for preserving the cultural identity of a country, safeguarding the economy, protecting historic landmarks, and preventing social unease.

Subsidence mitigation and adaptation policies are essential to address the potential impact on homeowners, who may face rising costs for maintaining and repairing their properties. Furthermore, it is essential to recognize the risks and costs associated with damage to buildings from land subsidence, even when it does not result in structural collapse.

In the Netherlands, managing and implementing policies to address subsidence involves multiple stakeholders with diverse interests, including homeowners, businesses and (agro)industry, institutions, and governmental agencies. Therefore, it is essential to raise awareness about the impact of land subsidence. Clear comprehension of the relationship between subsidence and resulting damages is essential for making informed decisions. The research presented in this dissertation, which is part of the project Living on Soft Soils (LOSS): Subsidence and Society (grantnr.: NWA.1160.18.259), is expected to contribute to this.

SAMENVATTING

Bodemdaling is een bekend fenomeen dat de geleidelijke verlaging van het grondoppervlak ten opzichte van het zeeniveau beschrijft. Bodemdaling beinvloedt veel dichtbevolkte gebieden in Noord-Amerika, Azië en Europa. In Nederland hebben de westelijke en noordelijke gebieden van het land al gedurende eeuwen te maken gehad met bodemdaling, als gevolg van de veen- en kleirijke ondergrond incombinatie met natuurlijke processen en menselijke activiteiten. Het voortdurende proces van bodemdaling vereist zorgvuldige planning en kostbare maatregelen om het huidige grondgebruik te behoudenen leidt tot schade aan gebouwen en infrastructuur.

Bovendien evolueren de kosten van bodemdaling door klimaatverandering, veranderende neerslag, grondwaterstanden en bodemvochtigheid. Deze veranderende condities versterken het bodemdalingproces, wat leidt tot onvoorspelbaardere en versnelde bodemdaling in de gebieden waar dit voorkomt.

Sociale gevolgen van bodemdaling omvatten onzekerheid voor woningeigenaren en economische verliezen. Individuen en publieke organisaties maken zich steeds meer zorgen over hoe bodemdaling het gebouwde erfgoed beinvloedt. Nederlandse steden staan wereldwijd bekend om hun metselwerkgebouwen, gebouwd met gebakken klinkers, een traditie ook nu nog voortduurt in de moderne architectuur. Metselwerk is echter een bros materiaal met beperkte treksterkte en is daarom kwetsbaar voor verschilzettingen, waardoor scheuren in muren kunnen optreden die de esthetiek, functionaliteit en/of veiligheid van gebouwen kunnen beïnvloeden. Oude metselwerkgebouwen met ongewapende ondiepe funderingen zijn bijzonder gevoelig voor bodemdaling.

Bodemdaling op de schaal van individuele gebouwen kan worden veroorzaakt door verschillende processen, waaronder stedelijke (bouw)activiteiten en veranderingen of aanpassingen in het grondwater, zeker in het geval van ruimtelijk heterogene en samendrukbare organische bodemlagen in de ondergrond. Bovendien wordt bodemdaling verergerd door de toenemende frequentie en intensiteit van droogtes als gevolg van klimaatverandering. De gelijktijdige aanwezigheid van verschillende triggerfactoren kan leiden tot ruimtelijk variabele grondvervormingen, bekend als *verschilzettingen*, die op hun beurt de gebouwen beïnvloeden. Daarentegen kunnen door verschillen in gebouweigenschappen sommige gebouwen verschilzettingen beter opnemen dan andere, waardoor de effecten van bodemdaling op verschillende tijdstippen naar voren komen. Bodemdaling kan langzaam en bijna onopgemerkt optreden, maar na verloop van tijd kan het een punt bereiken waarop de effecten onhoudbaar worden voor gebouwen in een specifiek gebied, wat maatschappelijke invloed heeft op hele gemeenschappen.

Dit proefschrift onderzoekt de relatie tussen bodemdaling en schade aan bestaande metselwerkgebouwen ter ondersteuning van activiteiten op het gebied van risicoanalyse, mitigatie- en aanpassing.

ONDERZOEKSRAAMWERK EN DOELSTELLINGEN

Dit PhD-onderzoek integreert informatie uit de literatuur, metingen van bestaande gebouwen, numerieke modellering en "engineering judgement" om een beter begrip te krijgen van hoe bodemdalingsprocessen gebouwen beïnvloeden.

Het project richt zich op twee onderzoeksgebieden: het onderzoeken van hoe bodemheterogeniteit zettingen op de schaal van gebouwen beïnvloedt en het ontwikkelen van statistische hulpmiddelen om de kans op schade aan metselwerkgebouwen door zettingen te schatten. Voor het aspect bodemheterogeniteit is een gebied in Nederland met een dicht netwerk van beschikbare in-situ metingen geselecteerd voor analyse. Deze waarnemingen dienen als input voor numerieke analyses om te beoordelen hoe varieties in de dikte van bodemlagen mogelijk ruimtelijk variabele bodemdaling kunnen veroorzaken of verergeren. Het onderzoek legt de nadruk op de ruimtelijke variabiliteit van de bodem als een potentiële oorzaak van zettingen die gebouwen kunnen beïnvloeden.

Wat betreft de kans op schade aan metselwerkgebouwen, omvat het onderzoek zowel empirische als numerieke gegevens. Allereerst worden schadeonderzoeken, uitgevoerd aan bestaande metselwerkgebouwen in Nederland, verzameld. De verzamelde informative omvat technische rapporten, foto's van de schade en metingen van de verplaatsingen van de gebouwen veroorzaakt door grondvervormingen. Analyses worden uitgevoerd om probabilistische relaties tussen de intensiteit van de zettingen en de kans op schade aan de gebouwen te achterhalen.

De empirische inzichten worden aangevuld met numerieke analyses. Niet-lineaire numerieke modellen worden gemaakt om de effecten van zettingen op metselwerkgebouwen te simuleren. Aanvankelijk evalueren deze simulaties hoe verschillende geotechnische en constructieve factoren de kwetsbaarheid van gebouwen voor zettingen beïnvloeden. Vervolgens worden aanvullende numerieke analyses uitgevoerd om de probabilistische relatie tussen de intensiteit van de zettingen en de kans op constructieve schade vast te stellen, volgens een vergelijkbare benadering als de analyses op basis van empirische informative.

Ten slotte worden de resultaten van de analyses vergeleken en gevalideerd aan de hand van de wetenschappelijke literatuur en de huidige normen voor gebouwen die worden beïnvloed door zettingen.

DE INVLOED VAN BODEMHETEROGENITEIT OP DE ZETTING

Variaties in bodemstratigrafie, met name in de dikte van de lagen, kunnen leiden tot verschil zettingen op de schaal van individuele gebouwen, wat tot meer schade leidt dan homogene/gelijkmatige zettingen.

Het effect van bodemheterogeniteit wordt onderzocht door middel van een gebied met dicht op elkaar geplaatste sonderingen (typisch op afstanden van ongeveer 1,25 m tot 5,0 m). Deze aanpak maakt een gedetailleerde karakterisering van bodemlagen en hun variaties in dit gebied mogelijk.

Een-dimensionale (1D), twee-dimensionale (2D) en drie-dimensionale (3D) numerieke analyses worden gebruikt om zettingen in het studiegebied te berekenen onder een uni-

forme belasting. Deze benadering wordt gebruikt om de impact van bodemheterogeniteit op de zetting te beoordelen.

De "correlatielengte", een maatstaf die wordt gebruikt om de afstand te beschrijven waarop waarnemingen significant gecorreleerd blijven, wordt ingezet om de ruimtelijke variabiliteit (de variatie van een bepaalde eigenschap op verschillende locaties binnen een geselecteerd domein) van de materiaaldikte van elke bodemlaag en de berekende zettingen te kwantificeren.

De resultaten geven aan dat de waarden van de correlatielengte van de berekende zettingen voor elke bodemlaag, verkregen via numerieke modellering, overeenkomen met de waarden van de correlatielengte van de bodemdikte. Bovendien wordt de ruimtelijke variabiliteit van de berekende zettingen gekwantificeerd door een correlatielengte variërend van ongeveer 1 tot 10 meter, wat overeenkomt met de schaal van typische gebouwen. Dit benadrukt hoe ruimtelijke variaties in de verdeling van bodemlagen kunnen leiden tot ongelijke zettingspatronen in bestaande gebouwen, wat mogelijk het risico op constructieve schade verhoogt.

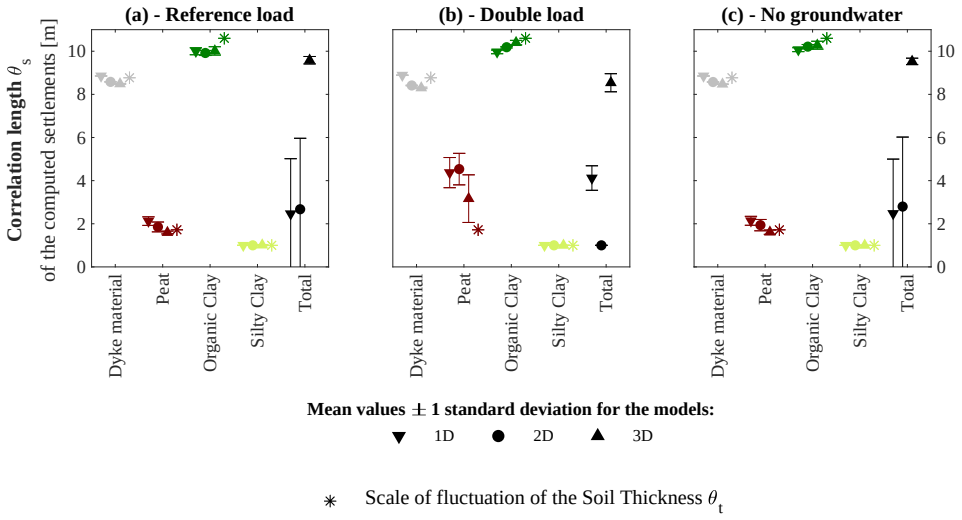

Figure 5: Relatie tussen de variabiliteit van bodemlagen en de berekende zettingen, gekwantificeerd door de gevonden correlatielengte. De resultaten tonen een verband aan tussen bodemvariabiliteit en maaiveldzettingen op de schaal van gebouwen.

Verdere numerieke analyses zijn uitgevoerd met behulp van een landsdekkend model om de ondergrond in het studiegebied te discretiseren. De resultaten van deze aanvullende analyses hebben een goede overeenkomst met die van de in-situ modellen, wat de opschaling en integratie van effecten van een heterogene bodem in regionale risico-evaluatiestudies ondersteunt.

EMPIRISCHE INZICHTEN OVER GEBOUWEN BLOOTGESTELD AAN ZETTINGEN DOOR BODEMDALING

Empirische waarnemingen van werkelijke gebouwen die worden beïnvloed door zettingen zijn essentieel voor het verbeteren van ons begrip van de gevolgen van bodemdaling voor die gebouwen. Er is een verzameling samengesteld van informatie over 386 onderzochte metselwerkgebouwen, waarvan 122 op ondiepe funderingen en 264 op funderingen met palen. De verzamelde informatie omvat handmatige hoogtemetingen en geregistreerde schade voor gebouwen die zettingen ervaren door verschillende, niet geregistreerde oorzaken.

Met de beschikbare lintvoegmetingen voor elk gebouw worden zettingsintensiteitsparameters berekend, waaronder *verschil zetting, rotatie, relatieve hoekverdraaiing* en *deflectie ratio*. Het is hierdoor mogelijk om de meest effectieve indicator voor zettingsintensiteit te identificeren voor het voorspellen van schade aan gebouwen. De analyses bevestigen dat de vervorming van gebouwen, gemeten via de twee parameters *rotatie* of *relatieve hoekverdraaiing*, betrouwbare voorspellers zijn van schade aan gebouwen. Met de beschikbare lintvoegmetingen is het mogelijk te onderzoeken of de vervormingen van de gemeten gebouwmuren herkenbare vormen hebben.

Conclusie is dat de vervormingen van gebouwen door bodemdaling een Gausskromme volgen, vergelijkbaar met de vormen die zijn waargenomen bij zettingen door tunnels, mijnbouw en andere graafwerkzaamheden.

Tot slot zijn empirische, probabilistische relaties vastgesteld die de kans op schade koppelen aan de intensiteit van de zettingen.

EINDIGE-ELEMENTMODELLEN

Niet-lineaire eindige-elementanalyses worden vaak gebruikt om de gevolgen van verschillende belastingen op gebouwen te onderzoeken. De meeste toepassingen en onderzoek naar de invloed van zettingen op gebouwen richt zich meestal op grondbewegingen die worden veroorzaakt door activiteiten zoals het aanleggen van tunnels, mijnbouw of andere graafwerkzaamheden. Er is echter behoefte aan modellen specifiek gericht zijn op gebouwen die worden beïnvloed door bodemdaling.

Daarom wordt in dit onderzoek een vergelijking van bestaande benaderingen voor modellering gemaakt om de optimale modelleringsstrategie te selecteren voor het beoordelen van schade aan gebouwen door zettingen ten gevolge van bodemdaling.

Als resultaat is een 2D-modelleringsbenaderinggeselecteerd voor de analyses. Het geselecteerde model kan de invloed van zetting op het gebouw simuleren, en houdt rekening met de relevante constructieve eigenschappen van oude Nederlandse metselwerk gebouwen , zoals het effect van scheidingswanden tussen huizen.

Zowel 2D- als 3D-niet-lineaire numerieke analyses worden uitgevoerd en vergeleken met het voorgestelde 2D-model. Alle geselecteerde modellen maken gebruik van de uitgesmeerde- scheurmodel om scheurinitiatie en -propagatie in het metselwerk te simuleren. De analyses richtten zich voornamelijk op het gedrag van de gevel in het vlak, hoewel ook uit-het-vlak effecten werden beoordeeld in de geselecteerde 3D-modellen.

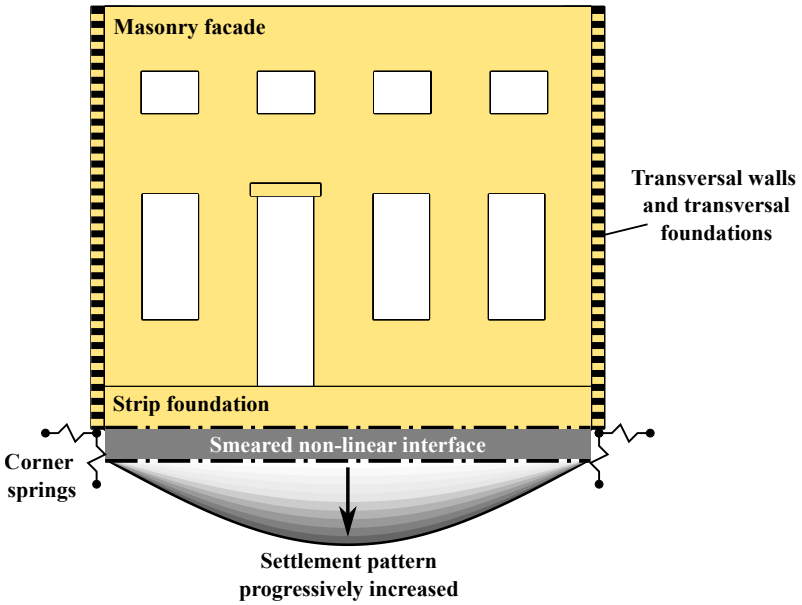

Figure 6: Schematische illustratie van een 2D niet-lineair eindige-elementmodel van een metselwerk gevel op strokenfundering, blootgesteld aan zettingen, met toenemende zettingen opgelegd aan de onderkant van het model. Interfaces simuleren de interactie met de ondergrond. Het model omvat het effect van dwarswanden en funderingen, ondersteund in de vorm van veren.

De vervormingen, spanningen en scheurvorming van het voorgestelde tweedimensionale model komen overeen met die van de complexere driedimensionale modellen. Bovendien heeft de voorgestelde 2D-modelleringsbenadering een lagere complexiteit dan 3Dmodellen en is deze 9 tot 40 keer sneller qua rekentijd, wat betekent dat elke simulatie aanzienlijk sneller wordt uitgevoerd.

EEN OBJECTIEVE BEOORDELING VAN SCHADE IN DE VORM VAN SCHEUREN

Scheuren worden vaak beschouwd als een maatstaf voor schade aan gebouwen die door zettingen worden beïnvloed. Metingen van de scheurwijdte worden vaak gebruikt om inzicht te verkrijgen in de ernst en omvang van schade aan gebouwen. Echter kunnen scheuren zich bevinden op ontoegankelijke delen van gebouwen of moeilijk waarneembaar zijn voor onervaren waarnemers. In Nederland leidt schade aan metselwerkgebouwen door zettingen meestal tot kleinere, minder significante constructieve problemen. Deze schade wordt doorgaans gekarakteriseerd als "*licht*", wat moeilijk objectief te detecteren en meten kan zijn. Bovendien bieden het aantal scheuren en hun lengte, naast hun breedte, waardevolle extra inzichten in de omvang van de schade, die niet over het hoofd gezien mogen worden.Een continue schadeparameter Ψ, afgestemd op bestaande schade-schalen, wordt gebruikt om de schade uit de numerieke analyses objectief te kwantificeren. Bovendien biedt de parameter Ψ direct inzicht in zowel niet-waarneembare (scheurwijdte kleiner dan 0,1 mm) als zichtbare schade. Deze schadeparameter, die in dit proefschrift wordt gebruikt, biedt een effectieve manier om het

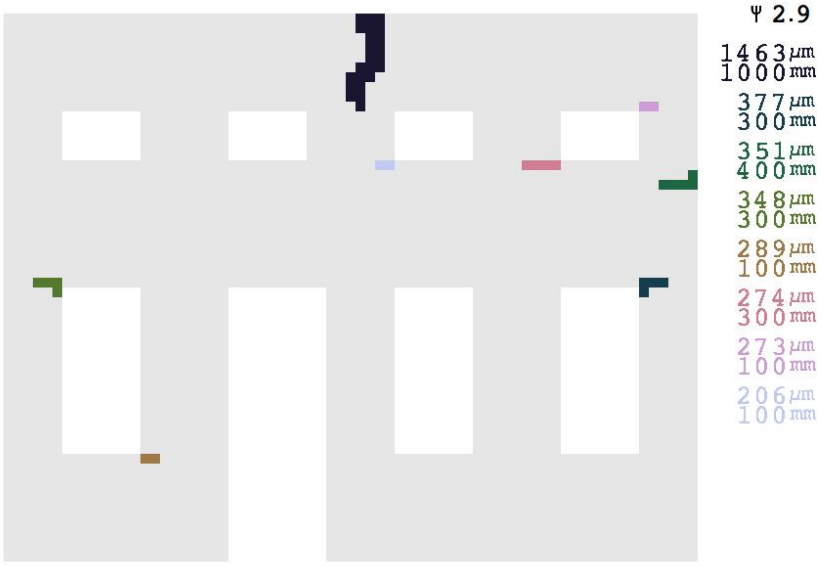

Figure 7: Voorbeeld van de automatische identificatie van scheuren en berekening van Ψ op basis van de resultaten van een gevelmodel blootgesteld aan een symmetrische hogging-zetting. In de legenda wordt de scheurwijdte uitgedrukt in μm en de scheurlengte in mm.

ontstaan van schade en de accumulatie ervan tijdens de voortgang van de zetting te observeren.

DE INVLOED VAN GEBOUWKENMERKEN EN ONDERGROND OP GEBOUWSCHADE

Verkennende numerieke analyses zijn uitgevoerd om de invloed van verschillende constructieve en geotechnische aspecten, zoals bouwmateriaal, gebouwindeling (geometrie en openingen), fundering en bodem, te evalueren. Belangrijke observaties worden hieronder beschreven:

De schade aan het gebouw hangt sterk af van de vorm van de zetting.

De flexibiliteit van de gebouwen wordt beïnvloed door de mate van schade: naarmate de verzakking toeneemt, neemt de schade toe en wordt de constructie flexibeler.

Er moet zorgvuldig worden nagedacht over het verschil tussen zetting van de en deformatie van de gebouwen, omdat deze aanzienlijk kunnen verschillen afhankelijk van de grond constructie interactie.

Conform de huidige stand van zaken, beinvloedt de verhouding tussen de lengte en hoogte van het gebouw sterk de invloed van de zakking op het gebouw.

Gevelsmet openingen zijn kwetsbaarder dan blinde muren.

De respons van dhet gebouw wordt bepaald door de ondergrond waarop deze rust: gebouwen op slappere bodem (klei) moeten grotere verplaatsingen ondergraan om hetzelfde niveau van schade te bereiken als bij gebouwen op stijvere bodem (zand). In

feite gedraagt het gebouw zich stijver op slappee bodem en flexibeler op stijvere bodem. Echter, in absolute zin zullen waarschijnlijk grotere zettingen optreden in slappe ondergrond, terwijl kleinere verplaatsingen worden verwacht in stijvere ondergrond.

Gewapende betonnen strokenfunderingen blijken de stijfheid van het gebouw ten opzichte van de ondergrond te vergroten in vergelijking met ongewapende metselwerkfunderingen. Dit resulteert erin dat gebouwen met gewapende betonnen strokenfunderingen over het algemeen minder schade ondervinden. Het effect is het meest significant in geval van symmetrische zettingspatronen, waarbij trekspanningen zich concentreren aan deonderkant van het gebouw. In dergelijke scenario's kunnen de wapeningsstaven in de betonnen funderingen deze trekspanningen tegengaan en zo schade verminderen. Dit gunstige effect is echter minderaanwezig in hogging-scenario's, waarbij trekspanningen zich aan de bovenkant van het gebouw ontwikkelen.

NUMERIEKE KWETSBAARHEIDSFUNCTIES

Kwetsbaarheidsfuncties zijn statistische hulpmiddelen die de kansuitdrukken dat een gebeurtenis zich voordoet als functie van een risico-metriek. In de context van schade aan gebouwen beschrijven kwetsbaarheidscurves de relatie tussen (de intensiteit van) de zettingen en de kans op het veroorzaken of overschrijden van een specifiek schade-niveau.

Kwetsbaarheidscurves worden ontwikkeld door middel van numerieke analyses specifiek voor oude metselwerkgebouwen op strokenfunderingen blootgesteld aan bodemdaling, als functie van de hoekverdraaiing van het gebouw. De curves worden ontwikkeld met realistische scenario's en variaties in de bodem- en gebouwkenmerken in de niet-lineaire numerieke modellen, waaronder 8 geometrieën, 3 metselwerkmaterialen, 2 ondiepe funderingssystemenen en 2 bodemtypes. Bovendien zijn 72 variaties van mogelijke symmetrische en asymmetrische zettingprofielen in de modellen opgenomen. In totaal zijn 6912 analyses uitgevoerd.

Twee sets curves zijn beschikbaar, waarbij onderscheid wordt gemaakt op basis van de vervormingen gemeten in de ondergrond en de vervormingen gemeten aangebouwen.

De curves op basis van de vervormingen gemeten aan gebouwen, rekening houdend met alle toegepast variaties van de beschouwde constructieve en geotechnische kenmerken, tonen aan dat 1 op de 2 gebouwen scheuren tot 5 mm kan hebben bij een hoekverdraaiing gelijk aan 1/500 (of 2 ‰), een grenswaarde die door internationale en nationale normen wordt aanbevolen als een acceptabele limiet voor gebouwen.
De voorgestelde kwetsbaarheidsfuncties bieden waardevolle inzichten in het gedrag van oude Nederlandse metselwerkgebouwen op ondiepe funderingen enzullen dienen als input in schade- en risico-evaluatiekaders.

BEPERKINGEN EN AANBEVELINGEN

De voorgestelde empirische en numerieke kwetsbaarheidscurves zijn onderling vergeleken. De resultaten geven aan dat numerieke kwetsbaarheidscurves meer conservatieve schattingen van de kans op schade geven dan de empirische curves voor een gegeven zettingsintensiteit.

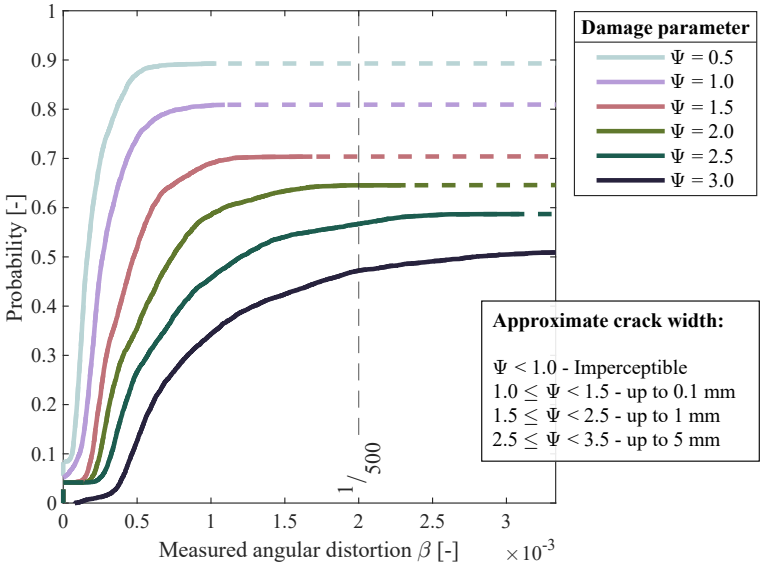

Figure 8: Kwetsbaarheidscurves op basis van gemeten hoekverdraaiing. De curves tonen eenkans op scheuren tot 5 mm (corresponderend met $\Psi = 3.0$) van ongeveer 47% voor een hoekverdraaiing gemeten op het gebouw gelijk aan 2 ‰(of 1/500).

Hoewel de toegepaste numerieke analyses zijn opgezet met eigenschappen afgeleid van experimentele campagnes en de modelleringbenaderingen ook zijn toegepast in eerdere studies over gebouwschade veroorzaakt door andere soorten belasting, laten de waargenomen verschillen tussen de empirische en numerieke resultaten zien dat het noodzakelijk is om de modellen te kalibreren met meer gedetailleerde integratie van empirische, experimentele en monitoringsgegevens . Gezien de langzame ontwikkeling van bodemdaling, is het monitoren van bestaande gebouwen over een langere periode complex en kostbaar. Ook is niet zeker dan : i) schade door zetting zal optreden en toenemen; ii) schade uitsluitend zal optreden door zetting, waarbij andere oorzaken worden uitgesloten. Deze beperkingen maken duidelijk dat het opzetten van gestructureerde experimenten nodig is.

Andere beperkingen van de analyses zijn:

Op dit moment is er beperkte kennis over hoe de ruimtelijke variabiliteit van de bodem de verzakkingsoccurrence op verschillende schalen beïnvloedt. De voorlopige resultaten suggereren een correlatie tussen verschillende schalen. Het blijft onduidelijk hoe gebruikelijk het is dat bodemlagen significante ruimtelijke variaties vertonen die de respons van individuele structuren kunnen beïnvloeden. Bovendien vereist de relatie tussen bodemruimtelijke variabiliteit en grondverzakkingen verdere studie in toekomstig onderzoek.

In dit onderzoek worden gevels gebruikt om het gedrag van volledige gebouwen te simuleren. In werkelijkheid bieden de 3D-effecten van gebouwen een extra bron van complexiteit en moeten deze verder worden bestudeerd. Ook kunnen de zettingen een 3D-ruimtelijke variatie vertonen, welke in dit onderzoek niet zijn meegenomen. Bek-

end is dat er significante horizontale rekken gemeten zijn bij zettingen veroorzaakt door tunnels, mijnbouw en ontgravingen welke effect hebben op schade aan gebouwen. Momenteel zijn er geen aanwijzingen dat vergelijkbare horizontale rekken kunnen optreden bij bodemdaling.

Een andere bron van onzekerheid ligt in de eigenschappen en constitutieve relaties die zijn aangenomen in de numerieke analyses. De eigenschappen die worden gerapporteerd in normen en richtlijnen zijn vaak afgeleid uit metingen op kleine monsters. Als gevolg hiervan kunnen er discrepanties ontstaan tussen de eigenschappen van metselwerk gebaseerd op monsters van verschillende afmetingen en bestaande gebouwen vanwege schaaleffecten. Wat betreft de constitutieve relatie wordt een "smeared cracking" benadering gebruikt om het metselwerk als een equivalent continuum te representeren. Aangezien metselwerk echter een composietmateriaal is, kan het model de complexe interacties tussen de individuele componenten mogelijk niet volledig representeren. Bovendien houdt het model geen rekening met langetermijneffecten: visco-elastische effecten kunnen optreden in bestaande gebouwen blootgesteld aan langzame zakkingen, wat de verschillen met de uitkomst van modellen verder kan vergroten.

De informatie over het bouwmateriaal, funderingssystemen en geometrische kenmerken zoals de verdeling van ramen en deuren in muren zijn voorbeelden van belangrijke gegevens die doorgaans niet beschikbaar zijn. De beschikbaarheid van gegevens over bestaande gebouwen vormt een uitdaging voor pogingen tot schadebeoordeling te maken over grotere gebieden. Voorlopige analyses kunnen echterworden uitgevoerd door dergelijke informatie af te leiden via correlaties met beschikbare gegevens.

MAATSCHAPPELIJKE RELEVANTIE

Bodemdaling is een doorlopend en onomkeerbaar fenomeen. Dit georisico wordt verergerd door steeds frequenter voorkomende en intensere weersomstandigheden als gevolg van klimaatverandering. De gevolgen van bodemdaling vormen uitdagingen voor de bouwopgave en inrichting van het land. In deze context is het begrijpen van de impact op bestaande gebouwen cruciaal voor het behoud van de culturele identiteit van een land, het beschermen van de economie, het behoud van historische monumenten en het voorkomen van negatieve sociale effecten zoals verloedering van de omgeving.

Beleidsmaatregelen voor het beperken van bodemdaling en maatregelen ter reductie of aanpassing zijn essentieel om de potentiële impact op huiseigenaren aan te pakken, die mogelijk te maken krijgen met stijgende kosten voor het onderhouden en repareren van hun eigendommen. Bovendien is het belangrijk om de risico's en kosten in verband met schade aan gebouwen door bodemdaling te erkennen, zelfs wanneer dit niet leidt tot ernstige constructieve effecten.

In Nederland houdt het ontwikkelen en implementeren van beleid om bodemdaling aan te pakken in dat meerdere belanghebbenden met diverse belangen betrokken zijn, waaronder huiseigenaren, bedrijven, instellingen en overheidsinstanties. Daarom is het essentieel om bewustzijn te creëren over de impact van bodemdaling.

Duidelijk begrip van de relatie tussen bodemdaling en de als gevolg hiervan optredende schade is essentieel voor het nemen van weloverwogen beslissingen. Het onderzoek

gepresenteerd in dit proefschrift, dat deel uitmaakt van het project Living on Soft Soils (LOSS): Subsidence and Society (grantnr.: NWA.1160.18.259), is bedoeld om hieraan positief bij te dragen.

Table of Contents

Propositions vii

Summary ix

Samenvatting xix

Table of Contents xxix

Chapter 1 Introduction 1

1.1 Problem statement . . . 3

1.2 Research Goal . . . 5

1.3 Research questions . . . 6

1.4 Thesis outline and methodology . . . 6

1.5 Highlights of this research . . . 8

1.6 NWA-LOSS research programme: Living on Soft Soils . . . 9

Bibliography of Chapter 1 . . . 15

Chapter 2 Literature review 17

2.1 Introduction . . . 20

2.2 Definitions . . . 21

2.2.1 "Subsidence" and "settlements" . . . 21

2.2.2 Damage and its expressions . . . 21

2.3 Masonry buildings in the Netherlands . . . 23
2.3.1 Building typologies . . . 23
2.3.2 Characteristics of the masonry buildings . . . 25
2.3.3 Foundation systems . . . 25

2.4 Causes of settlements . . . 27
2.4.1 Predisposing factors: soft soil and soil heterogeneity . . . 27
2.4.2 Triggering causes and mechanisms . . . 27

2.5 The response of structures to settlements . . . 30
2.5.1 Greenfield displacements . . . 30
2.5.2 The settlement shape and its influence . . . 31
2.5.3 Settlement intensity metrics for buildings . . . 31
2.5.4 The soil-structure interaction . . . 33
2.5.5 Damage classification due to ground settlements . . . 36
2.5.6 Criteria for damage to buildings . . . 37

2.6 Finite element analyses of masonry structures undergoing settlements . . . 43
2.6.1 Crack modelling for masonry structures . . . 44

2.7 Regional assessment of subsidence-induced damage to buildings . . . 46

2.8 Knowledge gaps, challenges and research focus . . . 49

Bibliography of Chapter 2 . . . 58

Chapter 3 The role of the soil heterogeneity on the settlement occurrence **59**

3.1 Introduction . . . 61
3.1.1 Soil heterogeneity . . . 61

3.2 Methodology and Underlying concepts . . . 61
3.2.1 Case study and available datasets . . . 63
3.2.2 Finite Elements models . . . 65
3.2.3 Correlation length . . . 69

3.3 Results of the Finite Elements analyses . . . 70
3.3.1 Correlation length of the soil thickness . . . 70
3.3.2 Correlation length of the computed settlements . . . 71
3.3.3 The influence of the dataset resolutions . . . 73

3.4 Discussion . . . 74
3.4.1 The variability of the soil thickness . . . 75
3.4.2 The variability of the computed settlements . . . 75
3.4.3 Comparison between the different resolutions . . . 78

3.5 Conclusions . . . 78

Bibliography of Chapter 3 82

Chapter 4 Empirical insights into masonry structures exposed to settlements: Recurrent settlement patterns and empirically-based fragility curves **83**

4.1 Introduction 85

4.2 Methodology and Underlying concepts 85
4.2.1 Data collection and processing 85
4.2.2 Recurrent settlement shapes 88
4.2.3 Receiver operating characteristic (ROC) curves 90
4.2.4 Fragility curves 92
4.2.5 Approach 1 93
4.2.6 Approach 2 93

4.3 Collected building information and settlement intensity parameters 94
4.3.1 The intensity of the computed settlement parameters 95

4.4 Recurrent settlement shapes 98

4.5 ROC curves 101

4.6 Empirically-based Fragility curves 102
4.6.1 Approach 1 102
4.6.2 Approach 2 104

4.7 Discussion 107

4.8 Conclusions 108

Bibliography of Chapter 4 113

Chapter 5 Exploratory FE analyses of masonry buildings on strip foundations exposed to variable settlement patterns: Using existing FE models to assess the influence of building and soil features on damage **115**

5.1 Introduction 117

5.2 Methodology and modelling approach 118
5.2.1 Façade and foundation variations 119
5.2.2 Material properties 121
5.2.3 Applied settlement configurations 123
5.2.4 Interface properties representing the soil-foundation interface 125
5.2.5 Method to characterize and quantify the damage 126

5.3 Results of sensitivity analyses involving variations in building and soil features 127
5.3.1 Relationship between settlement troughs and damage 127
5.3.2 Influence of the settlement configurations 129
5.3.3 Influence of the material properties 130
5.3.4 Effects of the façade features 130
5.3.5 Influence of the foundation, soil and interface 131
5.3.6 Results of the sensitivity analyses 132
5.3.7 Differences between applied and retrieved settlements 134
5.3.8 Comparison with the available limit values 136

5.4 Discussion 138

5.5 Conclusions 139
5.5.1 Implications for this thesis 140

Bibliography of Chapter 5 144

Chapter 6 Finding an optimal modelling strategy for masonry buildings on strip foundations subjected to subsidence: A Review of Existing Models and Development of the most suitable 2D Approach **145**

6.1 Introduction 147

6.2 Finite Element modelling strategies and method 148
6.2.1 Methodology 148
6.2.2 The selected 2D and 3D modelling strategies 148
6.2.3 Model Geometry 149
6.2.4 FEM discretization 150
6.2.5 The inclusion of the lateral walls 150
6.2.6 Material properties 151
6.2.7 Interface elements at the bottom of the strip foundation 152
6.2.8 Loadings: applied settlement shapes 153
6.2.9 Damage assessment 154

6.3 Results and comparisons of selected modelling approaches 154
6.3.1 Crack patterns and Damage severity 154
6.3.2 Building model displacements 157
6.3.3 Stresses at the bottom of the interface 159
6.3.4 Features and performance of the models 160

6.4 Discussion 161

6.5 Conclusion 162
6.5.1 Implications for this thesis 163

Bibliography of Chapter 6 167

Chapter 7 Preparatory steps for developing numerical fragility functions: Methodology, selection of the facade geometries, set-up of the numerical models and preliminary sensitivity analyses **169**

7.1 Introduction and methodology . . . 172

7.2 Selection of the facade geometries . . . 175
7.2.1 Available dataset and post-processing . . . 175
7.2.2 Age of construction . . . 176
7.2.3 Walls geometry . . . 176
7.2.4 Results of the preliminary analyses of the geometry of the walls . . . 178
7.2.5 Limitation and uncertainties . . . 178
7.2.6 The use of the wall geometries and statistics . . . 179
7.2.7 The selected facades geometries . . . 181
7.2.8 The representativeness of the selected facades . . . 182

7.3 Set-up of the Finite element models . . . 185
7.3.1 The inclusion of the effect of the transversal walls . . . 185
7.3.2 Selected foundation systems . . . 185
7.3.3 Masonry materials . . . 187
7.3.4 Concrete, Steel and Timber . . . 188
7.3.5 Soil materials . . . 189
7.3.6 Boundary conditions and Interface elements . . . 189
7.3.7 Finite element discretization . . . 190
7.3.8 Imposed settlement actions . . . 190
7.3.9 Loads of roof, floors and veneer . . . 192
7.3.10 Loading scheme and iteration procedure . . . 193
7.3.11 "Applied" and "measured" distortions . . . 195

7.4 Preliminary sensitivity analyses of the numerical features . . . 196
7.4.1 Relationship between the max. crack width and the damage parameter Ψ . . . 196
7.4.2 The influence of the analyses settings . . . 197

7.5 Discussion . . . 200

7.6 Conclusions . . . 201

Bibliography of Chapter 7 . . . 214

Chapter 8 Numerically-based fragility curves for masonry buildings on shallow foundations subjected to subsidence 215

8.1 Numerically-based fragility curves . . . 217

8.1.1 The influence of the number of analyses . . . 219
8.1.2 The influence of the masonry material . . . 221
8.1.3 The effect of hogging and sagging settlement profiles . . . 222
8.1.4 The influence of the foundation system . . . 223
8.1.5 The interface stiffness . . . 225
8.1.6 The effect of the L/H ratio . . . 226
8.1.7 Comparison of the influence of the different parameters . . . 227
8.1.8 The effect of existing damage . . . 231

8.2 Discussion . . . 233
8.2.1 Comparison with numerical fragility curves from previous studies . . . 233
8.2.2 Comparison with existing empirical fragility curves . . . 237
8.2.3 Comparison with available limit values from codes and standards . . . 243

8.3 Conclusions . . . 248

Bibliography of Chapter 8 . . . 252

Chapter 9 Conclusions and Outlook **253**

9.1 Conclusions . . . 255
9.1.1 Returning to the research questions . . . 255

9.2 Relevance and contributions . . . 259
9.2.1 Scientific contributions . . . 259
9.2.2 Societal relevance . . . 259
9.2.3 Utilisation: Integrating the results into a Systematic Regional Scale Damage Assessment . . . 260

9.3 Recommendations for Further research . . . 263
9.3.1 Soil heterogeneity: combining the lithological heterogeneity with the spatial variability of the material properties . . . 263
9.3.2 The influence of the horizontal soil strains . . . 264
9.3.3 Time-dependent behaviour of masonry . . . 264
9.3.4 Scale effect on the engineering properties of masonry . . . 264
9.3.5 Integrating of laboratory tests, monitoring data, measurements and numerical analyses . . . 265
9.3.6 Modelling approaches, numerical robustness and constitutive models 265
9.3.7 Cyclic ground movements: settlement and uplift . . . 266
9.3.8 The effect of existing damage and simultaneous actions . . . 267

Bibliography of Chapter 9 . . . 272

List of Publications **273**

Appendix A Appendix to Chapter 4 **275**

A.1 Differences from the results published in [1] . . . 276
A.1.1 Corrections to the dataset . . . 276
A.2 Differences between the fragility curves . . . 277
Bibliography of Appendix A . . . 279

Appendix B Appendix to Chapter 5 **281**

B.1 An example of the calculation of the relative bending stiffness for the reference model in Ch. 5 . . . 282

Appendix C Appendix to Chapters 7 and 8 **285**

C.1 Geometries of the models adopted in Chapters 7 and 8 . . . 286
C.2 Results of the sensitivity analysis for all the selected facades . . . 290
C.2.1 Results for hogging . . . 290
C.2.2 Results for sagging . . . 296
C.3 The influence of the number of analyses . . . 303
C.4 The influence of the masonry material . . . 305
C.4.1 The effect of hogging and sagging settlement profiles . . . 305
C.5 The influence of the foundation system . . . 305
C.6 The interface stiffness . . . 307
C.7 The effect of existing damage . . . 308
C.8 The effect of the L/H ratio . . . 309

Appendix D Supervised MSc Projects **311**

Appendix E Datasets **313**

List of Figures **314**

List of Tables **330**

Curriculum Vitae **333**

Acknowledgements **335**

CHAPTER 1
INTRODUCTION

CHAPTER 1: TABLE OF CONTENTS

1.1 Problem statement **3**

1.2 Research Goal **5**

1.3 Research questions **6**

1.4 Thesis outline and methodology **6**

1.5 Highlights of this research **8**

1.6 NWA-LOSS research programme: Living on Soft Soils **9**

Bibliography of Chapter 1 . . . . . **15**

1.1. PROBLEM STATEMENT

Land subsidence is a geological hazard responsible for the progressive lowering of the ground surface relative to the sea level. Subsidence affects many densely populated areas in North America, Asia and Europe [1], [2]. The potential consequences of subsidence processes include increased flood risk, aquifer salinization, reduced aquifer-system storage capacity, storm surges, earth fissures, damage to agricultural activities, greenhouse gas (GHG) emissions and damages to buildings and infrastructure [1], [3]–[14]. The latter is the focus of this work.

In the Netherlands, subsidence mainly affects the western part and northern part of the country [1], [12], [15]. The subsurface of these areas is characterized by sequences of peat and clay strata, often referred to as "*soft soils*". The presence of soft soils predisposes the occurrence of long-term (decades or even centuries) ground deformations ([15]–[19]). Subsidence processes are influenced not only by the presence but also by the spatial variability of such highly compressible soil strata. Climate change aggravates subsidence processes due to higher temperatures and more frequent and intense droughts.

In addition, different natural and human drivers, such as urban expansion, groundwater abstraction and management, and the oxidation of soil organic matter, trigger and enhance ground lowering. Furthermore, some factors create vicious circles, such as in the case of groundwater management in the western and northern regions of the Netherlands: water level reductions in ditches and watercourses impact groundwater tables, causing subsidence due to peat decomposition and leading to further need for drainage [20].

The subsidence-induced ground lowering is observed at different scales ranging from individual buildings to entire cities or regions. The intensity of subsidence in a given area is often measured by its overall rate, *i.e.*, the speed of the phenomenon at different locations, typically expressed in *mm/year*. Current predictions of land subsidence that include the effect of climate change for 2050 (Fig. 1.1a) show that the densely populated western and northern parts of the Netherlands are expected to exhibit high rates of land subsidence. Due to land subsidence, spatially variable ground settlements, known as "*differential settlements*", occur at the scale of individual structures. The effects of subsidence-related differential settlements are visible in the Dutch landscape, as buildings, dykes, bridges, side paths and roads sink, tilt or show cracks. Subsidence can also result in damage to underground infrastructure, *e.g.*, sewers, and water distribution systems [1], [3]–[12].

Masonry buildings, which are the most common structural type built in the Netherlands, rest on either shallow foundation systems or piles and are exposed to subsidence-related settlements. Given that masonry is a brittle material, it can only withstand minimal tensile stresses, making it especially vulnerable to settlements. While buildings on piles are less affected by ground movements, as the piles reach deeper, more stable soil layers, those on shallow foundations are directly exposed to settlements. Although it is common that houses in the Netherlands mainly rest on piles, shallow foundations were widely used in the Netherlands until the 1970s [21], and they are still adopted for new structures built on sand. The estimates published in a recent report by the Council for the Environment and Infrastructure (*De Raad voor de leefomgeving en infrastructuur* in Dutch, Rli) revealed

that about 70% of the buildings in the Netherlands rest on shallow foundations, 5-6 % on timber piles and the remaining on more modern concrete piles [22]; Thus, many old masonry buildings that rest on shallow foundations (Fig. 1.1b) could experience differential settlements that pose a risk for damage. The consequences of the subsidence

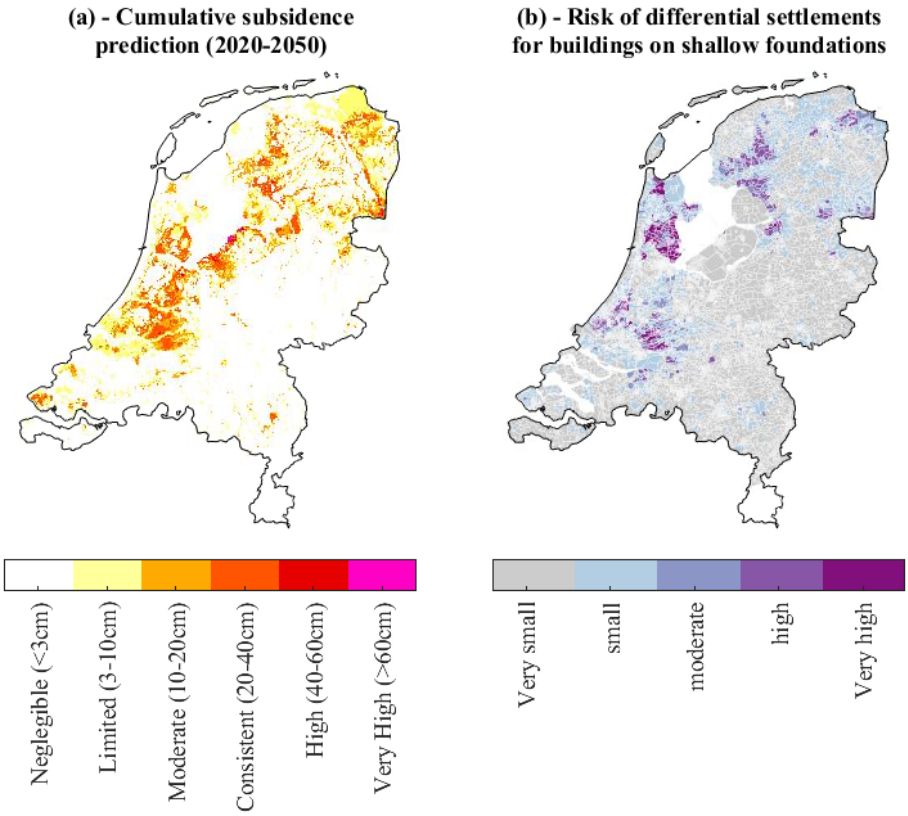

Figure 1.1: (a) Cumulative subsidence prediction map for the period 2020-2050, including the effect of climate change and (b) Risk of differential settlements for buildings on shallow foundations. Data retrieved from klimaateffectatlas.nl [23], [24].

processes include social problems and economic and cultural losses [2], [25]–[27]. For instance, subsidence is correlated to reduced property values [28] and poses a distinct threat to low-income families due to the damage to privately owned buildings. Moreover, the possible engineering actions and solutions, such as foundation repair or strengthening to counteract the effect of subsidence and foundation problems, are associated with high costs and are limited by the adjacency of structures: in Dutch neighbourhoods with old buildings, foundation repairs or strengthening works may not be carried out for a single structure without affecting the surrounding ones. This is particularly true for row houses that share the same foundation system.

Although the Netherlands has undergone subsidence for centuries [13], the problem has received increasing attention in the last decade, considering the influence of climate

change, the increasing population and the demand for urban expansion.

Research programs are currently carried out to map land subsidence, predict its occurrence (*i.e.*, when? where? and how much?) and assess the consequences to urban and agricultural areas. The present PhD study has been part of the LOSS (Living on Soft Soil) research programme [13] (grantnr.: NWA.1160.18.259). Further details about the LOSS programme are provided in section 1.6.

1.2. RESEARCH GOAL

This thesis embraces the necessity to assess (and predict) the damage to structures over wide areas exposed to subsidence processes. The damage assessment requires the availability of data on the exposed structures and subsurface conditions, coupled with insights into how such buildings respond to subsidence-induced ground movements.

This study aims to produce probabilistic relationships to assess the probability of damage to masonry structures due to the occurrence of subsidence-related settlements.

Additionally, part of this study aims to evaluate the influence of the spatial variability of the soil and its impact on the differential settlements at the scale of structures.

The findings and tools proposed in this PhD research find their application in the cost-benefit analyses to evaluate measures to reduce the impact of land subsidence.

1.3. RESEARCH QUESTIONS

This project aims to investigate the response of masonry buildings resting on strip foundations, typical of the Dutch-built heritage, exposed to subsidence-induced settlements. The following overarching research question can be formulated:

What is the relationship between subsidence and damage to existing masonry structures?

The main question can be decomposed into the following sub-questions:

- *What is the influence of the variability of the soil on the occurrence of differential settlements at the building scale?*
- *How can empirical insights into existing structures exposed to ground settlement and their damage be utilized to assess the probability of damage?*
- *What structural and geotechnical parameters (*i.e.*, geometry, foundation, material properties and soil) influence the relationship between imposed soil settlements and the resulting damage to buildings?*
- *What are the best modelling strategies to evaluate the response of structures subjected to subsidence?*
- *How can numerical analyses be used to develop probabilistic relationships between subsidence and the damage to existing masonry structures?*

This research question and the sub-questions will be answered throughout the dissertation, according to the outline presented in Section 1.4 and schematized in Figure 1.2.

1.4. THESIS OUTLINE AND METHODOLOGY

This project combines the use of empirical data with analytical and numerical analyses to answer the research questions. This thesis is structured as follows:

- **Chapter 2** presents the underlying concepts relevant to this thesis. A literature review is thus carried out, reviewing the state-of-the-art assessment of damage for buildings exposed to settlements. Based on the literature review, the knowledge gaps and challenges are identified.
  The features of the masonry buildings exposed to subsidence processes in the Netherlands are introduced and discussed, highlighting the focus of the work presented in this thesis.
- **Chapter 3** describes the role of soil heterogeneity as a predisposing factor for the occurrence of uneven subsidence at the scale of structures. The soil heterogeneity, in the form of variations in the thickness of the soil strata, is expected to influence the occurrence of uneven settlements. This problem can be further augmented by the heterogeneity of the loading conditions acting on the ground surface. In this Chapter, the effect of the soil heterogeneity at the scale of the single structure

is evaluated for a study area, located in the Netherlands. The study area is chosen due to the availability of closely spaced in-situ measurements, allowing for the assessment of soil stratigraphy and the variability of soil strata at the building scale. Numerical analyses are used to study the effects of the identified soil variability. Moreover, the analyses also explore the influence of the boundary conditions (groundwater levels) and the magnitude of the driver, *i.e.*, the load that triggers the settlement occurrence.
A novel method is proposed to quantify the soil heterogeneity, *i.e.*, how much the soil layers are variable, with the purpose of including it in risk assessment analyses over wide areas.

- **Chapter 4** reports the empirical insight gained from a sample of surveyed existing masonry buildings resting on either shallow or piled foundations. Thanks to the availability of in-situ measurements and reports of masonry structures located in the Netherlands reportedly exposed to settlements, a rich sample of almost 400 cases is collected.
  This chapter aims to achieve three goals:

  1. The measurements and reported damage are used to evaluate the empirical relationship between the settlement and the damage for the collected cases.
  2. Four intensity parameters that describe the intensity of the settlements are selected from the state-of-the-art. Their capacity to be used as predictors of building damage is assessed.
  3. The measurements of the buildings' deformation are used to identify recurrent deformation patterns of the settlements, which are then used as input for the numerical analyses.

- In **Chapter 5**, exploratory finite element analyses are carried out to evaluate the effect of different settlement deformations on the response of buildings using existing modelling approaches. The analyses consider realistic variations of geotechnical and structural aspects: the influence of the building's geometry, material, wall wythe, type of foundation and soil-structure interaction is studied.
  One model is selected as the reference case; Then, the effect of each feature is evaluated using a scenario-based approach: the selected feature is varied while keeping the others constant. Through the adopted approach, it becomes feasible to measure which features have the greatest influence on the building's response. These aspects are included in the development of numerical fragility curves, in Chapters 7 and 8.

- **Chapter 6** reviews the performance of different existing and purposely defined modelling strategies to assess the damage to buildings due to subsidence-related settlements. The aim is to identify the optimal modelling approach for the development of numerical fragility functions in Chapter 7. Among the selected models, the method adopted in Chapter 5, is further refined to include the influence of the house-to-house variability on the building's response. The results provide insight for the selection of the modelling strategy adopted in Chapter 7; Accordingly,

the selection of the modelling strategy is carried out not only by comparing the results of the different models, but it is also based on the modelling burden and computational time.

- **Chapters 7 and 8** focus on the development of fragility curves for Dutch masonry buildings on strip foundations subjected to settlements by means of numerical simulations. The modelling strategy discussed in Chapters 5 and 6 is used to generate the models:

  1. In Chapter 7, realistic facade geometries and features are selected from literature sources to build FE models. Preliminary analyses are carried out to evaluate the influence of the settings of the numerical analyses on the relationship between the settlements and the damage.
  2. In Chapter 8, 6912 numerical analyses are carried out to include realistic variations of the buildings, soil features and soil deformation patterns.
     The results of the models are used to generate probabilistic relationships that link the intensity of the settlements with the damage to buildings.

- **Chapter 9** discusses the results gathered in the previous Chapters. The use of the results is discussed, while the limitations are highlighted. The main steps and conclusions of this dissertation are recalled while answering the research questions. Suggestions for further research are provided. Finally, the relevance of this dissertation for practitioners and policy makers is discussed.

A schematic overview of the outline of this thesis is shown in Figure 1.2.

1.5. HIGHLIGHTS OF THIS RESEARCH

- This thesis introduces a new approach to quantifying soil heterogeneity and its effects on the differential settlements at the scale of single structures.
- A proof-of-concept is presented for including the effect of local soil heterogeneity in risk analyses that focus on a regional scale using the available subsurface data at different resolutions.
- A rich dataset of surveyed buildings provides insight into the behaviour of masonry structures subjected to ground settlements. The empirical insight is used to assess the fragility of existing structures and to evaluate the most common settlement patterns of buildings.
- Exploratory analyses are carried out using existing modelling strategies to evaluate the effect of realistic variations of structural and geotechnical on the building response.
- Different modelling strategies are considered and their results are compared; This step provides background for the selection of the modelling techniques that require less modelling burden and computational costs.

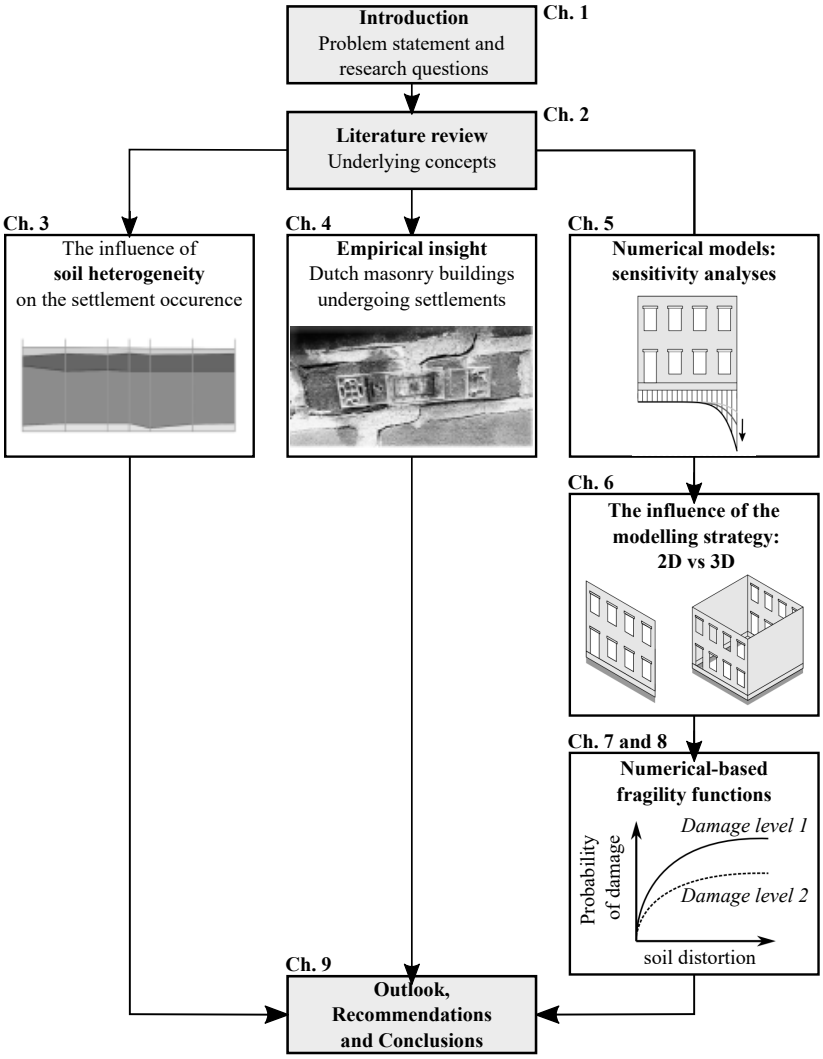

Figure 1.2: Outline of the dissertation. In the flowchart, schematic illustrations are included as graphical abstracts for each chapter.

- The probabilistic relationships between the imposed ground settlements and the resulting damage for masonry buildings on shallow foundations are retrieved by means of numerical analyses.

1.6. NWA-LOSS RESEARCH PROGRAMME: LIVING ON SOFT SOILS

The research presented in this dissertation is part of the project *Living on Soft Soils (LOSS): Subsidence and Society* (grantnr.: NWA.1160.18.259) [13]. The LOSS research program is

run by a broad consortium of research institutes and societal partners in the Netherlands.

The program consists of five work packages (WP), four scientific and a fifth one on knowledge utilization:

- WP1 – Measuring and monitoring of subsidence rates at local and regional scales.
- WP2 – Mechanisms and Green-house-gasses (GHG) emissions.
- **WP3 – Impact analysis**.
- WP4 – Measures and governance approaches.
- WP5 – Knowledge utilization and entrepreneurship.

A detailed overview of the work packages and their links is shown in Fig. 1.3. This thesis project is part of **Work Package 3 - Impact analysis** (in particular, this thesis project is internally referred to as **WP 3.2**); Work Package 3 focuses on the estimates of subsidence-related damage to infrastructure, buildings and agriculture, besides GHG emissions, as input for socio-economic cost-benefit analyses.

The results of this PhD research provide input for socio-economic cost-benefit analysis (as part of Work Package 3 in Figure 1.3), and for the development of different scenarios of the impact of land subsidence. Such knowledge can be integrated into the definition of measures and governance approach (Work Package 4 in Figure 1.3).

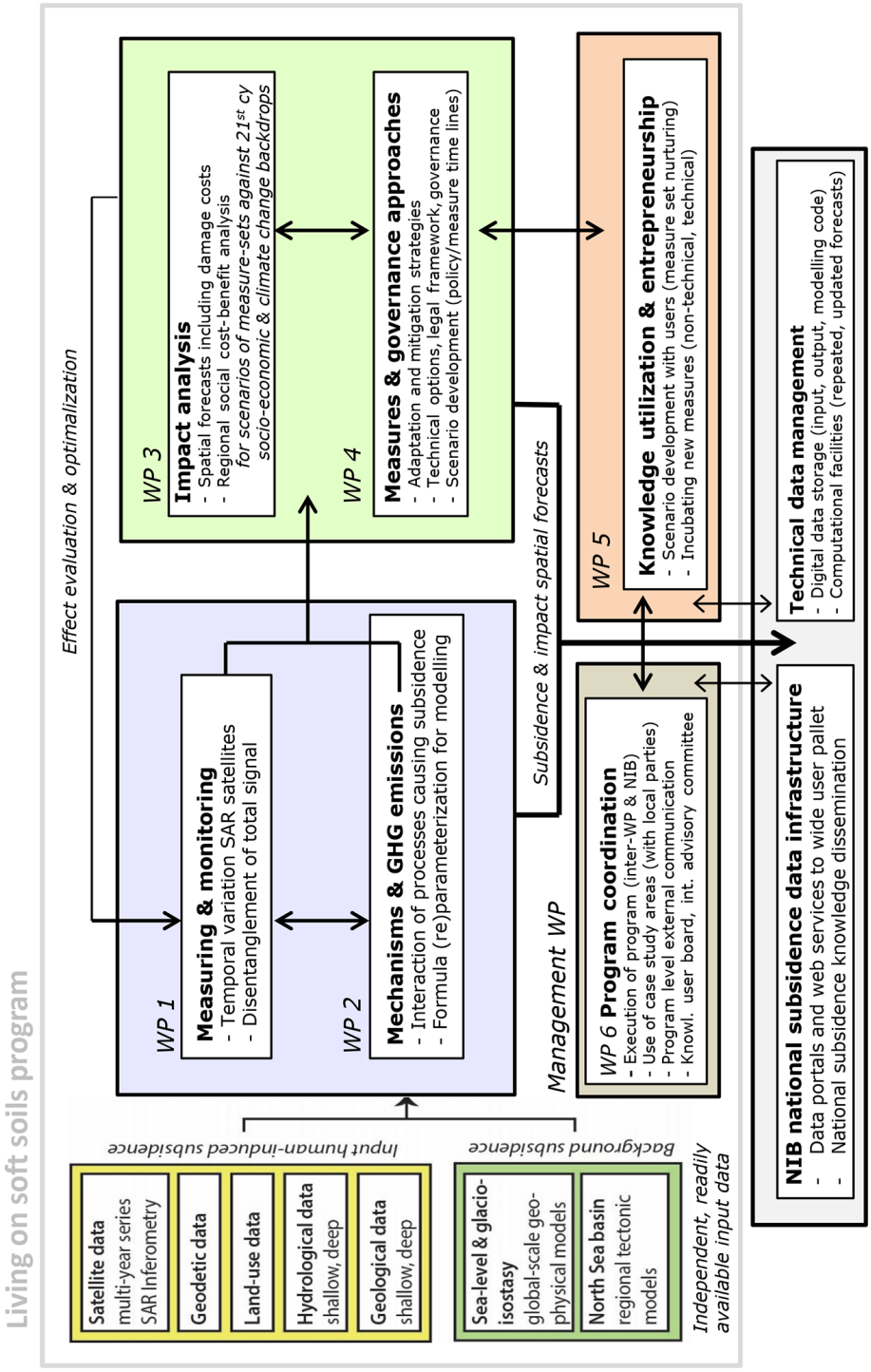

Figure 1.3: LOSS research program structure, retrieved from [13].

BIBLIOGRAPHY OF CHAPTER 1

[1] G. Herrera-García, P. Ezquerro, R. Tomás, *et al.*, "Mapping the global threat of land subsidence," *Science*, vol. 371, no. 6524, pp. 34–36, 2021.

[2] T. Bucx, C. Van Ruiten, G. Erkens, and G. De Lange, "An integrated assessment framework for land subsidence in delta cities," *Proceedings of the International Association of Hydrological Sciences*, vol. 372, no. 372, pp. 485–491, 2015.

[3] R. Brolsma, J. Buma, H. van Meerten, M. Dionisio, and J. Elbers, "Effect van droogte op stedelijk gebied, kennisinventarisatie," 2012.

[4] A. L. Costa, S. Kok, and M. Korff, "Systematic assessment of damage to buildings due to groundwater lowering-induced subsidence: Methodology for large scale application in the netherlands," *Proceedings of the International Association of Hydrological Sciences*, vol. 382, pp. 577–582, 2020.

[5] G. Nicodemo, D. Peduto, and S. Ferlisi, "Building damage assessment and settlement monitoring in subsidence-affected urban areas: Case study in the netherlands," *Proceedings of the International Association of Hydrological Sciences*, vol. 382, pp. 651–656, 2020.

[6] D. Peduto, S. Ferlisi, G. Nicodemo, D. Reale, G. Pisciotta, and G. Gullà, "Empirical fragility and vulnerability curves for buildings exposed to slow-moving landslides at medium and large scales," *Landslides*, vol. 14, pp. 1993–2007, 2017.

[7] D. Peduto, G. Nicodemo, J. Maccabiani, and S. Ferlisi, "Multi-scale analysis of settlement-induced building damage using damage surveys and dinsar data: A case study in the netherlands," *Engineering geology*, vol. 218, pp. 117–133, 2017.

[8] D. Peduto, G. Nicodemo, J. Maccabiani, S. Ferlisi, R. D'Angelo, and A. Marchese, "Investigating the behaviour of buildings with different foundation types on soft soils: Two case studies in the netherlands," *Procedia Engineering*, vol. 158, pp. 529–534, 2016.

[9] D. Peduto, M. Korff, G. Nicodemo, A. Marchese, and S. Ferlisi, "Empirical fragility curves for settlement-affected buildings: Analysis of different intensity parameters for seven hundred masonry buildings in the netherlands," *Soils and Foundations*, vol. 59, no. 2, pp. 380–397, 2019.

[10] A. Saeidi, O. Deck, and T. Verdel, "Development of building vulnerability functions in subsidence regions from empirical methods," *Engineering Structures*, vol. 31, no. 10, pp. 2275–2286, 2009.

[11] S. van Asselen, G. Erkens, E. Stouthamer, H. A. Woolderink, R. E. Geeraert, and M. M. Hefting, "The relative contribution of peat compaction and oxidation to subsidence in built-up areas in the rhine-meuse delta, the netherlands," *Science of the Total Environment*, vol. 636, pp. 177–191, 2018.

[12] D. Peduto, A. Prosperi, G. Nicodemo, and M. Korff, "District-scale numerical analysis of settlements related to groundwater lowering in variable soil conditions," *Canadian Geotechnical Journal*, vol. 59, no. 6, pp. 978–993, 2022.

[13] E. Stouthamer, G. Erkens, K. Cohen, *et al.*, "Dutch national scientific research program on land subsidence: Living on soft soils–subsidence and society," *Proceedings of the International Association of Hydrological Sciences*, vol. 382, pp. 815–819, 2020.

[14] K. Koster, A. Frumau, J. Stafleu, *et al.*, "Greenhousepeat: A model linking co 2 emissions from subsiding peatlands to changing groundwater levels," *Proceedings of the International Association of Hydrological Sciences*, vol. 382, pp. 609–614, 2020.

[15] K. Koster, J. Stafleu, and E. Stouthamer, "Differential subsidence in the urbanised coastal-deltaic plain of the netherlands," *Netherlands Journal of Geosciences*, vol. 97, no. 4, pp. 215–227, 2018.

[16] H. Nieuwenhuis and F. Schokking, "Land subsidence in drained peat areas of the province of friesland, the netherlands," *Quarterly Journal of Engineering Geology and Hydrogeology*, vol. 30, no. 1, pp. 37–48, 1997.

[17] E. Papadaki, "Modelling of peat compressed under sand bodies: Experimental and numerical approach," 2013.

[18] G. Nicodemo, "Vulnerability analysis of buildings in areas affected by slow-moving landslides and subsidence phenomena," 2017.

[19] A. Prosperi, G. Nicodemo, M. Korff, and D. Peduto, "Multi-source monitoring data and numerical analyses for the assessment of settlements affecting built-up areas in variable soil conditions," in *11th International Symposium on Field Monitoring in Geomechanics (ISFMG2022)*, International Society for Soil Mechanics and Geotechnical Engineering, 2022.

[20] F. C. Dufour, *Groundwater in the Netherlands: Facts and figures*. 2000.

[21] S. Kok and L. Angelova, "Impact droogte op funderingen. in opdracht van. verbond van verzekeraars.," Report, 2020.

[22] The Council for the Environment and Infrastructure (Rli), "Goed gefundeerd: Advies om te komen tot een nationale aanpak funderingsproblematiek," Tech. Rep., 2024.

[23] G. Erkens, H. Kooi, and R. Melman, "Actualisatie bodemdalingsvoorspellingskaarten," *Deltares, Utrecht, Nederland*, 2021.

[24] Deltares, "Technische toelichting risicokaarten funderingen," Report, Apr. 2021.

[25] M. Hoogvliet, F. Van de Ven, J. Buma, *et al.*, *Schades door watertekorten en-overschotten in stedelijk gebied: quick scan van beschikbaarheid schadegetallen en mogelijkheden om schades te bepalen*. Deltares, 2012.

[26] E. Leusink, *Naar een kosteneffectieve aanpak van klimaatadaptatie in nederland*, 2018.

[27] G. Van den Born, F. Kragt, D. Henkens, *et al.*, "Dalende bodems, stijgende kosten: Mogelijke maatregelen tegen veenbodemdaling in het landelijk en stedelijk gebied: Beleidsstudie," 2016.

[28] W. Willemsen, S. Kok, and O. Kuik, "The effect of land subsidence on real estate values," *Proceedings of the International Association of Hydrological Sciences*, vol. 382, pp. 703–707, 2020.

CHAPTER 2
LITERATURE REVIEW

CHAPTER 2: TABLE OF CONTENTS

2.1 Introduction **20**

2.2 Definitions **21**
2.2.1 "Subsidence" and "settlements" 21
2.2.2 Damage and its expressions 21

2.3 Masonry buildings in the Netherlands **23**
2.3.1 Building typologies 23
2.3.2 Characteristics of the masonry buildings 25
2.3.3 Foundation systems 25

2.4 Causes of settlements **27**
2.4.1 Predisposing factors: soft soil and soil heterogeneity . . . 27
2.4.2 Triggering causes and mechanisms 27

2.5 The response of structures to settlements **30**
2.5.1 Greenfield displacements 30
2.5.2 The settlement shape and its influence 31
2.5.3 Settlement intensity metrics for buildings 31
2.5.4 The soil-structure interaction 33
2.5.5 Damage classification due to ground settlements 36
2.5.6 Criteria for damage to buildings 37
Limiting values of the building's distortions 38
Limiting tensile strain method (LTSM) 40

2.6 Finite element analyses of masonry structures undergoing settlements **43**
2.6.1 Crack modelling for masonry structures 44

2.7 Regional assessment of subsidence-induced damage to buildings 46
Hazard 47
Exposure 47
Vulnerability 48

2.8 Knowledge gaps, challenges and research focus **49**
Subsidence processes and greenfield ground movements 49

Exposed buildings and vulnerability 49
Addressing Knowledge Gaps within this thesis 50

Bibliography of Chapter 2 . . . . . **58**

2.1. INTRODUCTION

This Chapter introduces the underlying concepts relevant to the buildings exposed to subsidence and, in turn, to this dissertation. First, some general definitions employed in the following Chapters are presented and discussed. The features of the Dutch masonry buildings are described. A literature review details the state-of-the-art assessment of damage for buildings exposed to settlements. This Chapter further distinguishes the procedures for the damage assessment carried out for a single structure, from damage assessment at a regional scale. Finally, based on the literature review, the focus of this thesis is presented while discussing the identified knowledge gaps, challenges and sources of uncertainties. An overview of the content of this Chapter is shown in Figure 2.1.

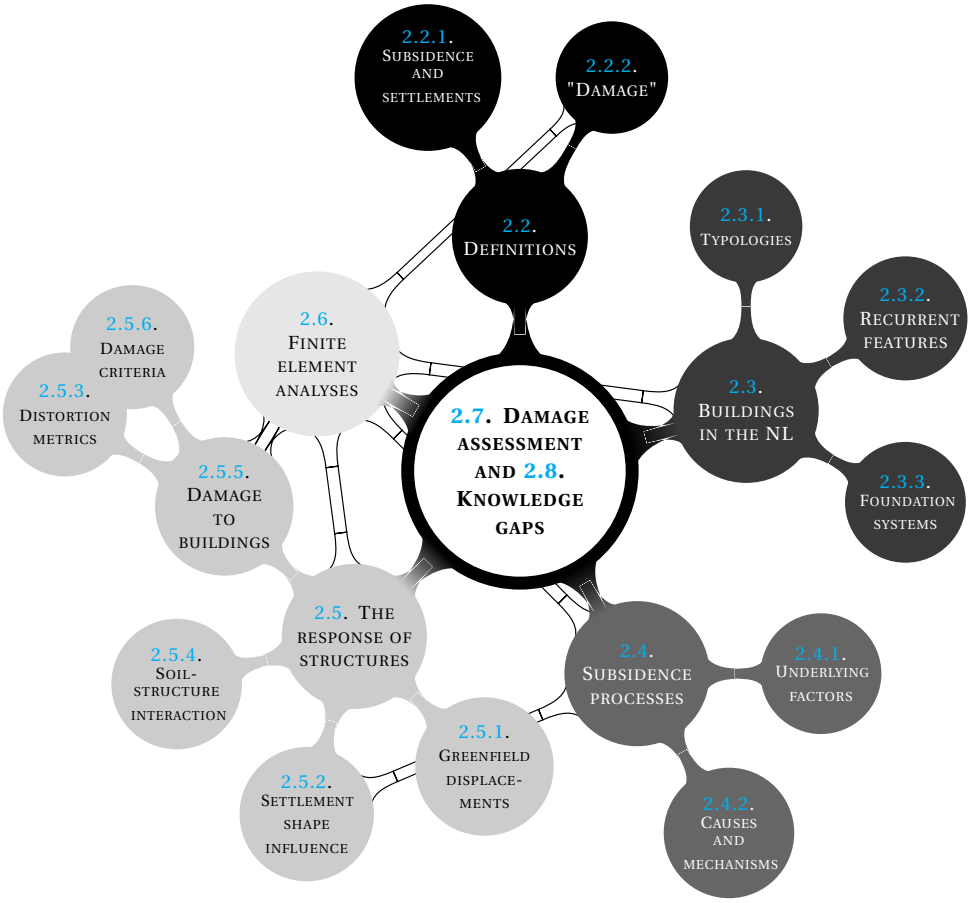

Figure 2.1: Mind map that connects the sections of this Chapter.

2.2. DEFINITIONS

This section reviews and discusses the terminology often adopted in the state-of-the-art and this dissertation.

2.2.1. "SUBSIDENCE" AND "SETTLEMENTS"

In civil engineering jargon, the terms "*subsidence*" and "*settlements*" are both used to identify the downward displacements that are observed at ground level. The word "settlement" is sometimes also used to identify the displacements recorded on the building; When this happens, "ground settlements" or "ground movements" are used to differentiate the displacements of the soil.

"Ground movements", however, is an expression used for both dynamic and quasi-static displacements, such as the dynamic displacements induced by earthquakes or the quasi-static heave and uplift soil displacements. Therefore, the expression "ground movements" is general and can be used to describe the displacements occurring in the soil due to different phenomena.

The definitions and use of the words "*subsidence*" ("*bodemdaling*" in Dutch) and "*settlements*" ("*zettingen*" in Dutch) are not limited by the scale, magnitude, rates or causes of the process; Thus, "*subsidence*" can be used to identify the displacements at the scale of a single structure, and the ground movements of an entire region. However, "*deep subsidence*" and "*shallow subsidence*" are terms used to differentiate between ground-lowering processes occurring deep within soil strata and those occurring near the ground surface, respectively. Therefore, depending on the context "*subsidence*" and "*settlements*" are not always synonymous, and it is important to introduce a distinction between them.

In this dissertation, the words "*subsidence*" and "*settlements*" are distinguished when structures are included in the analyses:

- "*Bodemdaling*" contains the words "*de bodem*", which means "*the soil*" and "*de daling*", "*the decline*". Thus, "*subsidence*" is used to identify the sinking of the ground surface.
- "*De zetting*", which can be translated as "*the settling*". Thus, "*settlements*", identifies the displacements of the building.

2.2.2. DAMAGE AND ITS EXPRESSIONS

Damage can be defined as any harm that alters the original or intended state of a structure [1]. Damage occurs when there is a perceptible manifestation of a defect. Moreover, damage can be expressed and evaluated in many forms, such as cracking, deformations, a reduction of water-tightness and thermal insulation, and an alteration of the functionality or accessibility of the building [1], [2]. In other words, the term "damage" lacks a single, clear definition, and it is thus intrinsically subjective [2]. Damage assessment procedures usually refer only to one prominent expression of damage, depending on the considered action that affects the structure. For instance, cracking, *i.e.*, the occurrence of cracks on or through walls and other elements [1], is often considered as an expression of damage induced by many actions, such as subsidence, vibrations and overloading [2]–[6].

During the life span of a structure designed for housing, some minor damage, such as small cracks in the plaster or non-structural elements, is likely to occur as the consequence of wear and tear, expansion or shrinkage due to daily or seasonal temperature changes, chemical actions and repetitive traffic-induced vibrations [1], [2], [7]. The design of structures typically accepts that some degree of damage will occur and can be repaired during ordinary maintenance works, to keep the project economically and technically affordable [8]. Nevertheless, the occurrence of minor damage can be the initial symptom caused by an external action. For instance, small cracks can be an expression of the ageing of the building or the results of other sources, such as ground settlements.

For this reason, the diagnosis of the driver(s) that cause the damage to the structure represents a complex task and typically requires detailed observations and evaluation. As an example, cracks that occur with a uniform width along their length are usually the results of thermal or chemical actions and are unlikely to progress significantly in time; In contrast, other phenomena, such as ground settlements, result in a time-dependent crack growth [7].

Furthermore, cracks can also seal due to autogenous self-healing [9], or close due to seasonal effects, *e.g.* seasonal thermal variations or change of soil moisture, resulting in periodic shrinkage and swelling cycles.

As a result, cracks can be distinguished in:

- active cracks: These progress over time;
- passive cracks: These stabilized over time;
- breathing cracks: These open and close over time;

To summarize, the following key concepts can be highlighted:

- The definition of damage is subjective;
- Damage assessment procedures are typically limited to one indicator of damage;
- Minor damage inevitably occurs as a result of wear and tear;
- In some cases, minor damage can be the initial symptom of more severe phenomena;
- Damage is time-dependent: it can get more severe or be recovered to a certain extent.

2.3. MASONRY BUILDINGS IN THE NETHERLANDS

Masonry is ubiquitous in the Netherlands, and it is the predominant construction material for old bridges, quay walls, windmills, water towers, and housing [2], [10]–[12]. For older structures, unreinforced masonry is typically used, lacking bracing from reinforcing materials like steel rebars found in concrete. For instance, a survey carried out in the Groningen region revealed that about 80% of existing buildings are built with unreinforced masonry [13].
This section briefly introduces the main features of the Dutch masonry buildings.

2.3.1. BUILDING TYPOLOGIES

Figure 2.2: Examples of masonry buildings located in Delft, the Netherlands. Photographs taken by the Author.

The Dutch masonry structures indented for housing can be classified into macro-typologies, based on the number of storeys and adjacency with other buildings:

- **Detached houses** in Fig. 2.3a (*Vrijstaand* in Dutch), free-standing structures with no attachments to other buildings. Detached houses are more frequent outside cities, in less densely populated areas; This category can also include farmhouses (Boerderijen) which combine residential and agricultural functions in the same structure.

- **Semi-detached houses** in Fig. 2.3b (*Twee-onder-een-kapwoning* in Dutch), are structures that share at least one wall with another building.

- **Terraced houses** (*Rijtjeshuis* in Dutch) in Fig. 2.3c: low-rise (one or two storey)

structures built as part of a continuous row, characterized by more uniform façades and structural layout between the single housing units [14].

- **Canal houses** (*Grachtenpanden* in Dutch) in Fig. 2.3d, are structures individually built against each other; In Amsterdam, the old canal houses are the most famous example of this building typology. The alternation of narrow façades with three up to six storeys characterizes the landscape of historical city centres in the Netherlands.

- **Apartments** in Fig. 2.3e, are structures of multi-unit residential buildings, varying in height, found in many urban areas. Only the exterior walls are typically made of masonry. However, for buildings up to 3-4 storeys it is also possible to have load-bearing walls made of calcium silicate masonry.

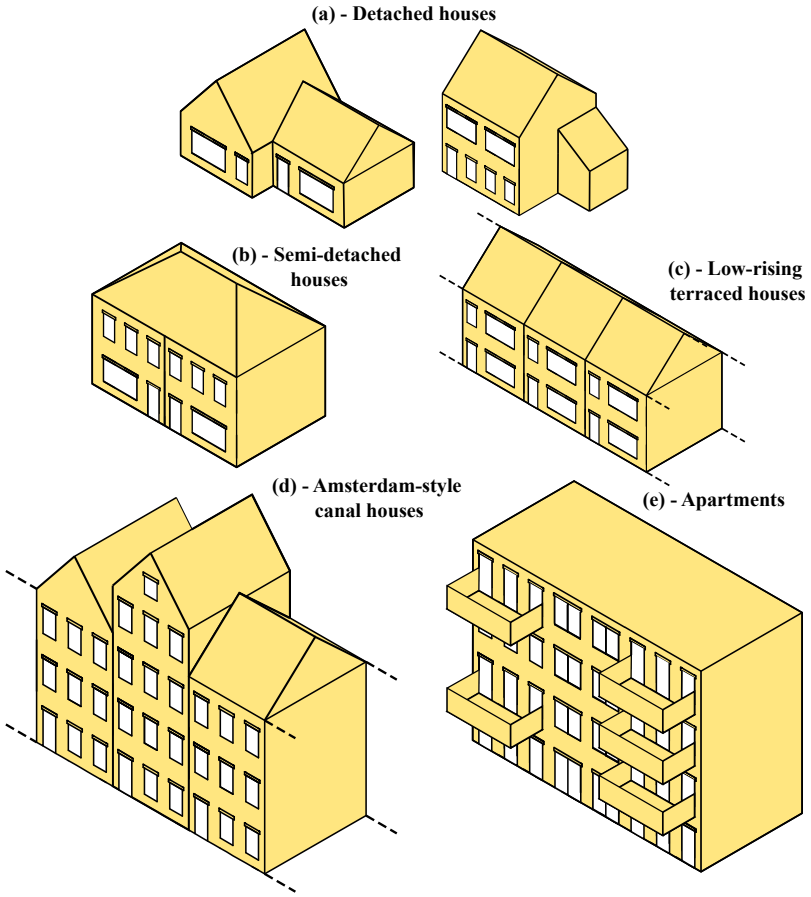

Figure 2.3: Schematic illustration of the housing typologies in the Netherlands.

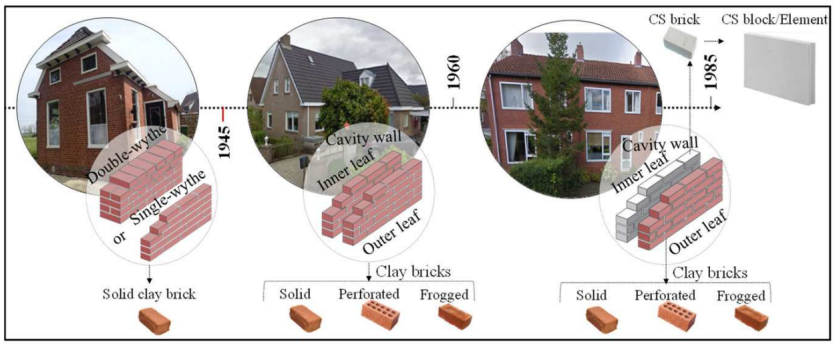

Figure 2.4: The relationship between the age of masonry buildings and the types of walls and masonry used in the Netherlands. Retrieved from [15].

2.3.2. CHARACTERISTICS OF THE MASONRY BUILDINGS

Masonry buildings in the Netherlands are often irregular in plan and characterized by slender façades with large openings, connected at the edges with long transversal walls [16], [17]. Examples of such buildings and façades are shown in Figure 2.2.

Structures built before WW2 often present double wythe walls (*steensmuren*) with timber diaphragms used for the floors and roof. After 1945, cavity walls (*spouwmuren*) and concrete floors started being adopted [15].
Before 1960, both the inner and outer leaves of the cavity walls were made mainly of single-wythe clay bricks, whereas afterwards calcium silicate bricks and calcium-silicate blocks or larger elements made of clay bricks as structural parts are used for the load-bearing inner leaf [14], [15]. An overview is provided in Figure 2.4.

The veneer of cavity walls is typically non-loadbearing.

Various materials have been historically used for lintels above doors and windows. Older buildings often feature timber lintels or masonry lintels with vertically laid bricks, while newer structures typically utilize concrete and steel lintels.

Depending on the age of the building and the type of walls, different floor systems can be observed. Older buildings with double-wythe walls often feature timber floors, while newer buildings with cavity walls typically have reinforced concrete floors.

2.3.3. FOUNDATION SYSTEMS

Masonry buildings in the Netherlands rest either on shallow foundations or piles, depending on the characteristics of the soil and the load of the structure. The illustration in Figure 2.5 shows some examples of shallow and piled foundations.

Strip foundations (Fig. 2.5a, b, and d) represent the prime example of shallow foundations, adopted until 1925, with some examples dating back to the 1970s [10]. Old strip foundations were made of unreinforced masonry: the wythe of the wall increases progressively (up to 1 - 1.5 meters) with the depth, which can reach 2 meters below the ground surface (Fig. 2.5a). Another typology of strip foundations is characterized by the use of unreinforced concrete for foundation beams (*Stampbeton* in Dutch, Fig. 2.5b), as

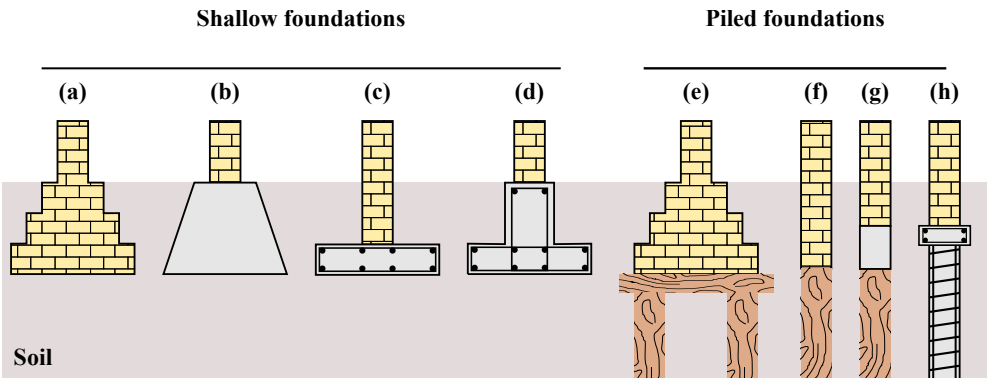

Figure 2.5: Schematic illustration of some examples of shallow and piled foundations common in the Netherlands.

an alternative to unreinforced masonry ones. Reinforced concrete (RC) foundations are more common in practice, especially for more recent structures: the masonry walls can rest on reinforced concrete plates (*Strokenfundering* in Dutch, Fig. 2.5c). More recent applications include RC strips with T-shaped RC sections under the masonry walls (Fig. 2.5c), which are still being adopted for new structures. In some extreme and rare cases, thin unreinforced concrete rafts were placed under masonry strips. In other cases, the superficial soil was removed and a layer of sand was used to replace the previous soil before the construction of the foundation.

As for piled foundations, timber (Fig. 2.5e to g) and later concrete (Fig. 2.5h piles) deeply driven into stable soil, have been widely used [18]. Although structures on piles are not directly exposed to shallow subsidence, timber piles can be exposed to fungi or bacteria which lead to degradation or additional negative skin friction due to the lowering of the surrounding soil [19]–[21]. As the use of concrete has become common practice in the last decades, recent structures use concrete piles as an alternative to timber ones, providing in fact a solution to degradation processes. Nevertheless, structures on piles can still be exposed to the effects of deep subsidence (refer to section 2.4.2 for the distinction between shallow and deep subsidence).

2.4. CAUSES OF SETTLEMENTS

During and just after their construction, structures typically experience settlements due to their own weight. This process can continue throughout the first few decades of their lifespan and is not necessarily a symptom of defects [22]. However, a wide variety of predisposing factors and drivers can enhance the settlements or trigger additional ground movements leading to damage.

2.4.1. PREDISPOSING FACTORS: SOFT SOIL AND SOIL HETEROGENEITY

The susceptibility of a specific location to the settlement occurrence depends on the characteristics of the subsurface. In the western part of the Netherlands, the subsurface is characterized by highly compressible soil strata rich in organic matter, namely "*soft soils*". Soft soils, which represent sequences of clayey and peaty layers of the Holocene age and can attain thicknesses up to 20 meters (Figure 2.6), predispose the occurrence of subsidence processes [23], [24]. Due to their depositions and loading history, the soil

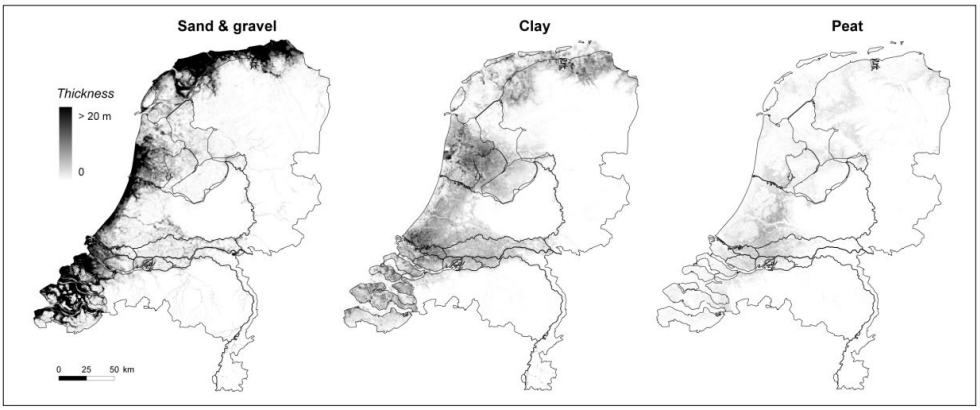

Figure 2.6: The cumulative thickness of Holocene deposits in the Netherlands, retrieved from [24].

strata have hydro- geo- mechanical properties, such as permeability or compressibility, that can vary depending on the location and depth. The variability of the soil properties within a layer is referred to as "**inherent spatial soil variability**" [25]–[27].
Moreover, a soil layer can be characterized by a thickness that varies from point to point, or presents an inclination. In some cases, a lens of weak soil can lie between a more uniform and stronger soil. The variability of the soil strata in terms of typology, unit thickness and inclination is referred to as "**lithological heterogeneity**" [25]–[27].
The combination of the "**lithological heterogeneity**" and the "**inherent spatial soil variability**" characterizes the "**soil heterogeneity**", which predisposes and can enhance the consequences of subsidence processes.

2.4.2. TRIGGERING CAUSES AND MECHANISMS

The subsurface in the Netherlands presents natural and anthropogenic subsidence drivers which can be divided into deep and shallow sources [29], as shown in Figure 2.7; Deep

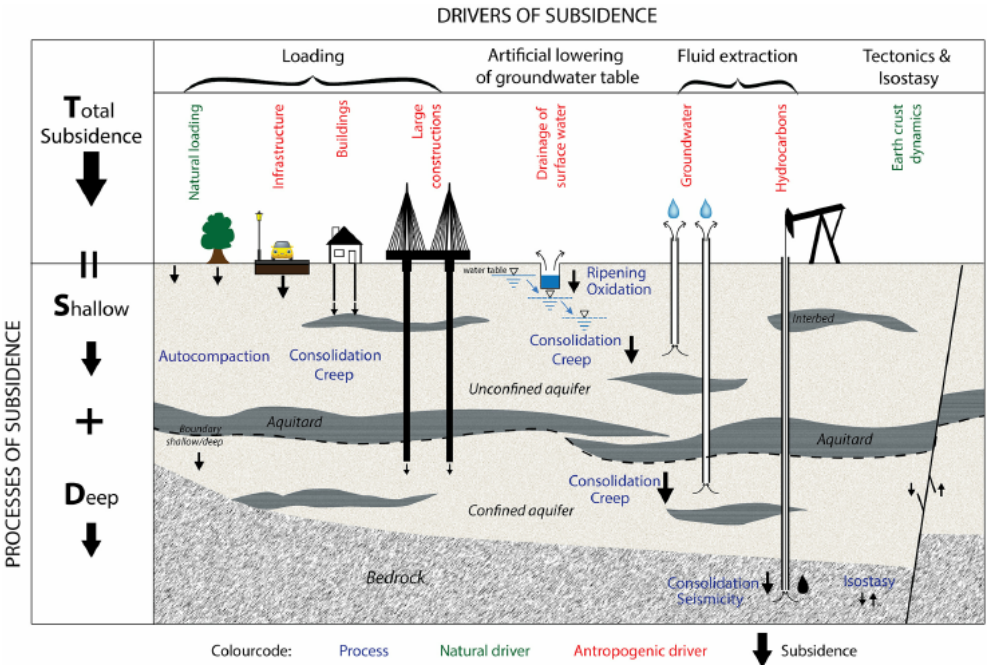

Figure 2.7: Schematic illustration of the different possible subsidence drivers and mechanisms, retrieved from [28]. Natural and human-induced drivers are distinguished, as well as the depth at which they occur.

subsidence sources represent processes that occur in soil layers deeper than about 50 meters from the ground surfaces.
The natural drivers of subsidence include:

- Groundwater absorption by tree roots inducing shrinkage in clayey soils;
- Changes in the soil moisture, triggering shrinkage and swelling in clay;
- Water table fluctuations due to seasonal or climate-induced effects, *e.g.*, rain and droughts;
- Tectonic processes and postglacial isostasy.

Whereas, anthropogenic drivers include the following:

- Underground leaking pipes, broken sewers and malfunctioning drainage systems;
- Water table management policies (*e.g.*, due to deindustrialization, drainage in rural and urban areas);
- Urban development causing additional loads on the ground surface;
- Mining, vibrations and extraction of resources from the deep subsurface;
- Tunnelling and excavations.

The above-mentioned subsidence drivers impact both rural and urban areas.
In the above-mentioned cases, the following mechanisms are triggered and contribute to the observed ground movements:

- **Consolidation** referred to as the change of the soil volume triggered by an additional load. When a load is applied to a saturated compressible soil, it is initially transferred to pore water; This happens because the water is relatively incompressible compared to the soil skeleton. If the water drains from the soil pores, the increase of pressure that results in the water, typically referred to as "*excess pore pressure*", gradually decreases and the load increment is shifted to the soil structure [30]. Two stages are typically distinguished during the consolidation process:

  1. *Primary consolidation* refers to the change of the volume in time due to the drainage of the pore water from the soil structures due to load changes.
  2. *Secondary consolidation* occurs even under constant stresses due to creep phenomena. The soil volume changes are largely controlled by the soil skeleton, which itself, yields, compresses, and creeps after the excess pore pressure completely dissipates [31].

- **Shrinkage** and **swelling**, represent the soil volume changes depending on the soil moisture content. Shrinkage produces downward movements, whereas swelling is responsible for soil uplift. These processes are particularly relevant for clay soils and can be enhanced by rain or droughts.

- **Organic soil oxidation**, refers to the degradation of the organic matter which triggers a change in the soil volume. This mechanism is particularly relevant for peat soil such as in the Western and Northern areas of the Netherlands.

In some specific cases, settlements could also result from defects in the design or construction of the foundations or the buildings.

The combination of the effects of the different drivers results in ground movements that are observable at a regional scale, with localized effects as differential settlements may arise at the scale of individual structures or infrastructure.

2.5. THE RESPONSE OF STRUCTURES TO SETTLEMENTS

2.5.1. GREENFIELD DISPLACEMENTS

When engineers assess the impact of ground movements on structures, they typically begin by estimating "*greenfield displacements*". The "*greenfield displacements*" indicate the vertical downward displacements that would occur on the ground surface if there were no buildings or structures present. This allows for verifying the magnitude of settlements and distortions before taking into account the influence of structures on the ground surface.

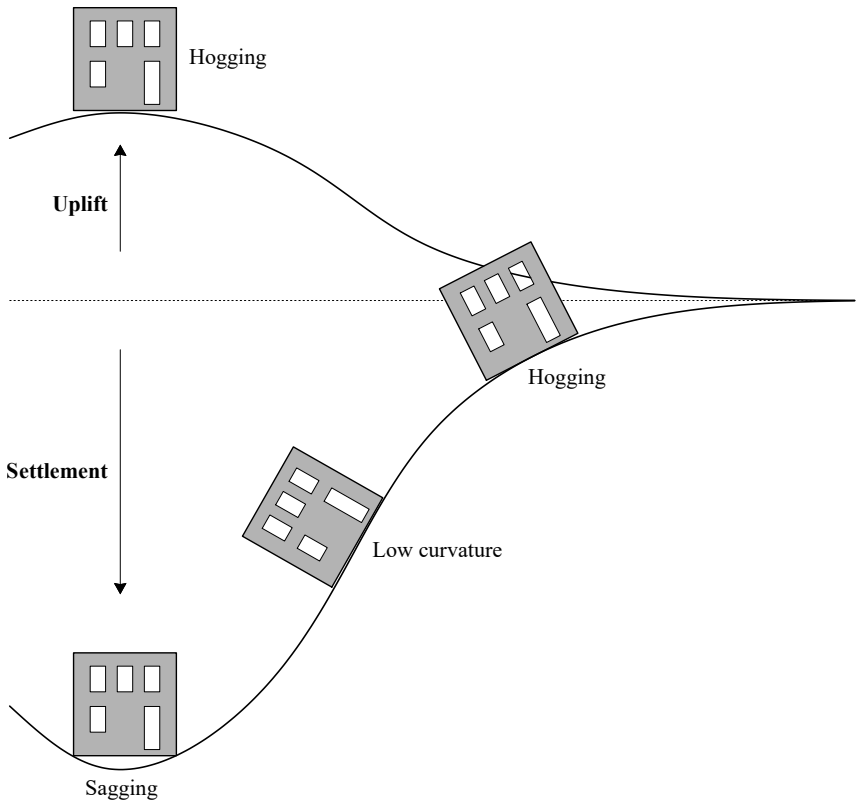

Figure 2.8: Illustration of the possible sagging and hogging settlement patterns, with reference to the ground movements. The response of the building and how the displacements are transferred from the soil to the structures is influenced by the soil-structure interaction, see section 2.5.4.

It is possible to estimate the magnitude and spatial distribution of ground displacements for certain sources of settlements, such as tunnelling. For tunnelling projects, analytical formulations are commonly employed to predict ground movements, under the assumption that these movements follow a Gaussian probability distribution [32] (an example of ground movements that resemble a Gaussian curve is shown in Figure 2.8).

The analytical relationships establish correlations between the greenfield displacements at a given location on the ground surface and factors such as tunnel depth, diameter, and distance. These methods provide quick estimates based on simplified assumptions, and their accuracy is supported by empirical observations.

Nevertheless, the soil surface can sink due to different drivers and their unpredictable combinations, as discussed in 2.4. Therefore, it is currently unknown whether the depression that forms on the ground surface above an area experiencing subsidence, known as the "subsidence bowl," resulting from drivers other than tunnelling, could be predicted using a Gaussian surface.

2.5.2. THE SETTLEMENT SHAPE AND ITS INFLUENCE

Ground movements may cause structures to “settle”: translate, rotate, and/or deform. The settlement patterns are often categorized in two typologies (or a combination of those), depending on their shape (as shown in Figure 2.8):

- **Sagging**, if the curve that describes the settlement pattern has a downward curvature.
- **Hogging**, if the settlement pattern has an upward curvature.

It is a popular premise, confirmed by empirical evidence, that buildings are usually more susceptible to hogging settlement patterns rather than sagging ones [6], [7], [33], [34]. The response of structures varies depending on the spatial distribution of the ground movements:

- If the ground movements occur uniformly, the affected structure is expected to displace uniformly without showing any damage, However, problems could arise with connections to services to the accessibility to the building [35].
- If the ground movements are uneven, the uneven settlements may be transferred to the buildings which then will be distorted so that cracking may occur. If the building is rigid enough relative to the soil, the building may only exhibit rigid body rotation, often referred to as "*tilt*". In some extreme cases, even a rigid body rotation without cracking can impair structural stability.

2.5.3. SETTLEMENT INTENSITY METRICS FOR BUILDINGS

The displacements of the buildings can be used to compute metrics that quantify the distortions that the structure is experiencing; In the case of masonry buildings, measuring the displacements of the building can be achieved with bed-joint measurements along façades. With the bed-joint levelling measurements the deformations of a masonry building over its life can be traced back to measuring the loss of horizontality of points along the brickwork courses, as these were usually laid strictly levelled, thus allowing reproducing the resulting deformation profile of the building over its length due to the ground settlements. A popular alternative is represented by the use of air- or space-borne methods to measure and monitor the displacements of structures [36].

If the measurements or predictions of the building deformation are available, then deformation metrics can be used to assess the intensity of the displacements and distortions. In this dissertation, the deformation parameters defined by [34] and shown in Figure 2.9 are used:

- the settlement ρ is the vertical displacement of a point;
- the **differential settlement** $\Delta\rho$ is the difference between the settlements of two points;
- the **relative deflection** Δ is the maximum displacement of the settlement profile between two points and a straight line connecting them;
- the **deflection ratio** Δ/L is the ratio of the relative deflection between two points to the length between them;
- the **rotation** θ is the gradient of a straight line connecting two points;
- the **tilt** ω is the body rotation of the part of the structure defined by two points;
- the **angular distortion** β (or **relative rotation**) is the rotation of the straight line connecting two points relative to the tilt of the building.

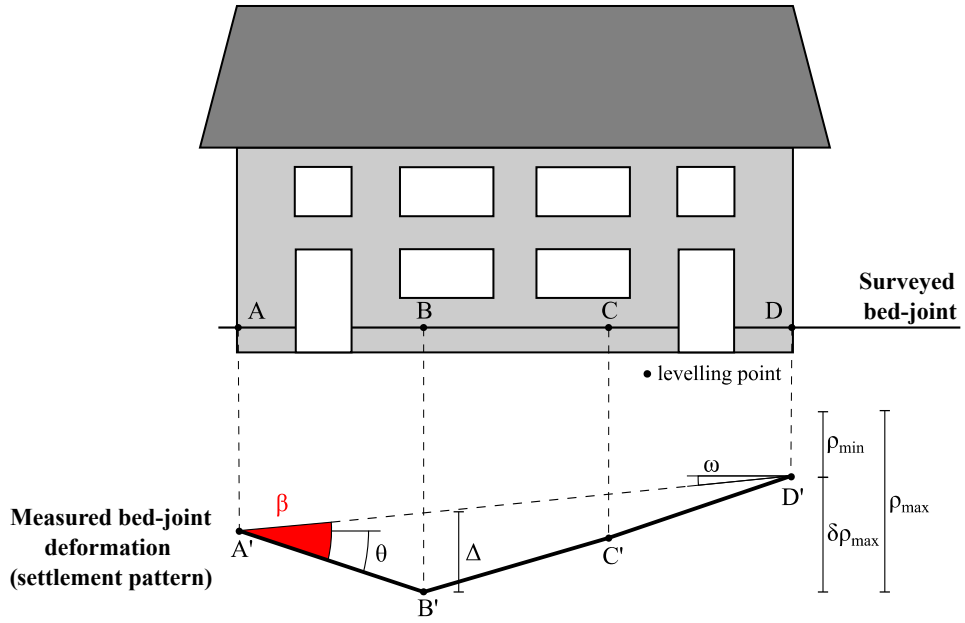

Figure 2.9: Illustration of the settlement parameters, according to the definition proposed by [34]. Measurements collected with manual surveys are typically collected only for a limited number of levelling points, providing a limited picture. Straight segments are typically used to connect the measurements.

The settlement parameters illustrated in Figure 2.9 are often computed in one plane, typically for the façade of a building, and refer to the vertical displacements. In other words, they are often used for single walls, whereas more complex metrics that consider the effects of the three-dimensional spatial distribution of the settlement, such as torsion, are not widely adopted [34]. In the case of horizontal ground displacements, their intensity is measured by additionally referring to the **horizontal strain** (or **lateral distortion**), which is defined as the average strain between two reference points due to the relative horizontal movement [37].
In the following sections, the settlement parameters and the horizontal strains are discussed in relation to the response of the structure.

2.5.4. THE SOIL-STRUCTURE INTERACTION

Different drivers can trigger displacements on the ground surface that affect the existing structures. However, the presence of the building also influences the ground movements and the transmission of the displacements and strains to the superstructure: this process is typically referred to as "**soil-structure interaction**".

The soil-structure interaction plays a fundamental role for structures exposed either to dynamic load, such as earthquake and vibration or quasi-static loads, such as settlements; The latter is the focus of this section and, more generally, this thesis.

The evaluation of the effect of the soil-structure interaction represents a key problem for studies of settlement effects on buildings. From previous studies related to tunnelling, mining and excavation, the principles of the judgement of the effects of the soil-structure interaction are available and can be thus applied to other subsidence sources [33]. It is known that the soil-structure interaction is influenced mainly by three aspects [7]:

- The stiffness of the building relative to the one of the subsurface on which it rests;
- The weight of the building;
- The contact interaction between the foundation and the soil.

The above-mentioned factors, related to the presence of the building, play a role in the development of the ground deformation: the green-field settlement profile, *i.e.*, the ground displacements that would occur if the building would not be present, is modified due to the presence of the structure. In particular, field measurements and models confirm that the weight and stiffness of the structure flatten down the curvature that is observed in the greenfield settlement profile [38]; The stiffer the building relative to the soil, the larger the difference between the soil displacements and the ones of the structures [7].

The effect of the building stiffness relative to the one of the soil has been quantified in the literature: with reference to the assessment of tunnelling to buildings, Potts and Addenbrooke, 1977 [39] introduced two parameters to account for the bending and axial stiffness (ρ^* in equation 2.1 and α^* in 2.2 respectively) of both the structure and the soil:

$$\rho* = \frac{EI^*}{E_s H^4} \tag{2.1}$$

$$\alpha* = \frac{EA^*}{E_s H} \tag{2.2}$$

Where:

- The building is considered to be represented as an isotropic elastic equivalent beam;
- "H" is half the length of the beam;
- "E" and "E_s" represent Young's moduli of the building and the soil respectively;
- "I" is the second moment of area of the beam and "A" is the area of the beam section;
- the parameters ρ^* and α^* for plain strain conditions; EI* and EA* have dimensions of kNm^2/m and kN/m respectively, thus α^* is dimensionless while ρ^* has dimensions of m^{-1};

With reference to excavation effects on buildings, Goh, 2010 [40], [41] modified the bending stiffness parameter ρ^* as (Eq. 2.3) :

$$\rho* = \frac{EI^*}{E_s L^3} \tag{2.3}$$

Where "L" represents the length of the building in either hogging or sagging based on the greenfield settlement trough. This results in dimensionless values of ρ^* for plain-strain finite elements analyses, in which "EI*" is computed with dimensions of kNm^2/m.

With reference to existing buildings, the bending stiffness "EI*" can be computed over a width of 1 meter; This, however, is suitable for floors, roofs and slabs, but unfeasible for walls, which can have cross-sections smaller than 1 meter. Korff, 2013 [7] reports the calculation of the relative bending stiffness for the existing White House building, located in Rotterdam (Table 2.1). Accordingly, the inertia of the walls is computed with reference to their cross-section of base b_{wall} and height H_{wall}, further divided by the distance between the front and back facade $b_{building}$. The approach adopted by [7] is coherent with the formulation of ρ^* (Eq. 2.4) proposed by Mair 2013, [42]:

$$\rho* = \frac{EI}{E_s L^3 W} = \frac{EI^*}{E_s L^3} \tag{2.4}$$

Where:

- "EI" is the bending stiffness of the superstructure computed in kNm^2.
- "EI*" is the EI per running meter and has dimensions of kNm^2/m.
- "L" is the length of the structure in either hogging or sagging and W is the longitudinal length of the building.

For the sake of completeness, it should be noted that another formulation of ρ^* was proposed by [43] specifically for tunnelling problems.

Table 2.1: Calculated (relative) bending stiffness White House. Retrieved from [7].

Description	Calculated value
Number of storeys	11 + basement, floor slabs 0.2m
Width building	20 * $\sqrt{2} = 28m$
Length building	20 * $\sqrt{2} = 28m$
Foundation	Slab cement/masonry 0.3m + piles
E soil	$E_{0.01\%} = 3$ MPa Soft Clay
E slab and floors / wall	10 GPa / 6 GPa
I building m^4/m: • Slab + floors • 2 walls 0.6 m	• 1m * $0.3^3/12$ + 11 * $0.2^3/12$ = 0.01 • 2 * b_{wall} / $b_{building}$ * $H_{wall}^3/12$ = 2 * 0.6/20 * $30^3/12$ = 135
$\rho^*_{Goh} = \frac{EI}{E_s L^3}$ • Slab + floors • 2 walls 0.6 m	• $1.5 * 10^{-3}$ • 1.2 (including reduction for openings)

Additionally, Potts and Attenbrook, 1977 [39] proposed a ratio, namely the modification factor (MD), to account for the difference between the deformation of the soil and the building, defined as (Eq. 2.5):

$$MD = \frac{\frac{\Delta}{L}building}{\frac{\Delta}{L}greenfield} \tag{2.5}$$

Where:

- "MD" is the modification factor;
- $\frac{\Delta}{L}building$ is the deflection ratio computed from the displacements of the structure;
- $\frac{\Delta}{L}greenfield$ is the deflection ratio computed from the greenfield settlement profile.

The values of the relative bending stiffness ρ^* can be plotted against the modification factor to evaluate the effect of the building stiffness in altering the ground deformation; For instance, in Fig. 2.10, modification factors from field data are plotted.
The values of the modification factors shown in Fig. 2.10 clearly highlight how the stiffness of the building relative to the one of the soil influences the reduction of the distortions and deformation transmitted from the soil to the building. In particular, buildings with a high relative bending stiffness ρ^* (right of the plot in Fig. 2.10) present a stiffer behaviour and thus low modification factors, *i.e.*, a high reduction of the ground deformation; Conversely,

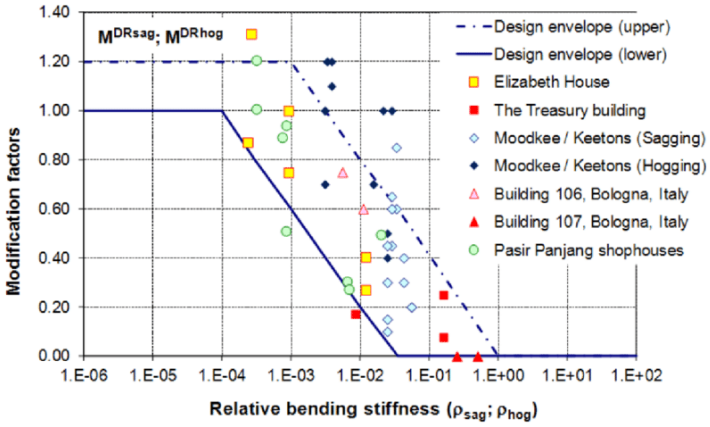

Figure 2.10: Modification factors from field data versus relative bending stiffness according to [40], [42], [44]. Image retrieved from [7]. The field data confirms the design envelopes by [40], based on numerical analyses.

flexible buildings (left of the plot in Fig. 2.10) better follow the ground deformation and present high modification factors.

This observation, confirmed in the literature, highlights how variable the response of different buildings could be, due to the variation of their geometry, material, composition and in turn, stiffness, which, in turn, influences their stiffness relative to the soil on which they rest.

Nevertheless, it is important to remember that the response of the structures is influenced by their non-linear behaviour: The bending stiffness of the building progressively changes with the progression of cracking, and so the interaction between the soil and the structure is influenced. The accumulation of damage to masonry elements is thus associated with a reduction of stiffness [45], [46]. The building may be able to better follow the ground deformation but at the expense of cracking, thus exhibiting progressively a more flexible behavior.

2.5.5. DAMAGE CLASSIFICATION DUE TO GROUND SETTLEMENTS

When a structure is not able to withstand the ground settlements, cracking of structural or non-structural elements alike, tilting and distortions are likely to occur, leading to a loss of cosmetic, functional, durability or structural-functional aspects [2].
When damage to buildings occurs due to ground movements, the form of damage typically considered in the assessments is cracking. masonry, concrete and other quasi-brittle materials are strong in compression, but they are weak and easily crack in tension. The distortions of the settlements lead to tensile stresses and, in turn, cracks. Cracking that occurs as a consequence of ground settlements is recognizable by the following aspects: cracks due to settlements are usually tapered, occur in both structural and non-structural elements and can continue below and above the ground [7]. Another indication that cracks could be caused by settlements is related to their location, which depends on the shape of the ground movement, *i.e.*, hogging, with tension and crack predominantly at

Figure 2.11: Crack patterns due to different settlement shapes modes [47]. Retrieved from [7].

the top of the building, or sagging, with tension and crack predominantly at the bottom of the building, as shown in 2.11.

The damage to buildings significantly varies depending on the structural (*e.g.*, the building's geometry, type of construction material, and foundation system) and subsurface features. In the state-of-the-art, the severity of damage to structures due to ground settlement is assessed by considering the crack pattern and ease of repair, following the system originally proposed by [48] and summarized in Table 2.2.
Although Table 2.2 defines a framework for the evaluation of the damage severity, the classification is quite general and there may be an overlap of the damage categories [37]. For instance, the classification in Table 2.2 indicates that damage depends on the number of cracks, without specifying how many cracks correspond to each damage level. As a result, the assessment of the damage severity can be influenced by subjectivity. Moreover, cracking could occur in parts of the buildings which are not accessible, posing an issue in the detectability of the damage. It should be mentioned, however, that these limitations are common to damage assessments for causes other than settlements.

2.5.6. CRITERIA FOR DAMAGE TO BUILDINGS

This section gives a brief review of the damage criteria for buildings exposed to settlements.

Table 2.2: Damage scale with classification of visible damage based on ease of repair and the crack width [48]. The category of damage was later introduced by [37] and refined by [5].

Category of damage	Damage class	Approximate crack width	Ease of repair
Aesthetic damage	Negligible	up to 0.1 mm	Hairline cracks of less than about 0.1 mm width.
	Very slight	up to 1 mm	Fine cracks which can easily be treated during normal decoration. Perhaps isolated slight fracturing in building. Cracks in external brickwork visible on close inspection.
	Slight	up to 5 mm	Cracks easily filled. Re-decoration probably required. Some re-pointing may be required. Several slight fractures showing inside of building. Cracks are visible externally and some repainting may be required externally to ensure water tightness. Doors and windows may stick slightly.
Functional damage, affecting serviceability	Moderate	5 to 15 mm or a number of cracks > 3 mm	The cracks require some opening up and can be patched by a mason. Re-current cracks can be masked by suitable linings. Repointing of external brickwork and possibly a small amount of brickwork to be replaced. Doors and windows sticking. Service pipes may fracture. Weather-tightness often impaired.
	Severe	15 to 25 mm, but also depends on number of cracks	Extensive repair work involving breaking out and replacing sections of walls, especially over doors and windows. Windows and door frames distorted, floors sloping noticeably. Walls leaning or bulging noticeably, some loss of bearing in beams. Service pipes disrupted.
Structural damage, affecting stability	Very Severe	Higher than 25 mm, but depends on number of cracks	This requires a major repair involving partial or complete rebuilding. Beams loose bearing, walls lean badly and require shoring. Windows broken with distortion. Danger of instability.

LIMITING VALUES OF THE BUILDING'S DISTORTIONS

In the state-of-the-art, limit values are proposed for the distortions (*i.e.*, the parameters reported in section 2.5.3) of existing and new buildings to prevent the occurrence of damage [34], [37], [49]–[53].

Among the different settlement parameters, limit values are often proposed for the angular distortion β. For instance, Skempton and MacDonald (1956) [49] recommended a value of β ranging between 1 ‰ and 2 ‰ (or 1/1000 to 1/500 respectively) to avoid the occurrence of any settlement damage. Bjerrum (1963) [53] supported the value of β equal to 2 ‰ (1/500) as a safe limit for buildings where cracking is not permissible. However, Meyerhof (1956) [54] discussed that limit values of the angular distortions β should include a margin of safety, thus, values of β ranging from 1/1000 to 1/500 were proposed. Similarly, Burland and Wroth (1975) [34] discussed how the limit of angular distortion β of 1/500 may be satisfactory for frame buildings, but it may be unsafe for load-bearing walls. Meyerhof (1982) [51] proposed tentative safe limits of β for unreinforced load-bearing walls equal to 0.5 ‰ (or 1/2000) and 1 ‰ (or 1/1000) for hogging and sagging settlements.

Regarding the response to excavation-induced settlements, Boscardin and Cording (1989)

[37] proposed a set of curves that relate damage to a combination of the angular distortion β and the horizontal strains for brick bearing-wall structures (shown in Fig. 2.12), which were validated in further research, for instance in [55]. The plot in Fig. 2.12 distinguishes the condition for which buildings are subjected to both horizontal strains and angular distortions, due to mining, excavation or tunnelling activities, from buildings subjected predominantly to angular distortion, as their settle due to their weight; In general, structures settling due to their weight are predominantly subjected to curvature and hardly horizontal strains [37].

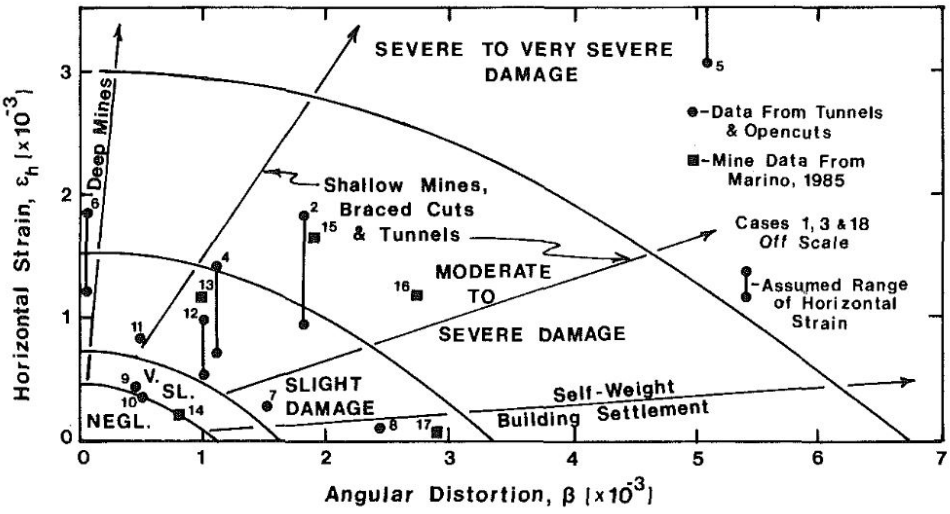

Figure 2.12: Relationship of damage to angular distortion and horizontal extension strain, retrieved from [37].

Regarding the available guidelines, the Eurocode 7 Annex H [56] recommended two ranges of β, which are also adopted in the Dutch standard [57], [58], to prevent the occurrence of a serviceability limit state (the condition under which the structure is still considered functional and serviceable) for the structure:

- β ranging from 1/2000 to 1/300 for sagging settlements;
- β ranging from 1/5000 to 1/600 for hogging settlements.

In terms of cracking, Rankin (1988) [50] linked the occurrence of cracks wider than 5 millimetres with functional and serviceability damage to the structure, *i.e.*, "Moderate" to "Severe" in Table 2.2.

From the above, it becomes clear that limit values of β range significantly in literature and standards. Although the knowledge of the topic developed and increased in the last decades, the discrepancies in the limit values of the angular distortion β are likely to be related to different aspects:

- The construction details, in terms of material, geometry, presence and disposition

of the openings, foundation system, and interlocking between the walls, influence the response of each individual structure;

- The ratio length to height (*i.e.,* L/H) of the structure influences the amount of distortions that the building can withstand;
- If settlements occur over a long period of time, the structural material could undergo creep and relaxation, which implies that the structure could be able to better accommodate the soil deformations [33].
- Many studies do not specify if the angular distortion β is computed from the displacements measured on buildings or on the soil surfaces;

It is evident that limiting the values of some distortion parameters has the advantage of being simple and practical, but it is challenging to confirm the general validity of such limit values [56], [59].

LIMITING TENSILE STRAIN METHOD (LTSM)

The limiting tensile strain method (LTSM) is an empirically-based analytical method to predict the damage induced to buildings exposed to settlements [34], [37], [60]. The following assumptions are involved in the method [60], [61]:

- The building is represented as a weightless, rectangular and isotropic elastic beam in two dimensions; The behaviour of this equivalent beam is governed by four parameters, the length "L", the height "H", the Young's modulus "E" and the shear modulus "G";
- The method assumes the full transfer of the ground movements to the structure, neglecting the effect of the soil-structure interaction.

The procedure of the LTSM involves subsequent steps (Fig. 2.13):

1. The calculation of the greenfield ground movements, neglecting thus the presence of the building.
2. The greenfield displacements are imposed on the simplified linear-elastic beam model representing the building.
3. The strains of the equivalent beam model are computed by means of analytical formulations and related to a possible damage level.

Detailed discussions and reviews of the LTSM are presented in [7], [60], [61]. It is evident that the method is applicable only if the greenfield ground movements can be estimated, by means of measurements, analytical or numerical methods. This may be the case for specific sources of settlements, such as tunnels, mining and excavations; However, limited insight is available for other subsidence drivers, thus the estimates of the ground movements are not always available. This limitation affects the applicability of this method in this thesis.

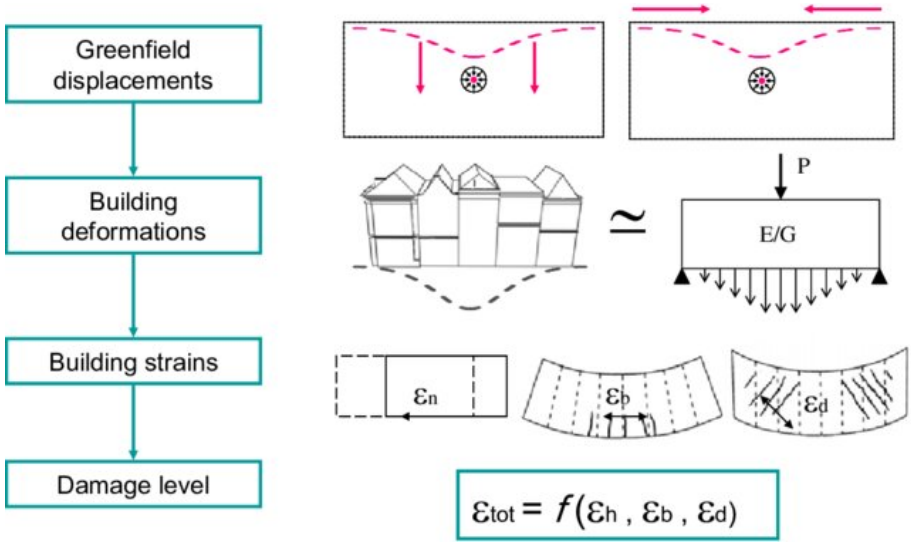

Figure 2.13: Schematization of the LTSM approach after [34], [37]. Retrieved from [61], [62]. This illustration shows the application of the method in the case of tunnelling-induced settlements.

In its original formulation by [34], the deflection ratio Δ/L computed from the equivalent beam is used to compute the maximum bending and diagonal strains, $\epsilon_{b,max}$ and $\epsilon_{d,max}$ respectively in Table 2.3, whereas the horizontal ϵ_h was later added to the method by [37]; These strains are then used to assess the expected damage to the building.

Table 2.3: Bending and shear strains for the equivalent beam model. Retrieved from [7]. The term "t" represents the distance of the neutral axis to the edge of the beam, assumed to be equal to 0.5H in sagging and H in hogging. Δ/L represents the deflection ratio.

	Maximum strain (bending)	Diagonal strain (shear)
Central point load	$\frac{\Delta}{L}=\left[\frac{L}{12t}+\frac{3I}{2tLH}\frac{E}{G}\right]\varepsilon_{b\max}$	$\frac{\Delta}{L}=\left[1+\frac{HL^2}{18I}\frac{G}{E}\right]\varepsilon_{d\max}$
Uniform load	$\frac{\Delta}{L}=\left[\frac{5L}{48H}+\frac{3I}{2tLH}\frac{E}{G}\right]\varepsilon_{b\max}$	$\frac{\Delta}{L}=\left[\frac{1}{2}+\frac{5HL^2}{144I}\frac{G}{E}\right]\varepsilon_{d\max}$

Although the LTSM is in principle a conservative method of assessment, [61] addressed that some of the assumptions do not necessarily lead to conservative results:

- The LTSM is based on linear-elastic assumptions and does not include non-linear progressive cracking of the building's material, which may lead to incorrect predictions of the damage and structural failure patterns.
- Neglecting 3D effects of the problem, such as the torsional behaviour of the structure due to the settlement, could lead to non-conservative estimates for complex non-symmetric settlement patterns [43];
- A reduction of the stiffness of the equivalent beam could account for the presence of

doors and windows. Nevertheless, when cracks occur, they often localize in the corners of openings, and this aspect can be included in the LTSM only approximately [63], [64].

- The full transfer of the ground movements is conservative for the vertical displacements, but for horizontal displacements, it can lead to an underestimation of the damage [33].

2.6. FINITE ELEMENT ANALYSES OF MASONRY STRUCTURES UNDERGOING SETTLEMENTS[1]

Ideally, the assessment and prediction of building damage due to settlements follow steps that progressively increase in complexity to enhance the accuracy of the analyses:

1. Engineers start with empirical criteria (section 2.5.6) and analytical methods (section 2.5.6) to determine whether a structure can withstand the ground settlements and distortions.

2. As analytical and empirical methods are expected to conservatively estimate structural damage, more refined analyses may not be necessary if the structure is predicted to be able to withstand the ground movements without damage. Conversely, if the structure is predicted to suffer damage, further complex analyses are performed to more accurately predict the damage.

Finite element analyses are tools that enable an accurate investigation of the structural response, as an alternative to empirical and analytical methods.

The advent of high-performance computational resources has enabled the simulation of complex structural behaviour and the interaction with the soil to be more detailed and accurate [66]. The models of the structure subjected to settlement improved from equivalent approaches, such as linear-elastic beams with equivalent axial and bending stiffness, to more complex and detailed 2D and 3D models, which include the non-linear cracking behaviour of the materials, and thus are able to investigate the damage progression with increasing settlements [66]–[77]. In some modelling approaches, *i.e.*, coupled analy-

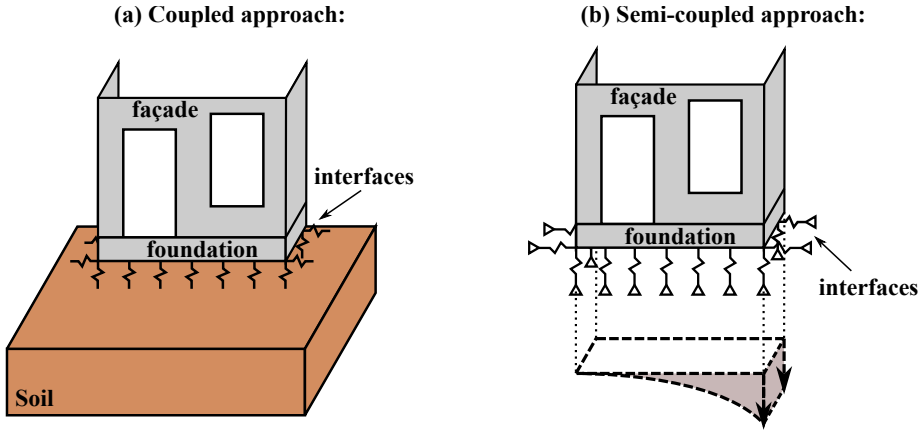

Figure 2.14: Scheme of coupled and semi-coupled modelling techniques for building subjected to settlements.

ses in Fig. 2.14a, the soil and the soil-structure interaction are included in the models. Whereas previous studies included the soil as an elastic mass, later approaches include

[1] Section 2.6 is a revised version of the content published in [65]

its non-linear behaviour to accurately predict the settlements and the interaction with the structure [66], [67], [78], [79].
However, detailed and complex analyses, such as the above-mentioned coupled models, require the generation of complex meshes that, in turn, require high computational efforts [66].

Therefore, an alternative is represented by semi-coupled analyses (Fig. 2.14b), in which the response of the structure is evaluated without the inclusion of the soil volume and the soil-structure interaction are represented by interfaces that captures bedding, gapping and friction. The ground settlements are imposed at the base of the interface that represents the foundation and the soil-structure interaction [66], [70], [80].
In some recent studies, the settlement is applied to an interface accounting for the soil-foundation interaction, while the strip foundation system is included in the model [66], [76], [81]–[83].

2.6.1. CRACK MODELLING FOR MASONRY STRUCTURES

Masonry is a quasi-brittle anisotropic made of brick units and mortar joints. The material exhibits highly non-linear behavior, with poor performance in tension and shear, and is susceptible to crushing and splitting under compression [15]. As a brittle material, masonry often exhibits damage in the form of cracks, mostly at the bond between bricks and mortar, where the material is weakest [84]. Figure 2.15 shows an overview of local failure mechanism of the masonry material.

The inherent properties of masonry render it vulnerable to both in-plane and out-of-plane failure mechanisms. In particular, in-plane failure occurs when a wall is subjected to forces acting within its plane, such as those caused by ground settlements. Conversely, out-of-plane failure arises when loads are applied perpendicular to the wall's plane. The focus of this thesis is on the in-plane failure induced by ground settlements.
In finite element analyses, the non-linear behaviour of the masonry material, with progressive tensile cracking and tensile softening is included in the incremental-iterative analyses. Three main approaches are available for the analysis of the material (Fig. 2.16), denoted as [87]–[89]:

- **detailed micro-modelling**, which consists of a detailed representation of both the brick, the mortar as well as brick/mortar interface. This approach is computationally demanding and only suitable for small structures, for detailed analyses.
- **simplified micro-modelling**, in which mortar joints including the two contact faces with the bricks are represented by a single interface. The thickness of the interface elements is typically set to zero to avoid unbalances in the moment equilibrium.
- **macro-modelling**, in which the masonry material is regarded as an equivalent anisotropic composite. Thus, the bricks, mortar and their interaction are represented in a smeared manner by an equivalent continuum element.

The required modelling and computational burden may vary depending on the scale and type of problem. In this thesis, the focus is on large-scale walls, facades and buildings.

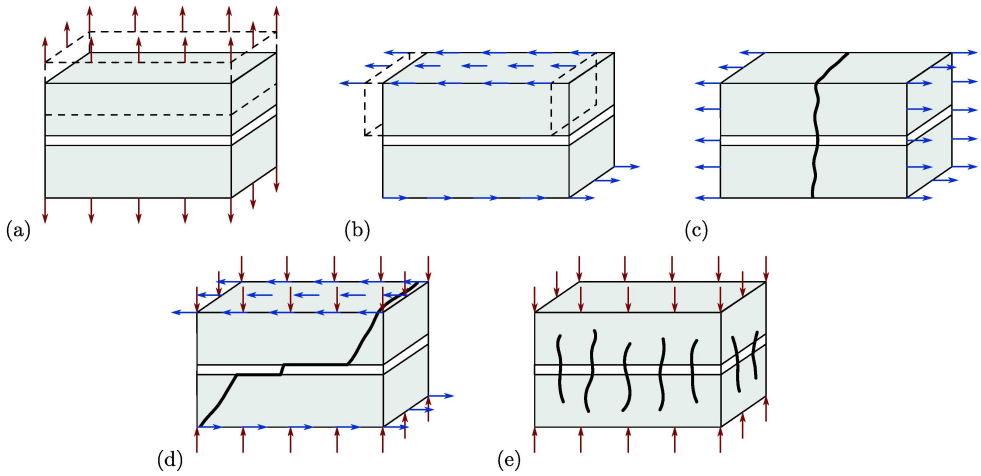

Figure 2.15: Examples of local failure mechanisms of the masonry material: (a) joint tensile failure, (b) joint shear failure, (c) brick and mortar tensile failure, (d) diagonal masonry failure and (e) masonry crushing, splitting and spalling under compression. Image retrieved from [84], and published in [85], originally adapted from [86]

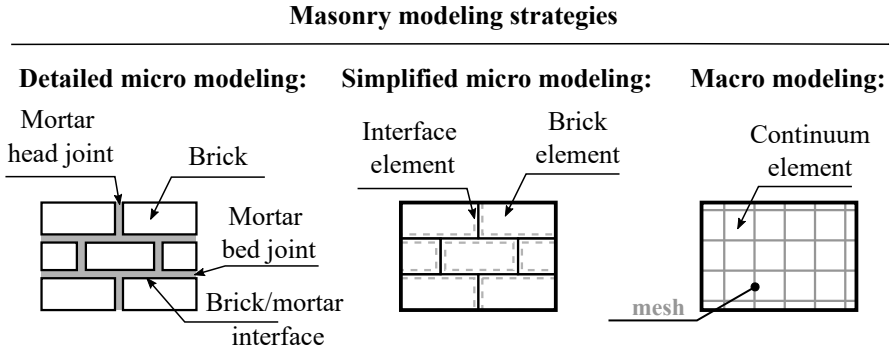

Figure 2.16: Modelling strategies for the masonry material [87]–[89]. While the micro models distinguish the brick and mortar joints, macro models describe the material via anisotropic continuum elements.

Thus, a detailed brick-to-brick model is not deemed feasible. Therefore, the smeared continuum-based macro models are used, as described later in this thesis.

When macro-models are adopted, the damage is smeared out in the continuum element, spreading out over the area that belongs to the integration points. This concept is referred to as "**smeared cracking**" [88]. This approach is also adopted later in this thesis.

2.7. REGIONAL ASSESSMENT OF SUBSIDENCE-INDUCED DAMAGE TO BUILDINGS

In the literature, damage assessment procedures are carried out for structures exposed to various hazards, such as earthquakes, flooding, landslides, tunnelling, mining and excavation activities [90]–[95].

As described in section 2.4, in the Netherlands, land subsidence is a geo-hazard that affects wide areas and induces the necessity to assess its consequences to buildings and infrastructure. Damage assessment for existing buildings in the areas exposed to subsidence is required to be integrated into the risk analysis to address policy making, adaptation and mitigation strategies [96], [97].

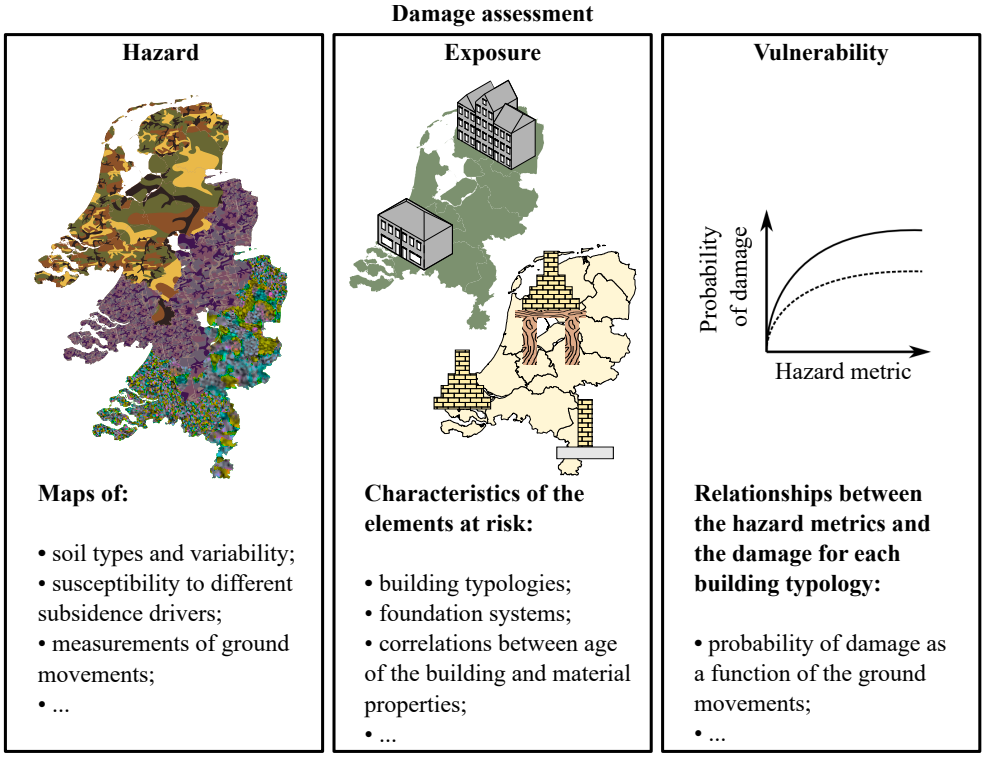

Figure 2.17: Schematic illustration of the components required for damage assessment in the Netherlands. The maps are not based on actual data and are used only for illustration purposes.

In general, a systematic regional or countrywide assessment of damage to the built heritage requires (Fig. 2.17) [97]:

- the **hazard**, triggering the process leading to damage;
- the **exposure**, an inventory of the buildings exposed to the event causing damage;

- the **vulnerability**, defining the correlation between the magnitude and rates of the event with the degree of damage.

The hazard, combined with the vulnerability and the exposure equals the risk. In the following sections, the three above-mentioned components will be detailed.

When the damage assessment procedure is carried out after the occurrence of the disaster *i.e.*, post-disaster, it is possible to refer to the measured hazard intensity, such as peak ground acceleration for earthquakes, or ground motion rates for landslides and settlements. From the insight gained from post-disaster assessments, researchers and professionals can retrieve the relationships between the measured hazard metric and the induced damage to the exposed structures: In other words, it is possible to investigate and evaluate the vulnerability of the structures that were exposed to the hazard; Such insight is helpful for those analyses that aim to predict the damage over wide areas due to the occurrence of a similar hazard. In such cases, a prediction of the (future) hazard intensity is obtained via models or estimates and subsequentially used to predict the damage to buildings.

If the damage assessment focuses on the prediction of the response of the structure, the hazards are quantified by values obtained by models or estimates, which are then employed to predict the damage to structures; Nevertheless, such estimates of the hazard should be available not only for wide areas but also at the scale of each structure; This is a required step to assess the response of each structure.

HAZARD

The quantification of subsidence is certainly not straightforward, and the employed metrics may vary depending on the type of analysis. For instance, subsidence maps that cover entire regions of the Netherlands typically express displacement rates in terms of *mm/year*. However, structures are not only influenced by the overall downward displacements but by the distortions induced by the difference in the displacements of the soil at scale and location of the buildings (as described in section 2.5). This induces a problem, as subsidence maps that include distortion rates at the scale of structures are not currently available.
Measurement-based, analytical or numerical methods can be used to estimate the magnitude and the extent of the ground deformation, and, in turn, the hazard metric on the single-structure scale (for instance, in terms of horizontal ground strains, curvature, vertical settlements), making use of conventional monitoring techniques (as levelling or Global Positioning System) or remote-based observations (images acquired by Spaceborne Synthetic Aperture Radar) as supportive tools and geomechanical models as predictive tools.

EXPOSURE

When structures are subjected to a widespread hazard, it is key to collect information on the exposed structures to identify the most sensitive features/building typologies.
The collection of structural features of the exposed structures can be challenging when the analysis focuses on a single structure, but even more demanding when the study deals with a population of buildings over a larger area. Nevertheless, key indicators (such as the

foundation system, and the construction material, the building typology) for the exposed structures can be identified to deal with the variable conditions of the structures in each area.
The availability of this information represents a limitation for any damage assessment attempt since databases with the identified key features are limited to some municipalities (e.g. foundation system map for Rotterdam city) or non-existent.

VULNERABILITY

The definition of the vulnerability of the exposed structures requires upscaling the available knowledge of the building damage due to settlements from individual structures to building clusters in wide areas.
As discussed in section 2.5, existing methods to assess the damage are often suitable for individual structures.
Nevertheless, probabilistic tools can be developed to assess the relationship between the intensity of the ground settlements, measured with the parameters discussed in section 2.5.3, and the probability of damage to buildings: such probabilistic relationships, namely *fragility curves*, allow to retrieve the relationship between the damage severity level and a hazard intensity parameter for a given structural typology [98].

2.8. KNOWLEDGE GAPS, CHALLENGES AND RESEARCH FOCUS

Drawing upon the literature review conducted in the preceding sections, knowledge gaps and research challenges can be identified. This section outlines how the identified gaps and challenges are addressed in this thesis.

Due to the widespread presence of masonry buildings on shallow foundations in the Netherlands [99], the focus of this thesis lies in the response of such structures exposed to subsidence-related settlements. Therefore, buildings on piled foundations are outside the main scope of the analyses.
In the western and northern parts of the Netherlands, the subsurface is rich in peat and clay strata which predispose the occurrence of ground settlements. Therefore, masonry structures that rest on such soil strata are considered in this thesis.
Furthermore, this thesis focuses on low-rise buildings built before 1970 with clay-baked masonry, as they are expected to be the most susceptible to subsidence and foundation problems.

From the literature review, the following knowledge gaps, sources of uncertainties and challenges have been identified (labelled and enumerated with the prefix "G." to aid in further referencing them throughout this work):

SUBSIDENCE PROCESSES AND GREENFIELD GROUND MOVEMENTS

G.1 Specific processes responsible for subsidence and thus damage to the buildings are better understood than others. As an example, the effect of the variation of the soil strata on the damage response of the building requires further studies.

G.2 For tunnelling, mining and excavation phenomena, methods are available to predict the settlement patterns to which buildings are exposed. In the Netherlands, however, due to the presence of different drivers, it may be hard to accurately predict the settlement pattern that affects each structure over wide areas. Thus, this aspect represents a source of uncertainties for the damage assessment procedures.

EXPOSED BUILDINGS AND VULNERABILITY

G.3 Dutch masonry buildings present unique combinations of construction materials, geometry, openings, and foundation systems, and rest on highly compressible soil strata. These features should be considered when investigating their vulnerability to settlements.

G.4 Limiting values of the building's distortions and deformations are typically proposed in codes and standards. Generalizing the use of these thresholds could be difficult without demonstrating their overall validity;

G.5 The damage assessment should take into account the differences between the soil displacements and the consequential building deformations, due to the soil-structure interaction.

G.6 The assessment of damage due to settlements is typically carried out referring mainly to one expression of damage: cracking. Very often, the maximum recorded crack width is adopted to assess the degree of damage; Such procedures, however, could result in subjective assessments.

G.7 The damage assessed for a single structure describes the state of the building at a specific time. Although monitoring techniques are available for both the building deformations and damage, the assessment is typically performed after the occurrence of (observable) damage. The challenge lies in the empirical and statistical establishment of soil distortions that trigger damage initiation.

G.8 Damage predictions for buildings exposed to subsidence require developing probabilistic relationships which include the wide variability of the buildings' features, the soil conditions and the possible settlement patterns;

ADDRESSING KNOWLEDGE GAPS WITHIN THIS THESIS

This section briefly describes how the identified knowledge gaps and challenges are addressed within this thesis.

Chapter 3 investigates the role of soil heterogeneity (G.1) in the occurrence of settlement at the scale of single structures.

The empirical insight gained from the collected sample of buildings (Chapter 4) provides support information for the numerical analyses and further insight into the uncertainties related to the variability of limit values of the building distortion G.4. Based on measurements of the building deformations, different possible settlement patterns for the buildings are selected to be adopted in the consequential numerical analyses, addressing G.2.

The numerical analyses further include procedures that minimize the subjectiveness of the damage assessment (G.6). Furthermore, the analyses distinguish the soil deformation from the displacements of the building (G.5). Moreover, the variability of the buildings and soil features (G.3 and G.8) is considered in the numerical analyses presented in the following.
The numerical simulations enable observing of the progression of the damage, from its initiation, differently from the empirical insight collected from existing structures (G.7)

The research focus lies in developing probabilistic relationships between soil settlements and damage to structures, providing background information for damage assessment analyses over wide areas.

BIBLIOGRAPHY OF CHAPTER 2

[1] P. Korswagen, M. Longo, E. Meulman, and C. Van Hoogdalem, "Damage sensitivity of groningen masonry structures–experimental and computational studies," *Delft University of Technology. Report*, no. C31B69WP0-12, 2017.

[2] I. de Vent, "Structural damage in masonry," Ph.D. dissertation, Citeseer, 2011.

[3] P. A. Korswagen, M. Longo, E. Meulman, and J. G. Rots, "Crack initiation and propagation in unreinforced masonry specimens subjected to repeated in-plane loading during light damage," *Bulletin of Earthquake Engineering*, vol. 17, pp. 4651–4687, 2019.

[4] G. Giardina, A. Marini, M. A. Hendriks, J. G. Rots, F. Rizzardini, and E. Giuriani, "Experimental analysis of a masonry façade subject to tunnelling-induced settlement," *Engineering Structures*, vol. 45, pp. 421–434, 2012.

[5] G. Giardina, "Modelling of settlement induced building damage," 2013.

[6] I. of Structural Engineers (Great Britain), I. of Civil Engineers (Great Britain), I. A. for Bridge, and S. Engineering, *Soil-structure Interaction: The Real Behaviour of Structures*. Institution of Structural Engineers, 1989.

[7] M. Korff, *Response of piled buildings to the construction of deep excavations*. IOS Press, 2013, vol. 13.

[8] M. Korff, "Deformations and damage to buildings adjacent to deep excavations in soft soils," *Delft Cluster*, 2009.

[9] M. B. Gaggero, P. A. Korswagen, R. Esposito, and J. G. Rots, "Innovative application of self-healing technology to masonry: A proof of concept," in *International Conference on Structural Analysis of Historical Constructions*, Springer, 2023, pp. 332–345.

[10] P. A. Korswagen, M. Longo, A. Prosperi, J. G. Rots, and K. C. Terwel, "Modelling of damage in historical masonry façades subjected to a combination of ground settlement and vibrations," in *International Conference on Structural Analysis of Historical Constructions*, Springer, 2023, pp. 904–917.

[11] S. Sharma, M. Longo, and F. Messali, "A novel tier-based numerical analysis procedure for the structural assessment of masonry quay walls under traffic loads," *Frontiers in Built Environment*, vol. 9, p. 1 194 658, 2023.

[12] Y. Oktiovan, F. Messali, and J. Rots, "Detailed distinct element modeling of a utrecht wharf cellar for the assessment of the load-bearing capacity and failure mechanism," in *Proceedings of the Seventeenth International Conference on Civil, Structural and Environmental Engineering Computing*, Civil-Comp Press, vol. 6, 2023.

[13] H. Crowley, J. Uilenreef, and R. Scheefhals, "Exposure database (edb) v7 - data documentation technical report and exposure model," ARUP, Report, Apr. 2020. [Online]. Available: https://nam-onderzoeksrapporten.data-app.nl/reports/download/groningen/en/b0b54c89-45d5-4765-8843-6c79903a0ef8.

[14] F. Messali, R. Esposito, S. Jafari, G. Ravenshorst, P. Korswagen, and J. G. Rots, "A multiscale experimental characterisation of dutch unreinforced masonry buildings," in *16th European Conference on Earthquake Engineering*, Springer, Thessaloniki, Greece, 2018, pp. 18–21.

[15] S. Jafari, "Material characterisation of existing masonry: A strategy to determine strength, stiffness and toughness properties for structural analysis," 2021.

[16] D. Fusco, F. Messali, J. Rots, D. Addessi, and S. Pampanin, "Numerical study of pier-wall connections in typical dutch urm buildings," in *12th International Conference on Structural Analysis of Historical Constructions*, International Centre for Numerical Methods in Engineering, CIMNE, 2021, pp. 2217–2228.

[17] D. N. Grant, J. Dennis, R. Sturt, *et al.*, "Explicit modelling of collapse for dutch unreinforced masonry building typology fragility functions," *Bulletin of Earthquake Engineering*, vol. 19, pp. 6497–6519, 2021.

[18] R. K. Klaassen, "Bacterial decay in wooden foundation piles—patterns and causes: A study of historical pile foundations in the netherlands," *International biodeterioration & biodegradation*, vol. 61, no. 1, pp. 45–60, 2008.

[19] D. Peduto, M. Korff, G. Nicodemo, A. Marchese, and S. Ferlisi, "Empirical fragility curves for settlement-affected buildings: Analysis of different intensity parameters for seven hundred masonry buildings in the netherlands," *Soils and Foundations*, vol. 59, no. 2, pp. 380–397, 2019.

[20] K. Klaassen, A. Jorissen, and H. Keijer, "Life expectation of wooden foundations — a non-destructive approach," in *Proceedings of the International Symposium Non-Destructive Testing in Civil Engineering (NDT-CE), Berlin, Germany*, 2015, pp. 15–17.

[21] D. Jacobs, "The influence of negative skin friction on the bearing capacity of timber piles in amsterdam," 2021.

[22] M. DeJong, "Thematic keynote: Settlement effects on masonry structures," in *Structural Analysis of Historical Constructions: Anamnesis, Diagnosis, Therapy, Controls*, CRC Press, 2016, pp. 449–456.

[23] H. Rietveld, "Land subsidence in the netherlands," *IAHS-AISH publication*, no. 151, pp. 455–464, 1986.

[24] M. J. van der Meulen, A. J. van der Spek, G. de Lange, *et al.*, "Regional sediment deficits in the dutch lowlands: Implications for long-term land-use options (8 pp)," *Journal of Soils and Sediments*, vol. 7, pp. 9–16, 2007.

[25] T. Elkateb, R. Chalaturnyk, and P. K. Robertson, "An overview of soil heterogeneity: Quantification and implications on geotechnical field problems," *Canadian Geotechnical Journal*, vol. 40, no. 1, pp. 1–15, 2003.

[26] L. Houy, D. Breysse, and A. Denis, "Influence of soil heterogeneity on load redistribution and settlement of a hyperstatic three-support frame," *Geotechnique*, vol. 55, no. 2, pp. 163–170, 2005.

[27] R. Popescu, G. Deodatis, and A. Nobahar, "Effects of random heterogeneity of soil properties on bearing capacity," *Probabilistic engineering mechanics*, vol. 20, no. 4, pp. 324–341, 2005.

[28] P. Minderhoud, G. Erkens, V. Pham, B. Vuong, and E. Stouthamer, "Assessing the potential of the multi-aquifer subsurface of the mekong delta (vietnam) for land subsidence due to groundwater extraction," *Proceedings of the International Association of Hydrological Sciences*, vol. 372, no. 372, pp. 73–76, 2015.

[29] T. Candela, K. Koster, J. Stafleu, W. Visser, and P. Fokker, "Towards regionally forecasting shallow subsidence in the netherlands," *Proceedings of the International Association of Hydrological Sciences*, vol. 382, pp. 427–431, 2020.

[30] H. F. Winterkorn and H.-Y. Fang, "Soil technology and engineering properties of soils," in *Foundation engineering handbook*, Springer, 1991, pp. 88–143.

[31] R. D. Holtz, "Stress distribution and settlement of shallow foundations," in *Foundation engineering handbook*, Springer, 1991, pp. 166–222.

[32] R. B. Peck, "Deep excavations and tunneling in soft ground," *Proc. 7th ICSMFE, 1969*, pp. 225–290, 1969.

[33] H. D. Netzel, "Building response due to ground movements," 2009.

[34] J. B. Burland and C. Wroth, "Settlement of buildings and associated damage," Tech. Rep., 1975.

[35] J. Charles and H. Skinner, "Settlement and tilt of low-rise buildings," *Proceedings of the Institution of Civil Engineers-Geotechnical Engineering*, vol. 157, no. 2, pp. 65–75, 2004.

[36] D. Peduto, G. Nicodemo, J. Maccabiani, and S. Ferlisi, "Multi-scale analysis of settlement-induced building damage using damage surveys and dinsar data: A case study in the netherlands," *Engineering geology*, vol. 218, pp. 117–133, 2017.

[37] M. D. Boscardin and E. J. Cording, "Building response to excavation-induced settlement," *Journal of Geotechnical Engineering*, vol. 115, no. 1, pp. 1–21, 1989.

[38] J. N. Franzius, "The behaviour of buildings due to tunnel induced subsidence," *PhD. Thesis, Imperial College, University of London*, 2004.

[39] D. Potts and T. Addenbrooke, "A structure's influence on tunnelling-induced ground movements.," *Proceedings of the Institution of Civil Engineers-Geotechnical Engineering*, vol. 125, no. 2, pp. 109–125, 1997.

[40] K. Goh, "Response of ground and buildings to deep excavations and tunnelling," Ph.D. dissertation, University of Cambridge, 2011.

[41] K. Goh and R. Mair, "Building damage assessment for deep excavations in singapore and the influence of building stiffness," *Geotechnical Engineering Journal of the SEAGS & AGSSEA*, vol. 42, no. 3, pp. 1–12, 2011.

[42] R. Mair, "Tunnelling and deep excavations: Ground movements and their effects," in *Proc., 15th European Conf. on Soil Mechanics and Geotechnical Engineering—Geotechnics of Hard Soils—Weak Rocks (Part 4)*, IOS Press, Amsterdam, 2013, pp. 39–70.

[43] J. Franzius, D. Potts, and J. Burland, "Twist behaviour of buildings due to tunnel induced ground movement," in *Geotechnical Aspects of Underground Construction in Soft Ground: Proceedings of the 5th International Symposium TC28. Amsterdam, the Netherlands, 15-17 June 2005*, CRC Press, 2005, p. 107.

[44] R. P. Farrell, "Tunnelling in sands and the response of buildings," Ph.D. dissertation, University of Cambridge, 2011.

[45] N. N. S. d. Oliveira, J. A. d. Nascimento Neto, and G. A. Parsekian, "Computational modeling of structural masonry shear walls considering cracking effects at mortar joints," *Revista IBRACON de Estruturas e Materiais*, vol. 16, e16410, 2023.

[46] S. Prabhu and S. Atamturktur, "Assessment of strength degradation of historic masonry monuments due to damage: Load path–based approach," *Journal of Structural Engineering*, vol. 143, no. 9, p. 04 017 122, 2017.

[47] R. B. Bonshor, L. L. Bonshor, and R. Sadgrove, *Cracking in buildings*. Construction Research Communications Limited London, UK, 1996.

[48] J. B. Burland, B. B. Broms, and V. F. De Mello, "Behaviour of foundations and structures," 1978.

[49] A. W. Skempton and D. H. MacDonald, "The allowable settlements of buildings.," *Proceedings of the Institution of Civil Engineers*, vol. 5, no. 6, pp. 727–768, 1956.

[50] W. Rankin, "Ground movements resulting from urban tunnelling: Predictions and effects," *Geological Society, London, Engineering Geology Special Publications*, vol. 5, no. 1, pp. 79–92, 1988.

[51] G. Meyerhof, "Limit states design in geotechnical engineering," *Structural Safety*, vol. 1, no. 1, pp. 67–71, 1982.

[52] D. E. Polshin and R. Tokar, "Maximum allowable non-uniform settlement of structures," in *Proc., 4th Int. Conf. on Soil Mechanics and Foundation Engineering*, Butterworth's London, vol. 1, 1957, pp. 402–405.

[53] L. Bjerrum, "Allowable settlement of structures," in *Proceedings of the 3rd European Conference on Soil Mechanics and Foundation Engineering, Wiesbaden, Germany*, vol. 2, 1963, pp. 135–137.

[54] G. Meyerhof, "Discussion. the allowable settlements of buildings.," *Proceedings of the Institution of Civil Engineers*, vol. 5, no. 6, pp. 768–784, 1956.

[55] M. Son and E. J. Cording, "Estimation of building damage due to excavation-induced ground movements," *Journal of geotechnical and geoenvironmental engineering*, vol. 131, no. 2, pp. 162–177, 2005.

[56] B. EN *et al.*, "Eurocode 7: Geotechnical design-part 1: General rules," *British Standards Institution*, 2004.

[57] NEN9997-1+C2:2017nl, *Geotechnisch ontwerp van constructies - deel 1: Algemene regels (geotechnical design of structures - part 1: General rules)*, 2017.

[58] NEN9997-1:2023Ontw.nl, *Geotechnisch ontwerp van constructies - deel 1: Algemene regels (geotechnical design of structures - part 1: General rules)*, 2023.

[59] D. Peduto, M. Korff, G. Nicodemo, A. Marchese, and S. Ferlisi, "Empirical fragility curves for settlement-affected buildings: Analysis of different intensity parameters for seven hundred masonry buildings in the netherlands," *Soils and Foundations*, vol. 59, no. 2, pp. 380–397, 2019.

[60] H. Netzel, "Review of the limiting tensile strain method for predicting settlement induced building damage," in *Proc., Geotechnical Aspects of Underground Construction in Soft Ground: Proc. of the 5th Int. Symp. TC28, edited by KJ Bakker, A. Bezuijen, W. Broere, and EA Kwast*, 2005, pp. 159–164.

[61] G. Giardina, "Modelling of settlement induced building damage," 2013.

[62] G. Giardina, M. A. Hendriks, and J. G. Rots, "Assessment of the settlement vulnerability of masonry buildings," in *Proceedings of the 1st WTA International PhD Symposium-Buildings Materials and Building Technology for Preservation of the Built Heritage, Leuven, Belgium*, 2009, pp. 8–9.

[63] J. Pickhaver, H. Burd, and G. Houlsby, "An equivalent beam method to model masonry buildings in 3d finite element analysis," *Computers & structures*, vol. 88, no. 19-20, pp. 1049–1063, 2010.

[64] M. Son and E. J. Cording, "Evaluation of building stiffness for building response analysis to excavation-induced ground movements," *Journal of geotechnical and geoenvironmental engineering*, vol. 133, no. 8, pp. 995–1002, 2007.

[65] A. Prosperi, M. Longo, P. A. Korswagen, M. Korff, and J. G. Rots, "2d and 3d modelling strategies to reproduce the response of historical masonry buildings subjected to settlements," *International Journal of Architectural Heritage*, pp. 1–17, 2024.

[66] G. Giardina, A. V. Van de Graaf, M. A. Hendriks, J. G. Rots, and A. Marini, "Numerical analysis of a masonry façade subject to tunnelling-induced settlements," *Engineering structures*, vol. 54, pp. 234–247, 2013.

[67] D. Potts and T. Addenbrooke, "A structure's influence on tunnelling-induced ground movements.," *Proceedings of the Institution of Civil Engineers-Geotechnical Engineering*, vol. 125, no. 2, pp. 109–125, 1997.

[68] H. Burd, G. Houlsby, C. Augarde, and G. Liu, "Modelling tunnelling-induced settlement of masonry buildings," *Proceedings of the institution of civil engineers - geotechnical engineering*, vol. 143, no. 1, pp. 17–29, 2000.

[69] H. Netzel and F. Kaalberg, "Numerical damage risk assessment studies on adjacent buildings in amsterdam," in *ISRM International Symposium*, ISRM, 2000, ISRM–IS.

[70] J. Rots, "Computational modelling of cracking and settlement damage in masonry structures," in *Proc. 12th International Brick/Block Masonry Conference*, 2001, pp. 2171–2187.

[71] M. Son and E. J. Cording, "Estimation of building damage due to excavation-induced ground movements," *Journal of geotechnical and geoenvironmental engineering*, vol. 131, no. 2, pp. 162–177, 2005.

[72] M. Son and E. J. Cording, "Evaluation of building stiffness for building response analysis to excavation-induced ground movements," *Journal of geotechnical and geoenvironmental engineering*, vol. 133, no. 8, pp. 995–1002, 2007.

[73] H. D. Netzel, "Building response due to ground movements," 2009.

[74] W. Yiu, H. Burd, and C. Martin, "Finite-element modelling for the assessment of tunnel-induced damage to a masonry building," *Géotechnique*, vol. 67, no. 9, pp. 780–794, 2017.

[75] S. Ferlisi, G. Nicodemo, D. Peduto, *et al.*, "Numerical analysis of the behaviour of masonry buildings undergoing differential settlements," in *Proceedings of the XVII European Conference on Soil Mechanics and Geotechnical Engineering*, The authors and The Icelandic Geotechnical Society, IGS, 2019, pp. 1–8.

[76] J. Rots, P. Korswagen, and M. Longo, "Computational modelling checks of masonry building damage due to deep subsidence," *Delft University of Technology*, 2021.

[77] S. Ferlisi, G. Nicodemo, D. Peduto, C. Negulescu, and G. Grandjean, "Deterministic and probabilistic analyses of the 3d response of masonry buildings to imposed settlement troughs," *Georisk: Assessment and Management of Risk for Engineered Systems and Geohazards*, vol. 14, no. 4, pp. 260–279, 2020.

[78] D. Peduto, A. Prosperi, G. Nicodemo, and M. Korff, "District-scale numerical analysis of settlements related to groundwater lowering in variable soil conditions," *Canadian Geotechnical Journal*, vol. 59, no. 6, pp. 978–993, 2022.

[79] F. Niklas, "Behaviour of buildings due to tunnel induced subsidence," Ph.D. dissertation, PhD Thesis, Imperial College of Science, UK, 2003.

[80] H. Burd, W. Yiu, S. Acikgoz, and C. Martin, "Soil-foundation interaction model for the assessment of tunnelling-induced damage to masonry buildings," *Tunnelling and Underground Space Technology*, vol. 119, p. 104 208, 2022.

[81] A. Prosperi, M. Longo, P. A. Korswagen, M. Korff, and J. G. Rots, "Accurate and efficient 2d modelling of historical masonry buildings subjected to settlements in comparison to 3d approaches," in *International Conference on Structural Analysis of Historical Constructions*, Springer, 2023, pp. 232–244.

[82] M. Longo, M. Sousamli, P. A. Korswagen, P. van Staalduinen, and J. G. Rots, "Substructure-based 'three-tiered' finite element approach to soil-masonry-wall interaction for light seismic motion," *Engineering Structures*, vol. 245, p. 112 847, 2021.

[83] A. Prosperi, M. Longo, P. A. Korswagen, M. Korff, and J. G. Rots, "Sensitivity modelling with objective damage assessment of unreinforced masonry façades undergoing different subsidence settlement patterns," *Engineering Structures*, vol. 286, p. 116 113, 2023.

[84] M. Sousamli, "Orthotropic cyclic continuum constitutive model for masonry structures and comparative studies," 2024.

[85] J. Wambacq, J. Ulloa, G. Lombaert, and S. François, "A variationally coupled phase field and interface model for fracture in masonry," *Computers & Structures*, vol. 264, p. 106 744, 2022.

[86] P. B. Lourenço and J. G. Rots, "Multisurface interface model for analysis of masonry structures," *Journal of engineering mechanics*, vol. 123, no. 7, pp. 660–668, 1997.

[87] P. J. B. B. Lourenço, "Computational strategies for masonry structures.," 1997.

[88] Centre for Civil Engineering Research and Codes - J.G. Rots, *Structural Masonry: An Experimental/ Numerical Basis for Practical Design Rules (CUR Report 171)*. CRC Press, 1997. DOI: https://doi.org/10.1201/9781003077961.

[89] L. T. Hong and D. F. Laefer, "Micro vs. macro models for predicting building damage underground movements," in *CSM-2008 the International Conference on Computational Solid Mechanics*, 2008, pp. 27–30.

[90] G. Nicodemo, D. Peduto, and S. Ferlisi, "Building damage assessment and settlement monitoring in subsidence-affected urban areas: Case study in the netherlands," *Proceedings of the International Association of Hydrological Sciences*, vol. 382, pp. 651–656, 2020.

[91] D. Peduto, M. Santoro, L. Aceto, L. Borrelli, and G. Gullà, "Full integration of geomorphological, geotechnical, a-dinsar and damage data for detailed geometric-kinematic features of a slow-moving landslide in urban area," *Landslides*, vol. 18, pp. 807–825, 2021.

[92] A. Goretti and G. Di Pasquale, "An overview of post-earthquake damage assessment in italy," in *Eeri invitational workshop. An action plan to develop earthquake damage and loss data protocols, California*, 2002.

[93] A. Saeidi, O. Deck, and T. Verdel, "Comparison of building damage assessment methods for risk analysis in mining subsidence regions," *Geotechnical and Geological Engineering*, vol. 31, pp. 1073–1088, 2013.

[94] G. Giardina, P. Milillo, M. J. DeJong, D. Perissin, and G. Milillo, "Evaluation of insar monitoring data for post-tunnelling settlement damage assessment," *Structural Control and Health Monitoring*, vol. 26, no. 2, e2285, 2019.

[95] N. S. Romali and Z. Yusop, "Flood damage and risk assessment for urban area in malaysia," *Hydrology Research*, vol. 52, no. 1, pp. 142–159, 2021.

[96] E. Stouthamer, G. Erkens, K. Cohen, *et al.*, "Dutch national scientific research program on land subsidence: Living on soft soils–subsidence and society," *Proceedings of the International Association of Hydrological Sciences*, vol. 382, pp. 815–819, 2020.

[97] A. L. Costa, S. Kok, and M. Korff, "Systematic assessment of damage to buildings due to groundwater lowering-induced subsidence: Methodology for large scale application in the netherlands," *Proceedings of the International Association of Hydrological Sciences*, vol. 382, pp. 577–582, 2020.

[98] A. Saeidi, O. Deck, and T. Verdel, "Development of building vulnerability functions in subsidence regions from empirical methods," *Engineering Structures*, vol. 31, no. 10, pp. 2275–2286, 2009.

[99] The Council for the Environment and Infrastructure (Rli), "Goed gefundeerd: Advies om te komen tot een nationale aanpak funderingsproblematiek," Tech. Rep., 2024.

CHAPTER 3

THE ROLE OF THE SOIL HETEROGENEITY ON THE SETTLEMENT OCCURRENCE

CHAPTER 3: TABLE OF CONTENTS

3.1 Introduction **61**
3.1.1 Soil heterogeneity 61

3.2 Methodology and Underlying concepts **61**
3.2.1 Case study and available datasets 63
3.2.2 Finite Elements models 65
3.2.3 Correlation length 69

3.3 Results of the Finite Elements analyses **70**
3.3.1 Correlation length of the soil thickness 70
3.3.2 Correlation length of the computed settlements 71
3.3.3 The influence of the dataset resolutions 73

3.4 Discussion **74**
3.4.1 The variability of the soil thickness 75
3.4.2 The variability of the computed settlements 75
3.4.3 Comparison between the different resolutions 78

3.5 Conclusions **78**

Bibliography of Chapter 3 . . . . . **82**

3.1. INTRODUCTION

The lithological heterogeneity, *i.e.* lithological variations in the subsurface can trigger and/or enhance subsidence processes at the scale of individual structures, and thus, potentially cause a threat to the built heritage. However, although this observation is well-known in civil engineering, the effect of lithological variations on settlement occurrence at the scale of structure has never been fully investigated. This Chapter aims to test and quantify whether the variability of the stratigraphical conditions can predispose the occurrence of uneven settlements at the scale of single structures. Two independent datasets at high resolution (site-specific) and low resolution (national level) are used to retrieve the stratigraphic conditions for an area selected for the analyses. One-, Two- and Three- dimensional numerical models, based on the collected information, are used to simulate the consolidation and settlement due to a uniform load imposed on the surface level of the study area. Additional analyses investigate the influence of different loading conditions and groundwater tables. The parameter "correlation length" quantifies herein the spatial variability of the soil layer thickness and then of the computed settlements.

3.1.1. SOIL HETEROGENEITY

Both natural and man-made soils are strongly characterized by an anisotropic behaviour and spatial heterogeneity that originates from different depositional processes and loading histories [1]–[3]. Soil heterogeneity has been distinguished [2], [4], [5] in two typologies: i) **inherent spatial soil variability**, which describes the variability of the soil properties, such as the compressibility or permeability, from one point to another within a layer, and ii) **lithological heterogeneity**, which refers to the variation of the stratigraphical information, such as lithology, unit thickness, inclination of the soil strata. Soil heterogeneity affects the soil behaviour and can influence different engineering problems [1], [2], [6]–[9]. Subsidence serves as a prime example wherein soil heterogeneity can enhance the spatial distribution of the ground settlements, which in turn can cause damage to buildings [1], [10].

In the current state of research, previous studies typically include the variability of the soil properties and their influence on soil-structure problems and foundation settlements [1], [4], [5]. The results of these works proved that variation of the soil properties within a layer can augment differential settlements [1], [11]. Conversely, only a few analyses focused on the effects of stratigraphical variations (*e.g.*, [9], [12]–[14]), which are investigated in this Chapter.

3.2. METHODOLOGY AND UNDERLYING CONCEPTS

The approach adopted consists of three phases (Fig. 3.1):

In Phase 0, data at different resolutions are collected over the area of interest, including information about the stratigraphy and the hydro-geo-mechanical material properties. The correlation length, which represents the distance within significantly correlated observations occur, is computed to quantify the variability of the thickness of each soil layer detected in the stratigraphy. The subsoil information, retrieved from the dataset

with the highest resolution (in-situ specific), and the available hydro-geo-mechanical properties of the soil materials are then used as the inputs for the numerical models. Such numerical analyses are carried out to investigate the influence of soil lithological heterogeneity on the settlement occurrence at the scale of buildings.

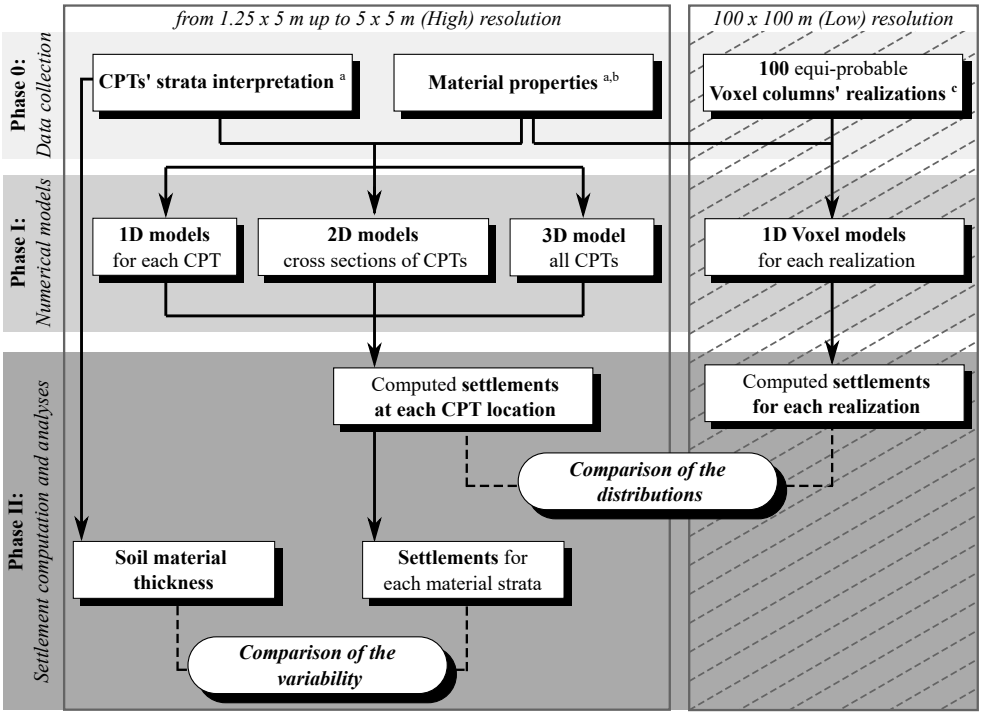

[a]de Gast, 2020; [b]Dutch norm (NEN9997-1+C2); [c]GeoTOP model;

Figure 3.1: Flowchart of the adopted procedure.

Toward this aim, one-, two- and three- dimensional numerical models are built in Phase I, based on the in-situ specific information. Additional 1D models, based on the stratigraphical information provided by the national-level subsurface model, are used to evaluate the response of the study area. Sensitivity analyses are further carried out to study the influence of the groundwater table and the different loading conditions on settlement occurrence and spatial variability.

In Phase II, the outputs of the numerical simulations are retrieved. First, a comparison between the in-situ specific 1D, 2D and 3D numerical models is carried out to investigate the difference. For each soil strata, the correlation length is computed using the computed settlements and compared with the one of the material thickness.

Finally, the results of the 1D, 2D and 3D analyses at the scale of the study area are compared with the ones of the 1D models at the national scale to evaluate the effects of the different resolutions and to determine the effect of lithological variations on the building scale.

3.2.1. CASE STUDY AND AVAILABLE DATASETS

The area selected for the analysis is the field of the Leendert de Boerspolder dyke (Fig. 3.2a), in the northwest of the Netherlands [15]. The available information encompasses: i) 100 CPTs data (Fig. 3.2b and c), their location and their interpretation in terms of lithotypes up to a depth of 11.70 m to NAP (*i.e.*, the Amsterdam Ordnance Datum or Normaal Amsterdams Peil in Dutch) (Fig. 3.2d), ii) hydro-geo-mechanical material properties (Table 3.1) [15], [16]. The closely spaced CPTs, located along the crest of the dyke and adjacent to the dyke, cover the study area of about 15 x 50 meters with an uneven grid (Fig. 3.2b and c) [17]–[19]. In particular, 29 CPTs were taken along the crest of the dyke, 28 CPTs along the slope and the remaining in the polder area (Fig. 3.2b) [19]. The distance between two adjacent CPTs varies from about 1.25 m up to 5.0 m, and the coarsest spacing of the CPTs' grid is equal to 5 m x 5 m [17], [18]; Thus, this dataset characterizes the study area at the in-situ level, hereinafter referred to as "high" resolution. The in-situ measurements reveal the presence of four soil strata, herein labelled as [15], [16], [18]:

- **dyke material**: a mix of clay, silt, sand and rumble that had been placed periodically starting from 1600 AD to form the embankment; The building and maintenance of this man-made layer have caused the underlying layers to compress [18].
- **peat**: organic layer affected by the overlying dyke materials;
- **organic clay**: clay in which the organic content decreases with the depth;
- **silty clay**: clay layer rich in silt, that continues until NAP -16.0m depth, beyond which sand is found.

The material properties shown in Table 3.1 are based on laboratory investigations [15], [16], further integrated by values available in the Dutch code [20] and estimates [15], [16]. Additional subsoil information is collected from the "GeoTOP model", which discretizes the surface area of the Netherlands (at the national level) up to a depth of 50 meters in rectangular blocks, namely "voxels", each measuring 100 m x 100 m x 0.5 m (height x width x depth) [21]–[23]. The data used to derive the GeoTOP model do not include the 100 CPTs available in the study area, and thus the two datasets are independent. Due to the size of the voxels, this set of data is herein referred for the study area to be at a "low" resolution, if compared with the closely spaced CPTs. The GeoTOP model provides estimates of the lithological classes for each voxel [23]: Anthropogenic material; Organic material (peat); Clay; Clayey sand, silty clay and loam; And Sand, distinguished according to the grain size in "Fine Sand", "Medium Sand" and "Coarse sand" and "Gravel". The lithological classes assigned to each voxel are the outcome of interpolation techniques; The procedure leads to a set of 100 realizations for each voxel. For additional details, the reader is referred to [23]. In other words, 100 realizations provide estimates of the soil type that lays within each voxel, *i.e.*, a cell that discretizes the surface at a certain depth; The group of voxels that discretizes the subsurface along the depth, *i.e.*, voxels that are piled on top of each other, at a certain location it's herein referred as "voxel column".

The studied area is covered by two voxel columns (Fig. 3.3a). 78 CPTs are included in the coverage of voxel column 1, whereas voxel column 2 only covers 22 CPTs (Fig. 3.3a). All the 100 equiprobable realizations for the two available voxel columns are shown in Fig.

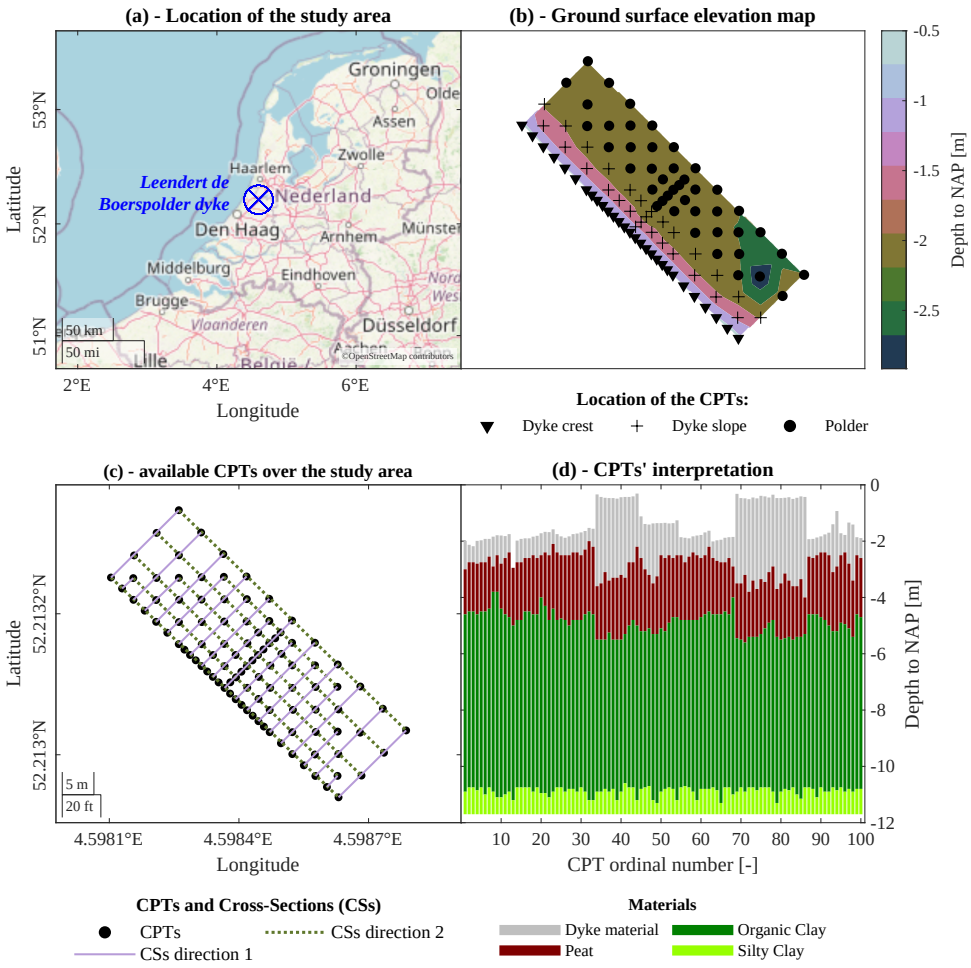

Figure 3.2: Location of the study area and the available cone penetration tests (CPTs). (a) show the location of the study area, plot (b) shows the elevation maps, (c) shows the selected cross-sections over the study area and (d) shows the stratigraphy at each location based on the interpretation of the CPT data [15].

3.3b and c. Each lithological class was assumed to have the same hydro-geo-mechanical properties as one of the four soil strata in the study area (Table 3.1), for consistency. This assumption is supported by similar stratigraphical conditions of both the GeoTOP realizations and the CPTs, with superficial strata of peat and clay, and deeper layers of silt and sand. Thus, each litho class is then assumed to have the same characteristics as one soil type for the study area, as shown in Fig. 3.4.

As briefly mentioned, the “dyke material” consists of sandy and clayey material. Due to that, it was assumed that its behaviour is similar to sand/loam, for the similarity between its material properties reported in Table 3.1 [15], [16] and the ones reported in the Dutch code. Moreover, as briefly mentioned above, the layers of peat and clay, which range between -2.8 m up to -10.90 m to NAP, are both characterized by an organic fraction

Table 3.1: Material properties of each soil layer. Sources: 1 - from [15]; 2 - from [20]; 3 - estimated values.

Parameter	Symbol	Unit of measure	Source	Materials			
				Dyke material/ sand	Peat	Organic Clay	Silty clay
Dry unit weight	γ_{dry}	kN/m^3	1	13.00	9.00	14.50	14.00
Saturated unit weight	γ_{sat}	kN/m^3	1	18.00	10.00	15.00	17.00
Modified compression index	λ^*	-	2	4.99×10^{-2}	2.00×10^{-1}	9.99×10^{-2}	2.22×10^{-2}
Modified swelling index	κ^*	-	2	2.50×10^{-2}	9.99×10^{-2}	5.00×10^{-2}	1.11×10^{-2}
Modified creep index	μ^*	-	2	2.00×10^{-3}	1.00×10^{-2}	5.00×10^{-3}	9.00×10^{-4}
Effective cohesion	c'	kN/m^2	1	5.00	2.50	4.40	1.90
Effective friction angle	φ'	°	1	33.00	28.80	29.50	30.00
Pre-overburden pressure	POP	kN/m^2	3	2.00	22.00	20.00	12.00
Hydraulic conductivity	k	m/day	1	3.46×10^{-1}	4.00×10^{-2}	7.52×10^{-4}	7.52×10^{-4}

[15], [16]. Thus, it is reasonable to assume that soil strata within the same range may be characterized by the presence of an organic fraction. The dyke material properties are thus assigned to the uppermost sand litho-classes of the GeoTOP realizations (Fig. 3.4), assumed to represent prevalently sandy layers with a small clay/organic fraction that undergoes creep.

3.2.2. FINITE ELEMENTS MODELS

In this study, 1D, 2D and 3D numerical analyses are carried out with the software PLAXIS 2D and 3D to investigate the effect of in-situ lithological heterogeneity on the settlements occurring at the scale of structures.

In the case of the 1D analyses (Fig. 3.5a), the geometry of the models corresponds to each CPT interpretation (Fig. 3.2d) and each voxel column (Fig. 3.3b and c).

It should be noted that all the CPTs were performed from the ground surface, which has a variable elevation in each location as shown in Fig. 3.2b and Fig. 3.2c, up to a depth of about 12 meters to NAP; Thus, the CPTs are characterized by different lengths along the depth. Therefore, the CPTs were herein truncated at the depth of 11.70 to NAP (Fig. 3.5a), which corresponds to the shallowest depth reached among all the CPTs. The mean length of the truncated CPTs, adopted hereafter, corresponds to 10.34 meters, while the standard deviation is equal to 0.64 meters.

Differently from the CPTs, the elevation of the top level of the voxel columns does not

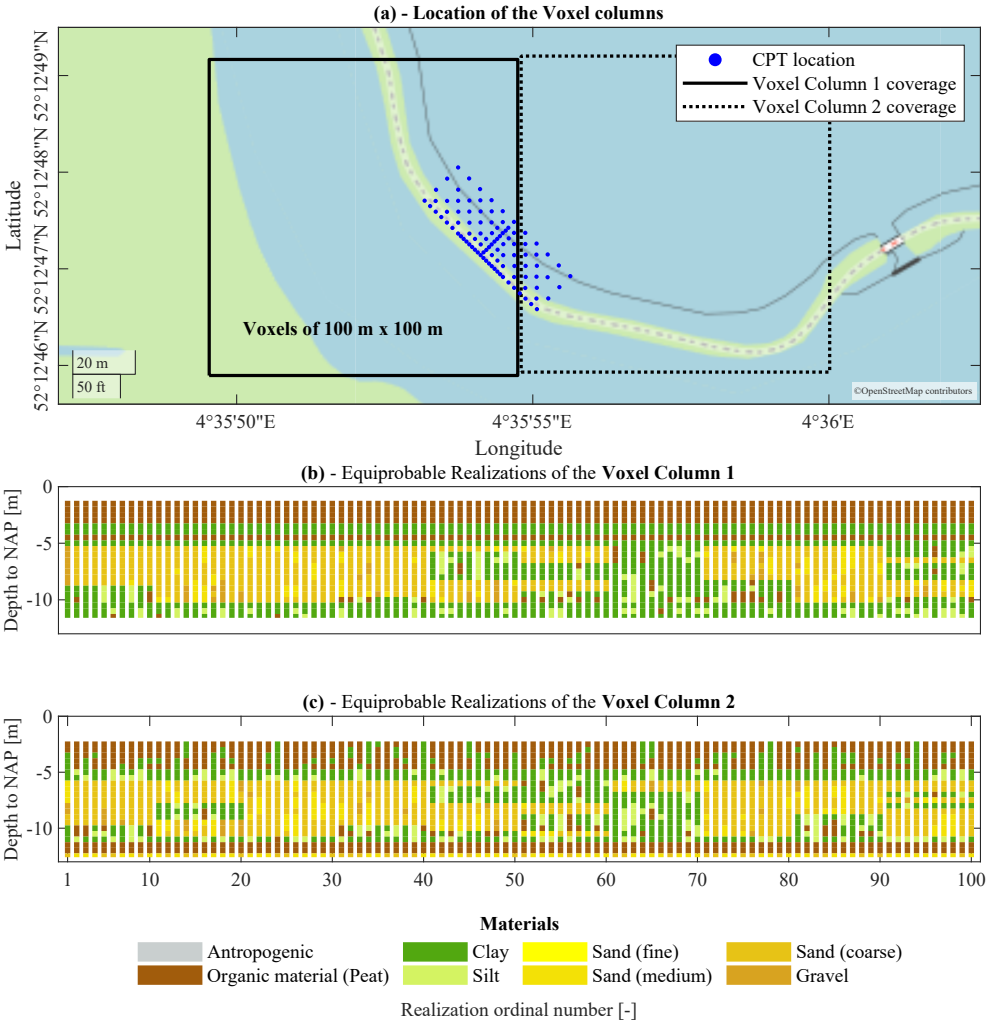

Figure 3.3: The voxel columns from the available GeoTOP model: (a) the location of the voxel columns, (b) and (c) the 100 equiprobable realizations for columns 1 and 2 respectively.

differ among the 100 realizations; Moreover, the voxel columns provide the stratigraphy up to a depth of 50 meters to NAP. In this study, however, only the portion of the voxel columns that cover the depth of the study area is considered. Therefore, each voxel column is truncated in a way that ensures a length of 10.34 meters (Fig. 3.3b and c), equal to the average length among all the CPTs. The 2D models represent the cross-sections obtained by linear interpolation of the stratigraphical information of the available CPTs (Fig. 3.5b) in the directions that correspond to the short and long sides of the CPTs' field (directions 1 and 2 in Fig. 3.2c respectively). The same procedure is applied to obtain the 3D model (Fig. 3.5c). The practical advantage of truncating the CPTs at the depth of 11.70 meters consists of having a horizontal boundary at the bottom of the 2D and 3D models (Fig. 3.5b and c), to avoid numerical issues. In all the models, a constant ground water

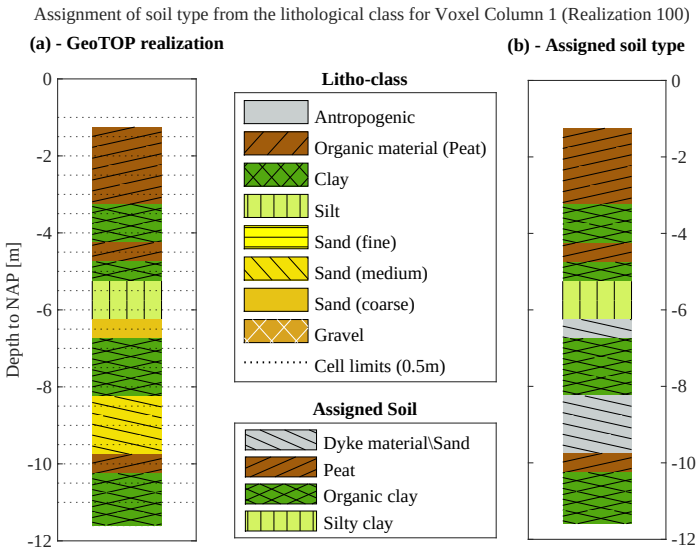

Figure 3.4: Schematic illustration of the relationship between (a) the computed soil lithoclass from the GeoTOP model and (b) the assigned soil type for each voxel column realization.

table of -3.94 meters to NAP is used, idealizing the in-situ conditions during the time the CPTs were made. The imposed groundwater level is different from the current in-situ conditions, as part of the study area is now submerged, as shown in Fig. 3.3a.

Table 3.2: The adopted phased analyses and numerical settings.

Phase	Calculation type	Pore pressure	Time [days]	Max steps	Tolerated error	Max number of iterations	Max load fraction per step
Initial phase	K0 procedure	-	-	-	-	-	-
Load application	Plastic	Use pressures from the previous phase	0	1000	0.01	60	0.5
From 1 up to 5000 years of consolidation (1, 10, 20, 30, 40, 50, 100, 500, 5000 years)			365 to 1.825×10^6				

For both 1D and 2D analyses, 15-node triangle plane strain elements are used to discretize the geometry, whereas the 3D models make use of 10-node tetrahedral elements. Meshing is performed by setting the global coarseness factor equal to 0.07 in all the models. For additional information on the coarseness factor and its influence on the element size, the reader is referred to [24]. The soil materials are modelled with the soft soil creep model (SSC), using material properties reported in Table 3.1. The SSC model is able to

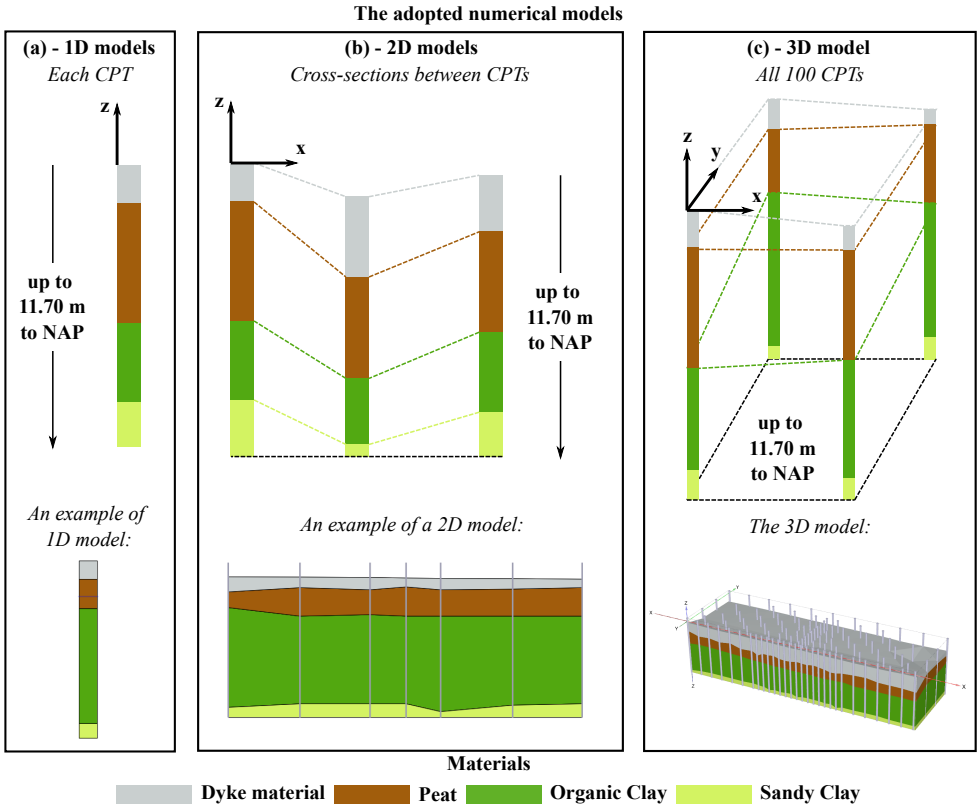

Figure 3.5: Schematic illustration of the adopted FE models. The directions x and y represent the local axis of the models. z is the vertical axis along the depth direction. The lower boundary at the bottom of the models is schematically illustrated.

account for the compressive behaviour and viscous effects of very soft soils and requires three stiffness parameters: the modified swelling index κ^*, the modified compression index λ^* and the modified creep index μ^*. SSC is also assigned to the "dyke material" for its clay fraction. In all the models, a constant load that simulates the deposition of 1 meter of sand with a volumetric weight of 17 kN/m^3 is applied on the surface to trigger the consolidation process (Fig. 3.6a). This loading condition is herein labelled as "reference load" (Fig. 3.6a). For the purpose of the sensitivity study, additional analyses are carried out by doubling the reference load ("double load" in Fig. 3.6b), and another set of analyses uses the reference load but the groundwater table was completely removed ("no groundwater" in Fig. 3.6c) by fictitiously setting the water head to -15 meters to NAP in the models, thus with no influence on the modelled domain. In all the models, phased analysis is used: First, the pore pressure and the stresses are initialized; Then, the load is applied in the Plastic phase; Finally, consolidation phases are used to simulate the consolidation process at different time intervals.

Additional information regarding the settings of the phased analyses for all the models is reported in Table 3.2.

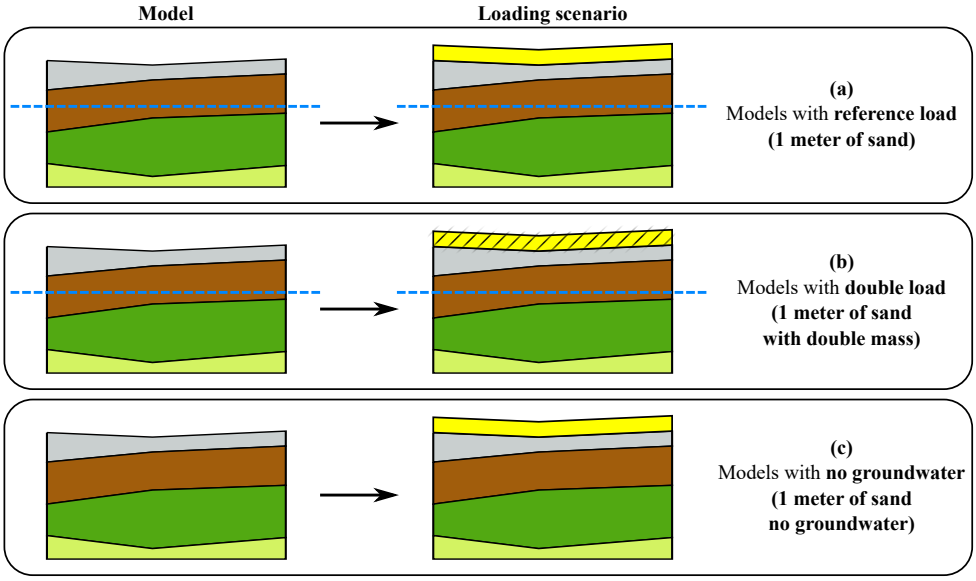

Figure 3.6: Schematic illustration of the three load scenarios for the 1D, 2D and 3D models. In the models with a double load (b), the load is applied by doubling the mass of the sand material rather than using 2 meters of sand. The decision to double the mass rather than the sand thickness was guided by the structure of the Python code used to generate the models, as it allowed for a more straightforward implementation.

The models aim to simulate a two-side drainage consolidation process due to the load application; During the K0 procedure, drainage is only blocked at the bottom of the model. Conversely, the hydraulic boundary conditions are set to simulate impermeable conditions at the vertical boundaries of the models (directions x and y in Fig. 3.5), and drainage is allowed at the top and the bottom of the model [25] (direction z in Fig. 3.5) during the Plastic and Consolidation phase. The horizontal displacements at the vertical boundaries are fixed while the vertical displacements are free.

3.2.3. CORRELATION LENGTH

The correlation length or scale of fluctuation, herein labelled as "θ", represents a convenient metric to describe the distance within significantly correlated observations [26]. The correlation length is determined by fitting the empirical determined auto-correlation function described in Eq. (3.1):

$$\hat{\rho} = \frac{\hat{\gamma}(\tau)}{\hat{\gamma}(0)} \tag{3.1}$$

Where $\hat{\gamma}(\tau)$ represents the empirical covariance function for the lag distance τ. For observations unevenly spaced on a grid, such as the grid represented by CPTs' locations of the study area herein presented, $\hat{\gamma}(\tau)$ can be computed as (3.2) [15]:

$$\hat{\gamma}(\tau) = \frac{1}{t-1} \sum_{j=1}^{t} (y_j - \hat{\mu})(y_{j+\Delta j} - \hat{\mu}) \tag{3.2}$$

Where $\hat{\mu}$ is the mean of the values, j is a counter representing the index of the first of a pair at lag distance τ, Δj represents the index spacing of a specific pair of observations for a non-uniformly distributed dataset and t is the number of pairs at lag distance τ. The lag distance τ represents the physical distance between the observations in the dataset.

In other words, for each lag distance τ, a sub-sample is defined as the number of pairs of observations t at that distance τ. The covariance $\hat{\gamma}(\tau)$ is then computed for the sub-sample, using the mean of the entire dataset $\hat{\mu}$. The empirically determined auto-correlation function $\hat{\rho}$ is fitted by the squared-exponential (Gaussian) function in Eq. 3.3:

$$\rho(\tau) = \exp\left[-\pi\left(\frac{|\tau|}{\theta}\right)^2\right] \tag{3.3}$$

A MATLAB algorithm is used to perform the fitting procedure to obtain the correlation length θ. In particular, data are grouped for intervals of lag distances τ of 1 meter. A lower bound of θ is imposed equal to the minimum distance between two CPTs of the study area (about 1 meter in this analysis). The lower bound is imposed to avoid values of θ smaller than the minimum distance between CPTs, which would have no physical meaning.

3.3. RESULTS OF THE FINITE ELEMENTS ANALYSES

3.3.1. CORRELATION LENGTH OF THE SOIL THICKNESS

The maps in Fig. 3.7a to Fig. 3.7d display the spatial distribution of the soil thickness for each soil material. The thickness of the dyke material is higher, as expected, in proximity to the dyke crest, whereas the thickness of the organic clay progressively increases toward the older.

The organic clay material exhibits, on average, the highest thickness (5.99 meters), see Fig. 3.2, followed by the peat (2.06 meters) the dyke material (1.46 meters) and the silty clay (0.82 meters).

The dispersion of the values of soil thickness is reported using the Coefficient of Variation (CoV) in Fig. 3.3a to Fig. 3.7d. The organic clay layer is associated with the smallest dispersion (0.07) followed by the peat (0.16), the silty clay (0.19) and the dyke material (0.68).

The variation of the soil thickness for each layer is visualized using box plots in Fig. 3.3e to Fig. 3.7h, which display the median (dashed lines), the interquartile range (the height of each rectangle) and the upper and lower bounds of the thickness of the soil strata of the available CPTs logs.

The soil thickness at each CPT location is used to determine the correlation length of the material thickness, labelled as θt, for each material (Fig. 3.7i, j, k and l), according to the procedure detailed in section 3.2.3; The dots in the plots represent the values of $\hat{\rho}$ obtained with equation (3.1), while the lines result from the fitting procedure that uses equation (3.3).

The organic clay is the soil strata associated with the highest value of the θt, followed by the dyke material, the peat and silty clay layer. However, the silty clay presents a θt equal to the lower boundary imposed in the fitting procedure, *i.e.*, 1 meter. This can be related to the fact that the silty clay has a limited (and truncated, as briefly described in section 3.2.2) thickness.

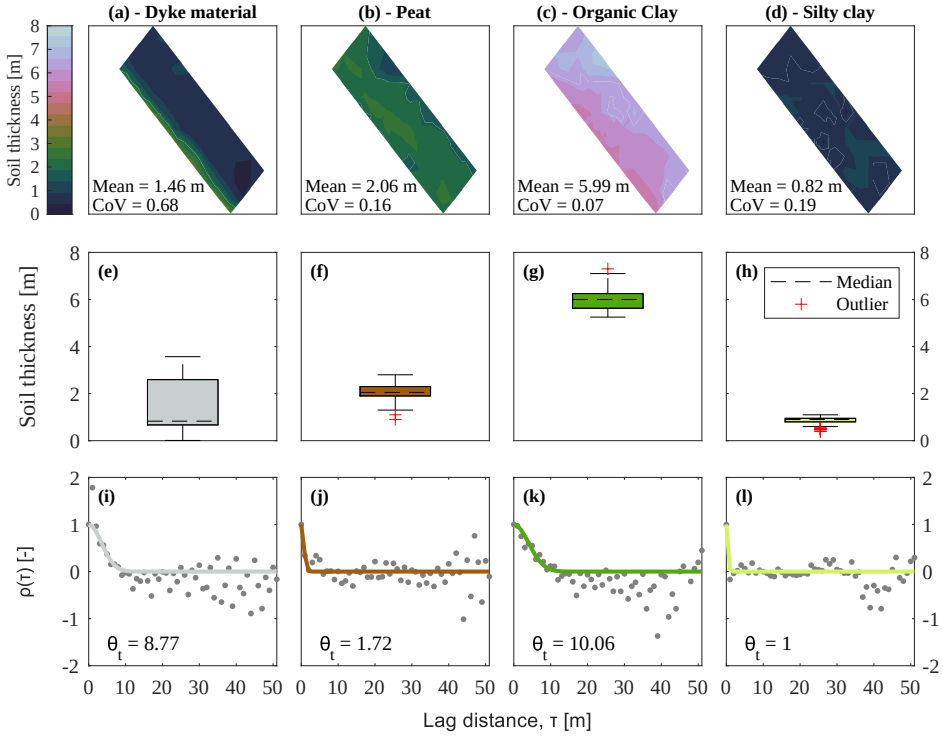

Figure 3.7: Maps obtained via linear interpolation and box plots of the soil layer thickness and the computed correlation length: (a) and (f) for Dyke material, (b) and (d) for peat, (c) and (g) for organic clay and (d) and (h) for silty clay. The bottom plots, from (i) to (l), show the results of fitting the autocorrelation function described in Eq. (3) through the points of the empirical autocorrelation function, Eq. (1), for each soil material.

3.3.2. CORRELATION LENGTH OF THE COMPUTED SETTLEMENTS

The numerical models give the vertical displacements of each soil strata (*i.e.*, dyke material, peat, organic clay, silty clay), and the cumulative vertical displacement, *i.e.*, the sum of all the contributions corresponding to the settlement of the ground surface, at the location of each CPT, for both the 1D, 2D and 3D analyses. In the case of the voxel columns, the material strata at a certain depth vary among the different realizations, thus it is not possible to retrieve the displacement of each material and only the cumulative vertical displacement is considered. An example of the results of the 1D numerical analyses is shown in Fig. 3.8 for the reference load. The organic clay material is the layer where the excess pore pressures develop the most (Fig. 3.8b) and, in turn, it's the layer

that contributes the most to the total settlement (Fig. 3.8c); On the contrary, as expected, the silty clay has the smallest contribution on the total settlement (Fig. 3.8c), which is also the results of its small thickness (Fig. 3.7d and h) and the low compressibility assigned (Table 3.1).

Fig. 3.9 shows the final (*i.e.*, 5000 years) settlement of each layer with maps obtained by linearly interpolating the results of the 1D, 2D and 3D models subjected to the reference load at all the CPTs' locations. The maps provide a picture of the spatial variability of the computed settlement. The results confirm how the layers "dyke material" (Fig. 3.9a1 to a3) and "silty clay" (Fig. 3.9d1 to d3) contribute the least to the overall settlements at all the CPTs' locations. As expected, for each soil strata, the areas with the highest and lowest settlements correspond to those of the soil thickness specific to that material (shown in Fig. 3.7). In other words, the spatial variability of the soil thickness matches one of the computed settlements for each material. Moreover, the values of the dispersion, *i.e.* CoV, of the computed settlements for each material (Fig. 3.9) match the ones of the material thickness for each soil (Fig. 3.7). In particular, The organic clay layer is associated with the smallest dispersion (from 0.06 to 0.08) followed by the peat (0.15 and 0.16), the silty clay (from 0.19 to 0.24) and the dyke material (from 0.64 to 0.78).

Each layer is observed to have settlements that only slightly change in terms of magnitude and spatial distribution among the 1D, 2D and 3D analyses; Nevertheless, the differences among the layers cumulate, and the total settlement varies among the analyses considered (Fig. 3.9e1 to e3).

In Fig. 3.9e3, it is observable how the 3D analyses better distinguish the behaviour of the three portions of the dyke, *i.e.*, the crest, slope and polder (Fig. 3.2b), whereas the settlement is more uniform in the case of 1D (Fig. 3.9e1) and 2D models (Fig. 3.9e2). The computed vertical displacements of each soil strata (shown for instance in Fig. 3.8) are used to obtain the correlation length of the settlement θs for five time steps, 1, 10, 50, 500 and 5000 years; Hence, the use of five time steps allow to investigate the time dependency of θs.

Fig. 3.10 shows the mean (markers) and the standard deviation interval (error bars) of the values of θs for each soil layer and of the total settlement, computed considering the selected time steps; The plots are distinguished by the type of loading scenario (Fig. 3.6). Additionally, the values of the correlation length of the soil thickness θt for each material, already reported in Fig. 3.7, are also plotted to allow a better visual comparison between the results.

The type of analyses (*i.e.*, 1D, 2D and 3D models) is not observed to influence significantly the values of θs. This can be attributed to the above-mentioned similarity between the spatial distribution of the computed settlements for each layer, shown in Fig. 3.9. However, the small localized differences in the computed settlement of each layer influence the spatial distribution of the total settlement, hence influencing its θs values.

In the case of the peat layer, the scale of fluctuation θs varies depending on the considered loading scenario: in the case of the double load, the peat layer exhibits higher mean and standard deviation values of θs for all the types of models. This is explained by the fact that in the case of the double load, the peat layer has a higher contribution to the overall

settlements at some specific CPT locations compared to the case of the reference load and the models with no groundwater. This can be a consequence of the low compressibility assigned to the peat layer (Table 3.1), which makes it the stratum that is influenced the most by a change in the applied superficial load.

The values of θt and θs are observed to be in good agreement for all the soil strata.

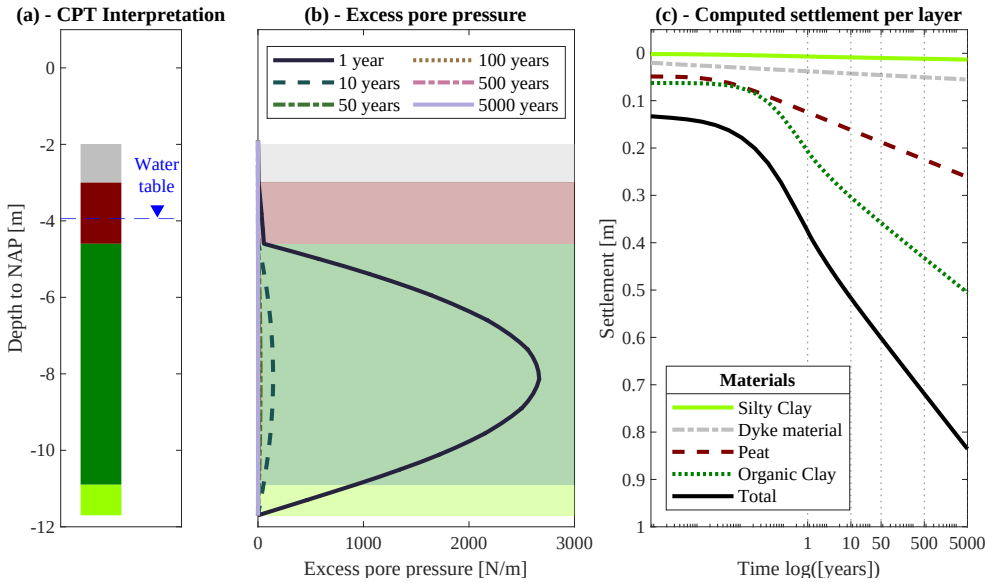

Figure 3.8: An example of the results of one of the 1D models subjected to the reference load: (a) the CPT interpretation and the groundwater level, (b) the development of the excess pore water pressure and (c) the computed settlements against the time.

3.3.3. THE INFLUENCE OF THE DATASET RESOLUTIONS

The settlement of the in-situ specific 1D, 2D and 3D models and the 1D voxel realizations are plotted as distribution to investigate their differences (Fig. 3.1); The distributions are shown for each analysis, each loading condition and each selected time step. Additionally, the values of the mean and coefficient of variation of the distributions are plotted, and they are reported in Table 3.3. Although for each loading scenario, the results of all the models have similar values of mean and dispersion (Table 3.3), their shapes slightly vary: the distribution of the computed settlement of the 3D models resembles a non-symmetric bi-modal distribution, due to the difference between the results of the dyke crest and slope, and the polder area; Conversely, the 1D and 2D models are more akin to unimodal distributions.

The 1D models of the voxel columns present values of the mean and dispersion similar to the ones of the 1D, 2D, and 3D in-situ specific analyses (Table 3.3). In particular, the computed settlement of voxel Column 1, which covers most of the study area (Fig. 3.3a), presents a bi-modal shape similar to the 3D in-situ specific models.

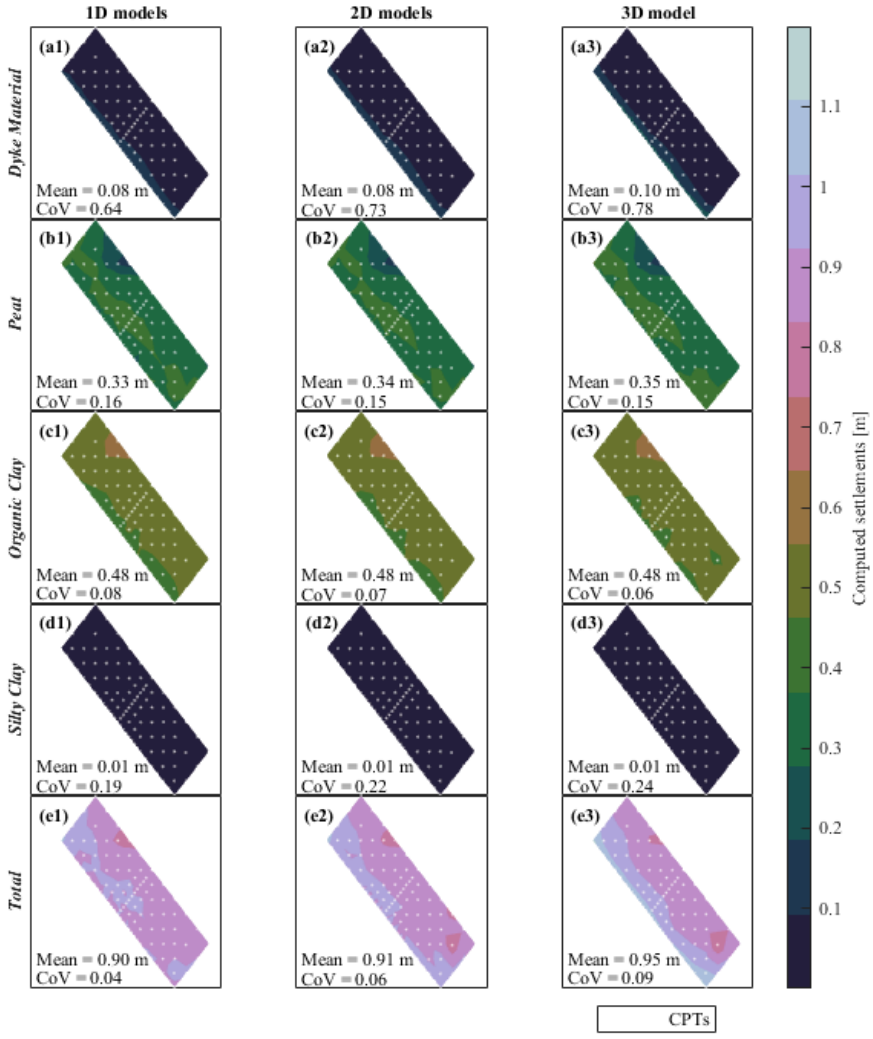

Figure 3.9: The settlement maps derived from the linear interpolation of the final (*i.e.*, 5000 years) settlement computed at each CPT location via the numerical models of the reference load (see Fig. 3.6).

3.4. DISCUSSION

In this study, an area is selected to investigate the lithological heterogeneity and its effects on the settlement occurrence; Toward this aim 1D, 2D and 3D numerical analyses subjected to different loading scenarios are carried out.

The loading conditions represent idealizations, they are not intended to reproduce realistic consolidation scenarios for the study area. Conversely, they enable observing how lithological heterogeneity influences the spatial variation of the computed settlement

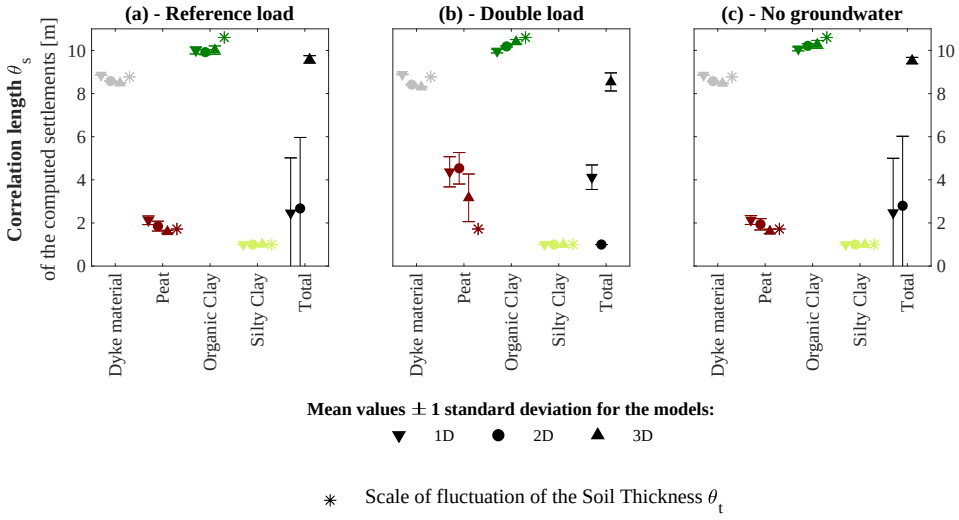

Figure 3.10: Values of the correlation length of the computed settlement of each soil stata for each loading condition. The values correspond to the mean and the standard deviation of θs considering the five time steps, *i.e.*, 1, 10, 50, 500 and 5000 years for: (a) reference load, (b) double load and (c) no groundwater (see Fig. 3.6).

due to different imposed loads. It should be noted that this study mainly focuses on the effects of soil stratification, while more complex loading conditions may further enhance the spatial variation of the computed ground settlements, as reported in [9]. Moreover, the effects of the variability of the hydro-geo-mechanical properties, *i.e.*, inherent spatial soil variability, are purposively neglected to focus on the sole impact of the lithological heterogeneity.

3.4.1. THE VARIABILITY OF THE SOIL THICKNESS

Regarding the scale of fluctuation of the material properties, [1] reported there is always a critical value that can augment differential settlements, that depends on the governing geometrical parameters and conditions of the considered problem. The analyses reported in [11] show that the differential settlement of the adjacent footings bears greater values for the scales of fluctuation ranging from 2 to 6 meters. This study focused on the spatial variability of the lithological conditions rather than the material properties. However, the computed values of the correlation length θt (Fig. 3.7) range between about 1 and 10 meters (Fig. 3.7). Therefore, even though the correlation length addresses herein lithological heterogeneity rather than the variability of the material properties, the values align with the ones reported in [11]. The results provide therefore an indication that the combination of both the spatial variability of the lithological conditions and material properties could enhance the differential settlements even more than the single contributions.

3.4.2. THE VARIABILITY OF THE COMPUTED SETTLEMENTS

The in-situ specific 1D, 2D and 3D numerical simulations enable computing the contribution of each soil layer on the total settlement, and their spatial variability θs, as shown in Fig. 3.10.

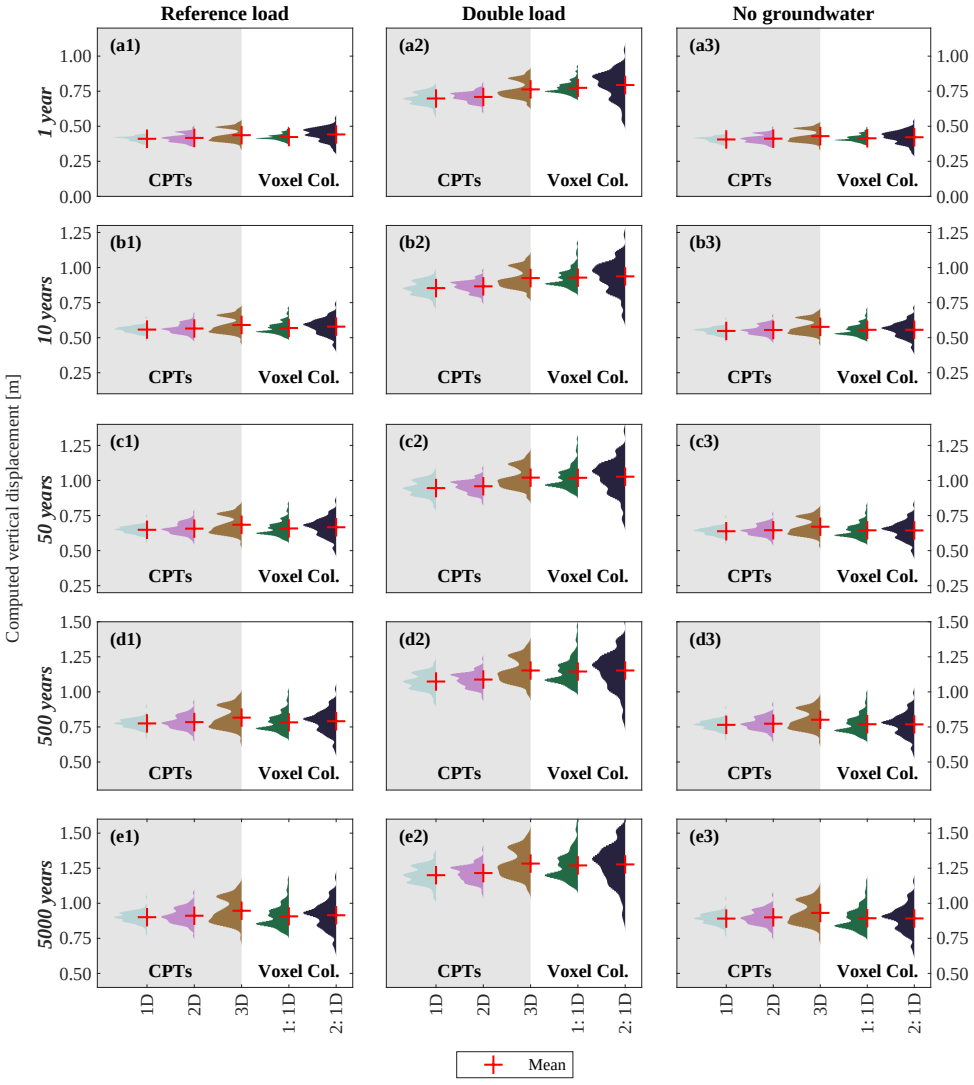

Figure 3.11: Empirical distribution functions of the total settlement computed for all the loading conditions and the numerical models, described in section 3.2.2, for the selected time steps. The distributions show the results at the 100 CPTs locations (Fig. 3.2) and the 100 realizations for two voxel columns (Fig. 3.3). The darker and lighter areas in the plots separate the results for the CPTs and the voxel columns, respectively. The red cross (+) markers show the mean of each distribution.

The computed values of the correlation length θs of all the soil layers do not depend on the groundwater conditions. In the case of the peat layer, the values of θs are observed to vary at different time steps of the model subjected to the doubled load.

For all the soil layers, a good match is observed between the values of θt and θs (Fig. 3.10), pointing toward a relationship between the two parameters; In other words, the analyses reveal that spatial variability of the material thickness of each soil layer matches

Table 3.3: Mean (μ) and coefficient of variation (CoV) values of the computed settlement at the surface level for all the numerical analyses and all the loading conditions. A colour scheme is applied to each parameter, *i.e.* μ and CoV, to distinguish the lowest (dark shades) and the highest (light shades) values.

	Computed settlements [cm] for the different loading conditions									
Reference load										
Time	**1D**		**2D**		**3D**		**Vox. Col. 1 - 1D**		**Vox. Col. 2 - 1D**	
[years]	**μ**	**CoV**	**μ**	**CoV**	**μ**	**CoV**	**μ**	**CoV**	**μ**	**CoV**
1	41	0.05	42	0.07	44	0.10	67	0.03	44	0.10
10	56	0.04	57	0.06	59	0.09	70	0.06	58	0.10
50	65	0.04	66	0.06	68	0.09	67	0.08	67	0.10
500	78	0.04	78	0.06	82	0.09	67	0.09	79	0.10
5000	90	0.04	91	0.06	95	0.09	61	0.13	91	0.10
Double load										
Time	**1D**		**2D**		**3D**		**Vox. Col. 1 - 1D**		**Vox. Col. 2 - 1D**	
[years]	**μ**	**CoV**	**μ**	**CoV**	**μ**	**CoV**	**μ**	**CoV**	**μ**	**CoV**
1	70	0.06	71	0.05	76	0.08	77	0.05	79	0.12
10	85	0.06	87	0.05	92	0.07	93	0.07	94	0.12
50	95	0.05	96	0.05	102	0.07	102	0.07	103	0.11
500	107	0.05	109	0.05	115	0.07	115	0.08	115	0.11
5000	120	0.05	122	0.05	128	0.07	127	0.08	128	0.11
No groundwater										
Time	**CoV**		**2D**		**3D**		**Vox. Col. 1 - 1D**		**Vox. Col. 2 - 1D**	
[years]	**μ**	**CoV**	**μ**	**CoV**	**μ**	**CoV**	**μ**	**CoV**	**μ**	**CoV**
1	41	0.05	41	0.07	43	0.10	41	0.06	42	0.10
10	55	0.04	55	0.06	58	0.09	56	0.07	56	0.10
50	64	0.04	65	0.06	67	0.09	64	0.08	64	0.10
500	76	0.04	77	0.06	80	0.08	77	0.08	77	0.10
5000	89	0.04	90	0.06	93	0.08	89	0.09	89	0.10

the one of their contribution to settlements. In particular, the dispersion (CoV) and spatial variability (θ) of the material thickness are observed to mirror the one of the computed settlements, as observed comparing Fig. 3.7 and Fig. 3.9; This supports the idea that lithological heterogeneity may directly influence the occurrence of differential settlements at the scale of structures, as often seen in practical scenarios, and, in turn, lead to damage.

Further studies that include the presence of the building and its response are recommended to test this conclusion.

The correlation length θs of the total settlement changes depending on the type of model, *i.e.*, 1D, 2D or 3D (Fig. 3.10); In particular, the 3D subsurface models present the highest values with the smallest dispersion. Moreover, 1D models in terms of total settlement (Fig. 3.9a3) are visually more uniform and present less variation compared to the results of the 2D and 3D models (Fig. 3.9a3 to e3 respectively).

In general, 3D models better represent the interaction between the different CPTs, com-

pared to 2D in which the interaction is limited to one of the directions (*i.e.*, x-axis in Fig. 3.5) and 1D models, in which it is excluded. Although in all the analyses the drainage of the excess pore water pressure is allowed only on the top and bottom of the numerical models, as briefly described in section 3.2.2, the excess pore water varies in the x-direction (Fig. 3.5b) in the 2D models, and in the x- and y- direction in the 3D models (Fig. 3.5c). Thus, this leads to the development of different stresses and, in turn, to the difference in the computed settlements. Thus, the 3D models better distinguish the behaviour expected from the different areas of the dyke, as described in section 3.3.3. This observation supports the use of 3D analyses to accurately depict the influence of lithological heterogeneity on similar problems.

3.4.3. COMPARISON BETWEEN THE DIFFERENT RESOLUTIONS

The distributions of the computed settlements of the 3D models resemble asymmetric bi-modal distributions for all the loading conditions and all the selected time steps (Figure 3.11. This effect, as mentioned in the previous section, is related to the different responses of the dyke crest, slope and polder. A similar shape is observed in the case of Voxel column 1. Voxel column 1 may better idealize the in-situ subsoil conditions compared to voxel column 2, as it covers the same area covered by the majority of the CPTs (section 3.2.1). Therefore, the similarities in terms of the shape of the distribution, mean values and standard deviation between the results of the CPTs' models and the voxel models (Table 3.3) may indicate that both resolutions can depict the variability of the settlement in the study area. In other words, the 100 equi-probable realizations of the GeoTOP model at a specific location may provide a picture of the variability of the lithological conditions and, in turn, the variability of the settlement. However, it is important to mention that the 100 realizations differ not only as a result of the soil heterogeneity at a specific area but also due to the modelling assumptions used to derive it, as well as the adopted borehole logs, their number and quality [22], [27]. Thus, although in this analysis the variability of the settlements computed at the scale of single structures is reflected by the variability of the settlements of the Voxel realizations for the study area (see Fig. 3.11), additional analyses are required to further validate this conclusion in other areas.

To allow a consistent comparison, it was required to integrate the engineering judgment in the interpretation of the voxel realizations to better match the in-situ characteristics of the selected study area. The sand litho-classes of the GeoTOP models were herein assumed to have the same hydro-geo-mechanical properties of the superficial soil strata of the dyke (*i.e.*, "dyke material/sand" in Fig. 3.4), as briefly described in 3.3.33.2.1. This step was required to assign the parameters for the numerical simulations (*i.e.*, Table 3.1), and to allow a consistent comparison between the results of the two independent datasets removing the dependency from the material properties.

3.5. CONCLUSIONS

In this chapter, the effects of the in-situ lithological heterogeneity are investigated by employing numerical simulations. The numerical models depict the behaviour of the study area at high (in-situ level, over a very fine grid ranging from 1.25m x 5m up to 5m

x 5m) and low (national level, grid of 100m x 100m) resolutions. The effect of different loading and hydrostatic conditions is herein investigated. Thus, it is observed that:

- A good agreement is observed between the results of the two independent datasets at high (in-situ level) and low (country level) resolution; In particular, the distribution of the settlements computed using the models based on the two datasets agree in terms of mean, spread and shape.
- The values of the correlation length of the computed settlements for each soil strata, derived via numerical modelling based on the available high-resolution information, match the values of the correlation length of the soil thickness. In other words, the spatial variability of the material thickness matches the spatial variability of the soil settlements due to a uniform load, excluding the variation of the material properties.
- The values of the computed correlation length for the ground movements are in the same order of magnitude as the extension of typical structures, *e.g.*, houses, roads and embankments. This confirms how the spatial variability of the soil layers can lead to uneven settlement at the scale of the existing structures, potentially causing (structural) damage.
- In this study, the spatial variability of the lithological variations in the soil stratigraphy is observed to have the same order of magnitude as the one reported in previous studies for the material properties of soil layers. Therefore, the two effects could contribute with the same relevance in augmenting the differential settlements at the scale of structures.
- The spatial variability of the three-dimensional subsurface models better depicts the behaviour of different portions of the study area, compared to the two- and one-dimensional analyses. This suggests that 3D analyses are required to accurately account for the effects of lithological heterogeneity.

The analyses indicate that local variation in the soil stratigraphy can be a source of unevenness in the spatial distribution of the ground settlement. The results of this study are expected to be preliminary for the additional analyses that aim to evaluate the effect of the lithological heterogeneity, combined with the inherent variability of the soil properties, of the buildings resting in areas exposed to the occurrence of ground settlements.

BIBLIOGRAPHY OF CHAPTER 3

[1] D. Breysse, H. Niandou, S. Elachachi, and L. Houy, "A generic approach to soil–structure interaction considering the effects of soil heterogeneity," *Geotechnique*, vol. 55, no. 2, pp. 143–150, 2005.

[2] T. Elkateb, R. Chalaturnyk, and P. K. Robertson, "An overview of soil heterogeneity: Quantification and implications on geotechnical field problems," *Canadian Geotechnical Journal*, vol. 40, no. 1, pp. 1–15, 2003.

[3] M. Uzielli, S. Lacasse, F. Nadim, K. Phoon, *et al.*, "Soil variability analysis for geotechnical practice," *Characterisation and engineering properties of natural soils*, vol. 3, no. 4, pp. 1653–1752, 2007.

[4] L. Houy, D. Breysse, and A. Denis, "Influence of soil heterogeneity on load redistribution and settlement of a hyperstatic three-support frame," *Geotechnique*, vol. 55, no. 2, pp. 163–170, 2005.

[5] R. Popescu, G. Deodatis, and A. Nobahar, "Effects of random heterogeneity of soil properties on bearing capacity," *Probabilistic engineering mechanics*, vol. 20, no. 4, pp. 324–341, 2005.

[6] C. Bauduin, "Uncertainties and their relevance for the design of deep excavations near existing structures," in *Geotechnical problems with man-made and man influenced ground*, 2003, pp. 445–449.

[7] A. L. Costa, S. Kok, and M. Korff, "Systematic assessment of damage to buildings due to groundwater lowering-induced subsidence: Methodology for large scale application in the netherlands," *Proceedings of the International Association of Hydrological Sciences*, vol. 382, pp. 577–582, 2020.

[8] A. Fiamingo, M. Bosco, and M. R. Massimino, "The role of soil in structure response of a building damaged by the 26 december 2018 earthquake in italy," *Journal of Rock Mechanics and Geotechnical Engineering*, vol. 15, no. 4, pp. 937–953, 2023.

[9] D. Peduto, A. Prosperi, G. Nicodemo, and M. Korff, "District-scale numerical analysis of settlements related to groundwater lowering in variable soil conditions," *Canadian Geotechnical Journal*, vol. 59, no. 6, pp. 978–993, 2022.

[10] R. Gibson, "The analytical method in soil mechanics," *Geotechnique*, vol. 24, no. 2, pp. 115–140, 1974.

[11] R. Jamshidi Chenari, S. Pourvahedi Roshandeh, and M. Payan, "Stochastic analysis of foundation immediate settlement on heterogeneous spatially random soil considering mechanical anisotropy," *SN Applied Sciences*, vol. 1, pp. 1–15, 2019.

[12] E. Conte, G. Dente, and A. Troncone, "Settlements of three buildings founded on stratified soils," 2004.

[13] M. Ibrahim and M. Al-Obaydi, "Numerical analysis of a rectangular footing resting on two inclined layers of soil," in *IOP Conference Series: Earth and Environmental Science*, IOP Publishing, vol. 856, 2021, p. 012 039.

[14] N. Krzysztof, "Numerical analysis of settlement of a structure situated on a heterogeneous loess subsoil," in *IOP Conference Series: Materials Science and Engineering*, IOP Publishing, vol. 603, 2019, p. 052 036.

[15] T. de Gast, "Dykes and embankments: A geostatistical analysis of soft terrain," 2020.

[16] T. de Gast, M. A. Hicks, A. P. Van den Eijnden, and P. J. Vardon, "On the reliability assessment of a controlled dyke failure," *Géotechnique*, vol. 71, no. 11, pp. 1028–1043, 2021.

[17] T. de Gast, M. A. Hicks, and P. J. Vardon, *Cone penetration test (cpt) dataset to study soil heterogeneity*, Generic, 2020. DOI: 10.4121/uuid:0a9b77bc-3f6d-40e2-846c-ddb992dd78a6. [Online]. Available: https://data.4tu.nl/articles/dataset/Cone_Penetration_Test_CPT_dataset_to_study_soil_heterogeneity_/12764387.

[18] T. de Gast, P. Vardon, and M. Hicks, "Estimating spatial correlations under man-made structures on soft soils," in *Geo-Risk 2017*, 2017, pp. 382–389.

[19] T. De Gast, P. J. Vardon, and M. A. Hicks, "Assessment of soil spatial variability for linear infrastructure using cone penetration tests," *Géotechnique*, vol. 71, no. 11, pp. 999–1013, 2021.

[20] NEN9997-1+C2:2017nl, "Geotechnisch ontwerp van constructies - deel 1: Algemene regels (geotechnical design of structures - part 1: General rules)," 2017.

[21] P. P. Kruiver, A. Wiersma, F. H. Kloosterman, *et al.*, "Characterisation of the groningen subsurface for seismic hazard and risk modelling," *Netherlands Journal of Geosciences*, vol. 96, no. 5, s215–s233, 2017.

[22] J. Stafleu, D. Maljers, J. Gunnink, A. Menkovic, and F. Busschers, "3d modelling of the shallow subsurface of zeeland, the netherlands," *Netherlands Journal of Geosciences*, vol. 90, no. 4, pp. 293–310, 2011.

[23] J. Stafleu, M. J. van der Meulen, J. L. Gunnink, *et al.*, "Systematic 3d subsurface mapping in the netherlands," *Synopsis of current three-dimensional geological mapping and modelling in geological survey organizations. Alberta Energy Regulator/Alberta Geological Survey, AER/AGS Special Report*, vol. 112, pp. 179–190, 2019.

[24] Bentley, "Plaxis 2d - reference manual 2d," Report, Jun. 2023.

[25] L. S. Wong and S. Somanathan, "Analytical and numerical modelling of one-dimensional consolidation of stabilized peat," *Civil Engineering Journal*, vol. 5, no. 2, pp. 398–411, 2019.

[26] E. Vanmarcke and H. Saunders, "Random fields: Analysis & synthesis," 1985.

[27] J. Stafleu, D. Maljers, F. S. Busschers, J. Schokker, J. L. Gunnink, and R. M. Dambrink, "Models created as 3-d cellular voxel arrays," *Applied Multidimensional Geological Modeling: Informing sustainable human interactions with the shallow subsurface*, pp. 247–271, 2021.

CHAPTER 4

EMPIRICAL INSIGHTS INTO MASONRY STRUCTURES EXPOSED TO SETTLEMENTS: Recurrent settlement patterns and empirically-based fragility curves

This Chapter is a revised version of the study published in [1]. The differences are detailed in Appendix A and in [2].

CHAPTER 4: TABLE OF CONTENTS

4.1 Introduction **85**

4.2 Methodology and Underlying concepts **85**
4.2.1 Data collection and processing 85
4.2.2 Recurrent settlement shapes 88
4.2.3 Receiver operating characteristic (ROC) curves 90
4.2.4 Fragility curves 92
4.2.5 Approach 1 93
4.2.6 Approach 2 93

4.3 Collected building information and settlement intensity parameters **94**
4.3.1 The intensity of the computed settlement parameters . . 95

4.4 Recurrent settlement shapes **98**

4.5 ROC curves **101**

4.6 Empirically-based Fragility curves **102**
4.6.1 Approach 1 102
4.6.2 Approach 2 104

4.7 Discussion **107**

4.8 Conclusions **108**

Bibliography of Chapter 4 . . . . . **113**

4.1. INTRODUCTION

This Chapter provides empirical insight into the behaviour of masonry buildings subjected to subsidence-related settlements. The study focuses on a rich dataset of 386 surveyed masonry buildings, mainly low-rise (terraced) houses built before 1950, which was collected and used for the analysis. Of the total set of buildings, 122 cases rest on shallow foundations and 264 on piled foundations.

The available bed-joint levelling measurements for each surveyed case enabled the determination of building deformation caused by ground settlements. This also allowed for verification of whether current analytical formulations (*i.e.*, Gaussian curves, already adopted for tunnelling, mining and excavation settlements) could fit the data, enabling prediction of the settlement pattern. Accordingly, recurrent settlement patterns were observed.

For each building, the recorded damage is related to the settlement using four different intensity parameters, namely differential settlement, rotation, relative rotation and deflection ratio.

The Receiver Operating Characteristic (ROC) curves are used to evaluate the relative efficacy of the selected hazard parameters.

Two different approaches were used to retrieve fragility curves, where the probability of damage is described as a function of the settlement intensity parameters. Thresholds were set to distinguish between the light damage and the functional and structural damage state.

The chapter begins presenting the methodology and the underlying concepts in 4.2. The results of the data collection are presented in 4.3. Sections 4.4 (Recurrent settlement shapes), 4.5 (ROC curves) and 4.6 (Empirical fragility curves) present and discuss the findings of the analysis. An overall discussion of the method and results of this Chapter is detailed in section 4.7, whereas section 4.8 gathers the main conclusions.

This Chapter presents a revised version of the analyses presented in [1]. The differences and improvements from the original publication are detailed in Appendix A and are further discussed in [2].

4.2. METHODOLOGY AND UNDERLYING CONCEPTS

The procedure followed for the analyses consists of a preliminary data collection phase followed by two analysis phases (Figure 4.1).

4.2.1. DATA COLLECTION AND PROCESSING

In the preliminary phase (Phase 0 in Figure 4.1), damage surveys performed on masonry buildings, typical of the Dutch built heritage, were collected. The field surveys include: i) the measurements of bed-joint levelling along the buildings' walls, ii) the information about the damage documented in the field survey, iii) the foundation system noted (*i.e.* shallow or deep foundation).

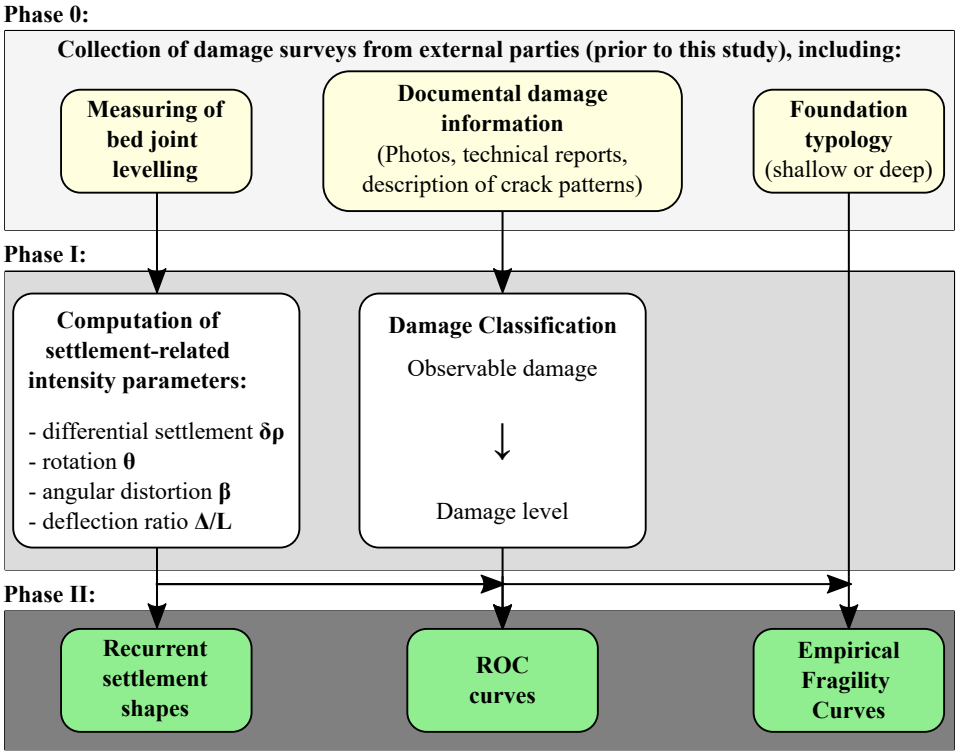

Figure 4.1: Flowchart of the adopted procedure. The definition of the settlement-related intensity parameters are detailed in Fig. 4.2.

In Phase I (Figure 4.1), the collected bed-joint levelling measurements for each building allowed to trace back a displacement profile assumed to correspond to the resulting settlement trough at the foundation level. Four SRI parameters, selected as representative of the intensity of the subsidence phenomena causing the damage to buildings, were computed for each case, according to the original definitions provided by [3], and as illustrated in Figure 4.2 for sagging and hogging examples:

- **Differential** (or **relative**) **settlement** $\delta\rho$, is calculated as the maximum difference in elevation between the recorded settlements;
- The **rotation** (or slope) θ, represents the maximum gradient among the lines connecting two reference points in the settlement profiles;
- The **relative rotation** or **angular distortion** [4] β, refers to the slope of the line joining two consecutive points in relation to the rigid rotation of the structure (or tilt) ω;
- The **deflection ratio** Δ/L, refers to the ratio between the maximum relative deflection and the corresponding length [3], [5], [6].

In other words, the chosen settlement parameters measure the extent of the building's

deformation. These parameters were used to establish the relationship between settlement and building damage in Phase II (Figure 4.1), as outlined in the following sections. Additionally, analyses were conducted to identify the most effective parameters for distinguishing "undamaged" cases from buildings that show signs of damage.

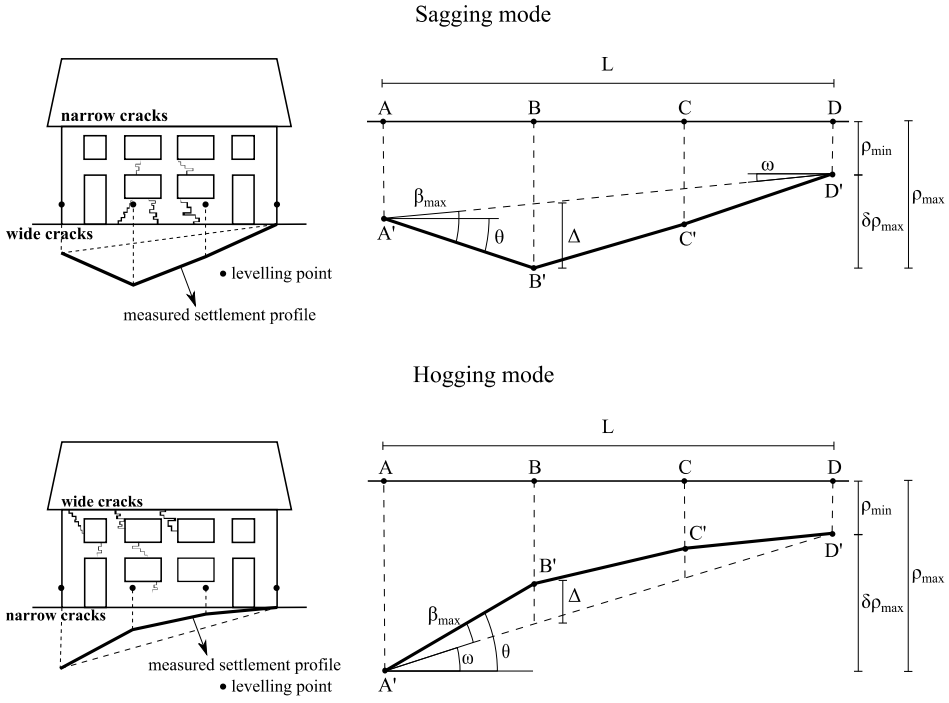

Figure 4.2: Typical building damage for sagging and hogging profiles and the definitions of the settlement parameters: maximum settlement ρ_{max}, minimum settlement ρ_{min}, differential settlement $\delta\rho_{max}$, rotation θ, relative rotation (or angular distortion) β, deflection Δ, deflection ratio Δ/L and tilt ω.

The damage severity of masonry buildings undergoing ground movements is typically assessed with the classification proposed by [7], later integrated by [8] and at its latest by [9] and [10] (Table 4.1) based on the ease of repair and the cracks' width as described in section 2.5.5 of this thesis. Three damage groups were considered (Table 4.1):

- "**No Damage**" or "**Undamaged cases**" to cases with no significant visible damage. Since visible damage is used as the criterion, this group may also include cases where damage exists but is not visible, such as when cracks are narrower than 0.1 mm.

- "**Light damage**" refers to aesthetic damage characterized by very fine/fine cracks up to 5 mm. The decision to categorise the initiation of light damage from a crack width of 1.0 mm upwards is related to the detectability of cracks on real structures during manual surveys.

- "**Moderate to severe damage**" implies moderate and severe damage that could affect the serviceability of the building or be associated with a risk to structural safety.

Table 4.1: Damage scale with the classification of visible damage based on ease of repair and the crack width (from [7]–[10]).

Category of damage	Damage class	Approximate crack width	Ease of repair	This study:
Aesthetic damage	Negligible	up to 0.1 mm	-	No Damage
	Very slight	up to 1 mm	Fine cracks which can easily be treated during normal decoration.	Light Damage
	Slight	up to 5 mm	Cracks easily filled. Re-decoration probably required. Some re-pointing may be required.	
Functional damage, affecting serviceability	Moderate	5 to 15 mm	The cracks require some opening up and can be patched by a mason. Re-current cracks can be masked by suitable linings. Repointing of external brickwork and possibly a small amount of brickwork to be replaced.	Moderate to severe damage
	Severe	15 to 25 mm	Extensive repair work involving breaking-out and replacing sections of walls, especially over doors and windows.	
Structural damage, affecting stability	Very Severe	Higher than 25 mm	This requires a major repair job involving partial or complete re-building.	

Accordingly, In Phase I (Figure 4.1) the collected hardcopies and information for each building in the dataset were used to assign the observed damage severity level.

The decision to consider three damage groups rather than the six damage classes (*i.e.* "Negligible" to "Very Severe" in Table 4.1) proposed by [7] is related to the availability of information: while for some buildings in the dataset manual measurements of the cracks' width were collected, for the rest only the reports or photos of the recorded crack patterns on the façade were available, from which it is challenging to objectively measure the width of each crack. Therefore, this study focuses on damage groups that align with the available data, potentially combining different damage classes (4.1).

4.2.2. RECURRENT SETTLEMENT SHAPES

Thanks to the availability of levelling measurements along the walls of the buildings in the dataset, analyses were carried out (Figure 4.1) to investigate the shapes of the settlement displacements for the buildings' dataset in Phase II (Fig. 4.1). The following method is used to verify the similarity between the measured displacements of each wall and the shapes computed with an analytical formulation:

1. First, all the settlement profiles have been made dimensionless to allow the comparison of the shapes among buildings with varying lengths.

2. Eight settlement shapes (Figure 4.3) were then computed from a Gaussian curve [11], described by equation 4.1, to idealize the observed recurrent bed joint measurements. The shapes were defined based on preliminary empirical observations of the collected wall deformations.

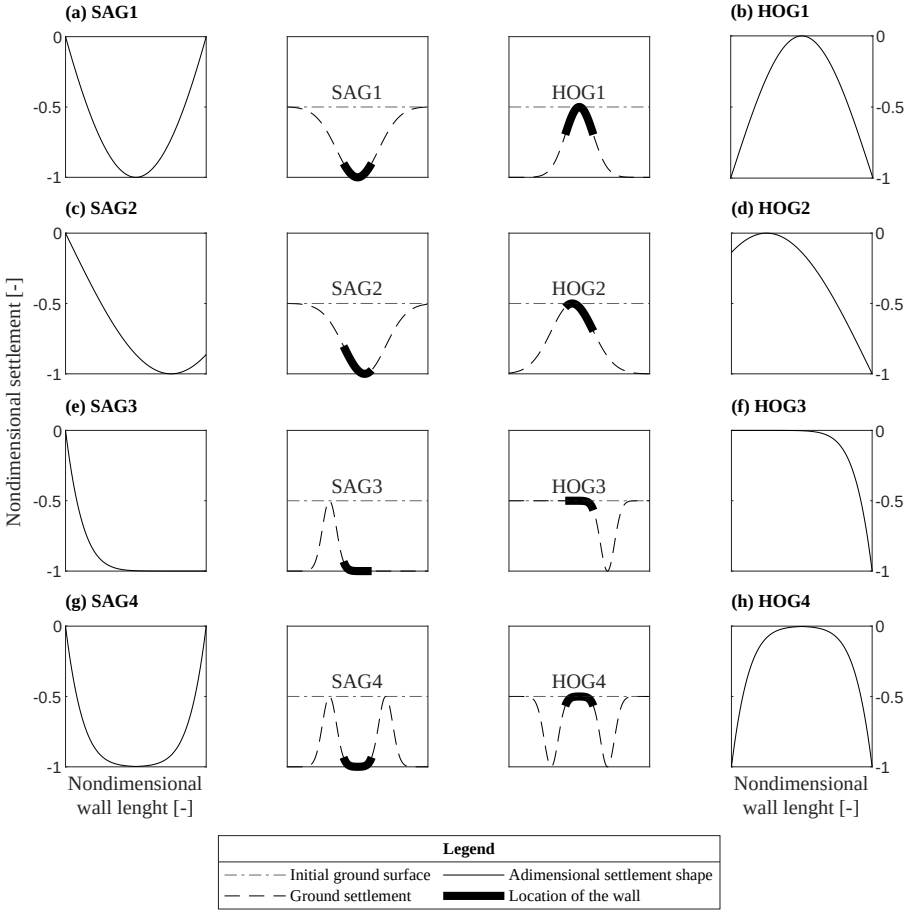

Figure 4.3: The selected settlement shapes, conformed to a Gaussian distribution that idealizes the most recurrent bed joint levelling measurement shapes, based on the visual observation: (a), (c), (e) and (g) idealize four settlement profiles while (b), (d), (f) and (h) the hogging ones. All the profiles are computed by means of equation 4.1 by varying the position of the wall x and the distance of the inflection point xi.

$$S_v(x) = (-1)^i e^{\left(\frac{-(x-D_x)^2}{2x_i^2}\right)} \tag{4.1}$$

Where "x" is the horizontal distance between the left and right sides of the wall; "D_x" is the distance between the symmetric axis of the Gaussian curve and the left side of the wall; "x_i" is the distance from the symmetric axis of the curve to the point of inflection. The parameter "ι" enables controlling the convexity of the Gaussian curve.

Table 4.2: Parameters adopted in equation 4.1 to generate the settlement shapes. The values of D_x and x_i should be multiplied by the length of the wall, which is unitary for the shapes shown in Figure 4.3. The shapes "SAG4" and "HOG4" correspond to the profiles "SAG3" and "HOG3" respectively, with the high distortion parts of the SAG3 and HOG3 curves mirrored (see fig:fig 4.4).

Settlement name	Convexity - ι	xi	Dx
SAG1	1	0.5	0.5
SAG2	1	0.75	0.75
SAG3	0	0.25	-0.5
SAG4	0	0.25	-0.5
HOG1	0	0.5	0.5
HOG2	0	0.75	0.25
HOG3	1	0.25	1.5
HOG4	1	0.25	1.5

The values of the parameters used in equation 4.1 are reported in table 4.2.

3. The settlement shapes computed with equation 4.1 have been made dimensionless as the bed-joint levelling measurements of the surveyed walls: Figure 4.3 shows that the selected settlement shapes have y-coordinates that go from -1 to 0.

4. For each settlement profile of the surveyed walls, the coefficient of determination R^2 was calculated with equation (4.2) for each of the j-th defined representative shapes:

$$R_j^2 = 1 - \frac{\sum_i \left(y_i - f_{i,j}\right)^2}{\sum_i \left(y_i - \overline{y}\right)^2} \tag{4.2}$$

where "y_i" is the vertical displacement of the i-th point, "$\overline{y}_i$" represents the mean settlement value of each dimensionless bed-joint profile and "$f_{i,j}$" is the vertical displacement of the i-th point for the j-th proposed settlement profile (Figure 4.3).

5. The R^2 of the fit to a horizontal line passing through the average values of each settlement profile was computed to check the reliability of the procedure. Accordingly, the settlement profile of each wall was sorted as one of the eight proposed shapes by selecting the maximum R^2 among the computed ones.

4.2.3. RECEIVER OPERATING CHARACTERISTIC (ROC) CURVES

Receiver operating characteristic (ROC) curves represent a useful tool to compare the predictor efficiency of different parameters for the same expected outcome and to find

optimum thresholds [12]. In the context of building damage, ROC curves can be used to assess how a parameter correlates with damage.

The ROC-curve technique has been used in structural health monitoring applications, geotechnical and seismic engineering [13]–[15]. ROC curves can be used to compare the predictor efficiency of different intensity parameters for which fragility curves are derived (*e.g.* in [15]).

For a binary classification problem characterized by the distributions of "positive" (*i.e.*, damaged cases) and "negative" (*i.e.*, undamaged cases), a cut-off (or threshold) value allows segregating the observations in one of the two distributions (Figure 4.4a). The accuracy of the classifier depends on the selected cut-off value defining four possibilities: a true positive (TP) representing a case both classified and observed as positive; a true negative (TN) referring to a negative outcome of both the prediction and observation; a positive prediction that fails in reality is referred as false positive (FP); and, on the other hand, a false negative (FN) refers to a negative prediction associated with a positive observation. The observed and the predicted binary results can be summarized in a two-by-two contingency table, as shown in Table 4.3 [13].

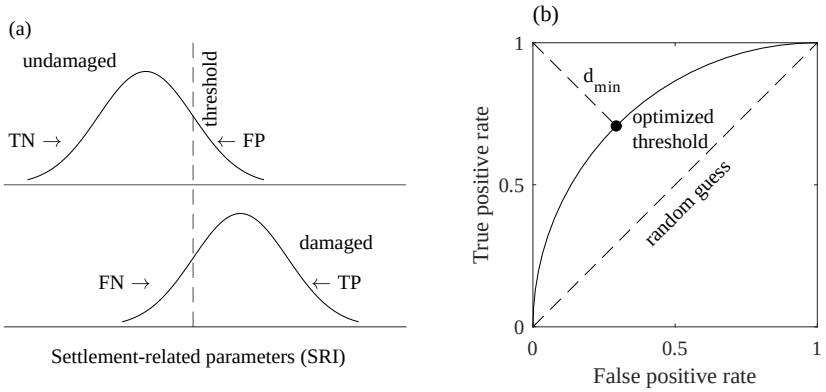

Figure 4.4: Explanatory illustration of ROC curve: (a) distribution of undamaged and damaged cases as a function of the settlement-related parameter; (b) conceptual ROC curve, the optimized threshold value is determined using the closest-to-(0,1) criterion [16], which identifies the sensitivity pair that is at the minimum distance (d_{min}) from the perfect classifier (0,1).

Table 4.3: Contingency table.

		Predicted		
		Undamaged (-)	**Damaged (+)**	**Total**
Observed	**Undamaged (-)**	TN	FP	O (-)
	Damaged (+)	FN	TP	O (+)
	Total	P (-)	P (+)	N

Accordingly, in Table 4.3, O(-) defines the total number of negative observations and O(+) the positive ones, while P(-) and P(+) respectively stand for the total number of negative and positive predictions.

ROC curves are plotted with the true positive rate (TPR) versus the false positive rate (FPR). Each point of a ROC curve represents the performance of the classifier for a given value of the threshold and it is defined by a sensitivity-pair (TPR versus FPR). The values of the TPR and FPR can be calculated using eq. (4.3) and (4.4):

$$TPR = \frac{TP}{O(+)} \tag{4.3}$$

$$FPR = \frac{FP}{O(-)} \tag{4.4}$$

The ROC analysis was performed for each of the four SRI parameters. In particular, the diagnostic test was performed considering the binary results, undamaged (referred to as "negative" results) and damaged (*i.e.*, cumulative of the buildings with "light" or "moderate to severe" damage, referred to as "positive" results), for the N cases, further subdivided by the foundation type.
In other words, the two subsets of buildings with either shallow or piled foundations were categorized into "no damage" and "damaged" with the latter group combining buildings with "light" or "moderate to severe" damage. ROC curves were then used to evaluate how effectively each computed settlement parameter (predictors) distinguished cases with damage from those without.

4.2.4. FRAGILITY CURVES

Fragility curves are statistical tools that retrieve the relationship between a hazard intensity parameter and the damage severity for a given structural typology [17]. Fragility curves display the probability of reaching or exceeding damage (or a specific degree of damage) as a function of a settlement intensity parameter. One of the most adopted analytical models used in the literature for empirical data is described in equation (4.5) in the form of a two-parameter lognormal distribution function. Such distributions are not only well established in the state of the art, but also they show a zero probability of producing negative or null SRI parameters [18]. In other words, fragility curves that follow a lognormal distribution do not provide a probability of damage for negative values of the intensity parameters, as they would have no physical interpretation.

$$F(SRI_i, \zeta_i) = \Phi\left[\frac{1}{\zeta_i} \ln\left(\frac{SRI_i}{\overline{SRI}_i}\right)\right] \tag{4.5}$$

where:

$\overline{SRI}_i$	is the median of the lognormal distribution;
ζ_i	is the standard deviation (or dispersion) of the lognormal distribution;
$\Phi[\bullet]$	is the standardized normal distribution function.

Two methods are adopted to obtain the parameters of the fragility curves, and are detailed in the following.

4.2.5. APPROACH 1 [1]

In Phase II (Figure 4.1) the parameters $\overline{SRI}_i$ and ζ_i of the lognormal distribution described in Eq. 4.5 were estimated using a non-linear fitting procedure, dividing the buildings according to the foundation system:

1. First, the exceedance probability distributions are obtained by counting the number of buildings reaching or exceeding each damage state (*i.e.*, "light damage" and "moderate to severe damage"), in relation to the total number of cases, for increasing values of each SRI parameter.

2. Then, the fragility parameters $\overline{SRI}_i$ and ζ were computed by fitting the cumulative probability functions by means of a non-linear Least Squares Estimation (LSE) [19]–[21], through the iterative Levenberg-Marquardt algorithm. The fitting procedure was carried out with a MATLAB algorithm, where lower bounds are imposed for both $\overline{SRI}_i$ and ζ to avoid negative values.

4.2.6. APPROACH 2

The procedure proposed by [22] is often adopted in the literature to retrieve the parameters $\overline{SRI}_i$ and ζ_i of the lognormal distribution described in equation 4.5.

The maximum likelihood (ML) method is used to estimate the parameters. The procedure assumes a unique ζ value for the different damage levels, avoiding the intersection of the fragility curves [23]. First, the likelihood function "$\mathcal{L}$" is determined as (Eq. 4.6) [24]:

$$\mathcal{L}(\overline{SRI}_i,\zeta) = \prod_{j=1}^{N}\prod_{i=0}^{k} {P_i}^{y_{ij}}\left(SRI_j;D_i\right) \tag{4.6}$$

Where:

P_i is the probability that the *j-th* building from the sample is at damage level Di when subjected to the SRI_j parameter value; "j" varies between 0 and "N" in the total number of buildings.

D_i indicates the considered damage severity level with "i" falling in the range of 0 to k (k equal to 0, 1, 2 for "no damage", "light" and "moderate to severe damage" in this study);

y_{ij} is equal to 1 if damage level Di occurs for the *j-th* building subjected to intensity value SRI_j; equal to 0 otherwise.

The maximum likelihood estimates of the parameters of the fragility function are obtained by solving the equations in 4.7 to maximise the likelihood function [22]:

$$\frac{\partial ln\mathcal{L}\left(\overline{SRI}_i,\zeta\right)}{\partial\overline{SRI}_i} = \frac{\partial ln\mathcal{L}\left(\overline{SRI}_i,\zeta\right)}{\partial\zeta} = 0 \tag{4.7}$$

[1] This approach was adopted in the published article [1]

4.3. COLLECTED BUILDING INFORMATION AND SETTLEMENT INTENSITY PARAMETERS

In the preliminary phase (Figure 4.4) the information from 386 field surveys over different Dutch provinces was collected into a database in MATLAB [25]. Each building corresponds to one database item, then categorized according to the recorded foundation system, including 122 buildings on shallow foundations and 264 on deep (piled) foundations. Additionally, information was retrieved from the available Addresses and Buildings Key Register (*Basisregistraties Adressen en Gebouwen (BAG)* in Dutch), allowing the retrieval and integration of the year of construction, into the surveys' information.

The masonry buildings were manually classified according to four typologies proposed in [26], based on the structural features and the adjacency with other structures. A schematic illustration of the selected building typologies is shown in Figure 4.5:

- **Unit House** (**UH**) in Figure 4.5a, refers to freestanding houses, (*e.g.* a single detached house) with an independent foundation system.
- **Block Unit Single** (**UBHS**) in Figure 4.5b, refers to a single building part of a homogeneous block (*e.g.* a single address of a block of row houses, or a part of a semi-detached house).
- **Block Unit Multiple** (**UBHM**) in Figure 4.5c, refers to a homogeneous building block, with the same foundation system (*e.g.* a block of row houses).
- **Others** (**OTH**) in Figure 4.5d, refers to cases not classified in the previous 3 categories (*e.g.* sheds or warehouses).

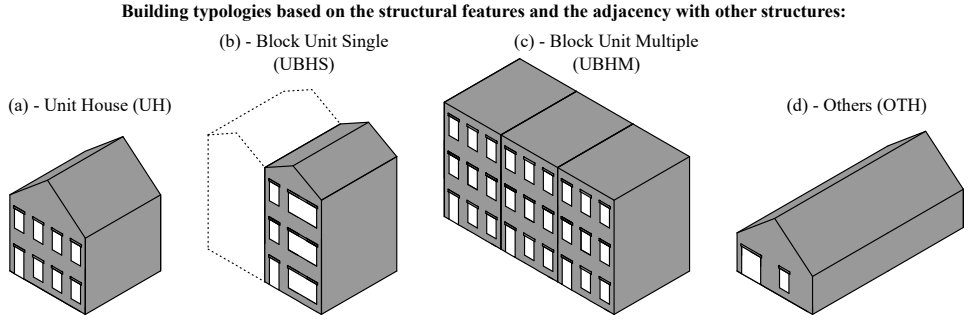

Figure 4.5: A schematic illustration of the selected building typologies based on the structural features and the adjacency with other structures: (a) Unit House (UH), (b) Block Unit Single (UBHS), (c) Block Unit Multiple (UBHM), and (d) Others (OTH).

A summary of all the available information is gathered in Table 4.4 in relation to their location (province). Most of the buildings were built between or right after 1900 and 1950. Moreover, all the buildings were observed to present similar structural features (*i.e.*, geometry, number of floors, etc.) based on the available information, and they are therefore assumed to be built using the same construction methods. Ideally, the

analysis herein presented may be enhanced by further classifying the buildings based on other features, such as the type of masonry and thickness of the walls, for instance. Such information was not available for all the cases in the buildings' sample. Moreover, further subdivisions would have resulted in samples too small to be considered in a probabilistic framework. Therefore, this study focuses on the distinction between buildings on shallow or deep foundations. Of the total set of 386 buildings, 269 cases were classified as UBHM, 44 as UBHS, 58 as UH and the remaining 15 could not be sorted into one of the defined typologies.

Table 4.4: Summary of building data for some provinces distinguished by foundation type, building typology and year of construction.

Province	Foundation type		Building typology (see Figure 4.5)				Year of construction (y)			
	Shallow	Deep	UH	UBHS	UBHM	OTH	y ≤ 1900	1900 <y ≤ 1950	1950 <y ≤ 2000	y > 2000
South-Holland	83	206	0	27	262	0	0	289	0	0
North-Holland	2	18	3	11	44	2	3	6	11	0
Utrecht	25	38	44	5	3	11	11	15	34	3
Other	12	2	11	1	0	2	0	10	4	0
Total	122	264	58	44	269	15	14	320	49	3

The buildings' dataset herein proposed, as any sample of structures collected to address post-disaster analyses, may not represent a random sample. In a truly random sample, every building in the Netherlands would have an equal chance of being selected and surveyed for analysis. Instead, the sample in question consists of cases gathered through desk research of damage information from various surveyors. Therefore, this sample could be categorized as a "convenience sample," which is susceptible to sampling errors and do not represent the behaviour of the entire population of buildings.

An example of the information collected for the buildings in the dataset is shown in Figure 4.6, including the levelling measurements and the damage information. Pictures of damage and the technical notes available in the collected reports have been used to assign to each building in the dataset a damage level, according to the approach discussed in section 4.2.1.

4.3.1. THE INTENSITY OF THE COMPUTED SETTLEMENT PARAMETERS

In Phase I (Figure 4.1), the level of masonry bed joints, assumed to have been built perfectly horizontally, has been used to decipher settlement profiles on the walls of buildings. Four SRI parameters were computed for each building from the settlement profiles and related to the assigned damage level, according to the methodology described in 4.2. In the case of buildings with multiple surveyed walls, the SRI parameters refer to the maximum among any of the walls.

From the work published in [27], the damage and foundation information of 262 cases in Schiedam, jointly with the available bed-joint measurements from an in-situ campaign

Levelling measurements:

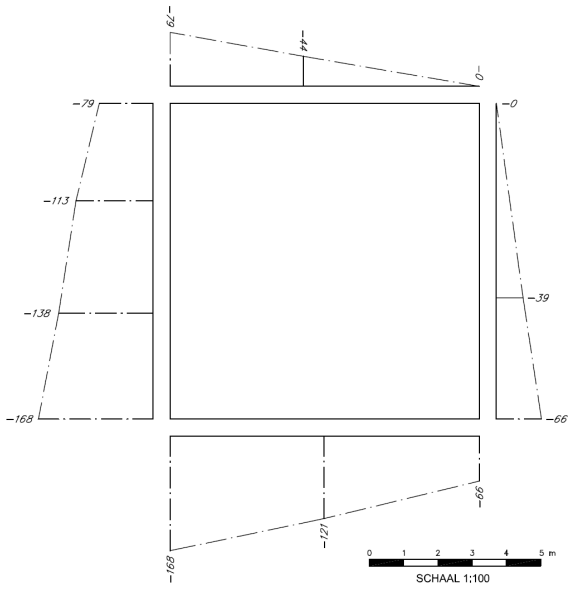

Pictures of damage:

Technical notes (originally in Dutch):

- Building in fair to poor structural condition;
- Significant visible cracking;
- Cracking near building corners is associated with relative rotation of walls;
- Cracking above lintels may also be partly related to temperature effects;

Figure 4.6: An example of the levelling measurements, pictures of damage and technical notes for one of the buildings in the collected dataset.

carried out during the year 2003, a decade earlier.

In Figure 4.7, box plots are used to display the median (crosses), the interquartile range (the height of each rectangle) and the upper and lower bounds for each SRI parameter and each damage severity group.

The box plots in Figure 4.7 illustrate that for buildings with shallow foundations (Fig. 4.7c, e, and g), the extent of damage generally increases as the mean of the selected SRI parameters increases, with the exception of differential settlements (Fig. 4.7a). This trend also holds true for buildings with piled foundations, although the increase in damage is notably more gradual (Fig. 4.7b, d, f, and h). The subsample of buildings on piles is associated, on average, with lower median values of the SRI parameters compared to buildings on shallow foundations, for all the damage levels.

It should be highlighted that in both cases, the number of buildings classified as “Moderate to Severe Damage” is small (23 and 11 cases for shallow and piled foundations

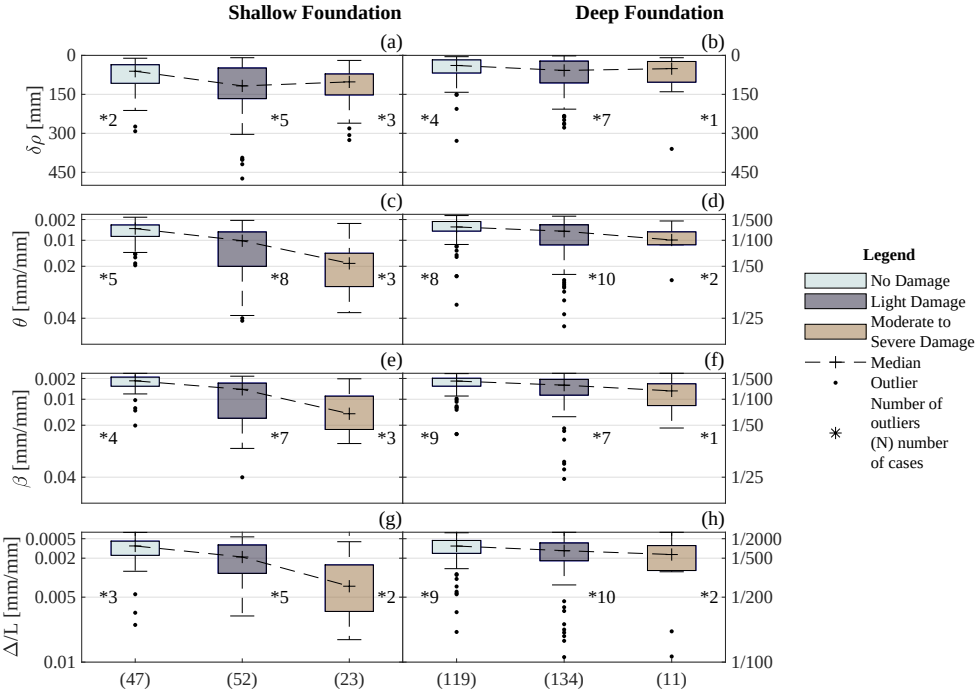

Figure 4.7: Box plot of damage level vs. settlement-related intensity parameters for (a), (c), (e) and (g) for shallow and b), d), f) and h) for deep foundations. The damage level generally increases as the selected SRI parameters increase.

respectively) compared with the other two damage levels. The relatively small sample size may therefore affect the reliability of the analyses for that damage level.

4.4. RECURRENT SETTLEMENT SHAPES

The shapes of the wall displacements for the building's dataset based on the bed-joint levelling measurements were compared with the idealized shapes discussed in 4.2.2.

The settlement profiles were sorted as one of the eight proposed shapes by selecting the maximum R^2 among the computed ones. In particular, among 615 surveyed walls, 116 cases were automatically excluded from the sorting procedure, because the maximum R^2 value was lower than 0.25 or because the profiles could not be sorted into one of the defined shapes. The 499 sorted settlement profiles and their average profile are shown for both sagging (Figure 4.8) and hogging shapes (Figure 4.9), further divided by the foundation system.
The analysis reveals how the most recurrent settlement shapes are associated with both deformations and an overall tilt (SAG2 in Figure 4.8b3 and HOG2 in Figure 4.40b3). Symmetric settlement shapes without tilt are less recurrent, as for SAG1 and SAG4 for Figure 4.8a3 and d3 and HOG1 and HOG4 for Figure 4.40a3 and b3. These findings with the observation by [28], which states *"In most practical situations, settlement will cause both distortion and tilt"* referring to sagging and hogging profiles with a non-uniform tilt.

It should be noted that Gaussian curves are used to fit the displacements measured on the walls, while the ground surface displacements might differ. It is widely known that buildings can flatten soil deformations due to soil-structure interaction (see section 2.5.4). Nevertheless, this aspect is expected to affect the difference between the distortions measured on the soil surface and the building, but the shape of the settlement pattern and its spatial distribution should be similar in both cases. In other words, if the wall displacements conform to Gaussian curves, the soil surface is likely more pronounced to exhibit a similar spatial distribution.

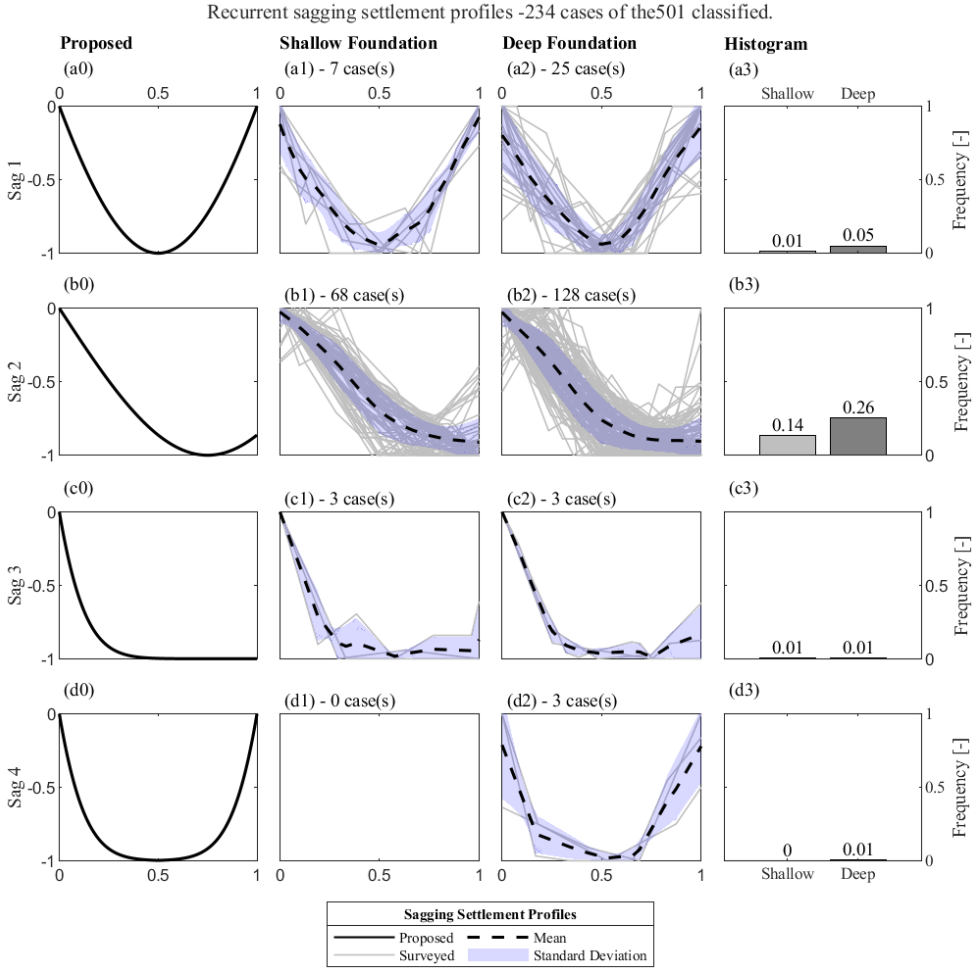

Figure 4.8: Non-dimensional sagging settlement profiles of the considered surveyed buildings: from (a0) to (d0) Proposed settlement profiles (Figure 4.3a,c,e and g); Settlement profile for: from (a1) to (d1) for buildings on shallow foundations, and from (a2) to (d2) for buildings on deep foundations. The number of cases for each foundation system is indicated on top of each bin from (a3) to (d3).

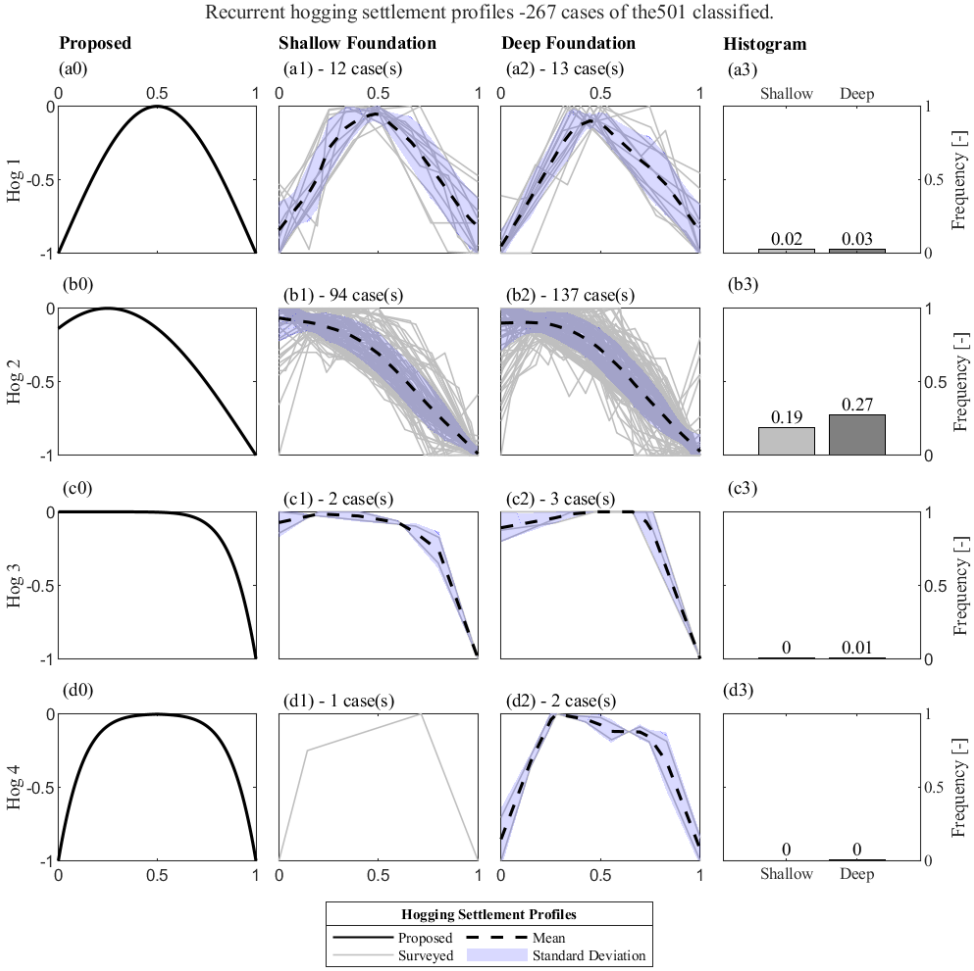

Figure 4.9: Non-dimensional hogging settlement profiles of the considered surveyed buildings: from (a0) to (d0) Proposed settlement profiles (Figure 4.3b,d,f and h); Settlement profile for: from (a1) to (d1) for buildings on shallow foundations, and from (a2) to (d2) for buildings on deep foundations. The number of cases for each foundation system is indicated on top of each bin from (a3) to (d3).

4.5. ROC CURVES

The ROC analyses conducted for each of the selected SRI parameters enabled the assessment of their effectiveness in predicting the damage. For each SRI parameter, the ROC curve was retrieved by computing the sensitivity pairs associated with values of the cut-off ranging from 0 and the maximum value of the considered SRI recorded in the database, per foundation type.

As shown in Figure 4.10 (with a black dot), in each ROC curve the sensitivity-pair with the highest distance from the diagonal line represents the optimized estimate of the threshold value that better predicts the binary outcome, determined using the closest-to-(0,1) criterion [16]. Accordingly, for each foundation typology, the AUC scores of the ROC curves for the selected SRI have been compared; the highest values for AUC scores are the ones retrieved, in order, for the rotation θ, the relative rotation β, and the deflection ratio Δ/L for both the foundation typologies. The differential settlement $\delta\rho$ is associated with the lowest AUC scores for building on shallow and deep foundations (Figure 4.10a and b).

Thus, based on the outcome of the ROC analyses herein presented the rotation θ and the angular distortion β are the best parameters to segregate "undamaged" cases from buildings that exhibit damage.

Regarding the values of the optimized threshold, these are observed to be relatively high if compared with the threshold proposed in the international standards. For instance, the Eurocode [29] proposes a value of angular distortion equal to 1/150 to avoid the occurrence of the ultimate damage state, whereas the thresholds obtained herein range between 1/273 and 1/210. This aspect is also discussed in the following and in detail in section 4.7.

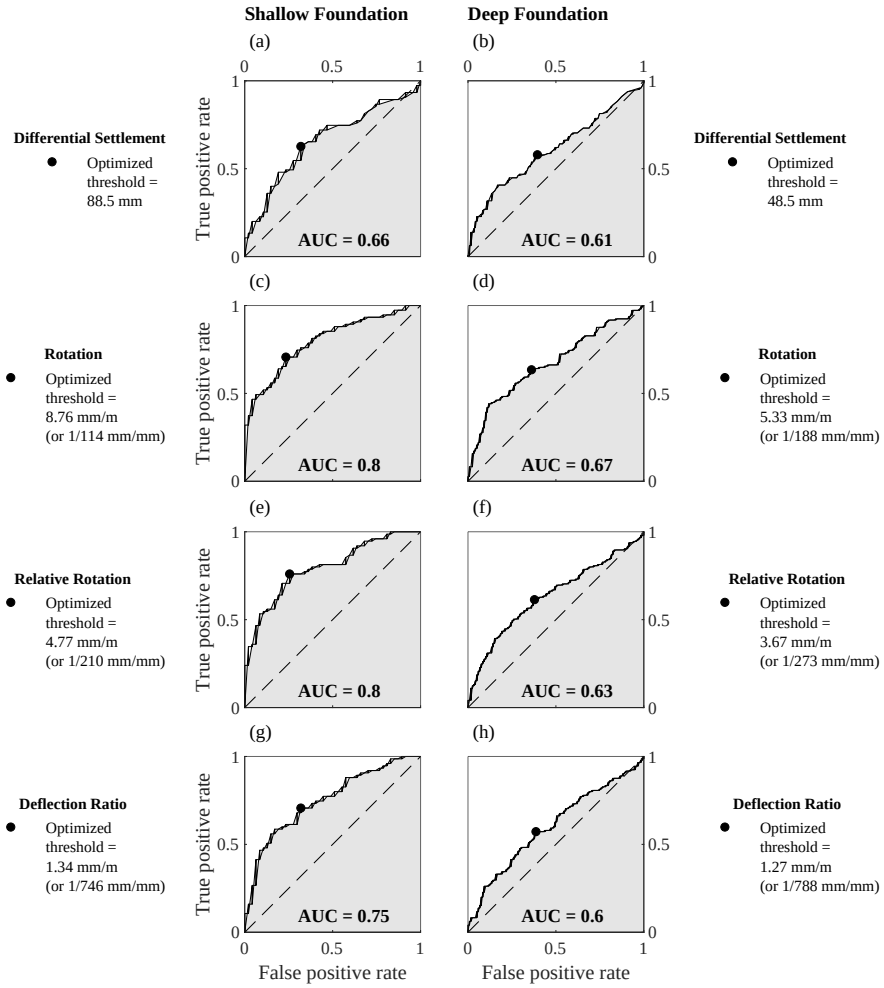

Figure 4.10: ROC curves for the selected SRI parameters (a), (c), (e) and (g) for shallow and b), (d), (f) and (h) deep foundations. Each SRI parameter varies between 0 and the maximum recorded value. The black dot shows the best sensitivity-pair. The shaded area represents the Area Under the Curve (AUC).

4.6. EMPIRICALLY-BASED FRAGILITY CURVES

4.6.1. APPROACH 1 [2]

In Phase II (Figure 4.1) the cumulative density functions of each damage level relative to the total number of cases and for each computed SRI parameter and foundation system were determined. The fragility curves shown in Figure 4.11a, c, e and h for buildings on shallow foundations and Figure 4.11b, d, f and h for buildings on deep foundations were retrieved by means of the non-linear least square fitting, according to the methodology described in 4.2.5. The estimated $\overline{SRI}_i$ and ζ parameters for each fragility curve are reported in Table 4.5.

[2]The difference between the results in this section and the published version [1] are detailed in Appendix A.

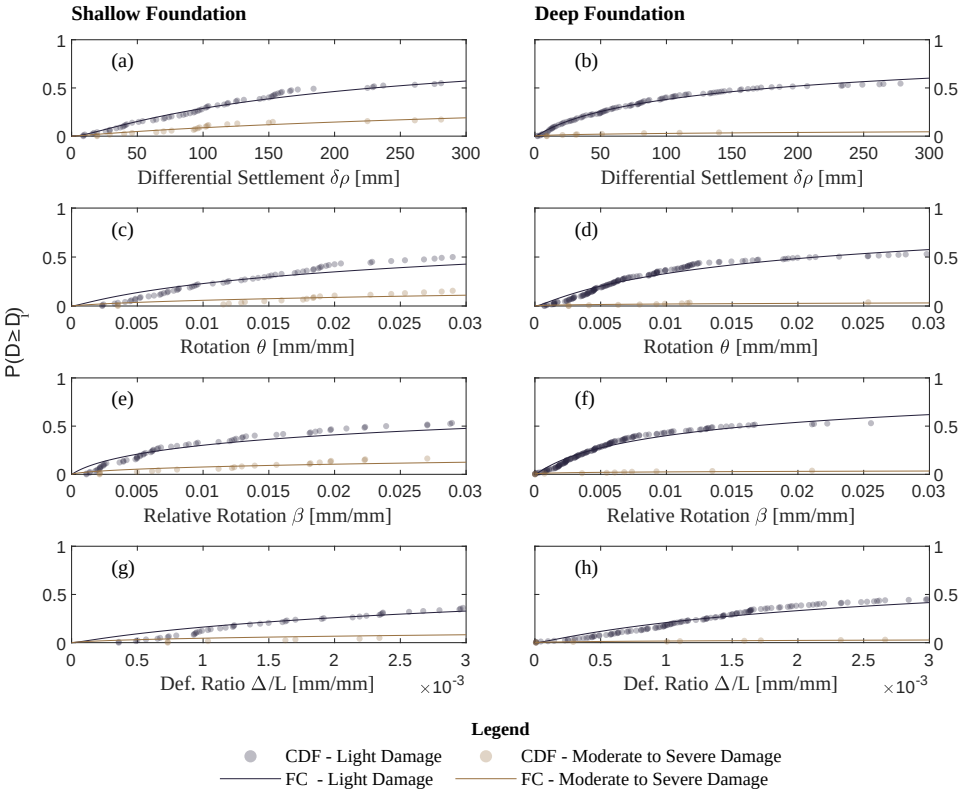

Figure 4.11: Fragility curves of buildings resting on shallow and deep foundations for all the SRI parameters obtained with "Approach 1" (section 4.2.5).

The proposed fragility curves reflect the behaviour of the buildings in the collected dataset: for instance, for a value of angular distortion equal to 2 ‰(or 1/500) the probability of light damage for buildings on shallow foundations is equal to 12%, whereas 15% for buildings on piled foundations. Such limit value of angular distortion is suggested in the Eurocode [29] as "*acceptable for many structures*". Therefore, the probabilities appear to align with this observation. Nevertheless, in the Eurocode, it is also stated that "*the relative rotation likely to cause an ultimate limit state is about 1/150.* For such a value of angular distortion, the probability of moderate to severe damage for buildings on shallow foundations is equal to 6%, whereas 2% for buildings on piled foundations. In other words, low probabilities of severe damage are observed, and this is not in agreement with the limit value proposed in the Eurocode. This can be the result of two different aspects:

- The surveyed buildings exhibit, on average, high values of displacements and distortions; Cases associated with low displacement and distortion are limited.
- Many buildings with high values of displacements and distortions are not associated with observable damage.
- The fragility curves determined with Approach 1 (section 4.2.5) strongly depend

on the number of cases collected for each damage level, *i.e.*, "undamaged", "light damage" and "moderate to severe damage".

Table 4.5: Median $\overline{SRI}_i$ and Standard deviation ζ of the lognormal distribution obtained with Approach 1 (section 4.2.5) for each considered settlement parameter distinguished by foundation type and damage level.

Parameter	Damage level	Shallow foundations		Deep foundations	
		$\overline{SRI}$	ζ	$\overline{SRI}$	ζ
$\delta\rho$ [mm]	Light	115	2.28	180	1.99
	Moderate to severe	4.51×10^{3}	3.42	7.43×10^{6}	5.96
θ [mm/mm]	Light	4.32×10^{-2}	2.45	2.94×10^{-2}	2.11
	Moderate to severe	6.95	4.63	109	4.81
β [mm/mm]	Light	3.79×10^{-2}	2.65	2.33×10^{-2}	2.53
	Moderate to severe	8.61	4.98	451	5.86
Δ/L [mm/mm]	Light	7.97×10^{-3}	2.28	6.14×10^{-3}	2.23
	Moderate to severe	2.83	5.23	176	5.97

The above-mentioned factors affect the shape of the fragility curves, and in turn the probabilities of damage.

4.6.2. APPROACH 2

The fragility curves shown in Figure 4.12a, c, e and h for buildings on shallow foundations and Figure 4.12b, d, f and h for buildings on deep foundations were retrieved by means of the approach described in 4.2.6. The estimated $\overline{SRI}_i$ and ζ parameters for each fragility curve are reported in Table 4.6.
The curves in Figure 4.12 are compared with the cumulative density function determined for each damage level independently.

Compared to the Fragility curves determined by fitting procedure (Fig. 4.11), the curves in figure 4.12 are associated with higher probabilities of damage.

For a value of angular distortion equal to 1/500 the probability of light damage for buildings on shallow foundations is equal to 12%, whereas 26% for buildings on piled foundations. Regarding "moderate to severe damage", for an angular distortion equal to 1/150, the probability of damage is 26% both for shallow foundations and piles.

Therefore, the fragility curves determined by Approach 2 in Figure 4.12 provide more conservative estimates of the probability of damage compared to the ones in Figure 4.11.

However, even the curves retrieved with Approach 2 present shortcomings:

- Low probabilities of damage are still observed for low values of distortions and displacements, as they are not limited in the collected datasets.

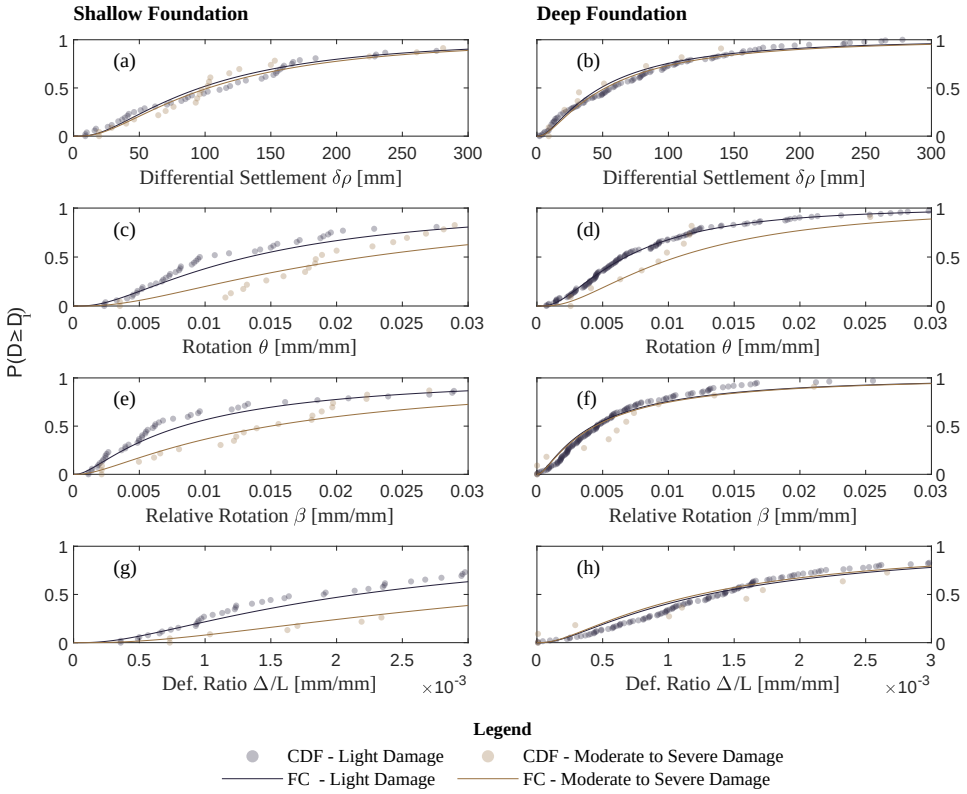

Figure 4.12: Fragility curves of buildings resting on shallow and deep foundations for all the SRI parameters obtained with "Approach 2" (section 4.2.6).

- The curves for piled foundations overlap, this is due to the limited number of cases in the "light damage" and "moderate to severe damage" subsets, and due to the limited increase of the SRI values with the increase of the damage class (Fig 4.7).

Table 4.6: Median $\overline{SRI}_i$ and Standard deviation ζ of the lognormal distribution obtained with Approach 2 (section 4.2.6) for each considered settlement parameter distinguished by foundation type and damage level.

Parameter	Damage level	Shallow foundations		Deep foundations	
		$\overline{SRI}$	ζ	$\overline{SRI}$	ζ
$\delta\rho$ [mm]	Light	96	0.88	48	1.05
	Moderate to severe	103	0.88	52	1.05
θ [mm/mm]	Light	1.33×10^{-2}	0.94	6.80×10^{-3}	0.85
	Moderate to severe	2.22×10^{-2}	0.94	1.07×10^{-2}	0.85
β [mm/mm]	Light	8.30×10^{-3}	1.16	4.30×10^{-3}	1.22
	Moderate to severe	1.50×10^{-2}	1.16	4.40×10^{-3}	1.22
Δ/L [mm/mm]	Light	2.22×10^{-3}	0.98	1.30×10^{-3}	1.08
	Moderate to severe	4.00×10^{-3}	0.98	1.20×10^{-3}	1.08

4.7. DISCUSSION

The analyses presented in this Chapter included the desk collection of the reports of 386 buildings for which levelling measurements, damage and foundation information are available.

The adopted procedure involved thus a digitalization process of data that were originally retrieved in hardcopies of different qualities and from different sources. The data were manually added to a MATLAB dataset, and thus the procedure is intrinsically subjected to human errors.

It should be noticed that in the state-of-the-art, there is currently a lack of procedures to collect data on structures exposed to settlement in a systematic way, from which probabilistic analyses can be developed. Thus, this study also highlights the necessity of detailed empirical data on existing structures exposed to settlements available for researchers and engineers.

Four SRI parameters (*i.e.*, differential settlement $\delta\rho_{max}$, rotation θ, relative rotation β, deflection ratio Δ/L) were chosen due to their wide usage in codes and regulations. The collection of other parameters could be suggested for future studies, such as the horizontal strain [30] that could also affect the occurrence of damage, although this parameter may be more suitable for studies related to tunnelling-induced, excavation-induced and mining-induced settlements rather than for climate-induced settlements. However, in the presented study, it was not possible to retrieve the horizontal (ground) displacements using the bed joint measurements.

Moreover, the displacements of only a few points are gathered at fixed, limited intervals with manual bed-joint levelling readings, thus suggesting that damage appears at higher values of distortion than what could be present. In addition, the level of accuracy of different surveyors is influenced by the tools, the time and the scope of the analyses. This factor could also affect the measurements of the wall deformations. An effect of this factor is the fact that all the buildings show values of SRI which are considered to be high if compared to standards and guidelines, whereas many existing buildings could experience lower SRI values (see Fig. 4.7). It should be noted, however, that different factors could influence the response of structures, allowing them to withstand also high distortion without exhibiting observable damage:

- Materials could exhibit viscoelastic effects, such as creep and relaxation, which can allow structures undergoing settlements over long times (such as decades) to conform to the ground movements with limited if any damage;

- It is widely known that the response of each structure strongly depends on its own features (structural layout, construction material, foundation etc.); This aspect contributes to the variation of values of the SRI computed for each structure.

Other prior studies also indicate a significant range in SRI values across various buildings. For example, [31]–[33] report angular distortion values for different structures, showcasing considerable variation, even among undamaged structures.

All the buildings in the dataset were classified according to the visible damage as “No Damage”, “Light Damage” and “Moderate to Severe Damage”. This classification is better applicable to the buildings in the dataset, compared to more detailed classification systems, as the damage was observed from the available information and was not quantified by detailed surveys. Moreover, all the visual damage to the surveyed buildings was assumed to be caused by the settlements, while other possible contributing causes were disregarded based on the lack of knowledge of major influences. Moreover, it should be noted that a limitation of this work is related to the detectability of damage: damage can occur in parts of the structures which are not easily accessible, or a detailed characterization of the damage could be missing in some reports.

Regarding the proposed fragility curves, two methods are used to retrieve the probabilistic relationship between the settlement parameters and the damage: the first method (Approach 1) uses a fitting procedure, whereas the second approach (Approach 2) is purely statistical [23] and makes use of the maximum likelihood estimation (MLE).

The curves retrieved with MLE method (Approach 2) are observed to be associated with higher probabilities of damage, however, the curves of "light damage" and "moderate to severe damage" overlap, due to the limited differences between the settlement parameters of the building in both subsets (see Fig. 4.7) especially in the case of piled foundations: in other words, when the SRI parameters do not increase with an increase of damage, the curves overlap. This is an effect of the relatively small subsamples of buildings for each damage level.

The curves retrieved with the fitting procedure (Approach 1) are also dependent on the sample size: for instance, if the number of "undamaged" cases were higher, the probability of damage of both "light" and "moderate to severe" damage would be lower. Therefore, the curves retrieved with Approach 1 describe the behaviour of the building. However, this sample-specific behaviour may not be easy to generalize.

4.8. CONCLUSIONS

The analyses presented in this Chapter provide empirical insight into the response of existing structures subjected to settlements. Accordingly, the analyses revealed:

- The wall deformations were observed to be associated with both an overall tilt and a curvature of the surveyed masonry wall. For the 501 walls displaying a consistent shape deformation, 90% of those present both tilt and curvatures; the investigated settlement profiles are observed to conform to a Gaussian curve.

- Empirical fragility curves for four selected settlement intensity parameters are retrieved using two different approaches. For a value of angular distortion equal to 2 ‰(or 1/500), the most conservative curves are associated with a probability of exceeding light damage, with cracks wider than 5mm, equal to 12%, whereas 26% for buildings on shallow and piled foundations respectively.

- The relative performance of the selected SRI parameters as classifiers was analysed by means of ROC analyses. Accordingly, the rotation and angular distortion are

identified as the best predictors of building damage, followed by the deflection ratio and the differential settlement.

It should be noted that the present analyses provide insight into the response of masonry structures subjected to ground settlements in the Netherlands, but it may be hard to generalize the conclusions, due to the relatively small sample size. Further analyses are therefore suggested to investigate the behaviour of complete masonry structures.

BIBLIOGRAPHY OF CHAPTER 4

[1] A. Prosperi, P. A. Korswagen, M. Korff, R. Schipper, and J. G. Rots, "Empirical fragility and roc curves for masonry buildings subjected to settlements," *Journal of Building Engineering*, vol. 68, p. 106 094, 2023.

[2] R. Straathof, P. Korswagen, and A. Prosperi, "Data verification for" empirical fragility and roc curves for masonry buildings subjected to settlements" report,"

[3] J. B. Burland and C. Wroth, "Settlement of buildings and associated damage," Report, 1975.

[4] A. W. Skempton and D. H. MacDonald, "The allowable settlements of buildings," *Proceedings of the Institution of Civil Engineers*, vol. 5, no. 6, pp. 727–768, 1956, ISSN: 1753-7789.

[5] A. Drougkas, E. Verstrynge, K. Van Balen, *et al.*, "Country-scale insar monitoring for settlement and uplift damage calculation in architectural heritage structures," *Structural Health Monitoring-an International journal*, p. 1 475 921 720 942 120, 2020, ISSN: 1475-9217. DOI: Artn147592172094212010.1177/1475921720942120.

[6] CEN, "Eurocode 7 geotechnical design - part 1: General rules. final draft, en 1997-1:2004 (e), (f) and (g)," Report, 2004.

[7] J. B. Burland, B. B. Broms, and V. F. De Mello, "Behaviour of foundations and structures," 1978.

[8] M. D. Boscardin and E. J. Cording, "Building response to excavation-induced settlement," *journal of Geotechnical Engineering-Asce*, vol. 115, no. 1, pp. 1–21, 1989, ISSN: 0733-9410. DOI: Doi10.1061/(Asce)0733-9410(1989)115:1(1).

[9] G. Giardina, A. V. Van de Graaf, M. A. N. Hendriks, J. G. Rots, and A. Marini, "Numerical analysis of a masonry facade subject to tunnelling-induced settlements," *Engineering Structures*, vol. 54, pp. 234–247, 2013, ISSN: 0141-0296. DOI: 10.1016/j.engstruct.2013.03.055.

[10] P. A. Korswagen, M. Longo, E. Meulman, and J. G. Rots, "Crack initiation and propagation in unreinforced masonry specimens subjected to repeated in-plane loading during light damage," *Bulletin of Earthquake Engineering*, vol. 17, no. 8, pp. 4651–4687, 2019, ISSN: 1573-1456.

[11] R. B. Peck, "Deep excavations and tunneling in soft ground," *Proc. 7th ICSMFE, 1969*, pp. 225–290, 1969.

[12] J. N. Mandrekar, "Receiver operating characteristic curve in diagnostic test assessment," *J Thorac Oncol*, vol. 5, no. 9, pp. 1315–6, 2010, ISSN: 1556-1380 (Electronic) 1556-0864 (Linking). DOI: 10.1097/JTO.0b013e3181ec173d.

[13] A. M. J. Mens, M. Korff, and A. F. van Tol, "Validating and improving models for vibratory installation of steel sheet piles with field observations," *Geotechnical and Geological Engineering*, vol. 30, no. 5, pp. 1085–1095, 2012, ISSN: 0960-3182. DOI: 10.1007/s10706-012-9506-5.

[14] C. Liu, J. Dobson, and P. Cawley, "Efficient generation of receiver operating characteristics for the evaluation of damage detection in practical structural health monitoring applications," *Proceedings of the Royal Society A: Mathematical, Physical and Engineering Sciences*, vol. 473, no. 2199, p. 20 160 736, 2017, ISSN: 1364-5021.

[15] M. Pellissetti, M.-C. Robin-Boudaoud, and P. Gehl, "Seismic fragility analysis based on vector-valued intensity measures; theory and application to fuel assembly grids," *NENE-2021*, 2021.

[16] N. J. Perkins and E. F. Schisterman, "The inconsistency of "optimal" cutpoints obtained using two criteria based on the receiver operating characteristic curve," *American journal of epidemiology*, vol. 163, no. 7, pp. 670–675, 2006.

[17] A. Saeidi, O. Deck, and T. Verdel, "Development of building vulnerability functions in subsidence regions from empirical methods," *Engineering Structures*, vol. 31, no. 10, pp. 2275–2286, 2009, ISSN: 0141-0296. DOI: 10.1016/j.engstruct.2009.04.010.

[18] M. Nguyen and D. Lallemant, "Order matters: The benefits of ordinal fragility curves for damage and loss estimation," *Risk Analysis*, vol. 42, no. 5, pp. 1136–1148, 2022, ISSN: 0272-4332.

[19] I. Ioannou, T. Rossetto, and D. Grant, "Use of regression analysis for the construction of empirical fragility curves," in *Proceedings of the 15th world conference on earthquake engineering, September*.

[20] C. Del Gaudio, G. De Martino, M. Di Ludovico, *et al.*, "Empirical fragility curves from damage data on rc buildings after the 2009 l'aquila earthquake," *Bulletin of Earthquake Engineering*, vol. 15, no. 4, pp. 1425–1450, 2017, ISSN: 1570-761X.

[21] M. Rota, A. Penna, C. Strobbia, and G. Magenes, "Direct derivation of fragility curves from italian post-earthquake survey data," in *Proceedings of the 14th world conference on earthquake engineering, Beijing, China, October*, pp. 12–17.

[22] M. Shinozuka, M. Feng, H. Kim, T. Uzawa, and T. Ueda, "Statistical analysis of fragility curves: Technical report," *Los Angeles (CA): University of Southern California*, 2003.

[23] S. Fotopoulou and K. Pitilakis, "Fragility curves for reinforced concrete buildings to seismically triggered slow-moving slides," *Soil Dynamics and Earthquake Engineering*, vol. 48, pp. 143–161, 2013.

[24] D. Peduto, M. Korff, G. Nicodemo, A. Marchese, and S. Ferlisi, "Empirical fragility curves for settlement-affected buildings: Analysis of different intensity parameters for seven hundred masonry buildings in the netherlands," *Soils and Foundations*, vol. 59, no. 2, pp. 380–397, 2019.

[25] *Matlab. version 9.12.0.1884302 (r2022a)*, Generic, 2022.

[26] H. Crowley, J. Uilenreef, and R. Scheefhals, "Exposure database (edb) v7 - data documentation technical report and exposure model," ARUP, Report, 2020.

[27] D. Peduto, M. Korff, G. Nicodemo, A. Marchese, and S. Ferlisi, "Empirical fragility curves for settlement-affected buildings: Analysis of different intensity parameters for seven hundred masonry buildings in the netherlands," *Soils and Foundations*, vol. 59, no. 2, pp. 380–397, 2019, ISSN: 0038-0806. DOI: 10.1016/j.sandf.2018.12.009.

[28] J. A. Charles and H. D. Skinner, "Settlement and tilt of low-rise buildings," *Proceedings of the Institution of Civil Engineers-Geotechnical Engineering*, vol. 157, no. 2, pp. 65–75, 2004, ISSN: 1353-2618.

[29] B. EN *et al.*, "Eurocode 7: Geotechnical design-part 1: General rules," *British Standards Institution*, 2004.

[30] M. D. Boscardin and E. J. Cording, "Building response to excavation-induced settlement," *Journal of Geotechnical Engineering*, vol. 115, no. 1, pp. 1–21, 1989.

[31] T. Ang and K. Masri, "Behaviour of residential structures on problematic ground," in *IOP Conference Series: Materials Science and Engineering*, IOP Publishing, vol. 513, 2019, p. 012 010.

[32] L. Zhang and A. Ng, "Probabilistic limiting tolerable displacements for serviceability limit state design of foundations," *Geotechnique*, vol. 55, no. 2, pp. 151–161, 2005.

[33] A. W. Skempton and D. H. MacDonald, "The allowable settlements of buildings.," *Proceedings of the Institution of Civil Engineers*, vol. 5, no. 6, pp. 727–768, 1956.

CHAPTER 5

EXPLORATORY FE ANALYSES OF MASONRY BUILDINGS ON STRIP FOUNDATIONS EXPOSED TO VARIABLE SETTLEMENT PATTERNS:

Using existing FE models to assess the influence of building and soil features on damage

This chapter has been published in [1].

CHAPTER 5: TABLE OF CONTENTS

5.1 Introduction **117**

5.2 Methodology and modelling approach **118**
5.2.1 Façade and foundation variations 119
5.2.2 Material properties 121
5.2.3 Applied settlement configurations 123
5.2.4 Interface properties representing the soil-foundation interface 125
5.2.5 Method to characterize and quantify the damage 126

5.3 Results of sensitivity analyses involving variations in building and soil features **127**
5.3.1 Relationship between settlement troughs and damage . . 127
5.3.2 Influence of the settlement configurations 129
5.3.3 Influence of the material properties 130
5.3.4 Effects of the façade features 130
5.3.5 Influence of the foundation, soil and interface 131
5.3.6 Results of the sensitivity analyses 132
5.3.7 Differences between applied and retrieved settlements . . 134
5.3.8 Comparison with the available limit values 136

5.4 Discussion **138**

5.5 Conclusions **139**
5.5.1 Implications for this thesis 140

Bibliography of Chapter 5 . . . . . **144**

5.1. INTRODUCTION

In this Chapter, the influence of different building features on the response of masonry façades on strip foundations subjected to ground settlements is investigated using non-linear finite element (FE) models.
The aim is to quantify the effects of the different selected features and to identify the ones that are the most influential for the model and the building's response; Features identified as strongly influencing the response of the models are thus highlighted and are further used in the analyses reported in Chapter 7.

The numerical simulations herein presented investigate the influence of the masonry material, the length over height (L/H) ratio of the façade, the wall thickness, the number and size of openings and different types of strip foundations (*i.e.*, reinforced concrete and unreinforced) is examined. The models depict the non-linear constitutive behaviour of both the masonry, via smeared cracking, and of the soil-foundation interaction, via nonlinear interface elements at the base of the foundation. A sensitivity study additionally investigates the influence of the interface stiffness and its constitutive model.

Eight Gaussian curves, including both symmetric and asymmetric profiles, are used to replicate the shape of the ground settlements; The settlement shapes are imposed in the FE and the angular distortion is used to measure their intensity. The extent of the induced damage to the façade is assessed objectively using a damage parameter that represents the number, length and width of cracks in a single scalar value.

The method distinguishes between the applied settlement profile at the bottom of the interface and the retrieved settlement profile measured on the façade.

The damage to the structure is computed from the results of the FE models using a scalar parameter; This provides an objective assessment of the damage level based on the cracks' number, width and length.

A distinction is made between the applied settlements, representing the loss of support underneath the foundation, and the retrieved displacements measured at the façade. This allows for studying the influence of the building's features and the shape of the settlements on the relationship between the applied settlements, the façade deformation and the resulting damage.

This Chapter begins with a detailed description of the methodology, the FE models and the investigated variations in section 5.2. The outcomes of the simulations are presented in section 5.3. In section 5.4 the findings of this chapter are discussed, and the main conclusions are presented in section 5.5.

Compared to the published manuscript (*i.e.*, [1]), in this dissertation a revised version of section 5.3.7 is presented. In the revised version, the calculation and the discussion are further refined. The refinements are discussed in detail and do not affect the discussion, findings or conclusions of the original publication.

5.2. METHODOLOGY AND MODELLING APPROACH

The analysis procedure followed consists of two main steps (Figure 5.1).

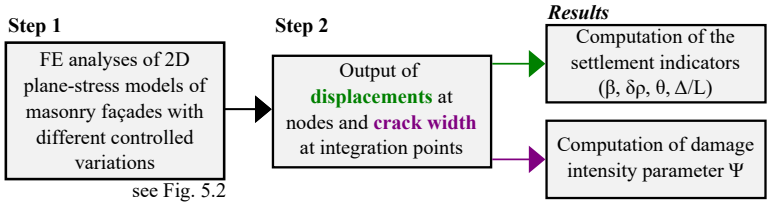

Figure 5.1: Flowchart of the adopted procedure.

In Step 1 (Figure 5.1), masonry façades were modelled in 2D plane stress with the software Diana FEA 10.5, including different materials, geometries, soil conditions and settlement loads.

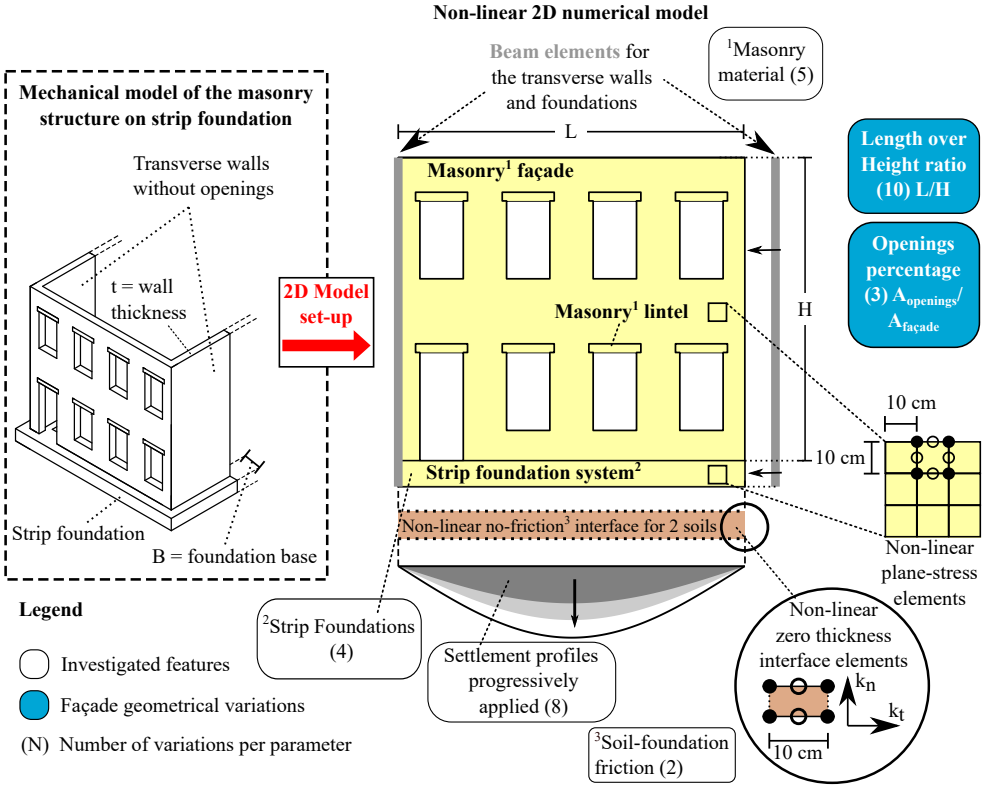

Figure 5.2: Illustration of the intended mechanical model and the adopted FE modelling approach, the features included and the variations investigated. Number of variations per parameter indicated in parenthesis (N). The foundation systems adopted in the model are shown in detail in Figure 5.4, while the settlement profiles applied at the bottom edge of the interface are shown in Figure 5.5.

All the investigated parameters are schematically presented in Figure 5.2. Particularly, below the façade, the strip foundation systems were explicitly modelled, to further investigate their role. Moreover, class-III Mindlin beam elements were placed on the two lateral sides of the façades to simulate the presence of transversal walls and transverse foundations; This was observed to aid the development of realistic crack patterns due to ground settlements [2]. The lateral beam elements simulate the additional stiffness at the sides of the façade due to the interlocking with the house-to-house separation walls which restrain the rotation of the façade's edges [2]. The models include openings underneath masonry lintels and 8-node quadratic plane stress elements with 3 x 3 Gaussian integration schemes adopted for the façade, lintels and strip foundation, with a mesh size of 100 mm x 100 mm. Three-noded elements were used for the beam elements, while six-noded line interface elements with the Lobatto integration scheme [3] were used to model the soil-foundation interaction, both with a mesh size of 100 mm.
The geometry (*i.e.*, length L, height H, opening percentage in Figure 5.2), the material properties (*i.e.*, the elastic-softening orthotropic material properties), the strip foundation system and the type of soil were varied to investigate their effect on the structural response in terms of damage.
Eight settlement configurations were considered to simulate the symmetric and non-symmetric hogging and sagging profiles due to the loss of support underneath the foundation. The settlement profiles specifically aim to represent urban subsidence phenomena and differ from those by excavations, tunnelling or mining works [4]–[6].

In Step 2 (Figure 5.1), the output of the numerical analyses was used to retrieve the relationship between the settlement profiles and the damage. The vertical displacements at the façade's base (top edge of the foundation) of all the models were selected to output the façade's displacements. In this regard, this study is framed by distinguishing with the term "applied" the prescribed displacements at the bottom of the interface (Figure 5.2), while the term "retrieved" is used for the resulting displacements at the façade's base (*i.e.*, top edge of the strip foundation). The crack widths at the integration points of the façade are used to quantify the extension and accumulation of the damage. The relationships between the applied, retrieved displacements (in terms of differential settlement, rotation, angular distortion and deflection ratio [7]) and the damage severity were then determined.

5.2.1. FAÇADE AND FOUNDATION VARIATIONS

A two-storey façade model with a total height of 7 meters and a length of 8 meters was selected as the reference case (Figure 5.3f). Additional geometries were modelled varying the length over height (L/H) ratio of the façade ranging from 0.57 in Figure 5.3a1 up to 5.00 in Figure 5.3e2. The dimensions of the openings for the reference façade were set to ensure similarity to previous studies (*e.g.*, [8]) and correspond to an opening percentage of 0.27. Additionally, two extra opening percentages of 0.10 and 0.20 were obtained by arbitrarily modifying the height of the openings, as shown in Figure 5.3h and g respectively, for the sensitivity analyses.

The load and the effect of the floors and roof are not included in the models; Thus, in terms of mass loads the façades are only loaded by their self-weight. A wall thickness of 210 mm was considered for all analyses ("t" in Figure 5.2). Such wall thickness was also

applied to the lateral beam elements. A model was developed in which the lateral beam elements were not included, to further investigate their influence.

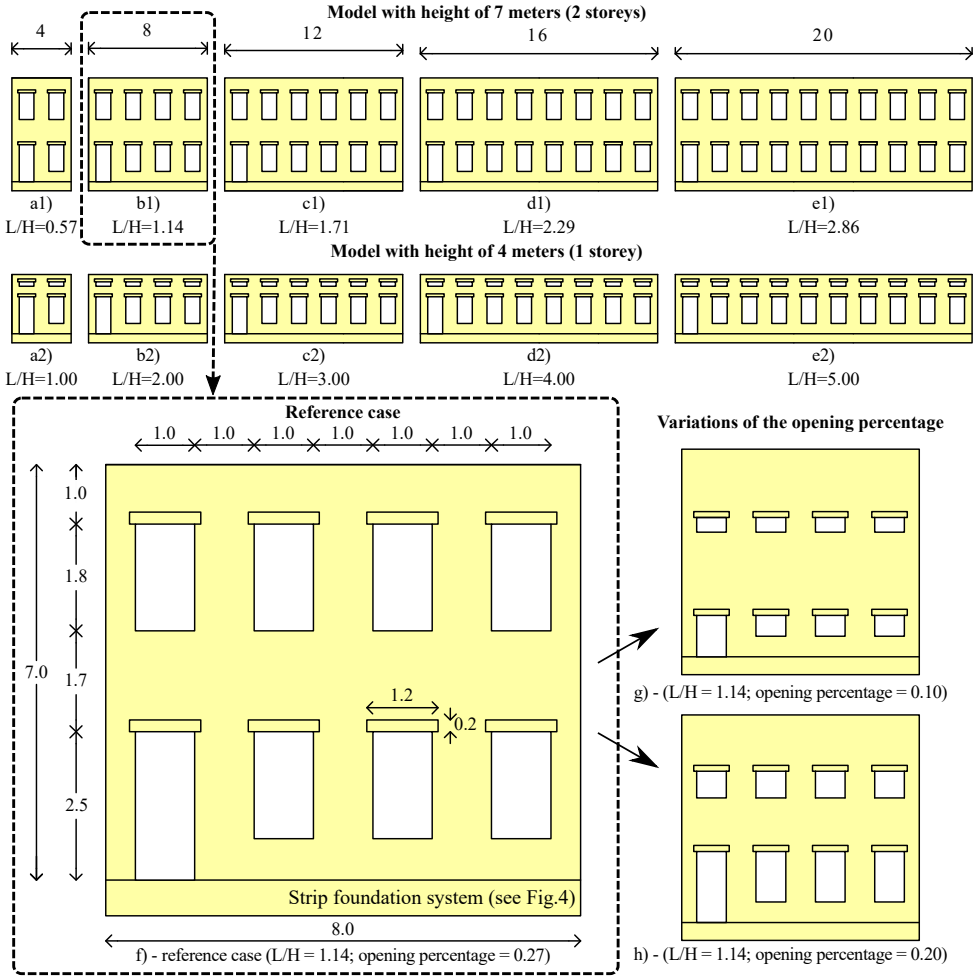

Figure 5.3: Reference geometries for the masonry facade. The geometries from a1) to e2) are characterized by an opening ratio ($A_{opening}/A_{facade}$) of 0.27. The model f) represents the reference case. The height of the openings of f) is modified arbitrarily for the geometries g) and h) to obtain the two selected opening percentages (*i.e.*, 0.10 and 0.20 respectively). The foundation systems adopted in the model are shown in detail in Figure 5.4. Not to scale. Measures in meters.

Each façade model rests on an Unreinforced Masonry (URM) strip foundation (Figure 5.4a). Additional reinforced concrete (RC) strip foundations were also modelled. Among those, an RC block foundation (Figure 5.4b), an RC strip foundation with a masonry layer on top (Figure 5.4c) and an RC strip foundation with an RC stiffening beam (Figure 5.4d). The top edge of each foundation system corresponds to the ground surface level. The longitudinal (*i.e.*, along the façade) rebar system was modelled as line reinforcement and

considered fully embedded in the concrete and no slipping behaviour was considered. The equivalent cross-section of the steel is shown in Figure 5.4 for each RC foundation.

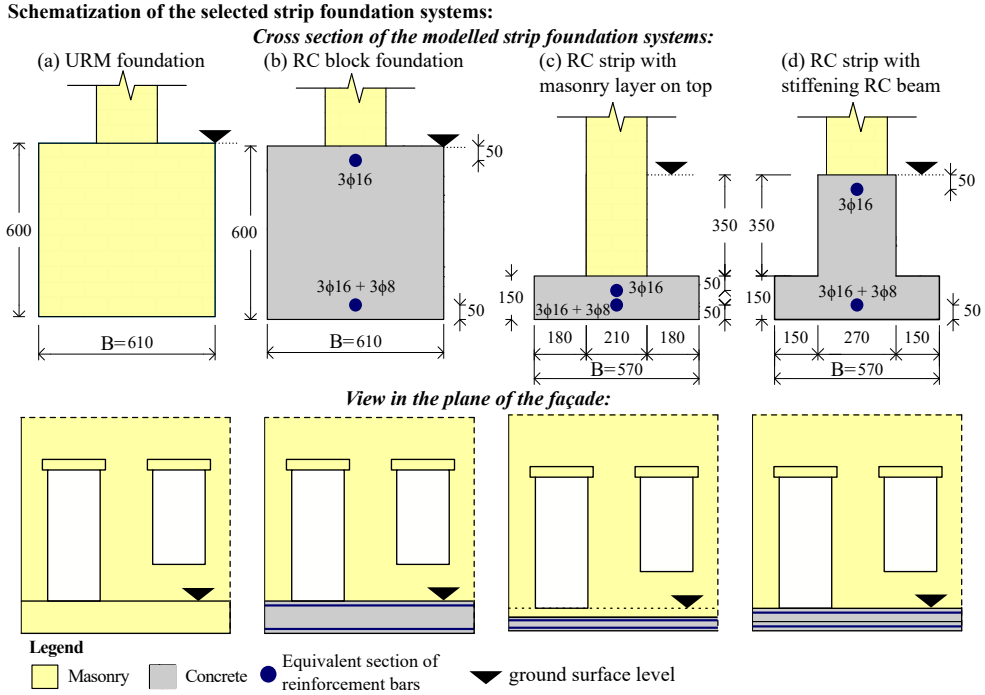

Figure 5.4: Sketch of the recurrent strip foundation systems in the Netherlands: (a) URM foundation, (b) RC block foundation, (c) RC strip with masonry layer on top and (d) RC strip with stiffening RC beam. The level of the ground surface and the view in the plane of the façade are shown for each foundation system. Upper and lower reinforcement bars are represented as equivalent embedded bars. The equivalent section of each bar was based on the design values of existing structures. Measures in millimetres.

5.2.2. MATERIAL PROPERTIES

The parameters of five different sets of masonry materials were retrieved from the Dutch Standard [9] and previous studies [10], [11] to investigate the response of both: baked clay (BC) and calcium-silicate (CS) brick masonry. Accordingly, in Table 5.1, the material properties are reported as:

- **M1** a poor version of M2 where the elastic and strength parameters were reduced by 50% to simulate the effect of an aged, pre-damaged material, as advised in the Standard [9];
- **M2** represents the material properties of a BC brickwork, built before 1945;
- **M3** is the material set used for clay masonry built after 1945;
- **M4** represents a CS brickwork with general purpose mortar;

- **M5** a CS block or large element masonry with thin mortar layers.

Table 5.1: Adopted material properties for the masonry in the numerical models.

Material Properties	Symbol	Unit of measure	M1	M2	M3	M4	M5
Young's modulus vertical direction	E_y	[MPa]	2500	5000	6000	4000	7500
Young's modulus horizontal direction	E_x	[MPa]	1250	2500	3000	2000	3750
Shear Modulus	G_{xy}	[MPa]	1000	2000	2500	1650	3000
Bed joint tensile strength	f_{ty}	[MPa]	0.050	0.100	0.200	0.100	0.200
Fracture energy in tension	$G_{t,I}$	[N/mm]	0.003	0.010	0.010	0.010	0.020
Compressive strength	f_c	[MPa]	4.25	8.50	10.00	7.00	10.00
Fracture energy in compression	G_c	[N/mm]	10.00	20.00	15.00	15.00	20.00
Friction angle	φ	[rad]	0.500	0.700	0.900	0.400	0.600
Cohesion	c	[MPa]	0.075	0.150	0.300	0.150	0.200
Fracture energy in shear	G_s	[N/mm]	0.025	0.100	0.200	0.100	0.200
Mass Density	ρ	[Kg/m^3]	1708	1708	1708	1763	1763

The masonry façades are assumed to be built with a running bond pattern, with typical brick dimensions of 210x50x100 mm for the BC bricks and 210x70x100 mm for the CS bricks. The mortar thickness is assumed to be 10 mm. An orthotropic, smeared crack/shear/crush constitutive law was employed to simulate the cracking behaviour of masonry. This constitutive model labelled as EMM (Engineering Masonry Model, [10]) is total-strain based and it describes tensile cracking, shear slip and compression crushing including their softening and specific unloading/reloading behaviour in the pre-fixed x,y-system aligned with the masonry bed and head joint orientations [12]. The selected material properties were applied to both the façade and masonry foundation. For the lintels, the same material properties were employed (Table 5.1), and a rotation of 90° of the local axes was applied to account for the different orientations of the masonry (soldier brick pattern). The head-joint failure (representing vertical cracking) is based on friction, so a higher vertical pre-compression positively contributes to the crack formation. The minimum head-joint strength (as no pre-compression is present) is set to 1.5 times the bed-joint tensile strength. The lateral beam elements make use of a linear elastic model, with the Young's modulus equal to 1/3 of the Ey for each M material, the Poisson's ratio of

0.15 and the same mass density of the considered M material [2].

Table 5.2: Adopted material properties for the reinforced concrete in the numerical models.

Material Properties	Symbol	Unit of measure	Concrete	Steel
Young's modulus	E	[MPa]	32000	210000
Poisson's ratio	ν	[-]	0.2	-
Fracture energy in tension	$G_{t,I}$	[N/mm]	0.137	-
Compressive strength	f_c	[MPa]	33	-
Tensile strength	f_t	[MPa]	2.565	-
Mass density	ρ	[Kg/m^3]	2350	-
Yield strength	f_y	[MPa]	-	400
Hardening curve	-	-	-	No Hardening

The long-term effects such as creep and relaxation of the masonry material were not included, due to a lack of available information. Moreover, there may be a discrepancy between the material properties of real full-scale masonry walls and those of the small-scale masonry laboratory test specimens on which the material properties of this study were based, even if these originate from real buildings.

For the variations with reinforced concrete foundations (Figure 5.4b, c and d), the non-linearity of the material was explicitly modelled with the Total Strain Rotating Crack Model. The Von Mises Plasticity model was employed for the steel material of the rebar in the RC foundations. A summary of such material properties is shown in Table 5.2.

5.2.3. APPLIED SETTLEMENT CONFIGURATIONS

In this chapter, eight possible settlement profiles were considered, reflecting symmetric and non-symmetric hogging and sagging shapes; The settlement shapes reflect different positions of the building on a long Gaussian settlement trough [13] and are computed with Eq. 5.1:

$$S_v(x) = S_{v,max} e^{\left(\frac{-x^2}{2x_i^2}\right)} \tag{5.1}$$

where:

x is the horizontal distance from the symmetric axis of the curve;

x_i is the distance from the symmetry axis of the curve to the point of inflection.

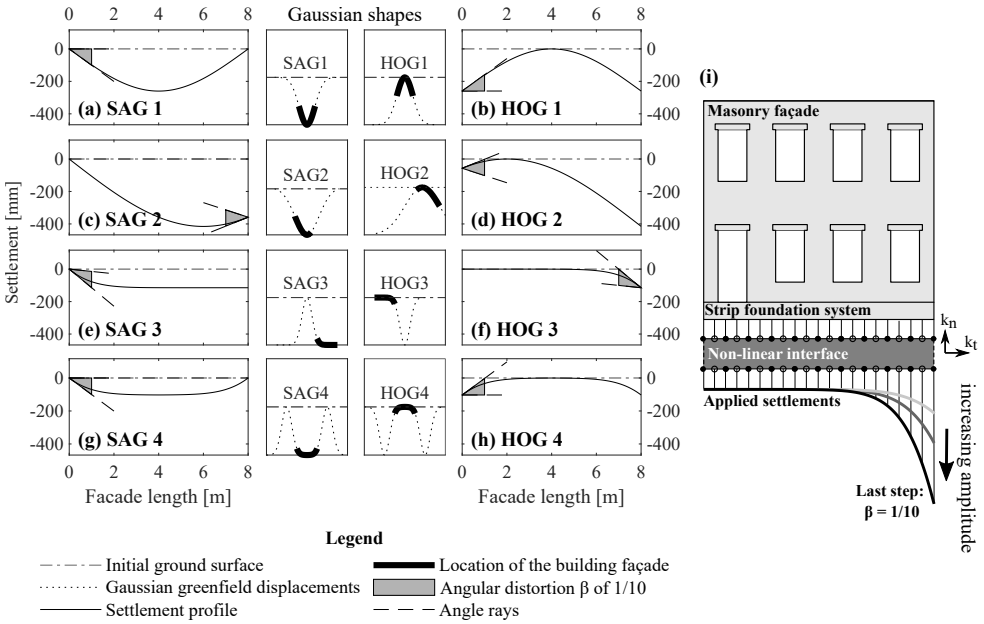

Figure 5.5: The applied settlement profiles, that reproduce a loss of support underneath the strip foundation, computed from a Gaussian shape for a façade of 8 meters and an angular distortion β equal to 1/10 (illustrated as a shaded area), defined according to the definition proposed by [7]: a) SAG1, b) HOG1, c) SAG2, d) HOG2, e) SAG3, f) HOG3, g) SAG4 and h) HOG4. All profiles were obtained by considering different positions of the façade over the displacement distributions, as schematically indicated in the centre pictures. The settlement shapes are applied in the numerical model with increasing amplitude as illustrated in i).

Although Gaussian curves are typically adopted for ground movements due to tunnelling, mining or excavations, they are herein employed to simulate the reduction of support underneath the foundation due to urban subsidence processes (*e.g.*, organic soil oxidation, soil shrinkage, groundwater lowering, etc.).

The angular distortion β was chosen to characterize the intensity of the profiles and to allow for comparison to previous studies [14]–[17]. It is worth stressing that the angular distortion refers to the slope of the line joining two consecutive points in relation to a line joining the two points at the sides of the façade [7]. Therefore, depending on the shape, the maximum vertical settlement $S_{v,max}$ of each settlement shape was imposed to ensure an identical distortion, equal to 1/10, in all the profiles. In particular, the imposed angular distortion refers to the maximum value along the façade. In other words, the maximum settlement of each of the considered shapes differs, while the angular distortion is the same (Figure 5.5).

The FE analyses make use of two steps procedure:

- First, gravity was applied to the structure to compute the stress states due to the self-weight (labelled as "Gravity" in Table 5.3); after this step, the resulting displacement field of the façade, characterized by displacements in the order of tenths of a millimetre, was then cleared to avoid the occurrence of deformations not related to the applied settlements.

- Then, the settlement profiles (labelled "Settlement" in Table 5.3) were applied as prescribed nodal displacements at the bottom of the interface elements that simulate the soil-foundation interaction.

The gravity load was applied in 10 steps. The number of steps used for the application of the settlements differs per shape. Three intervals with different step sizes were considered, in order to better observe the progression of the damage in the numerical model:

Table 5.3: Characteristics of the iterative scheme.

Load	Method	Convergence norm	Convergence tolerance	Satisfy all specified norms	Max. number of iterations
Gravity	Quasi-Newton	Displacement Force Energy	0.01 0.01 0.001	Yes	200
Settlement	Quasi-Newton	Energy	0.0001	Yes	200

1. 0.1 mm/step for a vertical displacement minor or equal to 10 mm;
2. 0.2 mm/step for a vertical displacement minor or equal to 100 mm;
3. 0.5 mm/step for higher vertical displacements.

The angular distortion was progressively increased from 0 (in the first step after the gravity load) up to 1/10. The variable step sizes ensure convergence after the occurrence of cracking and non-linearity. Both the gravity and the settlement loads make use of the Quasi-Newton incremental-iterative procedure (also referred to as the "Secant method" [3]). Additional information about the iterative procedure is reported in Table 5.3.

5.2.4. INTERFACE PROPERTIES REPRESENTING THE SOIL-FOUNDATION INTERFACE

The interface between soil and foundation was modelled by selecting a no-tension smooth discrete cracking model as constitutive law for the interface elements. Such an interface is added to avoid the application of the imposed settlement directly to the strip foundation. This means that no forces (either normal or tangential) were transferred at the interface level when normal tensile stresses were acting at the base of the model. With this approach, the applied settlement displacements do not pull the façade downward, as its self-weight makes the façade deform due to the loss of support.

The interface normal and tangential stiffness values were computed using the equations reported by [18] and proposed by [19] and [20], for arbitrarily shaped foundations on a homogeneous half-space [21]:

$$K_n = \frac{GL}{1-\nu}\left[0.73 + 1.54 \cdot \left(\frac{B}{L}\right)^{0.75}\right] \tag{5.2}$$

$$K_t = GL\left\{\frac{1}{2-\nu}\left[2+2.5\cdot\left(\frac{B}{L}\right)^{0.85}\right]-\frac{0.2}{2(0.75-\nu)}\left[1-\frac{B}{L}\right]\right\} \tag{5.3}$$

Where K_n, and K_t from equations (5.2) and (5.3) represent the static stiffness values for a rigid foundation respectively for the normal, and tangential (*i.e.*, in the plane of the façade) directions to the soil surface. B represents the foundation thickness, while L is the foundation length (equal to the length of the façade) (Figure 5.2).

Table 5.4: Material properties of the soil types considered.

Material Properties	Symbol	Unit of measure	Soil A	Soil B
Soil Material	[-]	[-]	Sandy soil	Clayey Soil
Shear Modulus	G	[MPa]	35	10
Poisson's Ratio	υ	[-]	0.3	0.45

The properties of two soil types (Soil A and B in Table 5.4) were based on the superficial (*i.e.*, the first five meters) soil stratigraphy in the Groningen region reported by Deltares [22]. In particular, G represents the small-strain shear modulus. The use of equations (5.2) and (5.3) has been validated in previous studies [21], [23]–[27]. The values of K_n, and K_t were then divided by B and L to obtain smeared values of the normal and shear linear stiffness (namely k_n, and k_t respectively, in Figure 5.2 and Figure 5.5) along the foundation footprint.

For the purpose of the sensitivity analysis, a simulation is performed using a Mohr-Coulomb interface to investigate the role of soil-foundation contact friction. The analyses were performed by considering the same stiffness values (*i.e.*, k_n, and k_t), and an arbitrarily defined friction angle of 30° and zero cohesion for soil A in Table 5.4.

5.2.5. METHOD TO CHARACTERIZE AND QUANTIFY THE DAMAGE

The severity of damage to buildings induced by ground displacements is measured with the damage classification proposed by [28] which is based on the ease of repair and the approximate width of the visible cracking. However, the objective quantification of the cracking damage requires considering not only the width, but also the length and the number of cracks in brick walls [29], [30]. In this study, a parameter Ψ in equation (5.4) proposed by [29] was employed to quantify the resulting progression and accumulation of the damage in the numerical models in one single scalar value:

$$\Psi = 2n_c^{0.15}\hat{c}_w^{0.3} \tag{5.4}$$

Where n_c is the number of cracks, $\hat{c}_w$ is the width-weighted and length-averaged crack width (in mm) calculated with equation (5.5):

$$\hat{c}_w = \frac{\sum_{i=1}^{n_c} c_{w,i}^2 c_{L,i}}{\sum_{i=1}^{n_c} c_{w,i} c_{L,i}} \tag{5.5}$$

Where $c_{w,i}$ is the maximum crack width along the i-crack in mm, while $c_{L,i}$ is the i-crack length in mm. The parameter Ψ was computed considering the output of the FE analyses, not including the foundation and the lateral beam elements. The length of each crack is computed according to its shape (automatically classified by a MATLAB script as horizontal, vertical or staircase-like).

A summary of the relation between Ψ and the approximate crack width for the various damage levels proposed by [29], is presented in Table 5.5.

Table 5.5: Damage scale with classification of visible damage based on the crack width and discretization of the damage parameter in sub-levels (adapted from [28], and [29]).

Damage level	Degree of damage	Approximate crack width	Parameter of damage
DL0	No Damage	Imperceptible cracks	$\Psi < 1$
DL1	Negligible	up to 0.1 mm	$1 \leq \Psi < 1.5$
DL2	Very slight	up to 1 mm	$1.5 \leq \Psi < 2.5$
DL3	Slight	up to 5 mm	$2.5 \leq \Psi < 3.5$
DL4	Moderate	5 to 15 mm	$\Psi \geq 3.5$

It is worth stressing that Ψ is limited to the assessment of the light damage (*i.e.*, up to cracks of about 5 mm wide), whereas damage that could affect the structural safety would require a different metric, possibly quantifying the reduction of the capacity of the structure.

5.3. RESULTS OF SENSITIVITY ANALYSES INVOLVING VARIATIONS IN BUILDING AND SOIL FEATURES

5.3.1. RELATIONSHIP BETWEEN SETTLEMENT TROUGHS AND DAMAGE

Figure 5.6 shows how the crack pattern (*i.e.*, cracks' orientation, width, length, number) varies depending on the considered shape of the settlements and the applied distortion. The models depict how cracks initiate around the corners of the openings, and in most cases propagate mainly either horizontally or vertically (Figure 5.6). Less frequently, some cracks develop diagonally (*e.g.*, crack "2" in Figure 5.6h).

Thanks to the presence of lateral beam elements, cracking never initiates from the façade's edges [2]. The observed crack patterns were validated against available literature data (e.g.[31]–[33]).

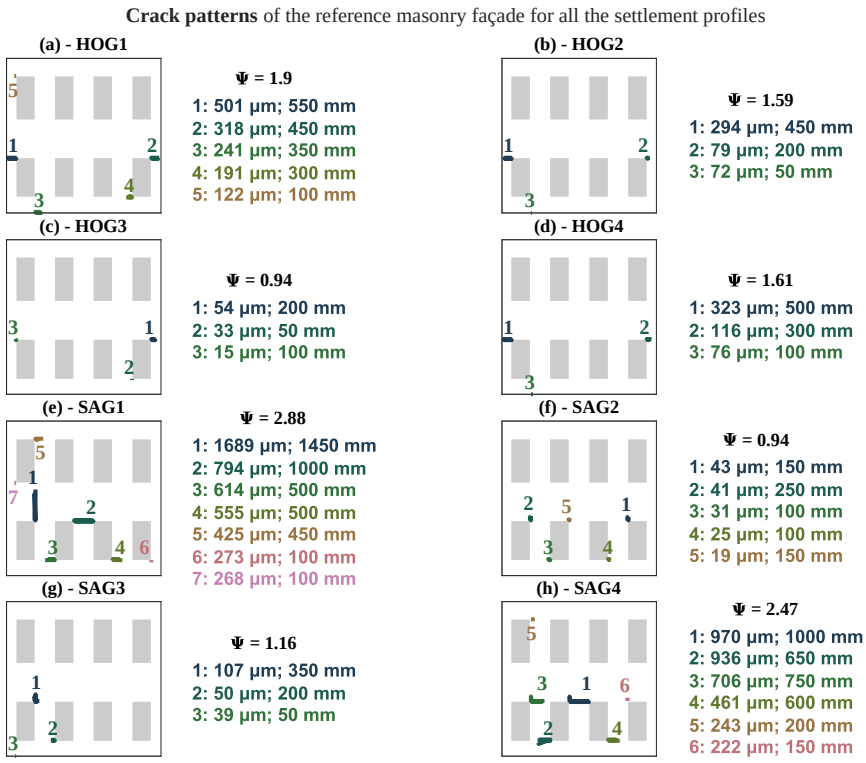

Figure 5.6: Crack patterns of the masonry façade for all the settlement profiles at step 60 (maximum applied settlement equals to about 11 mm) of the numerical model: a) HOG1, b) HOG2, c) HOG3, d) HOG,4 e) SAG1, f) SAG2, g) SAG3 and h) SAG4. Note that for a given numerical step the applied settlement configurations are not characterized by the same value of the angular distortion, due to the variable load step, as discussed in section 5.2. The cracks' width in the plots is exaggerated.

As discussed in section 5.2.3, each settlement profile was applied with a progressively increasing angular distortion in the FE model, allowing recording the vertical displacements of all the models at the façade's base (top edge of the foundation) for each step of the analysis. Accordingly, the four SRIs considered were computed both for the applied and the retrieved settlements (e.g., $\beta_{applied}$ refers to the applied angular distortion, while $\beta_{retrieved}$ corresponds to the one computed from the resulting displacements of the façade).

In the following sections, the differences between the values of both the applied and retrieved parameters for each Ψ value are presented per FE model variation (discussed in 5.2). The model of the façade with L/H = 1.14 (Figure 5.3f), M2 (Table 5.1) with DW thickness (*i.e.*, 210 mm) and an opening percentage = 0.27 (Figure 5.3f), resting on the soil A (Table 5.4) on an URM foundation (Figure 5.4a) is arbitrary assumed to be the reference case.

5.3.2. INFLUENCE OF THE SETTLEMENT CONFIGURATIONS

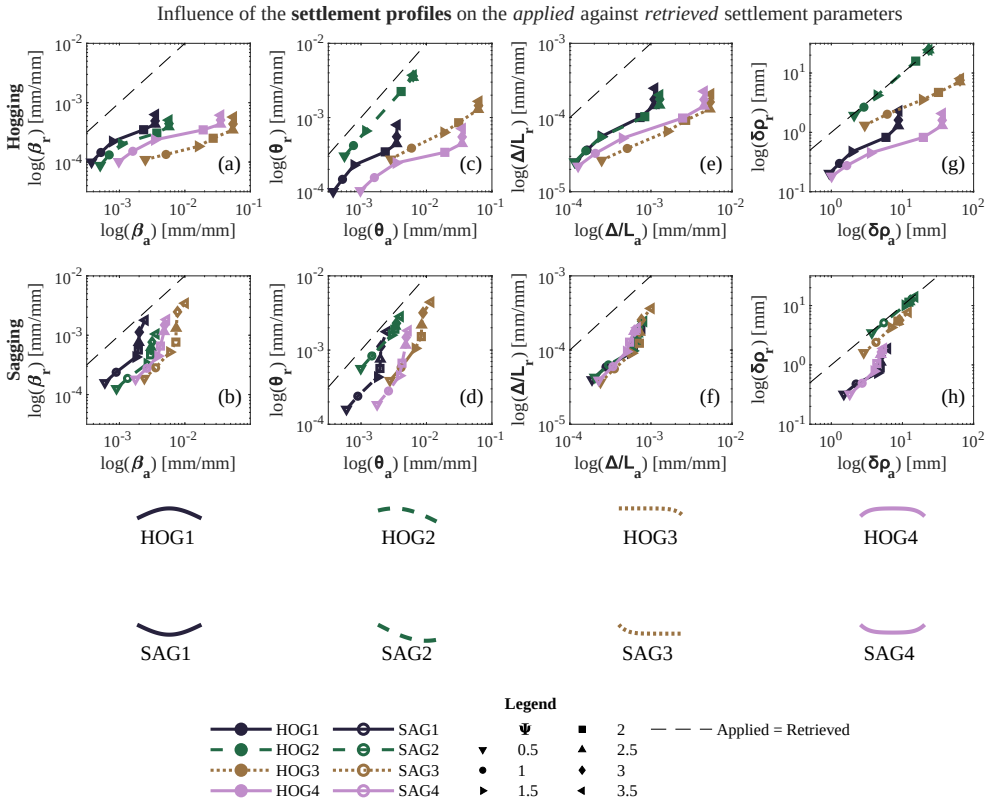

Figure 5.7: Influence of the settlement configuration on the applied vs. retrieved settlement parameters for each level of damage for: angular distortion for a) hogging and b) sagging, rotation for c) hogging and d) sagging, deflection ratio for e) hogging and f) sagging, differential settlement for g) hogging and h) sagging. The shapes of the settlement profiles (not to scale) are shown for clarity. Plots in the logarithmic scale.

For the reference case, the influence of each settlement shape on the applied against retrieved SRI is shown in Figure 5.7. A dashed line represents an idealization for which the applied and the retrieved parameters would be equal. The differences between applied and retrieved SRIs strongly depend on the shape of settlement (Figure 5.7). Due to this dependency, in the following sections, the results will be mainly presented referring to the angular distortion, chosen for consistency with previous studies [14]–[17]. Moreover, the average values of the angular distortion among the results of the eight settlement profiles is considered for both the applied and retrieved angular distortion (β_a and β_r respectively) for each Ψ level, allowing to remove the dependency of the results from the settlement configurations.

To keep a consistent comparison with other analyses, for those models, in which less than eight profiles reach a given Ψ value, the average value is omitted from the charts.

5.3.3. INFLUENCE OF THE MATERIAL PROPERTIES

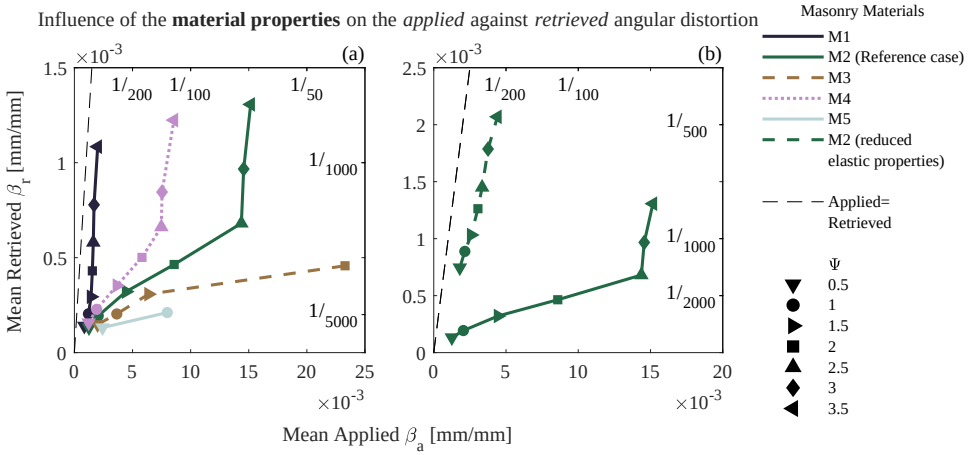

Figure 5.8: Differences of the applied vs. retrieved angular distortion for each level of damage for the variation of the: a) material typology, b) variation of the elastic parameters. The secondary x- and y- axes (on top and the right of the plots) show the values of the angular distortion as $1/\beta^{-1}$, as typically adopted in the literature.

In Figure 5.8a, the applied angular distortion is plotted against the retrieved one for each masonry typology. The results show that the ratio between the applied and the measured angular distortion ranges from about 2 up to 51. Moreover, the façade model with M5 does not reach a damage higher than Ψ=1.0. The lowest differences between applied and retrieved β are observed for M1, which represents a very weak material. The results of the material M2 were compared with a model in which the elastic parameters (*i.e.*, Ex, Ey and Gxy in Table 5.1) were further reduced by an order of magnitude, to investigate the role of the façade stiffness. The comparison proposed in Figure 5.8b shows indeed that the model with reduced elastic properties (and therefore associated with a more flexible behaviour) reaches all the damage levels for values of the applied distortions smaller than the other materials, and it also exhibits the smallest differences between the applied and retrieved distortions; while an order of magnitude of difference between the elastic parameters represents an extreme condition, it serves to highlight this observation.

5.3.4. EFFECTS OF THE FAÇADE FEATURES

The results for the models with different L/H ratios (Figure 5.3) are presented in Figure 5.9 using a log-log plot, to better illustrate the distinctions. Façades with an L / H lower than or equal to 1.00 were observed to not reach a Ψ value higher than 1.50 in any of the models, while only for a few settlement profiles a Ψ value of 1.00 is reached. A decrease in the L/H ratio (*i.e.*, squat facades) is associated with less damage, and with a bigger difference between applied and retrieved parameters.
The effects of the additional variations of the façade features are shown in Figure 5.10. A simulation is performed by doubling the mass of the reference façade's masonry material (M2). Figure 5.10a shows how an increase in the mass density leads to damage for smaller

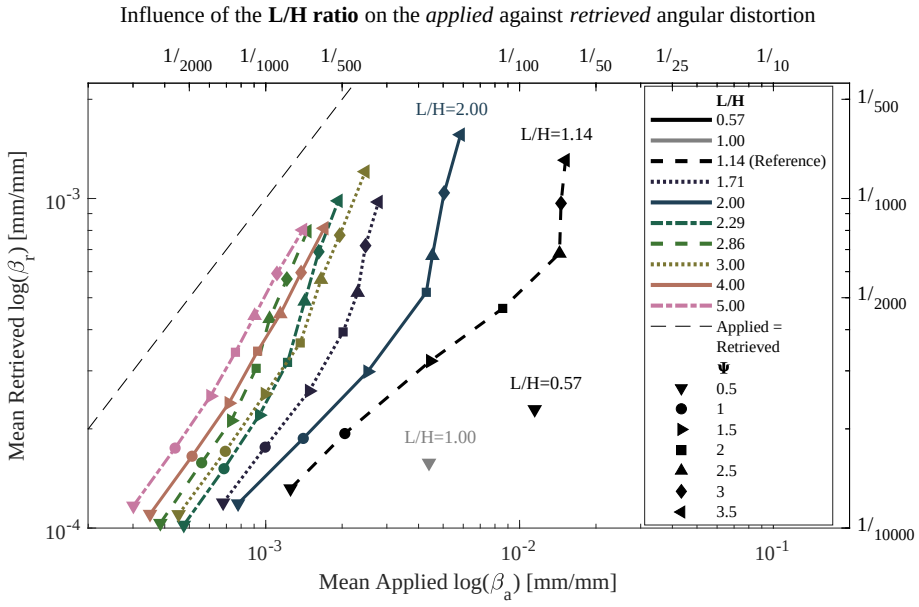

Figure 5.9: Influence of the length over height (L/H) ratio on the difference between applied vs. retrieved angular distortion. The secondary x- and y- axes (on top and on the right of the plots) show the values of the angular distortion as $1/\beta^{-1}$, as typically adopted in the literature.

values of the applied angular distortion, compared to the reference case. This effect could occur particularly when the loads of the storeys and/or the roof of the building are summed to the self-weight of the façade.

The influence of the opening percentage was investigated comparing the results for the models in Figure 5.3g and Figure 5.3h (which correspond to an opening percentage of 10% and 20% respectively) with the reference case. The results of these analyses are proposed in Figure 5.10b. The façade with the smallest opening percentage (*i.e.*, 10%) does not exhibit cracks wider than 0.1 mm (Ψ value higher than 1.0). As observed in the case of the elastic parameters, façades with large openings have a more flexible response and more damage, in agreement with the findings of previous studies (*i.e.*, [32], [34]). Figure 5.10c shows the comparison between the reference FE model and one without the inclusion of the lateral beam elements (Figure 5.2). For the model without lateral beam elements, the damage initially progresses similarly to the reference case and suddenly increases after reaching a value of Ψ equal to 1.5; the removal of the lateral beam elements decreases the difference between the applied and the retrieved angular distortion.

5.3.5. INFLUENCE OF THE FOUNDATION, SOIL AND INTERFACE

Figure 5.11 shows how the façades on RC foundations exhibit stiffer behaviour and consequently, on average, less damage. The influence of the interface features is shown in Figure 5.12. To investigate the role of the soil stiffness relative to the façade, a sensitivity analysis was performed by varying the adopted interface stiffness. Two variations were

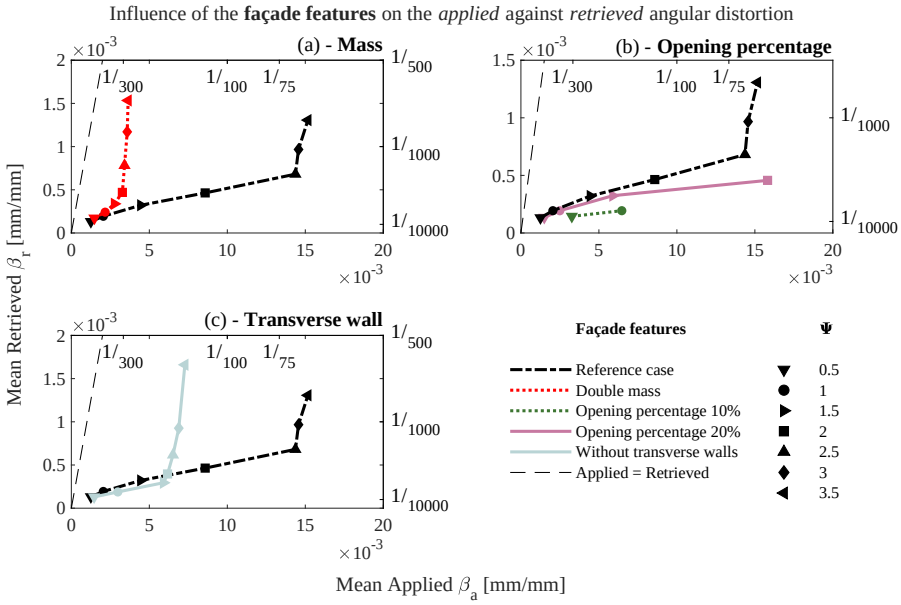

Figure 5.10: Differences of the applied vs. retrieved angular distortion for each level of damage for the variation of the: a) mass density, b) opening percentage and c) presence of the transverse walls. The secondary x- and y- axes (on top and on the right of the plots) show the values of the angular distortion as $1/\beta^{-1}$, as typically adopted in the literature.

selected by increasing and decreasing the values of normal and tangential stiffness of the reference model by an order of magnitude (k_n,k_t)*10, and (k_n,k_t)/10 in Figure 5.12a. The smallest difference between the applied and the retrieved angular distortion is observed in the case of the highest stiffness values, (k_n,k_t)*10. Similarly, Figure 5.12b shows the comparison between the reference model resting on sand (Soil A in Table 5.4) and a variation resting on clay (Soil B in Table 5.4), thus contrasting the shear modulus and Poisson's ratio.
The model resting on clayey soil exhibits less damage compared to the one on sand. The façade acts stiffer on the clayey soil than on the sandy one, thus increasing the differences between applied and retrieved displacements and leading to less damage. Figure 5.12c shows the comparison between the use of a smooth or a rough interface for the reference model, as described in section 5.3.5. Interestingly, the two analyses show similar results when Ψ is smaller than 1.5. However, the model with a rough interface is more susceptible to damage, as the damage occurs for smaller values of the angular distortion when compared with the reference case [35].

5.3.6. RESULTS OF THE SENSITIVITY ANALYSES

In Figure 5.13 an overview of the results of all the models is presented. Particularly, the mean applied angular distortion of each model is divided by the one of the reference case so that the effect of all the investigated variations can be compared. The L/H ratio is the one that is associated with the larger variability of the structural response. Accordingly,

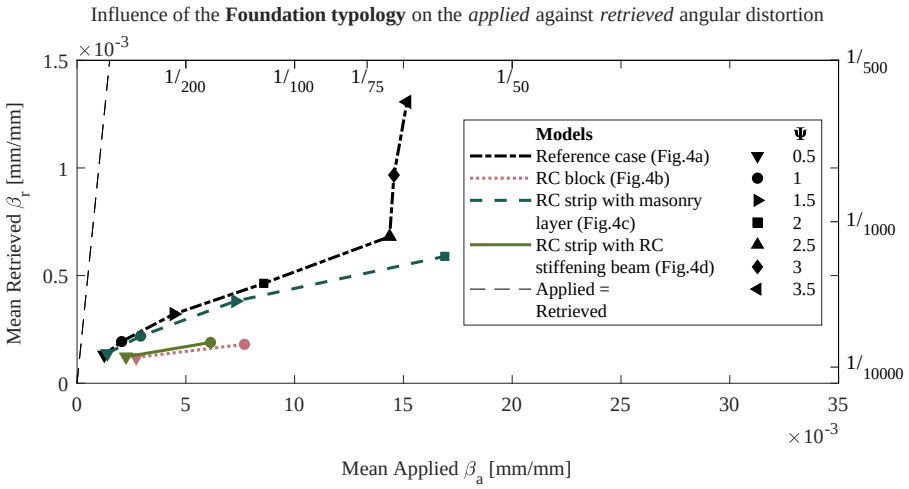

Figure 5.11: Differences of the applied vs. retrieved angular distortion for each level of damage for the variation of the foundation typology. The secondary x- and y- axes (on top and on the right of the plots) show the values of the angular distortion as $1/\beta^{-1}$, as typically adopted in the literature.

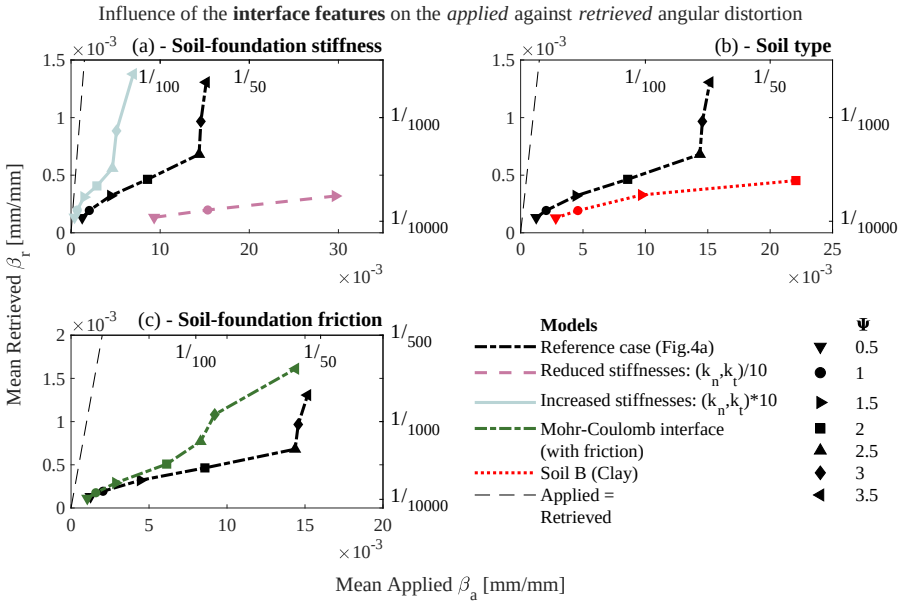

Figure 5.12: Differences of the applied vs. retrieved angular distortion for each level of damage for the variation of the: a) interface stiffness, b) interface model, c) soil type. The secondary x- and y- axes (on top and on the right of the plots) show the values of the angular distortion as $1/\beta^{-1}$, as typically adopted in the literature.

for Ψ equal to 0.5 the mean applied angular distortion βa ranges from values 4 times smaller (in the case of slender façade with high L/H values) to 9 times higher (for squat

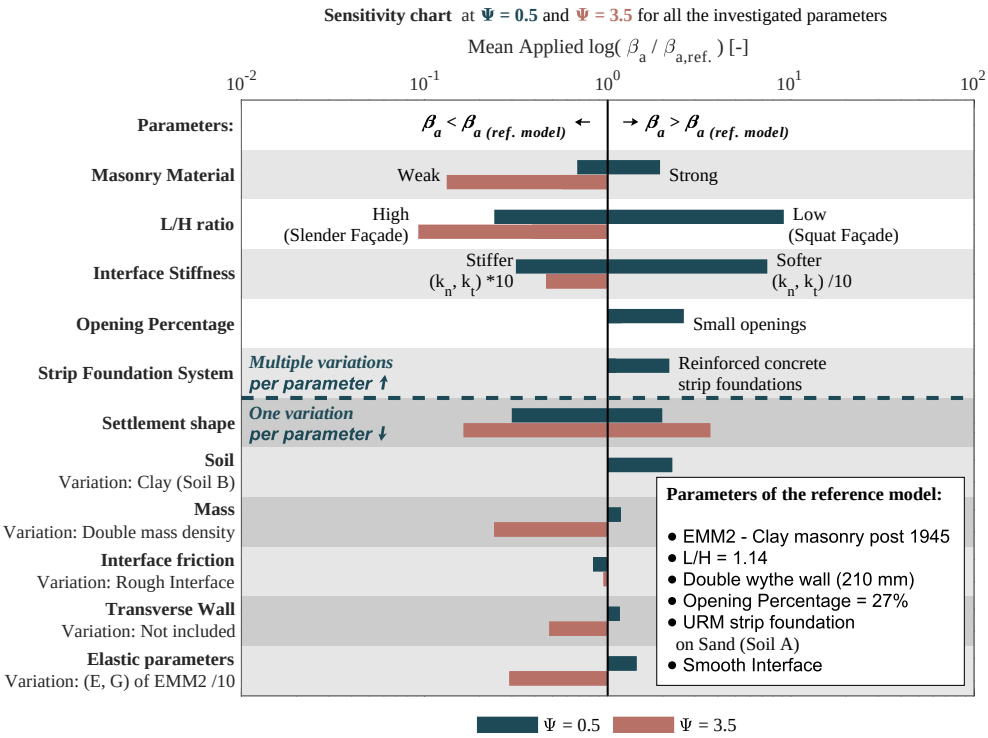

Figure 5.13: Sensitivity chart of the results of all the numerical models. The x-axis in the logarithmic scale shows the ratio between the mean applied angular distortion β_a and the one of the reference model. The results are categorized by the number of models used to study the influence of each parameter by a dashed line.

façades with small L/H values) compared to the reference case (L/H=1.14). A similar effect is observed when comparing the analyses with stiffer or softer interfaces. In the case of the foundation system, the RC strip foundation reaches a Ψ of 0.5 for values of βa about 2 times higher than the reference case, thus with a stiffer response. In comparison, higher Ψ values are not possible, as RC strip foundations don't exceed Ψ equal to 0.5. A similar effect is given by the opening percentage: models with a small opening percentage present values of βa about 4 times higher than the reference case. Depending on the shape of the settlement, The value of β_a varies between being 3 times smaller and 2 times higher than the reference case (which is based on the average of the 8 settlement profiles chosen for the analysis) when Ψ equals 0.5. As the damage progresses, this variation increases, ranging from 6 times smaller up to 6 times larger when Ψ equals 3.5. Other parameters have a smaller influence on the results.

5.3.7. DIFFERENCES BETWEEN APPLIED AND RETRIEVED SETTLEMENTS

This section presents a refinement of the calculations presented in section 3.7 of [1]. The difference is related to the calculation of the relative bending stiffness parameter, which is detailed in the following. The differences, however, do not influence the original results, findings and conclusions.

Many authors investigated the relationship between ground displacements and building deformations using the modification factor (MD); This factor corresponds to the ratio between the deflection ratio computed from the deformation of the building and the one of the green field profile [36]–[40] (see Eq. 2.5 in section 2.5.4), for tunnelling and excavations. The deflection ratio and the MD values were computed for all analyses herein presented, allowing to compare the results with the state of the art. The MD factor is plotted against a dimensionless ratio, made up of the relative bending stiffness [36], that takes into account the role of the relative stiffness between the soil and the building. It should be noted that the relative bending stiffness ρ is typically computed per meter stretch in the direction perpendicular to the building length, since it was originally proposed with reference to plain-strain numerical analyses [36]. In this Chapter, the following equation 5.6 is used [37], [40]:

$$\rho = \frac{EI}{E_s L^3 W} \tag{5.6}$$

where EI is the masonry façade stiffness, Es represents the soil stiffness and L is the length of the building in either hogging or sagging based on the greenfield settlement profile (equal to the length of the façade in this study) and W is the building width. In this study, the relative bending stiffness ρ is computed with (5.6), assuming W is equal to the base of each selected strip foundation (differently from [1], which assumed W to be equal to the length "L" of the façade). In particular, in this chapter, EI is estimated with (5.7), similarly to [41]:

$$EI = E_w I_w \alpha_w + E_f I_f \tag{5.7}$$

Where E_w is the Young's modulus of the masonry, I_w is the second moment of inertia of the façade, while E_f I_f is the contribution of the foundation.
In particular, I_w is computed by assuming the neutral axis close to the mid-height of the façade in sagging (*i.e.*, $I_w = H^3*t/12$ with "t" and "H" represented in Figure 5.2) and equal to the top edge of the foundation in hogging (*i.e.*, $I_w = H^3*t/3$) [7]. The moment of inertia I_f of the foundation is computed relative to its own middle plane [41]. Moreover, α_w represents the reduction factor to consider the presence of voids (doors or windows), as proposed by Melis and Ortiz [41], reported in Table 5.6.
An example of the calculation of the relative bending stiffness ρ is reported in section B.1 of Appendix B for the reference case. The computed modification factors are compared to the design curves proposed by [37] in Figure 5.14 for different values of the damage parameter Ψ. The points found lay between the two design curves (Figure 5.14), offering an indirect validation of the numerical analysis results.
Interestingly, the values of the modification factor increase for higher levels of damage (higher Ψ values): As cracking develops, the stiffness of the building can decrease significantly, allowing the building to conform more closely to the assumed ground movement [34], [42]. However, Equation 5.6 does not account for this reduction in stiffness, meaning that ρ remains the same (in Figure 5.14) across different levels of damage (different values of Ψ), varying only based on the considered model. The reduction in building stiffness is reflected by the fact that the MD values progressively approach 1 as damage increases, as the deflection ratio measured on the building aligns more closely with that of the soil as

damage progresses (Figure 5.14).
In other words, as the damage to the building accumulates, it results in a more flexible response.

Table 5.6: Reduction factor of wall bending stiffness EI (from Melis and Ortiz [41]).

Type of wall	L < 2H	L > 2H
Opening from 0 to 15%	0.70	0.90
Opening from 15 to 25%	0.40	0.60
Opening from 25 to 40%	0.10	0.15

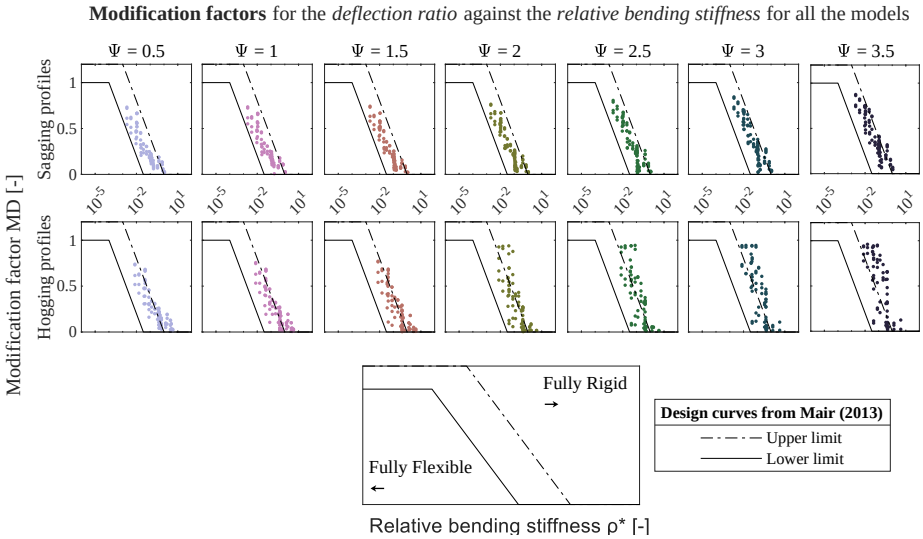

Figure 5.14: Modification factors for the deflection ratio with relative bending stiffness for all Ψ values. Design curves from [37]. The results refer to all the façade models and all the settlement profiles.

5.3.8. COMPARISON WITH THE AVAILABLE LIMIT VALUES

In Figure 5.15 the cumulative density functions (or exceedance curve) are retrieved for all the selected SRI parameters (*i.e.*, angular distortion, rotation, deflection ratio and differential settlement) for Ψ values ranging from 0.5 to 3.5. The exceedance curves were obtained by counting the number of models that exceed each threshold of damage (Ψ) in relation to the total number of analyses. It should be highlighted that the exceedance curves do not provide probabilistic information regarding the real population of masonry buildings, but only an insight into the results of the numerical analyses of this study. A more comprehensive analysis would require modelling a wider, realistic, set of cases and combinations of the investigated parameters.

Probability density functions of the damage for the *retrieved settlement parameters* for all the façade models

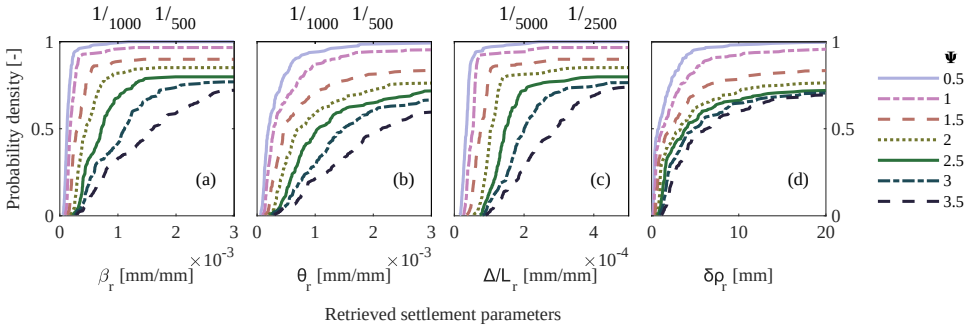

Figure 5.15: Cumulative density function for all the Ψ values for the retrieved: (a) angular distortion β_r, (b) rotation θ_r, (c) deflection ratio Δ/L_r and (d) differential settlement $\delta\rho_r$. The secondary x-axes (on top of the plots of the (a) angular distortion, (b) rotation and (c) deflection ratio) show the values of the parameters as $1/x^{-1}$, as typically adopted in the literature.

The limit values of the settlement parameters, often employed as guidelines or recommendations (*e.g.*, in [7], [14], [43]–[48]), are herein discussed in relation to the result of the numerical analyses proposed in this study. For each threshold, the frequency (or probability) of exceedance for the corresponding Ψ value is retrieved from the cumulative density functions shown in Figure 5.15. This allows assessing the performance of such limit values relative to the numerical analyses presented in this study. An overview of the available literature thresholds, in terms of the structures' angular distortion β and deflection ratio Δ/L, thus the "retrieved" settlement parameters, is presented in Table 5.7. Regarding other parameters, only a limited number of studies focus on the rotation and the differential settlements. For the rotation, there is a lack of limit values in the current state-of-the-art. In the case of the differential settlement, however, this parameter may not be sufficiently reliable in the definition of the relationship between the ground settlement and the resulting damage. For instance, although the differential settlement can be arguably easily computed in many cases, it does not provide any information regarding the distortion along the building. The differential settlements could also result from the uniform tilting of the building with small or null distortions in the structure unlikely to produce damage [5]. For each limit value in Table 7, the corresponding frequency of exceedance is reported from the curves of the retrieved settlement parameters (Figure 5.15). In all the encountered cases, if the goal is to prevent the occurrence of a Ψ value, the high probabilities of exceedance discussed indicate how the limit values may be too optimistic in relation to the results of the numerical model. For example, a Ψ higher or equal to 3.5 is associated with the occurrence of cracks above 5 mm wide (in this study), corresponding to the occurrence of a serviceability limit state [45]–[48]. In the Eurocode [46], the threshold values of the angular distortion β corresponding to the occurrence of a serviceability limit state ranges from 1/4000 to 1/300 depending on the shape of the settlement profile (Table 5.7). For such values of angular distortion, from 10 to 75 % of the models reach or exceed a Ψ of 3.5, thus the thresholds proposed in the guideline are observed to be too optimistic with respect to the results of this study.

Table 5.7: Overview of the available literature limit values [7], [14], [43]–[49] with the estimated Ψ values and corresponding probabilities of exceedance.

Reference	Parameter	Values [‰]	Fraction [1/ β^{-1}]	Description	This study	
					Ψ	Probability [%]
Meyerhof, 1982	β	0.5	1/2000	Safe limit for hogging	1	93
		1	1/1000	Safe limit for sagging	1	96
EN 1997-1 -2004	β	0.5 to 3.3	1/2000 to 1/300	sagging (serviceability limit state)	3.5	10 to 75
		0.25 to 1.7	1/4000 to 1/600	hogging (serviceability limit state)	3.5	0 to 52
Boscardin and Cording, 1989	β	1.5	1/667	Very slight damage (self-weight)	2.5	79
		3.3	1/300	Slight damage (self-weight)	3.5	75
Zhang and Ng., 2007	β	0.9	1/1100	Tolerable limit (load bearing walls)	1	96
		1.2	1/800	Tolerable limit (shallow foundations)	1	97
Polshin and Tokar, 1957	Δ/L	0.3 to 0.4	1/3300 to 1/2500	with L/H ≤ 3	1.5	89
		0.5 to 0.7	1/2000 to 1/1400	with L/H ≥ 5	1.5	89
		0.5	1/2000	no cracking limit	1	97
Burland et al. 1975	Δ/L	0.2 ‰	1/5000	Limit value for L/H =1	1.5	88

5.4. DISCUSSION

This chapter focuses on the settlements due to a combination of subsidence drivers (*e.g.*, organic soil oxidation, groundwater lowering, soil shrinkage) in urban areas. Detailed measurements of the ground settlements along strip foundation footprints are not available in the state of the art. Thus, the shapes of the imposed settlements, conformed to a Gaussian curve, fictitiously simulate the loss of support underneath the foundations without having the soil unrealistically pull on the foundations. Urban subsidence phenomena are characterized by smaller horizontal components of the ground movements compared to excavations, tunnelling or mining works [43]; Thus the horizontal ground deformations were purposely neglected. Furthermore, the 2D models do not account for variations in settlement in three dimensions. As a result, the intensity of the ground settlement is concentrated on the masonry facade. However, 3D settlement patterns are likely to cause damage to only specific exterior walls of a building, leaving others unaffected. Therefore, assuming that a single facade can serve as a proxy for evaluating the cracking damage of the entire structure was expected to provide conservative estimates.

A smooth interface was assumed for the analyses, due to the limited empirical knowledge of the transmission of the stresses and displacements from the soil to the foundations. However, a rough soil-foundation interface was observed to reduce the ratio between the applied and retrieved settlement deformations when compared to the smooth one.

Further improvements may include the effects given by the soil embedding the RC strip foundations (Figure 5.4c and d).

The geometry of the reference case is based on typical masonry structures. The chosen geometry represents an idealized rectangular facade, facilitating straightforward parametric analyses that consider variations in different geometric features of the models. However, real-world buildings may have walls with more complex shapes, such as single or double gable walls, or other intricate geometries. It is recommended to include the effect of different wall shapes in analyses focused on developing a probabilistic framework.

The Engineering Masonry Model has been utilized to simulate the non-linear cracking behaviour of masonry. While the model provides numerical stability [50], it has limitations in terms of damage localization, as cracks tend to appear diffuse rather than sharply localized [10], [50]. Despite this, the model has been successfully employed to replicate the crack patterns and behaviour observed in experimental tests with satisfactory accuracy [51].

Further improvements of the 2D modelling approach of the structure may include the calibration of the thickness of the lateral beam elements against a 3D model to better represent the effects of the house-to-house separation walls. This aspect is considered in Chapter 6.

In addition to the sensitivity analyses presented in this Chapter, the effects of different numerical settings (mesh size, load step size, convergence norms) should also be assessed, as they may affect the results of the numerical analyses. This aspect is further explored in Chapter 7.

5.5. CONCLUSIONS

The sensitivity analysis presented herein was carried out to investigate the non-linear response of the masonry façades subjected to different settlement shapes underneath their strip foundations. The effect of different buildings' features, material properties and settlement profiles was studied; Thus, we have observed:

- The results of the numerical analyses in terms of damage and deformation strongly vary depending on the shapes of the applied settlements. For instance, the initiation of damage for the reference model is achieved for values of the applied angular distortion ranging between 0.37 ‰(or about 1/2700) and 2.48 ‰(1/400) depending on the shape of the imposed settlements.
- As the damage increases, the façade tends to be more flexible, thus better accommodating the imposed settlement deformations.
- The façades on reinforced concrete strip foundations were observed, on average, to exhibit lower levels of damage with respect to the masonry ones.
- The façades with L/H smaller or equal to 1 were observed to have cracks of a maximum 1 mm, on average, without further progression of the damage afterwards, even for high values of the applied angular distortion (such as 0.1 or 1/10).

- On the contrary, some of the façades with L/H higher than 1 exhibit cracks equal to or wider than 5 mm for applied angular distortion of 0.35 ‰ (or 1/2833).
- The limit values of the settlement parameters (*i.e.*, angular distortion, deflection ratio, differential settlement, rotation) proposed in (inter)national codes and guidelines were found to be insufficient in preventing light damage, as compared to the results from the finite element models presented in this study.

5.5.1. IMPLICATIONS FOR THIS THESIS

The results of this Chapter are used as input for the development of a probabilistic framework in Chapter 7 and 8.

The influence of the lateral transverse walls is further investigated in Chapter 6, whereas the effect of different numerical settings is explored in Chapter 7. Among the scenarios selected for the numerical analyses presented in this chapter, the variations of L/H and opening percentage, settlement shapes, interface stiffness and masonry and soil material and mass significantly impact the models' responses. Nevertheless, some of the selected variations serve the sensitivity analysis's objectives and may not entirely reflect realistic conditions for buildings in the Netherlands; Thus, it is crucial to select and integrate realistic sets of the aforementioned features in the analyses to investigate the probabilistic response of buildings.

BIBLIOGRAPHY OF CHAPTER 5

[1] A. Prosperi, M. Longo, P. A. Korswagen, M. Korff, and J. G. Rots, "Sensitivity modelling with objective damage assessment of unreinforced masonry façades undergoing different subsidence settlement patterns," *Engineering Structures*, vol. 286, p. 116 113, 2023.

[2] P. A. Korswagen, M. Longo, E. Meulman, and J. Rots, "Experimental and computational study of the influence of pre-damage patterns in unreinforced masonry crack propagation due to induced, repeated earthquakes," in *13th North American Masonry Conference*, TMS, 2019, pp. 1628–1645.

[3] DIANA FEA, "Finite element analysis user's manual - release 10.5.," Report, 2021.

[4] J. Rots, P. Korswagen, and M. Longo, "Computational modelling checks of masonry building damage due to deep subsidence," *Delft University of Technology*, 2021.

[5] J. Charles and H. Skinner, "Settlement and tilt of low-rise buildings," *Proceedings of the Institution of Civil Engineers-Geotechnical Engineering*, vol. 157, no. 2, pp. 65–75, 2004.

[6] P. Van Staalduinen, J. Rots, and K. Terwel, "Onderzoek naar de oorzaken van bouwkundige schade in groningen: Methodologie en case studies ter duiding vande oorzaken," 2019.

[7] J. B. Burland and C. Wroth, "Settlement of buildings and associated damage," Tech. Rep., 1975.

[8] G. Giardina, A. V. Van de Graaf, M. A. Hendriks, J. G. Rots, and A. Marini, "Numerical analysis of a masonry façade subject to tunnelling-induced settlements," *Engineering structures*, vol. 54, pp. 234–247, 2013.

[9] NPR9998:2020en, *Assessment of structural safety of buildings in case of erection, reconstruction and disapproval - induced earthquakes - basis of design, actions and resistances*, 2021.

[10] G. Schreppers, A. Garofano, F. Messali, and J. Rots, "Diana validation report for masonry modelling," *DIANA FEA report*, 2016.

[11] P. A. Korswagen, M. Longo, E. Meulman, and C. van Hoogdalem, "Damage sensitivity of groningen masonry structures–experimental and computational studies: Stream 1," 2017.

[12] J. Rots, F. Messali, R. Esposito, S. Jafari, and V. Mariani, "Thematic keynote computational modelling of masonry with a view to groningen induced seismicity," in *Structural Analysis of Historical Constructions: Anamnesis, Diagnosis, Therapy, Controls*, CRC Press, 2016, pp. 227–238.

[13] R. B. Peck, "Deep excavations and tunneling in soft ground," *Proc. 7th ICSMFE, 1969*, pp. 225–290, 1969.

[14] G. Meyerhof, "Limit states design in geotechnical engineering," *Structural Safety*, vol. 1, no. 1, pp. 67–71, 1982.

[15] M. Son and E. J. Cording, "Estimation of building damage due to excavation-induced ground movements," *Journal of geotechnical and geoenvironmental engineering*, vol. 131, no. 2, pp. 162–177, 2005.

[16] L. Zhang and A. Ng, "Probabilistic limiting tolerable displacements for serviceability limit state design of foundations," *Geotechnique*, vol. 55, no. 2, pp. 151–161, 2005.

[17] T. Ang and K. Masri, "Behaviour of residential structures on problematic ground," in *IOP Conference Series: Materials Science and Engineering*, IOP Publishing, vol. 513, 2019, p. 012 010.

[18] NEHRP, "NIST GCR 12-917-21 soil-structure interaction for building structures," 2012.

[19] G. Gazetas, "Foundation vibrations," in *Foundation engineering handbook*, Springer, 1991, pp. 553–593.

[20] G. Mylonakis, S. Nikolaou, and G. Gazetas, "Footings under seismic loading: Analysis and design issues with emphasis on bridge foundations," *Soil Dynamics and Earthquake Engineering*, vol. 26, no. 9, pp. 824–853, 2006.

[21] S. Ferlisi, G. Nicodemo, D. Peduto, C. Negulescu, and G. Grandjean, "Deterministic and probabilistic analyses of the 3d response of masonry buildings to imposed settlement troughs," *Georisk: Assessment and Management of Risk for Engineered Systems and Geohazards*, vol. 14, no. 4, pp. 260–279, 2020.

[22] P. Kruiver, G. de Lange, A. Wiersma, *et al.*, "Geological schematisation of the shallow subsurface of groningen—for site response to earthquakes for the groningen gas field," *Deltares Report*, 2015.

[23] S. Ferlisi, G. Nicodemo, D. Peduto, *et al.*, "Numerical analysis of the behaviour of masonry buildings undergoing differential settlements," in *Proceedings of the XVII European Conference on Soil Mechanics and Geotechnical Engineering*, The authors and The Icelandic Geotechnical Society, IGS, 2019, pp. 1–8.

[24] M. Longo, M. Sousamli, P. A. Korswagen, P. van Staalduinen, and J. G. Rots, "Substructure-based 'three-tiered' finite element approach to soil-masonry-wall interaction for light seismic motion," *Engineering Structures*, vol. 245, p. 112 847, 2021.

[25] A. Drougkas, E. Verstrynge, P. Szekér, *et al.*, "Numerical modeling of a church nave wall subjected to differential settlements: Soil-structure interaction, time-dependence and sensitivity analysis," *International Journal of Architectural Heritage*, 2019.

[26] I. Anastasopoulos, N. Gerolymos, G. Gazetas, and M. Bransby, "Simplified approach for design of raft foundations against fault rupture. part ii: Soil-structure interaction," *Earthquake Engineering and Engineering Vibration*, vol. 7, pp. 165–179, 2008.

[27] P. A. Korswagen, M. Longo, and J. G. Rots, "High-resolution monitoring of the initial development of cracks in experimental masonry shear walls and their reproduction in finite element models," *Engineering Structures*, vol. 211, p. 110 365, 2020.

[28] J. B. Burland, B. B. Broms, and V. F. De Mello, "Behaviour of foundations and structures," 1978.

[29] P. A. Korswagen, M. Longo, E. Meulman, and J. G. Rots, "Crack initiation and propagation in unreinforced masonry specimens subjected to repeated in-plane loading during light damage," *Bulletin of Earthquake Engineering*, vol. 17, pp. 4651–4687, 2019.

[30] P. A. Korswagen, S. N. Jonkman, and K. Terwel, "Probabilistic assessment of structural damage from coupled multi-hazards," *Structural safety*, vol. 76, pp. 135–148, 2019.

[31] I. A. E. De Vent, "Prototype of a diagnostic decision support tool for structural damage in masonry," 2011.

[32] G. Giardina, "Modelling of settlement induced building damage," 2013.

[33] D. Peduto, G. Nicodemo, J. Maccabiani, and S. Ferlisi, "Multi-scale analysis of settlement - induced building damage using damage surveys and dinsar data: A case study in the netherlands," *Engineering geology*, vol. 218, pp. 117–133, 2017.

[34] M. Son and E. J. Cording, "Evaluation of building stiffness for building response analysis to excavation-induced ground movements," *Journal of geotechnical and geoenvironmental engineering*, vol. 133, no. 8, pp. 995–1002, 2007.

[35] H. Burd, W. Yiu, S. Acikgoz, and C. Martin, "Soil-foundation interaction model for the assessment of tunnelling-induced damage to masonry buildings," *Tunnelling and Underground Space Technology*, vol. 119, p. 104 208, 2022.

[36] D. Potts and T. Addenbrooke, "A structure's influence on tunnelling-induced ground movements.," *Proceedings of the Institution of Civil Engineers-Geotechnical Engineering*, vol. 125, no. 2, pp. 109–125, 1997.

[37] R. Mair, "Tunnelling and deep excavations: Ground movements and their effects," in *Proc., 15th European Conf. on Soil Mechanics and Geotechnical Engineering - Geotechnics of Hard Soils - Weak Rocks (Part 4)*, IOS Press, Amsterdam, 2013, pp. 39–70.

[38] K. Goh, "Response of ground and buildings to deep excavations and tunnelling," Ph.D. dissertation, University of Cambridge, 2011.

[39] A. Franza, S. Ritter, and M. J. Dejong, "Continuum solutions for tunnel–building interaction and a modified framework for deformation prediction," *Géotechnique*, vol. 70, no. 2, pp. 108–122, 2020.

[40] K. Goh and R. Mair, "Building damage assessment for deep excavations in singapore and the influence of building stiffness," *Geotechnical Engineering Journal of the SEAGS & AGSSEA*, vol. 42, no. 3, pp. 1–12, 2011.

[41] M. Melis and J. Rodriguez Ortiz, "Consideration of the stiffness of buildings in the estimation of subsidence damage by epb tunnelling in the madrid subway," in *International conference on the response of buildings to excavation induced ground movements*, 2001, pp. 387–394.

[42] B. Simpson and W. Grose, "Discussion: The effect of ground movements on rigid masonry facades," in *Proc., Int. Symp. on Geotechnical Aspects of Underground Construction in Soft Ground*, 1996, pp. 769–770.

[43] M. D. Boscardin and E. J. Cording, "Building response to excavation-induced settlement," *Journal of Geotechnical Engineering*, vol. 115, no. 1, pp. 1–21, 1989.

[44] D. E. Polshin and R. Tokar, "Maximum allowable non-uniform settlement of structures," in *Proc., 4th Int. Conf. on Soil Mechanics and Foundation Engineering*, Butterworth's London, vol. 1, 1957, pp. 402–405.

[45] W. Rankin, "Ground movements resulting from urban tunnelling: Predictions and effects," *Geological Society, London, Engineering Geology Special Publications*, vol. 5, no. 1, pp. 79–92, 1988.

[46] CEN, "Eurocode 7 geotechnical design - part 1: General rules. final draft, en 1997-1:2004 (e), (f) and (g)," Report, 2004.

[47] L. Zhang and A. M. Ng, "Limiting tolerable settlement and angular distortion for building foundations," in *Probabilistic applications in geotechnical engineering*, 2007, pp. 1–11.

[48] G. H. Yunusa, U. Hamza, A. Y. Abdulfatah, and A. Suleiman, "Geotechnical investigation into the causes of cracks in building: A case study," *Electronic Journal of Geotechnical Engineering*, vol. 18, pp. 2823–2833, 2013.

[49] A. W. Skempton and D. H. MacDonald, "The allowable settlements of buildings.," *Proceedings of the Institution of Civil Engineers*, vol. 5, no. 6, pp. 727–768, 1956.

[50] M. Sousamli, "Orthotropic cyclic continuum constitutive model for masonry structures and comparative studies," 2024.

[51] P. A. Korswagen, "Quantifying the probability of light damage to masonry structures: An exploration of crack initiation and progression due to seismic vibrations on masonry buildings with existing damage," 2024.

CHAPTER 6

FINDING AN OPTIMAL MODELLING STRATEGY FOR MASONRY BUILDINGS ON STRIP FOUNDATIONS SUBJECTED TO SUBSIDENCE: A Review of Existing Models and Development of the most suitable 2D Approach

The analysis presented in this Chapter has been published in [1]

CHAPTER 6: TABLE OF CONTENTS

6.1 Introduction **147**

6.2 Finite Element modelling strategies and method **148**
6.2.1 Methodology 148
6.2.2 The selected 2D and 3D modelling strategies 148
6.2.3 Model Geometry 149
6.2.4 FEM discretization 150
6.2.5 The inclusion of the lateral walls 150
6.2.6 Material properties 151
6.2.7 Interface elements at the bottom of the strip foundation . 152
6.2.8 Loadings: applied settlement shapes 153
6.2.9 Damage assessment 154

6.3 Results and comparisons of selected modelling approaches . . **154**
6.3.1 Crack patterns and Damage severity 154
6.3.2 Building model displacements 157
6.3.3 Stresses at the bottom of the interface 159
6.3.4 Features and performance of the models 160

6.4 Discussion **161**

6.5 Conclusion **162**
6.5.1 Implications for this thesis 163

Bibliography of Chapter 6 . . . . . **167**

6.1. INTRODUCTION

In this Chapter, 2D and 3D modelling strategies are used to represent the behaviour of historical masonry buildings on strip foundations undergoing settlements. The application focuses on a two-storey building, typical of the Dutch architectural heritage.

The aim is to provide background knowledge on the most suitable modelling techniques for masonry buildings undergoing ground settlement, with a focus on Dutch historic structures and their features.

Both two- or more complex three- dimensional modelling approaches can be used to study the structural behaviour. However, it is crucial to correctly identify and model the structural features that affect the response of the structure due to settlements, such as the effects of the lateral walls, *i.e.*, the walls connected to the façade perpendicularly, the floor and roof systems, and the foundation.

In the following, six 2D and 3D modelling strategies are selected from the state-of-the-art, and their results are compared to identify the most suitable and least cost-effective model(s) in terms of modelling and computational burden. Among the selected models, an improved 2D model, originally proposed in [2] and adopted in Chapter 5, includes the effects of the lateral walls in terms of stiffness and weight on the masonry building's response.

For all the selected models, the masonry strip foundation is modelled and supported by a no-tension interface, which represents the soil-foundation interaction. Two settlement configurations, hogging and sagging, are applied to the models, and their intensity is characterized using their angular distortion.

This chapter begins by introducing the Finite Element Models and the methodology in section 6.2. The results are presented in section 6.3 and discussed in section 6.4. In section 6.5, the conclusions are gathered.

The results presented herein represent further refinements of the analyses presented in 5, and provide additional background on the role of the different building features and the influence of the adopted modelling strategies.

The most suitable and least cost-effective model is selected to be used in the analyses presented in Chapter 7.

6.2. FINITE ELEMENT MODELLING STRATEGIES AND METHOD

6.2.1. METHODOLOGY

The adopted approach consists of three steps:

- In Step 0, the 2D and 3D modelling approaches for masonry structures subjected to ground settlements available in the state-of-the-art were reviewed.
- Based on this desk study, six modelling approaches were selected and used in Step 1 to generate the 2D and 3D numerical models for a two-storey building on masonry strip foundations.
- The results of the numerical analyses were compared in Step 2 to investigate their differences. Thus, models are compared in terms of displacements, damage and stresses. Among the selected modelling strategies, the most efficient is selected as the one associated with the lowest computational burden and costs.

6.2.2. THE SELECTED 2D AND 3D MODELLING STRATEGIES

Six modelling approaches were selected from the literature. The models are herein built with the finite element software Diana FEA 10.5 to analyse a masonry building undergoing settlements. The selected strategies include 2D plane-stress analyses and 3D models. A schematic illustration of the six selected models and their features is shown in Figure 6.1, and are herein labelled as:

- *2D FAçade model* (**2DFA** in Figure 6.1a), a **plane-stress** two-dimensional model of the building's façade [3]–[5];
- *2D façade model with Short Flanges* (**2DSF** in Figure 6.1b), a **plane-stress** two-dimensional model with one-brick lateral flanges, (i.e, 100 mm in the plane of the façade and 210 mm in the direction of the transverse walls) modelled with beam elements, that simulates the presence of lateral walls [6]–[8];
- *2D façade model with Long Flanges* (**2DLF** in Figure 6.1c), an improved **plane-stress** two-dimensional model with lateral flanges whose width is wider than one brick (*i.e.*, higher than 210 mm in the direction of the transverse walls). The overburden given by the floor and roof is also included, differently from 2DFA and 2DSF [2];
- *3D FAçade model* (**3DFA** in Figure 6.1d), a **shell-elements** three-dimensional model of the building's façade; This model does not differ significantly from 2DFA, and it is included to check whenever differences can be observed using shell-elements rather than plane stress elements.
- *3D BOX model* (**3DBOX** in Figure 6.1e), a **shell-elements** three-dimensional model of the entire building, without floors and party walls, similar to [9]–[12];
- *3D FULL model* (**3DFULL** in Figure 6.1f), a **shell-elements** three-dimensional model of the entire building including a timber floor, timber roof and an inner structural wall, similar to [10], [12]–[14].

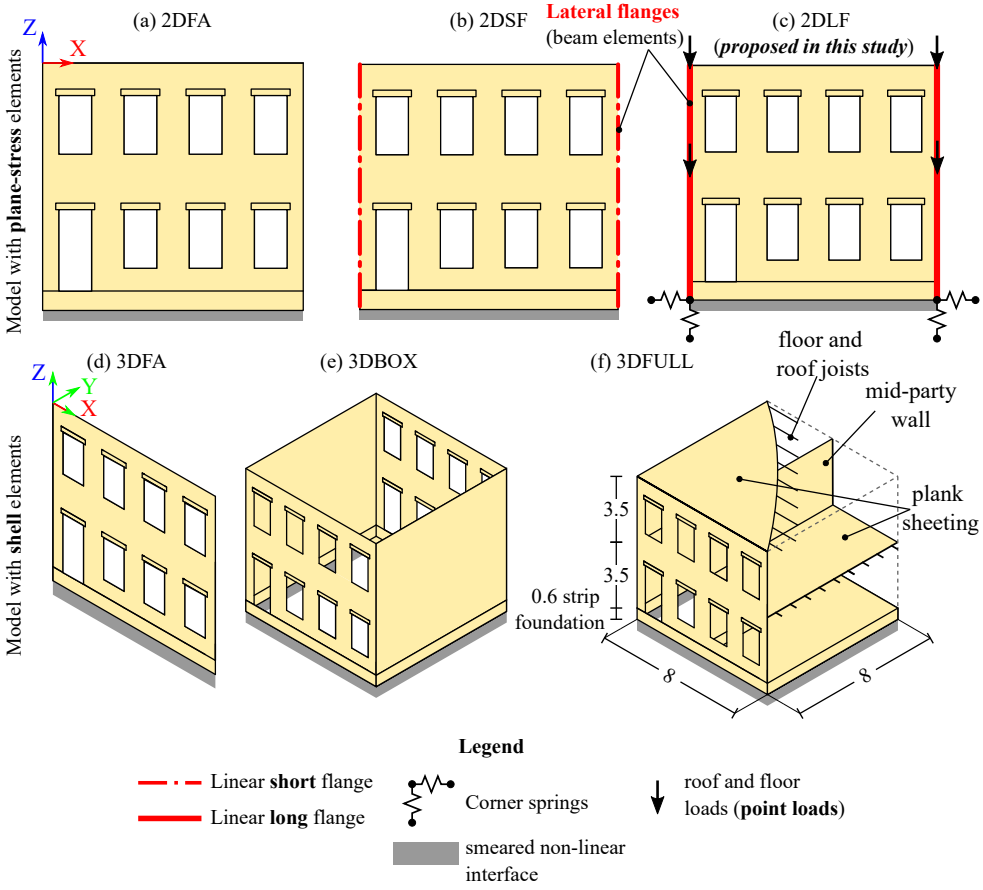

Figure 6.1: The six modelling approaches selected from the state-of-the-art: (a) 2D FAçade model (2DFA); (b) 2D façade with lateral Short Flanges (2DSF); (c) 2D façade with lateral Long Flanges (2DLF); (d) 3D FAçade model (3DFA); (e) 3D BOX model (3DBOX); (f) 3D FULL model (3DFULL). Measures in meters.

6.2.3. MODEL GEOMETRY

The selected modelling strategies are employed to investigate the behaviour of a two-storey masonry building. The façade of the selected building has a width of 8 meters (direction "X" in Figure 6.1), and a height of 7 meters. The selected building idealizes typical old Dutch houses [15]. Moreover, the façade represents a single-wythe wall (*i.e.* the width of one brick, equal to 100 mm, in direction "Y" in Figure 6.1) [7]. The lateral walls of the building have the same dimension and cross-section as the façade (Figure 6.1).

Below each wall, the unreinforced masonry strip foundations are modelled. In the Netherlands, unreinforced masonry strip foundations are commonly observed in old buildings that rely on shallow foundation systems. The foundation is characterized by a base (perpendicularly to the façade, direction "Y" in Figure 6.1) equal to 500 mm and a height of 600 mm. In all the models, the façade includes openings underneath masonry lintels.

6.2.4. FEM DISCRETIZATION

Regarding the mesh of the selected models, 8-node quadratic elements with 3 x 3 Gaussian integration schemes were adopted for the façade, lintels, and foundation for both the 2D and 3D analyses. A mesh size of 100 x 100 mm was used for the plane stress and curved shell elements, and 100 mm for the beam elements.

In the case of 3DFULL, the timber floor and timber roof, commonly observed in Dutch historical buildings, were modelled using the class-III Mindlin beam elements, representing the joists. Moreover, orthotropic shell elements were used for the plank sheeting. The floor, roof and mid-party wall were assumed to be disconnected from the front and back façades and to transmit the load to the transversal walls.

Similarly, in the case of the 2DSF and 2DLF models (Figure 6.1b and c respectively) Class-III Mindlin beam elements [16] were placed at the sides of the façade to model the effect of the transverse walls, following the approach implemented in [6], [8].

6.2.5. THE INCLUSION OF THE LATERAL WALLS

The lateral elements simulate the additional stiffness and weight due to the presence of lateral walls and prevent the rotation of the façade's edges [7], [8]. The inclusion of lateral elements was observed to aid the development of realistic crack patterns due to ground settlements in similar studies [7], [8].

In the case of model 2DSF (Figure 6.1b), the presence of lateral walls is modelled with one-brick flanges (*i.e.*, 100 mm in the plane of the façade and 210 mm in the direction of the transverse walls).

Regarding the improved 2D model, *i.e.*, 2DLF (Figure 6.1c), an analytical approach is proposed to compute the length values (perpendicularly to the façade) adopted for lateral beam elements. This length corresponds to the "*cooperating flange*" of walls subjected to shear loading [17], [18]; The cooperating flanges contribute added stiffness to the facade when it's subjected to shear action, provided a good interlocking between the transverse and the façade [17], [18]. In the case of Dutch buildings (*section 5.5.3* of [18]), the Dutch standard integrates this contribution with a normal compression force given by two areas: the normal compressive force is provided by the part of the building wall located next to the cooperating flange width (from [17]); this further contributes to the facade stability and the stress redistribution in the case of shearing actions.
In this chapter, the same value is used to describe the portion of the transversal walls that contribute to the response of the façade subjected to settlements. Accordingly, the length of the cooperating flanges corresponds to the sum of three contributions (A1, A2a and A2b in Figure 6.2):

- The first contribution (A1 in Figure 6.2) was computed by considering the minimum of the following transverse wall properties: i) a fifth of the wall height ii) half of the internal distance between party walls (Ls/2) iii) six times the wall thickness ($6t_w$), as described in [17]. The obtained value for the selected case is equal to 0.6 m;

- The second and the third contributions (A2a and A2b in Figure 6.2), correspond to

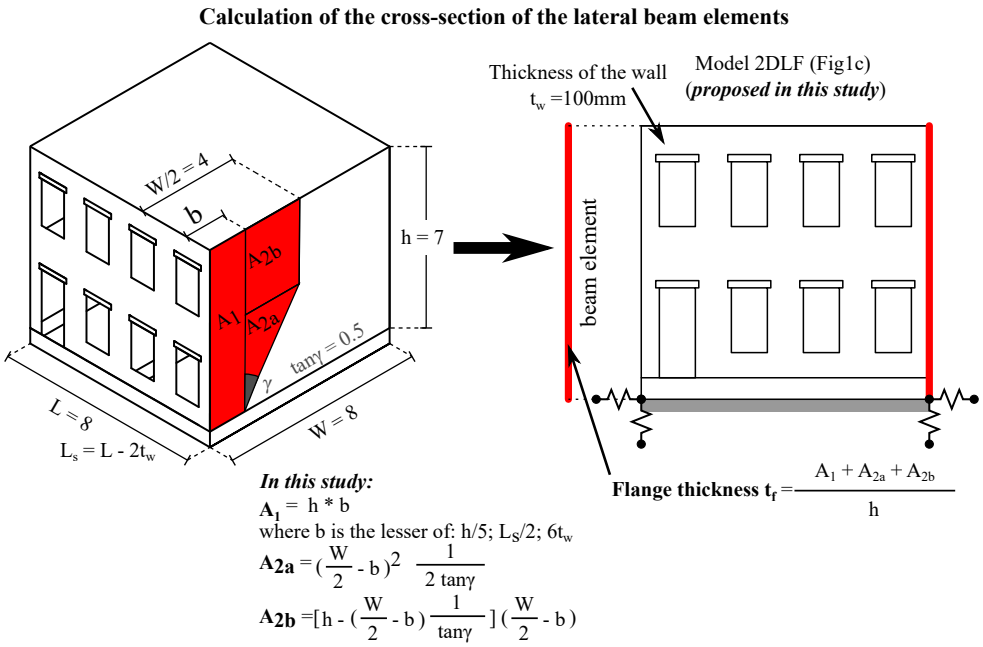

Figure 6.2: The calculation of the cross-section of the lateral beam elements used in the model 2DLF (Figure 6.1c). Measures in meters.

the contribution to the normal compression given by the flange, as described in [18].

The sum of the three contributions (Flange thickness t_f in Figure 6.2), *i.e.*, the length of the flange for the model 2DLF is 2.35 m for the selected case; Therefore, the computed value is about 11 times higher than the one used for the model with short flange 2DSF (which is equal to 210 mm), whereas the dimension is the same along the plane of the façade, *i.e.*, 100 mm.

6.2.6. MATERIAL PROPERTIES

The non-linear cracking behaviour of masonry behaviour of the masonry material was modelled employing an orthotropic, smeared crack/shear/crush constitutive law, *i.e.*, the Engineering Masonry Model [19], [20].

The parameters of the adopted constitutive law correspond to the material properties of the clay brick masonry (Table 6.1); Such material properties were retrieved from the Dutch Standard [21] and previous studies [19], [22]. The Engineering Masonry Model was adopted for the façade, the lintels and the foundation.

The Young's modulus equal to 1/3rd of the one of the masonry material (Ey in Table 6.1) a Poisson's ratio equal to 0.15 were used for the lateral flanges in both the models 2DSF and 2DLF. The addition of lateral flanges with a reduced Young's modulus follows the calibration and validation presented in [8]; Accordingly, achieving realistic crack patterns was observed [6], [8].

Table 6.1: Material properties adopted in the FE models.

Material Properties	Symbol	Unit of measure	Value
Young's modulus vertical direction	E_y	[MPa]	5000
Young's modulus horizontal direction	E_x	[MPa]	2500
Shear modulus	G_{xy}	[MPa]	2000
Bed joint tensile strength	f_{ty}	[MPa]	0.10
Minimum head-joint strength	$f_{tx,min}$	[MPa]	0.15
Fracture energy in tension	$G_{ft,I}$	[N/mm]	0.01
Angle between stepped crack and bed-joint	α	[rad]	0.50
Compressive strength	f_c	[MPa]	8.50
Fracture energy in compression	G_c	[N/mm]	20.00
Friction angle	φ	[rad]	0.70
Cohesion	c	[MPa]	0.15
Fracture energy in shear	G_s	[N/mm]	0.10
Mass density	ρ	[Kg/m^3]	1708

The timber floor and timber roof are herein modelled using elastic C24 class (table 3.4 of [23]) material for both the class-III Mindlin beam element and the orthotropic shell elements [16], calibrated according to the Appendix G of [21].

The selected soil is characterized by the shear modulus equal to 10 MPa and the Poisson's ratio equal to 0.45. The soil material properties were adopted for the interface elements.

6.2.7. INTERFACE ELEMENTS AT THE BOTTOM OF THE STRIP FOUNDATION

At the bottom edge of the strip foundation, a no-tension boundary interface was used to model the soil-foundation interaction [24]. The interface has zero tensile strength, while it acts linearly in compression and shear. When an opening occurs, the shear stiffness is reduced to zero at that location.

In the case of both 2D and 3D models, six-noded line interface elements and the Newton-Cotes integration scheme are used [16]. In particular, 2D models use 5 integration points, while for 3D models 3 integration points are used.

Interface elements require the definition of the normal (*i.e.*, in the direction of gravity) and tangential (along the façade) stiffness values. Such values are herein computed using the analytical formulations reported by [25]–[27]. The interface stiffness values depend on soil shear modulus G, Poisson's ratio ν, and foundation base and length, following the approach implemented in [7].

Additionally, the model 2DLF uses two corner springs below the transversal walls (Figure 6.1c) which are placed to support the additional weight of the lateral beam elements. The normal and tangential stiffness values computed for the interface elements are also assigned to the corner springs, by dividing the stiffness values by the area underneath the transversal wall.

6.2.8. LOADINGS: APPLIED SETTLEMENT SHAPES

In all the selected models, settlements are modelled as displacements imposed at the base of the interface. This approach enables to fictitiously simulate the loss of support below the foundation due to the settlements, without having the soil unrealistically pull on the foundations [7]. The settlement actions idealize the occurrence of two types of asymmetric deformations (*i.e.* hogging and sagging in Figure 6.3) [7]. The imposed settlement deformations are based on field data and literature [7], [28], [29]. In the case of tunnelling-induced settlements, the ground movements are often observed to resemble Gaussian probability curves. However, in this work Gaussian curves are also used to idealize the deformations due to other sources of subsidence, similarly to [7]. Therefore, the displacements imposed at the interface at the base of the foundation were computed using equation 6.1 [30], in the same way presented in section 5.2.3:

$$S_v(x) = S_{v,max} e^{\left(\frac{-x^2}{2x_i^2}\right)} \tag{6.1}$$

Where $S_v(x)$ represents the vertical ground settlement at the location x; xi is the distance from the symmetric axis of the Gaussian curve to the point of inflection, and $S_{v,max}$ is a value that enable imposing the same intensity for all the profiles. In particular, the intensity of the settlement profiles is measured by the angular distortion β, *i.e.* the slope of the line joining two consecutive points in relation to a line joining the two points at the sides of each settlement profile [31]; In particular, the angular distortion β is herein considered to be the maximum along the façade, following an approach implemented in [7]. Therefore, the $S_{v,max}$ is imposed so that the two settlement patterns are characterized by an angular distortion equal to 1/300. Equation 6.1 allows the computation of two-dimensional curves; In the case of the 3D models, the settlement shapes obtained with Eq.6.1 are extruded in the direction perpendicular to the plane of the façade. This enables a consistent comparison between the results of all the models, as the façade is always subjected to the same imposed displacements. Therefore, the obtained settlement actions do not include the effects of three-dimensional settlement variations, which are explored for instance in [32].
In the model 3DFULL (Figure 6.1f) the effect of the overburden given by the timber floor and timber roof is included. In the case of the improved 2DLF model (Figure 6.1c), the overburden of the floors was modelled by applying four equivalent point loads, two per floor at each side of the façade (Figure 6.1c); The intensity of the four equivalent point loads was computed considering the portion of the floor and roof that loads the length of the cooperating flanges.

The load application procedure includes two phases for all the selected models: First, the self-weight of the masonry structure, and eventually the overburden of the floors, was applied in 10 steps to obtain the initial stress-state. Then, the settlement is imposed at the base of the interface, and the intensity of the displacements is progressively increased in 195 steps (which correspond to a load rate of 0.02 mm/step).

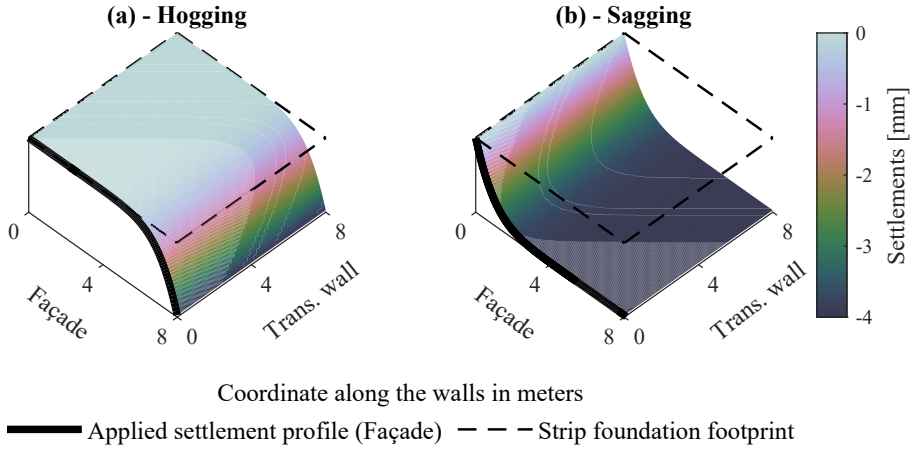

Figure 6.3: The two settlement shapes imposed at the base of the interfaces in the finite element models: (a) Hogging and (b) Sagging. The settlement profiles are conformed to a Gaussian curve. Their angular distortion is equal to 1/300. Measures in meters.

6.2.9. DAMAGE ASSESSMENT

For each step of the numerical analyses, the tabulated output of the FEM models can be used to quantify the damage progression and accumulation. Damage is then assessed using the parameter Ψ, with the same methodology presented in section 5.2.5 of this dissertation.

6.3. RESULTS AND COMPARISONS OF SELECTED MODELLING APPROACHES

6.3.1. CRACK PATTERNS AND DAMAGE SEVERITY

An example of the progression of the damage for the model 2DLF (Figure 6.1c) and 3DFULL (Figure 6.1f) is shown in Figure 6.4.

For each model, the vertical displacements at the façade's base (top edge of the foundation) were retrieved. A distinction is therefore introduced between the applied deformations at the interface level, herein labelled as "applied", and the resulting façade displacements, identified as "retrieved" [7]. Thus, the angular distortion imposed at the interface level is labelled as "βa", whereas "βr" is computed from the retrieved displacements.

Figure 6.5a and b show the relationship between the applied angular distortion β and the damage parameter Ψ.

It can be observed that the two façade models 2DFA (with plane stress elements) and 3DFA (with shell elements) show just minor differences (Figure 6.5). This observation confirms that no major differences can be attributed only to a change of the adopted finite elements (*i.e.* plane stress or shell elements).

The three-dimensional models, 3DBOX and 3DFULL, also show similar trends. More-

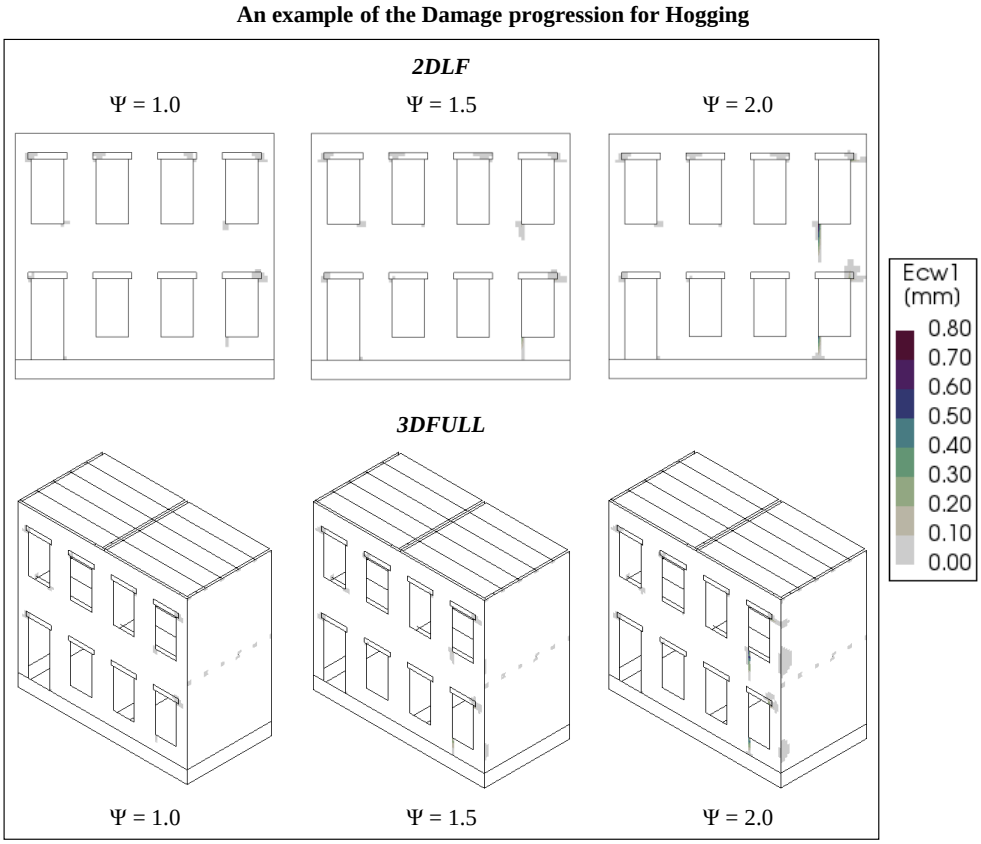

Figure 6.4: An example of the progression of the damage for model 2DLF (Figure 6.1c) and 3DFULL (Figure 6.1f) for the imposed hogging settlement (Figure 6.3a) for different values of imposed distortion βa. The principal crack width (Ecw1) is shown. 3DFULL depicts half the model.

over, the more detailed 3D model exhibits higher damage for the same applied angular distortion, compared to the simplified façade models, 2DFA and 3DFA.

The results show how the model with a short lateral flange, 2DSF exhibits a trend comparable with the other simplified 2D analyses, presenting slightly more damage in hogging, and less in sagging (similarly to the results presented in Fig. 5.10c). Conversely, the proposed 2D model with a long lateral flange (*i.e.*, 2DLF) shows a trend more similar to the more detailed 3D cases. Interestingly, smaller differences between the trends of the models are observed when the retrieved angular distortion βr is plotted against Ψ (Figure 6.5c and d); This observation proves that the retrieved deformation mainly depends on the shape and the stiffness of the façade itself. This is in agreement with the results of [7]. Regarding the ratio between the applied and the retrieved values of the angular distortion, shown in Figure 6.5e and f for hogging and sagging respectively, the plotted lines are compared with a dash-dotted line that represents the condition for which applied and retrieved values would be equal (Figure 6.5).

The results of the models 2DLF, 3DBOX and 3DFULL progressively get closer to the theo-

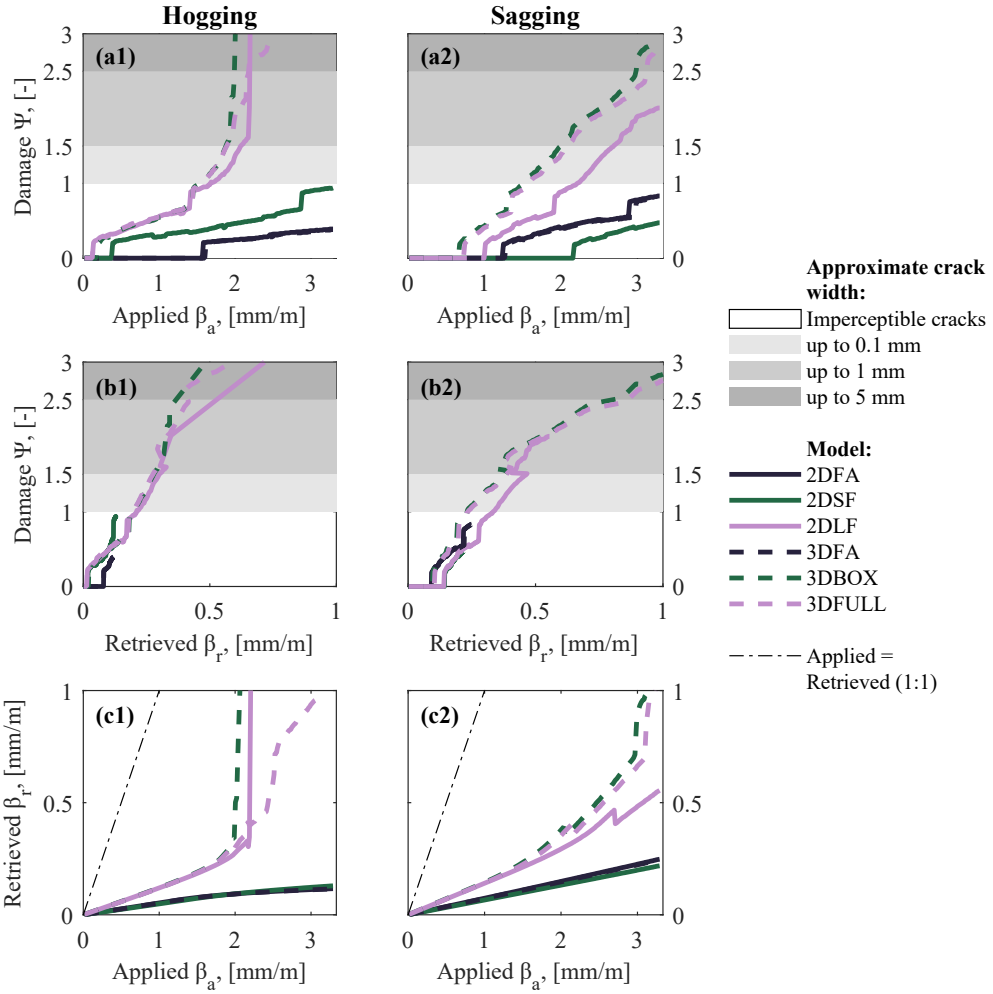

Figure 6.5: Applied and Retrieved angular distortion β against the resulting damage parameter Ψ for all the FE models for both hogging and sagging. The results of the models 2DFA and 3DFA overlap in all the plots.

retical line as the damage accumulates on the façade. Therefore, the 2DLF model better accommodates the imposed settlements with the damage progression. This behaviour is less clear for the model with short lateral elements, 2DSF. Conversely, the two simplified façade models, 2DFA and 3DFA, show a different trend.

For an applied angular distortion βa equal to 2 ‰(or 1/500), a comparison is shown in Figure 6.6 between the crack patterns (*i.e.* location and direction of the cracks) exhibited by all the models for both hogging and sagging. For the selected angular distortion, the simplified façade models, 2DFA and 3DFA, and the model with short lateral elements, 2DSF, underestimate the damage (in terms of Ψ), both in hogging and sagging when compared with 3DFULL.

The 3DBOX model, in which the effects of the party wall and floors are not included,

shows the highest damage in both hogging and sagging. The damage and crack patterns of the models 2DLF and 3DFULL are observed to be in good agreement.

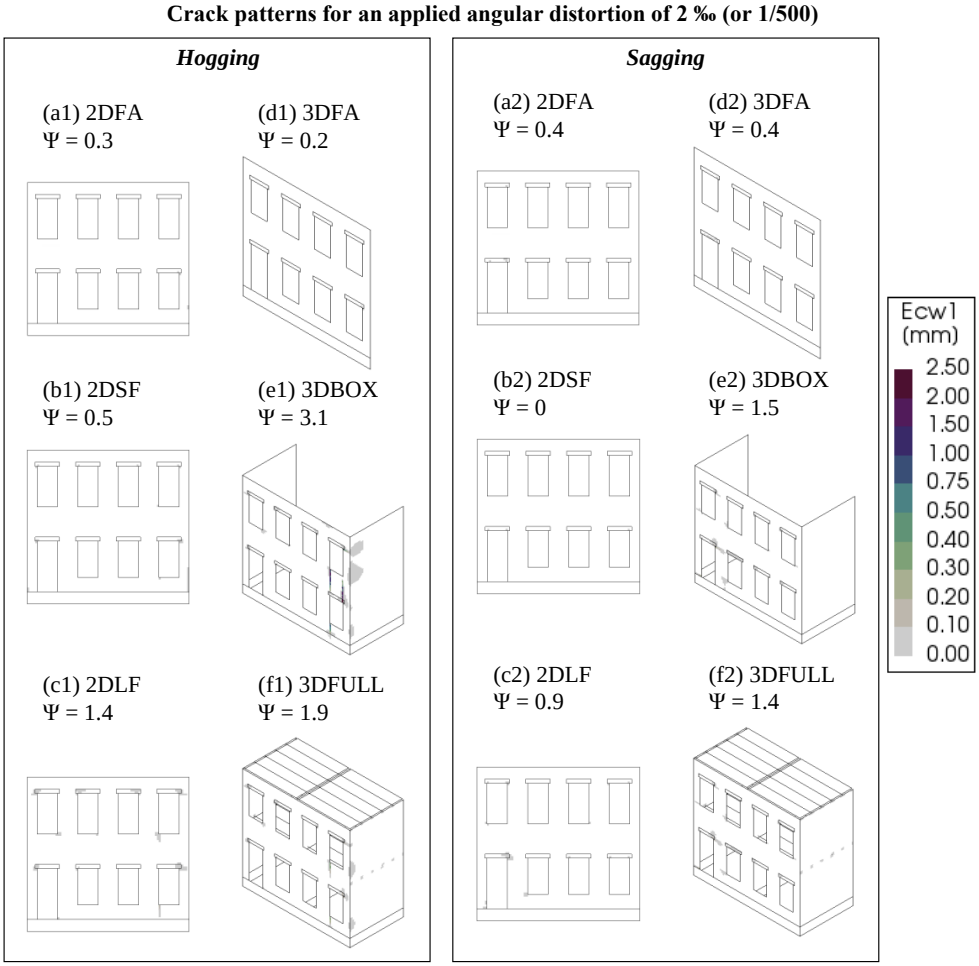

Figure 6.6: Resulting crack patterns for all the FE models at an applied angular distortion of 2 ‰(or 1/500). The principal crack width (Ecw1) is shown. The damage parameter Ψ is reported for every model. (e1), (f1), (e2) and (f2) depict half the model.

6.3.2. BUILDING MODEL DISPLACEMENTS

Figure 6.7 shows the comparison in terms of vertical (*i.e.*, in the direction of gravity) displacements. The models, 2DFA, 3DFA and 2DSF exhibit different stiffer behaviour, *i.e.*, less deformation, when compared to the models 2DLF, 3DBOX and 3DFULL in hogging and sagging (Figure 6.7).This is in agreement with the trends shown in Figure 6.5.

The inclusion of a flexible diaphragm in 3DFULL shows that the additional lateral con-

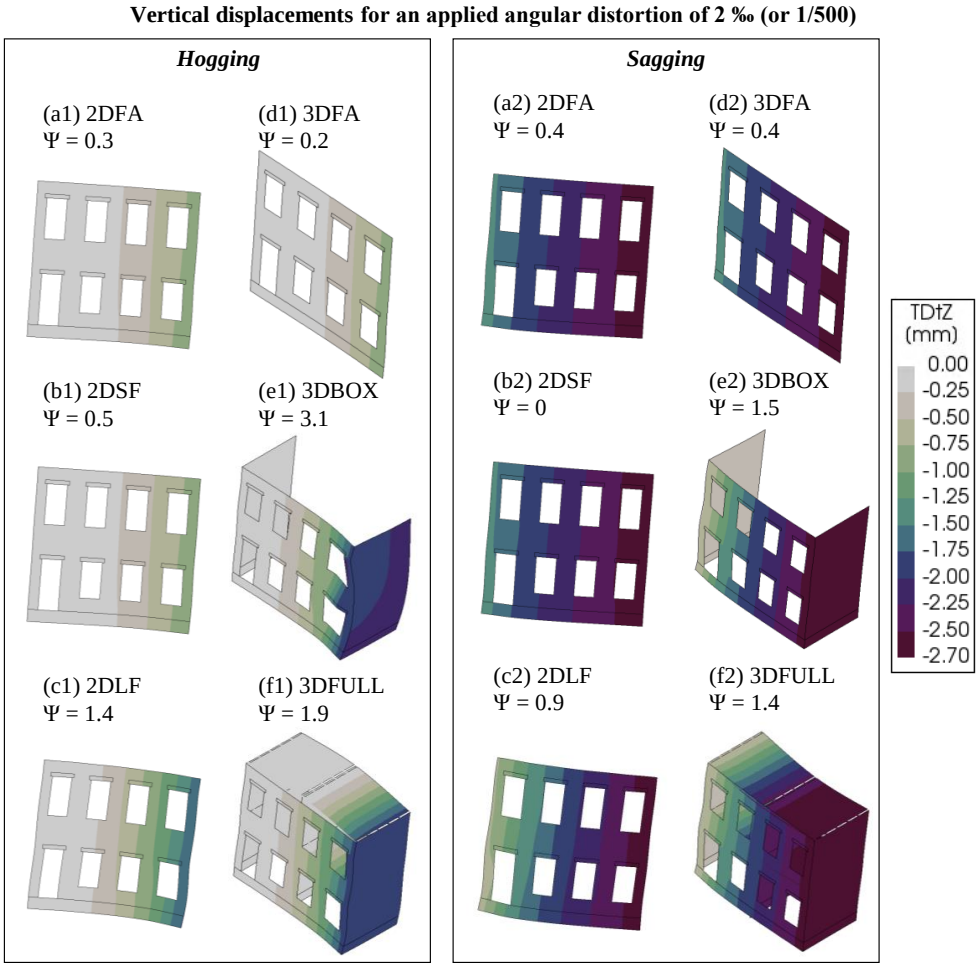

Figure 6.7: The resulting vertical displacements (TDtZ in the Legend) for all the FE models at an applied angular distortion of 2 ‰(or 1/500). Deformations are exaggerated (The magnification factor is equal to 500). The damage parameter Ψ is reported for every model. (e1), (f1), (e2) and (f2) depict half the model.

finement and extra overburden of the transversal walls do not influence the initiation and progression of the displacement-crack of the front facade. A small difference between 3DBOX and 3DFULL becomes visible when Ψ reaches a value of about 2.0. This confinement reduces the brittleness of the mechanism and avoids larger out-of-plane displacement of the transversal walls. The confinement effect of the floor is mainly predominant when hogging deformation occurs (Figure 6.5).

Out-of-plane (OOP) displacements, *i.e.*, perpendicular to the plane of the façade, are observable in the 3D models, differently from 2D ones, which do not include this feature. Figure 6.8 shows the out-of-plane displacements for the models 3DBOX and 3DFULL. Interestingly, the two models exhibit different OOP displacement patterns, both in hogging and sagging (Figure 6.8). For the selected value of angular distortion equal to 2 ‰(or

1/500), the maximum absolute value of OOP displacement is equal to 0.25 millimetres.

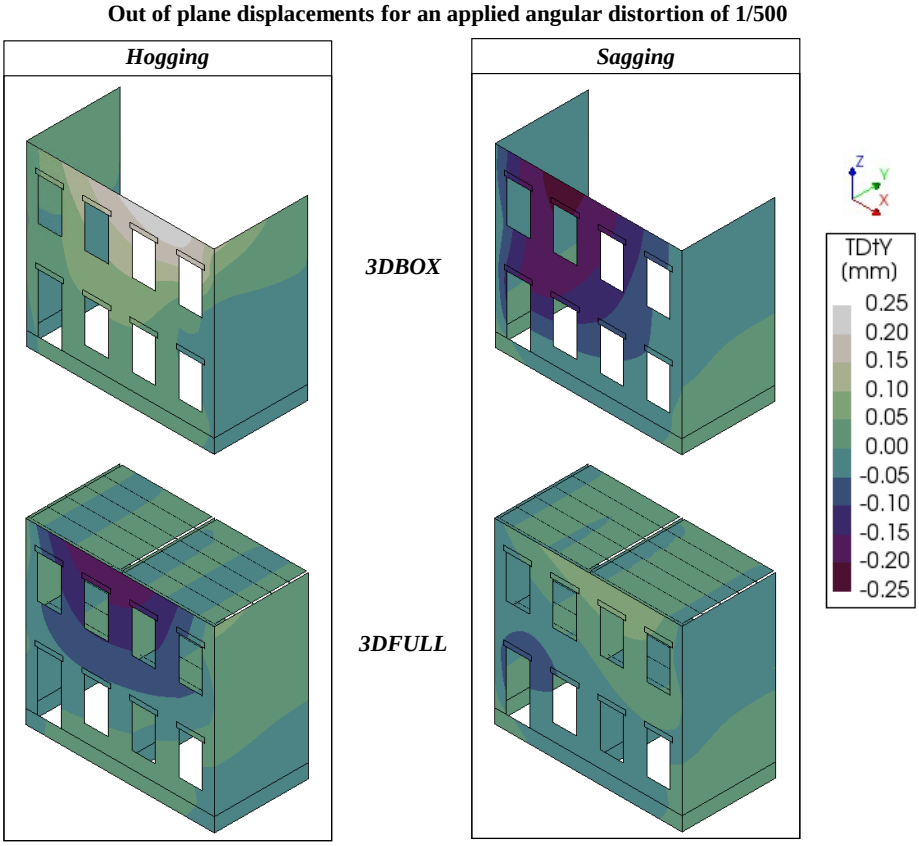

Figure 6.8: Out-of-plane (OOP) displacements (TDtY in the Legend) for all the FE models 3DBOX and 3DFULL at an applied angular distortion of 2 ‰(or 1/500) for both hogging and sagging. Deformations are shown and exaggerated along the direction of the transverse walls (The magnification factor is equal to 5000). The plots depict half the models.

6.3.3. STRESSES AT THE BOTTOM OF THE INTERFACE

For the selected settlement intensity, *i.e.*, βa equal to 2 ‰(or 1/500), a comparison between the normal interface stresses is proposed in Figure 6.9. Accordingly, Figure 6.9 shows the results for both hogging and sagging. In both hogging and sagging, a good agreement is observed between the results of the models 2DLF, 3DBOX and 3DFULL. For instance, the stresses reveal that for the models 2DLF, 3DBOX and 3DFULL the entire interface is subjected to compression in the case of hogging. On the contrary, the models 2DFA, 2DSF and 3DFA show the formation of a gap at the right side of the façade, which means that that location reached zero compressive stress.

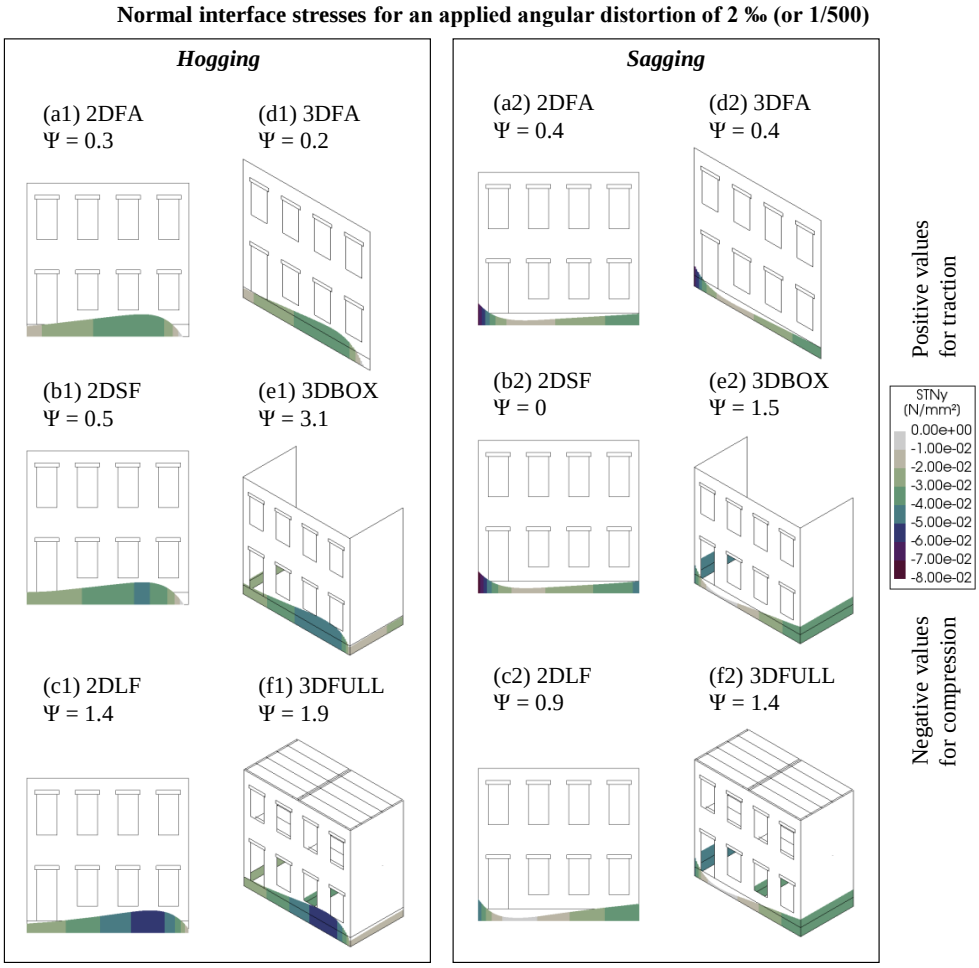

Figure 6.9: Normal (*i.e.*, direction of gravity) interface stresses for hogging and sagging, with applied angular distortion of 2 ‰(or 1/500). Positive values represent tension, and negative ones, compression. (e1), (f1), (e2) and (f2) depict half the model.

6.3.4. FEATURES AND PERFORMANCE OF THE MODELS

The features of the numerical models in terms of type of elements, number of elements and nodes are summarized in Table 6.2. The CPU time of the analyses with the hogging settlement action (Figure 6.3a) is reported. Additionally, as the 3D models can make use of the structural symmetry, two additional analyses that include this effect are included, and are herein labelled as 3DBOX-Half and 3DFULL-Half (Table 6.2). These estimates do not include the time to build the model, generate the mesh or set up the analyses. Moreover, the analysis time of each model was normalized to one of the proposed 2DLF model. The 2D models, 2DFA and 2DSF are the ones that require less computational time. The model 3DFA is 6 times slower than its plane-stress counterpart 2DFA. The models 3DBOX and 3DFULL are 37 to 40 times slower than the reference case, *i.e.*, 2DLF; Even

Table 6.2: A comparison of the performance of all the adopted models. The values of the proposed modelling approach 2DLF (Figure 6.1c) are shaded.

Model	Type of Elements	Elements	Nodes	Analysis Time [hh:mm:ss]	Normalized Analysis Time
2DFA	2D Plane Stress	4570	14414	00:08:41	0.36
2DSF	2D Plane Stress	4722	14414	00:08:25	0.35
2DLF	**2D Plane Stress**	**4724**	**14414**	**00:24:18**	**1.00**
3DFA	3D Shell	4650	14638	00:48:34	2.00
3DBOX	3D Shell	21620	66088	14:48:21	36.56
3DFULL	3D Shell	41580	121944	16:04:28	39.69
3DBOX-Half	3D Shell	10810	33198	03:50:18	9.48
3DFULL-Half	3D Shell	61436	20895	06:17:41	15.54

the models that make use of the structural symmetry, 3DBOX-Half and 3DFULL-Half, are 9 to 16 times slower than the reference case; Similar trends are observed in Sagging.

6.4. DISCUSSION

In this chapter, different 2D and 3D modelling strategies, inspired by the state-of-the-art, for masonry buildings on strip foundations undergoing settlements are compared. The imposed loads considered are settlement deformations applied at the bottom of a boundary interface underneath the foundation. The imposed settlements do not present variations along the direction perpendicular to the plane of the façade. This assumption, however, serves the purpose of achieving a consistent comparison among the different modelling strategies. In the cases of structures undergoing settlements that highly resemble 3D patterns, 2D analyses may not be suitable to accurately depict the building response.

Regarding the imposed settlement, only the vertical components of the ground displacements are idealized and considered. Conversely, the horizontal ground movements were purposely neglected. Horizontal ground movements play a key role in the case of settlement induced by human activities, such as tunnelling, mining or excavation works [33]; this chapter focuses instead on the effect of settlements that occur due to a combination of other subsidence sources (*e.g.* organic soil oxidation, groundwater lowering, soil shrinkage).

The soil deformations were herein imposed at the base of no-tension interfaces with a linear elastic behavior in shear. However, further analyses and future studies can benefit from the use of a soil friction angle to better simulate the contact at the base of the foundation, as shown in [7].

Regarding the limitation of 2D modelling strategies, ie., 2DFA, 2DSF and 2DLF, they are not able to include out-of-plane effects of the walls. In this chapter, out-of-plane displacements in the 3DFA were not activated, while detailed 3D models, 3DBOX and 3DFULL reach a maximum of 1.7 mm at the end of the settlement applications, which

is thus considered negligible. Previous studies, *i.e.*, [13], [34], show that the difference between a 3D façade model, in which the 3D effects in terms of transverse wall and foundations are not included (similar to 3DFA) and a 3D full-structure model (similar to 3DBOX) provides similar results in terms of strains and damage for specific tunnelling-induced settlements; It should be noted, however, that the damage was there assessed considering the magnitude on the building maximum tensile strain, differently from this chapter. Additionally, such studies considered a different type of constitutive relation of the masonry material.

The results herein presented suggest that including the 3D effect of the lateral walls is crucial: the interface stresses, displacements and cracking are all observed to be influenced by the weight and stiffness of lateral walls. The presence of a wider transversal wall (with additional weight) and the corner springs (additional stiffness) in the 2DLF model allows for a better representation of the three-dimensional effects. A similar effect at the side of the façades is expected when adjacent structures share transversal walls, in agreement with [12].

The considered clay masonry façade and lateral walls idealize the structural inner leaves of old Dutch houses with cavity walls; Therefore both the façade and the lateral wall are characterized by the same wythe equal to 100 mm. However, it is expected that the results of this chapter can provide background to the analyses of cases characterized by the façade and the transverse walls with different wythes, such as for single wythe façade interlocked with double wythe house-to-house separation walls.

Additionally, although the use of linear elastic lateral elements in the model 2DSF and 2DLF serve as a modelling strategy rather than an actual depiction of the behaviour of the lateral walls, it was confirmed that the traction stresses to which they are subjected during the application of the settlement load never exceed the (bed joint) tensile strength of the masonry material; Consequently, the use linear-elastic elements were deemed suitable for the lateral walls in this chapter.

Further improvements of the proposed modelling approach may include the effect given by lateral walls with openings or the lateral confinement by the floor system; The inclusion of such effects can be attained, for instance, by means of discrete lateral springs. In this case, however, a 3DBOX model that does not include the timber floor and roof and the lateral walls only slightly differs in terms of deformation, crack pattern and stresses from the 3DFULL model in which such effects are included. This indicates that, for the reference case, the effects in terms of stiffness of the timber floor and roof system may be negligible. This is in agreement with the work of [9], in which it is reported that "*most of the mass and stiffness of a masonry building lies in the masonry itself*".

6.5. CONCLUSION

The results of this chapter provide a background to the choice of the most suitable modelling strategy for masonry structures affected by ground distortions. It was observed that:

- It is key to pinpoint the structural features that affect the model response due to the settlement action: the simplified façade of the building, 2DFA and 3DFA, that

do not include the effects of the lateral walls, exhibit lower damage for a given applied angular distortion when compared with the more detailed three-dimensional models, 3DBOX and 3DFULL. For instance, for an applied angular distortion of 2 ‰(or 1/500), the models that do not include the effect of the transverse walls, *i.e.*, 2DFA and 3DFA exhibit a Ψ value from 2 to 7 times lower than the improved 2D modelling approach, labelled as 2DLF.

- The models without lateral walls exhibit lower vertical displacements than the models that include the effect of such walls. Therefore, the response of the masonry façade is influenced not only by the stiffness but also by the weight of the lateral walls.
- The behaviour of all the models considered is influenced by the stress components developed at the interfaces. These stresses, in turn, are influenced by the inclusion of the weight of the lateral walls, which results in different stresses at the façade's edges.
- The results of model 2D Long Flanges (2DLF), in terms of deformations, damage, displacements and interface stresses, are in good agreement with the ones of the more detailed 3D analyses. This observation suggests that the improved 2D modelling strategy, 2D with lateral Long Flanges, depicts with good accuracy the behaviour of the entire structure subjected to settlement.
- The improved 2D modelling strategy, 2D with lateral Long Flanges, was observed to require less time and computational burden than the full-scale 3D analyses. The model 2DLF was observed to be from 9 to 40 times faster in terms of computational time than 3D analyses, due to a low model complexity.

6.5.1. IMPLICATIONS FOR THIS THESIS

Based on the results of this Chapter, the 2D model with Long Flanges, herein labelled as "2DLF" is selected for the numerical analyses in Chapter 7.

The selected modelling strategy represents the best trade-off between the modelling burden, computational time and the accuracy of the results: It demonstrates a strong capability to replicate the outcome of more complex 3D analyses with lower use of computational resources and time.

BIBLIOGRAPHY OF CHAPTER 6

[1] A. Prosperi, M. Longo, P. A. Korswagen, M. Korff, and J. G. Rots, "2d and 3d modelling strategies to reproduce the response of historical masonry buildings subjected to settlements," *International Journal of Architectural Heritage*, pp. 1–17, 2024.

[2] A. Prosperi, M. Longo, P. A. Korswagen, M. Korff, and J. G. Rots, "Accurate and efficient 2d modelling of historical masonry buildings subjected to settlements in comparison to 3d approaches," in *International Conference on Structural Analysis of Historical Constructions*, Springer, 2023, pp. 232–244.

[3] G. Giardina, A. V. Van de Graaf, M. A. Hendriks, J. G. Rots, and A. Marini, "Numerical analysis of a masonry façade subject to tunnelling-induced settlements," *Engineering structures*, vol. 54, pp. 234–247, 2013.

[4] L. Bejarano-Urrego, E. Verstrynge, A. Drougkas, *et al.*, "Numerical analysis of settlement-induced damage to a masonry church nave wall," in *Structural Analysis of Historical Constructions: An Interdisciplinary Approach*, Springer, 2019, pp. 853–861.

[5] A. Drougkas, E. Verstrynge, P. Szekér, *et al.*, "Numerical modeling of a church nave wall subjected to differential settlements: Soil-structure interaction, time-dependence and sensitivity analysis," *International Journal of Architectural Heritage*, 2019.

[6] J. Rots, P. Korswagen, and M. Longo, "Computational modelling checks of masonry building damage due to deep subsidence," *Delft University of Technology*, 2021.

[7] A. Prosperi, M. Longo, P. A. Korswagen, M. Korff, and J. G. Rots, "Sensitivity modelling with objective damage assessment of unreinforced masonry façades undergoing different subsidence settlement patterns," *Engineering Structures*, vol. 286, p. 116 113, 2023.

[8] P. A. Korswagen, M. Longo, E. Meulman, and J. Rots, "Experimental and computational study of the influence of pre-damage patterns in unreinforced masonry crack propagation due to induced, repeated earthquakes," in *13th North American Masonry Conference*, TMS, 2019, pp. 1628–1645.

[9] H. Burd, G. Houlsby, C. Augarde, and G. Liu, "Modelling tunnelling-induced settlement of masonry buildings," *Proceedings of the institution of civil engineers - geotechnical engineering*, vol. 143, no. 1, pp. 17–29, 2000.

[10] H. Netzel and F. Kaalberg, "Numerical damage risk assessment studies on adjacent buildings in amsterdam," in *ISRM International Symposium*, ISRM, 2000, ISRM–IS.

[11] H. Burd, W. Yiu, S. Acikgoz, and C. Martin, "Soil-foundation interaction model for the assessment of tunnelling-induced damage to masonry buildings," *Tunnelling and Underground Space Technology*, vol. 119, p. 104 208, 2022.

[12] G. Giardina, "Modelling of settlement induced building damage," 2013.

[13] W. Yiu, H. Burd, and C. Martin, "Finite-element modelling for the assessment of tunnel-induced damage to a masonry building," *Géotechnique*, vol. 67, no. 9, pp. 780–794, 2017.

[14] S. Ferlisi, G. Nicodemo, D. Peduto, *et al.*, "Numerical analysis of the behaviour of masonry buildings undergoing differential settlements," in *Proceedings of the XVII European Conference on Soil Mechanics and Geotechnical Engineering*, The authors and The Icelandic Geotechnical Society, IGS, 2019, pp. 1–8.

[15] S. Jafari, "Material characterisation of existing masonry: A strategy to determine strength, stiffness and toughness properties for structural analysis," 2021.

[16] DIANA FEA, "Finite element analysis user's manual - release 10.5.," Report, 2021.

[17] B. Standard, "Eurocode 6—design of masonry structures—," *British Standard Institution. London*, no. 2005, 2005.

[18] NPR 9096-1-1:2012 nl, "Steenconstructies - eenvoudige ontwerpregels, gebaseerd op nen-en 1996-1-1+c1 (masonry structures - simple design rules, based on nen-en 1996-1-1+c1)," 2012.

[19] G. Schreppers, A. Garofano, F. Messali, and J. Rots, "Diana validation report for masonry modelling," *DIANA FEA report*, 2016.

[20] J. Rots, F. Messali, R. Esposito, S. Jafari, and V. Mariani, "Thematic keynote computational modelling of masonry with a view to groningen induced seismicity," in *Structural Analysis of Historical Constructions: Anamnesis, Diagnosis, Therapy, Controls*, CRC Press, 2016, pp. 227–238.

[21] NPR9998:2020en, *Assessment of structural safety of buildings in case of erection, reconstruction and disapproval - induced earthquakes - basis of design, actions and resistances*, 2021.

[22] P. A. Korswagen Eguren, M. Longo, E. Meulman, and C. van Hoogdalem, "Damage sensitivity of groningen masonry structures–experimental and computational studies: Stream 1," 2017.

[23] EN 1995-1-1, *Eurocode 5: Design of timber structures - part 1-1: General - common rules and rules for buildings*, 2004.

[24] M. Longo, M. Sousamli, P. A. Korswagen, P. van Staalduinen, and J. G. Rots, "Substructure-based 'three-tiered' finite element approach to soil-masonry-wall interaction for light seismic motion," *Engineering Structures*, vol. 245, p. 112 847, 2021.

[25] G. Gazetas, "Foundation vibrations," in *Foundation engineering handbook*, Springer, 1991, pp. 553–593.

[26] G. Mylonakis, S. Nikolaou, and G. Gazetas, "Footings under seismic loading: Analysis and design issues with emphasis on bridge foundations," *Soil Dynamics and Earthquake Engineering*, vol. 26, no. 9, pp. 824–853, 2006.

[27] NEHRP, "NIST GCR 12-917-21 soil-structure interaction for building structures," 2012.

[28] J. Charles and H. Skinner, "Settlement and tilt of low-rise buildings," *Proceedings of the Institution of Civil Engineers-Geotechnical Engineering*, vol. 157, no. 2, pp. 65–75, 2004.

[29] I. A. E. De Vent, "Structural damage in masonry: Developing diagnostic decision support," 2011.

[30] R. B. Peck, "Deep excavations and tunneling in soft ground," *Proc. 7th ICSMFE, 1969*, pp. 225–290, 1969.

[31] J. B. Burland and C. Wroth, "Settlement of buildings and associated damage," Tech. Rep., 1975.

[32] J. Zhao and M. DeJong, "Three-dimensional probabilistic assessment of tunneling induced structural damage using monte-carlo method and hybrid finite element model," *Computers and Geotechnics*, vol. 154, p. 105 122, 2023.

[33] M. D. Boscardin and E. J. Cording, "Building response to excavation-induced settlement," *Journal of Geotechnical Engineering*, vol. 115, no. 1, pp. 1–21, 1989.

[34] W. Yiu, H. Burd, and C. Martin, "Soil-foundation contact models in finite element analysis of tunnelling-induced building damage," in *Numerical Methods in Geotechnical Engineering IX, Volume 2*, CRC Press, 2018, pp. 989–997.

CHAPTER 7

PREPARATORY STEPS FOR DEVELOPING NUMERICAL FRAGILITY FUNCTIONS: Methodology, selection of the facade geometries, set-up of the numerical models and preliminary sensitivity analyses

CHAPTER 7: TABLE OF CONTENTS

7.1 Introduction and methodology . . . 172

7.2 Selection of the facade geometries . . . 175

7.2.1 Available dataset and post-processing . . . 175

7.2.2 Age of construction . . . 176

7.2.3 Walls geometry . . . 176

7.2.4 Results of the preliminary analyses of the geometry of the walls . . . 178

7.2.5 Limitation and uncertainties . . . 178

7.2.6 The use of the wall geometries and statistics . . . 179

7.2.7 The selected facades geometries . . . 181

7.2.8 The representativeness of the selected facades . . . 182

7.3 Set-up of the Finite element models . . . 185

7.3.1 The inclusion of the effect of the transversal walls . . . 185

7.3.2 Selected foundation systems . . . 185

7.3.3 Masonry materials . . . 187

7.3.4 Concrete, Steel and Timber . . . 188

7.3.5 Soil materials . . . 189

7.3.6 Boundary conditions and Interface elements . . . 189

Soil-foundation contact interaction and supports . . . 189

Steel lintel-masonry interface . . . 190

7.3.7 Finite element discretization . . . 190

7.3.8 Imposed settlement actions . . . 190

7.3.9 Loads of roof, floors and veneer . . . 192

7.3.10 Loading scheme and iteration procedure . . . 193

7.3.11 "Applied" and "measured" distortions . . . 195

7.4 Preliminary sensitivity analyses of the numerical features . . . 196

7.4.1 Relationship between the max. crack width and the damage parameter Ψ . . . 196

7.4.2 The influence of the analyses settings . . . 197

The influence of the settlement shape: sagging vs hogging . . . 198

The influence of the facade geometry 200

7.5 Discussion 200

7.6 Conclusions 201

Bibliography of Chapter 7 214

7.1. INTRODUCTION AND METHODOLOGY

This section introduces the steps used to develop numerical models and to generate numerical fragility functions for masonry buildings in the Netherlands.

The analyses presented in this Chapter are carried out in three steps (Fig. 7.1):

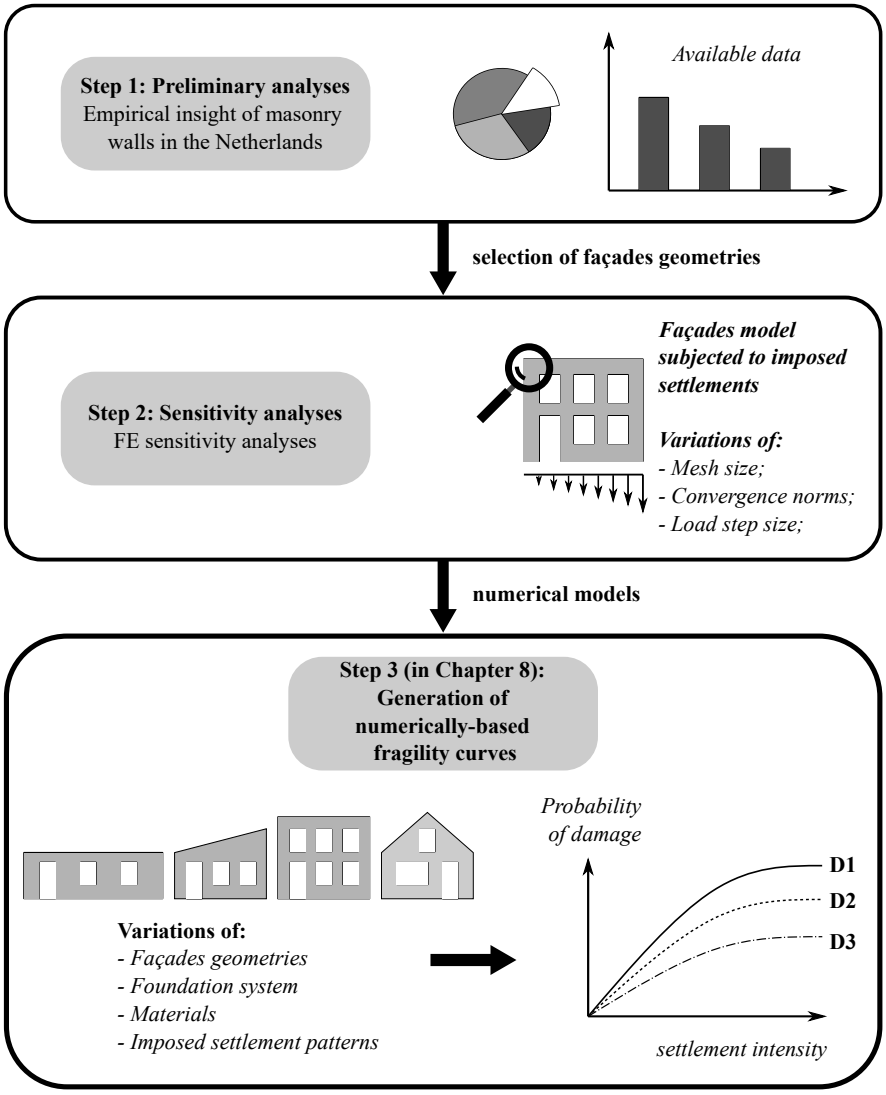

Figure 7.1: Flowchart of the adopted methodology. Steps 1 and 2 are detailed in Chapter 7, whereas Step 3 is in Chapter 8.

- **Step 1** details the preliminary analysis of the features of the masonry buildings in

the Netherlands. The analysis entails the use of available datasets to retrieve the recurrent dimensions and shape of the population of about 53 million facades in the Netherlands. Accordingly, eight facades are selected to idealize the characteristics of Dutch facades, and their representativeness is also evaluated.

- In **Step 2**, the set-up of two-dimensional numerical models of the selected facades is described. The models of the selected facades include realistic variations of the features which influence the buildings' response, as shown in Chapters 5 and 6, such as the number and size of openings which vary in each geometry, the masonry material, two different types of shallow foundations (*i.e.*, unreinforced masonry and reinforced concrete strips) and two soil materials. In particular, the properties of the soil materials are used to model interfaces at the bottom of the foundations to include the soil-structure interaction. Moreover, the effect of the lateral transverse walls is included in the models, with reference to the methodology described in Chapter 6 and further detailed in the following sections of this Chapter.

  Regarding the loads to which the models are subjected, in addition to the gravity load and the overburden given by the floors and roof, 72 settlement patterns are imposed at the bottom of the interface of the models to include the unpredictable settlement patterns that could be experienced by buildings due to different drivers. The intensity of each settlement pattern is measured using angular distortion β.

  The analyses also distinguish the imposed ground deformations, "***applied***" at the bottom of the soil-structure interfaces, by the "***measured***" distortion, retrieved on the structural model at the bottom of the facade.

  The damage parameter Ψ, already adopted in the previous Chapters of this thesis, has been used to assess the damage on the models. It should be noted that this study focuses on the occurrence of damage levels which can be classified as "***light damage***", ranging from cracks invisible to the naked eye up to 5 millimetres.

  Accordingly, preliminary sensitivity analyses are carried out to evaluate the influence of the features of the numerical analyses, such as the mesh size, the adopted load step size and the convergence norms.

  From this step, the settings that are employed in further numerical analyses are selected.

- In **Step 3**, the relationship between the imposed angular distortion β and the damage Ψ is retrieved by means of exceedance curves (*i.e.*, **fragility functions**). The proposed fragility curves allow the users to determine the probability of having or exceeding a certain level of damage for a given value of angular distortion. Moreover, the proposed curves are validated against different available literature sources. The differences and the limitations are discussed.

Step 1 and **Step 2** are discussed in this Chapter. **Step 3** is discussed in Chapter 8.

The results presented are expected to contribute to a better understanding of the relationship between the ground settlements due to multi-causal subsidence processes and the damage to the existing masonry structures.

The use of the developed numerical-based fragility functions in a systematic damage assessment is subsequently discussed in Chapter 9.

7.2. SELECTION OF THE FACADE GEOMETRIES

The administrative and spatial data of the buildings in the Netherlands are collected and discussed. Thanks to the availability of this information, it is possible to gain additional insight into the features of the buildings in the Netherlands, which integrates the review presented in Chapter 2, and aids the selection of recurrent facades geometries for the purpose of the numerical analyses.

7.2.1. AVAILABLE DATASET AND POST-PROCESSING[1]

In the Netherlands, a 3D building data set that covers the whole country is available (©3DBAG by tudelft3d and 3DGI [3]). 3DBAG is an enhanced version of the Dutch Basis-registraties Adressen en Gebouwen (BAG) data set, that includes the height information from different sources and measurements [4]; Thus, the information already provided in BAG, such as the age of construction of each building, its footprint and use, is further integrated with the height determined from aerial (laser) measurements.

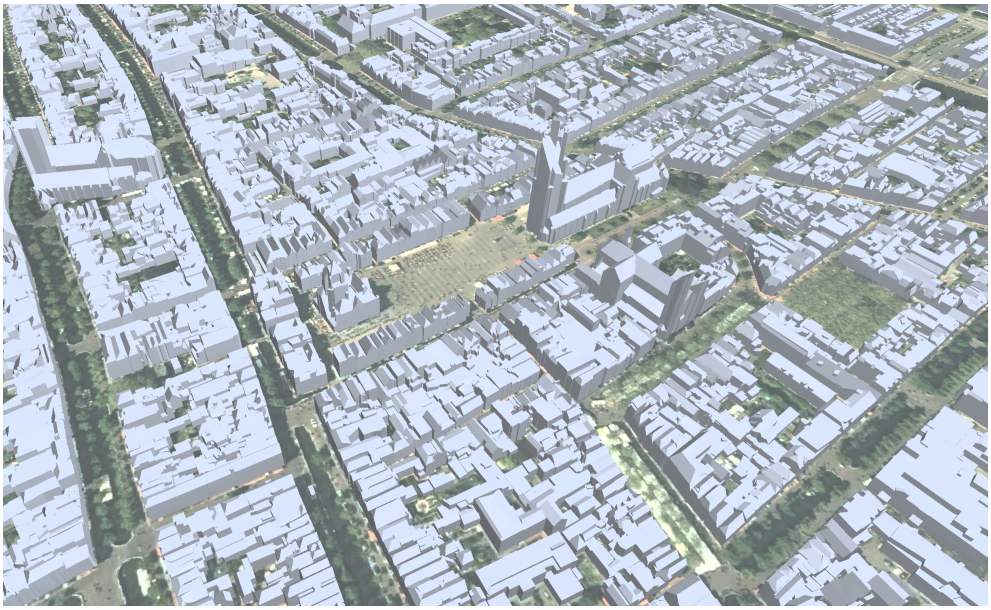

Figure 7.2: Aerial view of the ground and 3D view of city centre of Delft. From the website 3DBAG.nl [4].

The entire database has been downloaded and post-processed. Accordingly, the geometry data encoded with the PostGIS plugin for Postgres SQL is converted and imported into Matlab; In this way, the building geometry can easily be visualised and processed into statistics at a building population scale.

An algorithm was used to post-process the available information to obtain statistics about the shape, length and height of each wall in the dataset. In particular, the geometry of each

[1] This analysis was carried out as part of a previous research project, *i.e.*, [1], [2].

building was further processed to identify individual facades. The algorithm "unfolds" the available 3D geometry into a paper-like net by reconstructing the façades' shape from the roof geometry. The algorithm identifies what could be individual walls, and the imperfections of the 3D geometry are restored to produce clearly defined façades. Figure 7.3 presents an example from the unfolding algorithm. The algorithm thus determines the wall height and length and the overall shape of each wall.

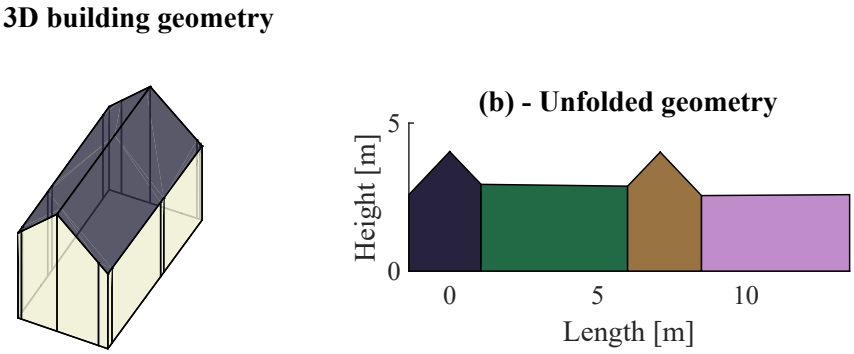

Figure 7.3: An example of the unfolded geometry of two buildings showing the individual walls' length and height: (a) the 3D visualization of the building and (b) the identified facades.

7.2.2. AGE OF CONSTRUCTION

The entire database includes information about 10 million buildings constructed in the Netherlands between 1770 and 2022. The dataset is limited to existing buildings, as it does not include those that have been demolished.

A histogram of the age of the construction of buildings is shown in Figure 7.4. The plot shows the effect of the uncertainty in the data, such as estimates of the construction year rounded to the nearest decade, and the impact of historical occurrences, such as World War 2 [1], [2].

Figure 7.4 shows that about 50% of the buildings in The Netherlands were built before 1975. In other words, about 50% of the Dutch buildings have reached and surpassed a lifespan of 50 years. Thus, although repair and maintenance works can be carried out, many of these buildings could be more susceptible to ground movements due to deterioration and degradation of the materials, and due to the accumulation of minor damage caused by different actions (see Ch. 2).

Although the information regarding the construction material is not available, buildings aged before 1960 are expected to be built mainly with baked clay masonry, as discussed in section 2.3.2 [5], [6].

7.2.3. WALLS GEOMETRY

The geometry of more than 53 million walls was analysed. Then, each wall was categorised based on its shape in one of the four categories shown in Fig. 7.5. The four

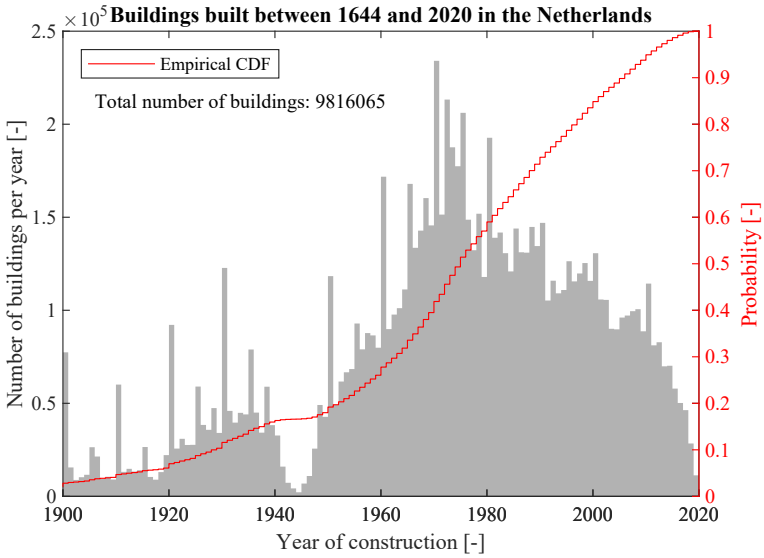

Figure 7.4: Histogram of the year of construction for existing buildings in the Netherlands available in the BAG 3D database [1], [2]. The data refers to the buildings identified as "in use" ("*pand in gebruik*", in Dutch [7]). The data for buildings that have been demolished is not available.

shape categories were based on preliminary empirical observations of the recurrent wall geometries, and correspond to:

- "**Flat**", rectangular wall geometries with a flat upper side;
- "**Twin-gable**", walls underneath roofs made of two sloping planes;
- "**Single-gable**", walls underneath roofs made of one sloping plane;
- "**Others**", geometries that do not fall in the previous categories;

In some cases the adopted algorithm failed to reconstruct the wall geometries, thus the walls are categorized as "**Unassigned**". The most common wall geometry is "Flat", followed by single- and double-gable walls. The histograms of the length, height and length over height ratio of the investigated walls are shown in Fig. 7.6. Most of the walls present a length between 2 and 10 meters, while longer walls are less common (Fig. 7.6a). Two peaks are observed in the histogram of the height at about 3 and 6 meters respectively, corresponding to single and double-storey houses (Fig. 7.6b).

The length and height of each wall are used to determine the length-over-height ratio. Fig. 7.6c shows how the common values of the length/height ratio range between 0.5 and 2.5.

Although the histograms represent the results for the dataset of buildings across the entire country, similar distributions are expected in areas specifically prone to subsidence.

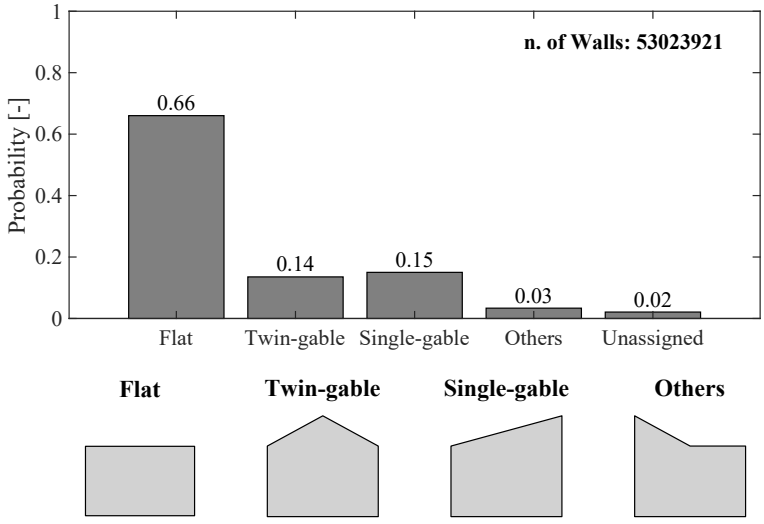

Figure 7.5: Recurrent shapes of the walls distinguished in found macro-categories. Each wall is automatically assigned to one of the categories.

7.2.4. RESULTS OF THE PRELIMINARY ANALYSES OF THE GEOMETRY OF THE WALLS

This section briefly summarizes the results of the preliminary analyses of the geometry of the walls. It has been observed that:

- 50% of the buildings located in the Netherlands have reached or surpassed a lifespan of 50 years;
- Most of the walls can be schematized as rectangular walls, followed by single- and double-gable walls;
- The height of the walls suggests that most of the walls belong to low-rise (one- or two- storey) buildings;
- Walls longer or higher than 10 meters are uncommon;
- Typical length/height ratios vary between 0.5 (high facades with short length) and 2.5 (short facades with long length).

7.2.5. LIMITATION AND UNCERTAINTIES

The retrieved information on the walls' geometry is associated with aleatory and epistemic uncertainties, which are briefly discussed in the following [1], [2].

The administrative and spatial data of the buildings may differ from reality, or be wrong or incomplete. Buildings may have been altered (demolition, renovation, extensions) and their record modified or simplified. Each dataset case is characterized by an "ID" which corresponds to buildings in real estate properties. It may be possible that different buildings could share the same "ID", or conversely multiple "IDs" differentiate properties that belong to the same structure.

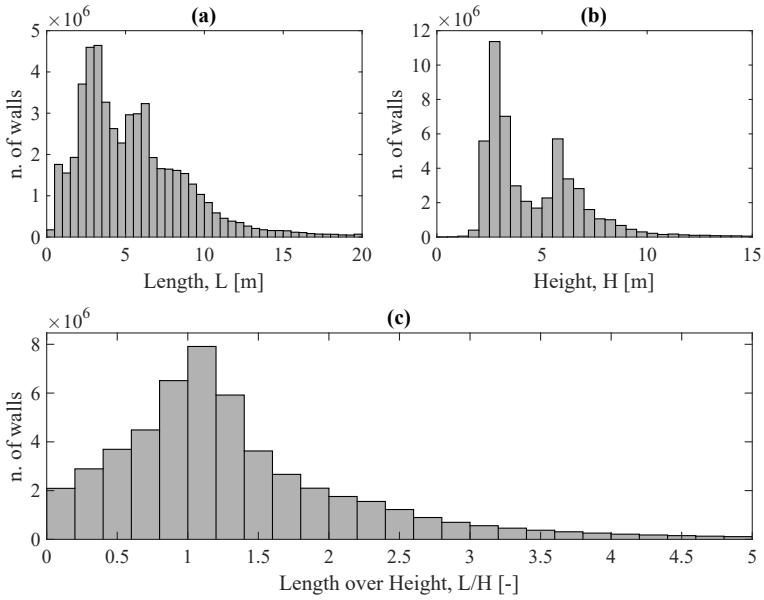

Figure 7.6: Histograms of the walls' length (a) and height (b). (c) shows the length-over-height ratio.

Moreover, the construction material of each building is not known.

Aerial measurements were used to derive the geometry of each building and then published in 3DBAG (©3DBAG by tudelft3d and 3DGI [3]). The geometry of the buildings is further processed to derive the information used for this study. Thus, the multiple steps and the amount of data required for the analysis increase the sources of uncertainties. Moreover, it has not been quantified the confidence of the process responsible for the automatic categorization of the wall geometries. This process may be influenced by inconsistent data or irregular geometries that, in some cases, influence the results of the unfolding algorithm.

Therefore, it cannot be stated that the geometry of all the buildings is properly represented and that the analyses are characterized by a high degree of confidence.

7.2.6. THE USE OF THE WALL GEOMETRIES AND STATISTICS

Although several limitations can be highlighted, as discussed in section 7.2.5, the analysis herein presented results in insightful statistical data that describe the features of the walls of buildings in the Netherlands.

The collected data does not include information about the construction material of buildings, nor the openings (windows or doors) of the exterior walls. It is not possible to obtain any information about the cross-section of walls: for example, cavity walls cannot be identified. Additionally, there is no correlation between the walls and the foundation system of the buildings.

Nevertheless, the collected information can be used to determine if a given wall geometry resembles the walls available in the dataset. In the following, facades are selected for

the numerical analyses and the collected dataset is used to check whether the facades represent realistic idealizations of the walls in the Netherlands.

7.2.7. THE SELECTED FACADES GEOMETRIES

Eight facade geometries are selected for the analyses and are shown in Fig. 7.7. The detailed information of each facade geometry is reported in the Appendix. C, whereas Table 7.1 summarises the main geometrical features of the facades and their transversal walls.

The selected geometries correspond to the exterior walls of existing structures and full-scale tests that have been reported and used in previous studies (for instance [8]–[10]). The geometries resemble typical Dutch facades (see for instance Fig. 2.2).

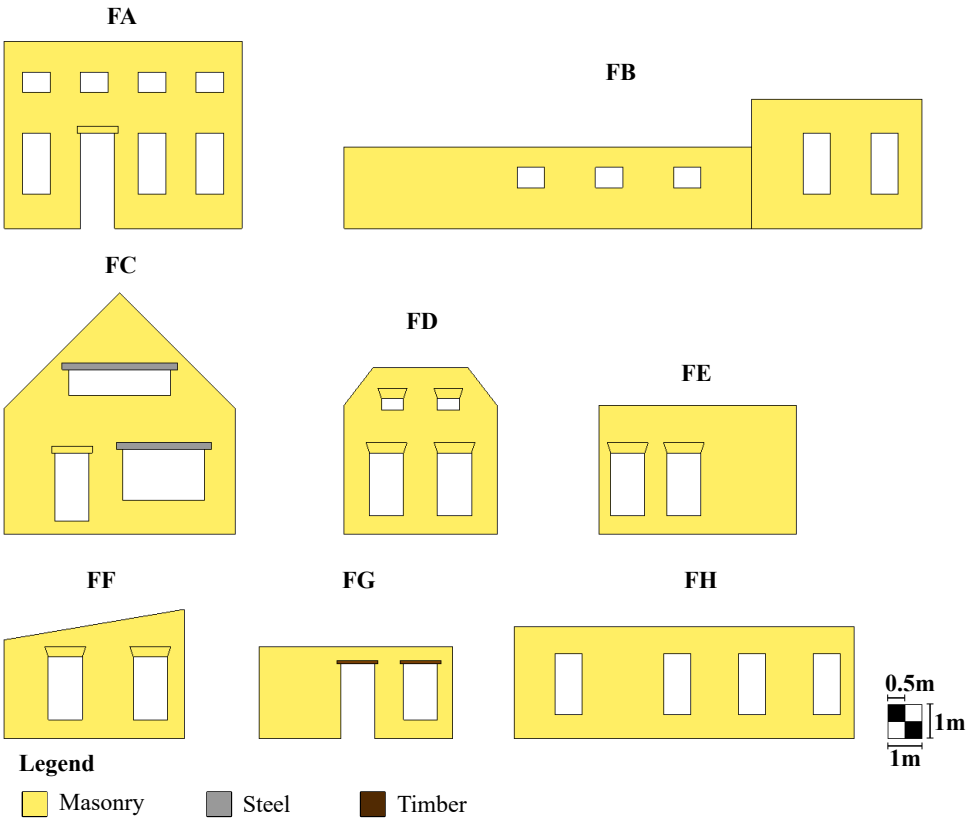

Figure 7.7: The selected facades adopted in the numerical models. Each facade is associated with an ID which is only used to further reference them.

Each facade was built with clay-baked masonry. As the facades idealize old clay-baked buildings, 6 facades are double-wythe walls (see Chapter 2, section 2.3.2 for further details), whereas only two facades are single-wythe (Table 7.1).

Masonry lintels are used for the openings in most cases (Fig. 7.7), *i.e.*, for the facades herein labelled as "FA", "FC", "FD", "FE", "FF", whereas one facade additionally uses steel lintels over large openings as observed in real structures, *i.e.*, "FC", one facade use timber

Table 7.1: Geometrical parameters of the selected facades shown in 7.7.

Parameter	Symbol	Units	Façade							
			FA	FB	FC	FD	FE	FF	FG	FH
Length	L	[m]	7.00	17.00	6.80	4.50	5.80	5.30	5.70	10.00
Height	H	[m]	5.50	3.80	7.10	4.90	3.80	3.80	2.70	3.30
Length over Height ratio	L/H	[-]	1.27	4.47	0.96	0.92	1.53	1.39	2.11	3.03
Façade thickness	t_f	[m]	0.21	0.21	0.10	0.21	0.21	0.21	0.21	0.10
Height Transversal Wall	h	[m]	3.80	2.40	3.00	3.80	3.80	2.90	2.70	3.30
Transversal Wall thickness	t_t	[m]	0.21	0.21	0.10	0.21	0.21	0.21	0.21	0.10
Distance between front and back façade	W	[m]	5.00	7.00	12.00	5.80	4.50	5.80	5.40	6.50

Note: The parameters "h", "t_t" and "W" that refer to the transverse walls and the distance between the front and back facades are illustrated and used in section 7.3.1.

lintels, *i.e.*, "FG", and two facades do not have lintels, *i.e.*, "FB" and *i.e.*, "FH".

7.2.8. THE REPRESENTATIVENESS OF THE SELECTED FACADES

The entire population of about 53 million walls include cases characterized by length and height values smaller than 2 meters, which could refer to (parts of) structures which are not representative of the exterior walls of buildings and be parts of annexes, extensions or sheds. Similarly, structures with lengths and heights higher than 20 meters have no bearing on detached or semi-detached houses, which represent the focus of this work.

Therefore, a subset of about 20 million walls with length and height values ranging between 2 and 20 meters is considered in the following. Walls with shapes classified as "Others" or "Unassigned" are not considered in the sub-sample. Moreover, the sub-sample purposely refers to walls from structures built before 1970, as they represent the focus of this thesis.

Figure 7.8a shows the relationship between Length L, and Height H for the selected 20 million subsets by means of a bivariate histogram. Each dataset item has a unique combination of shape, L, H and thus L/H. Therefore, the determination of facade geometries with the aim of representing the majority of the cases is not a straightforward task, due to the uniqueness of each wall. Moreover, any facade selected directly from the dataset may only represent a small number of cases.

An algorithm is used to check if any of the selected facades (Fig. 7.7) resemble the features of the 20 million cases, based on the similarity between the length over height L/H ratio, the length L and shape:

- First, the differences in terms of height H, and length over height L/H are computed between each selected facade and each case in the 20 million dataset;

- The facade that best resembles each wall in the dataset is selected as the one that has the same shape and the smallest differences in terms of H and L/H. The differences in terms of H and L/H, however, do not have an upper limit. Therefore, walls that have difference values in terms of H and L/H higher than 1.5 meters and 0.5 respectively for all the selected facades are classified as "Unassigned".

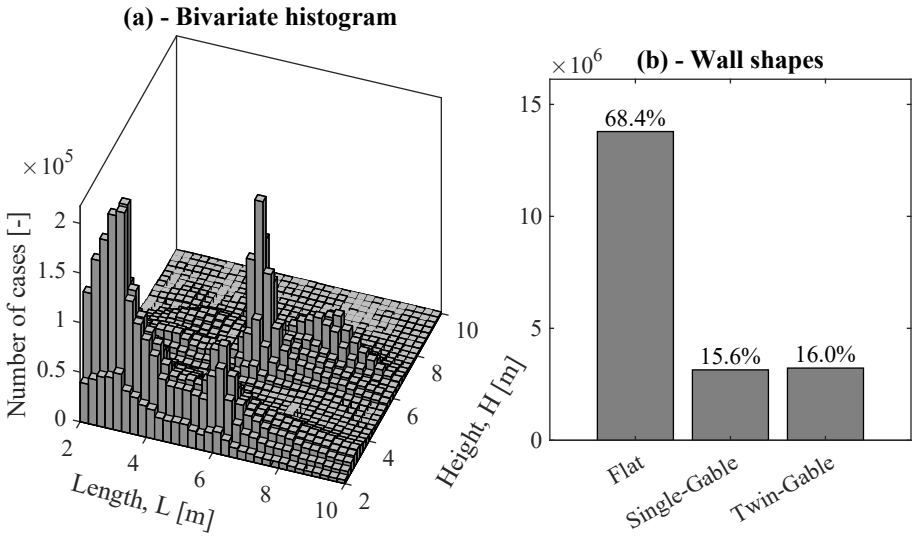

Figure 7.8: (a) Bivariate histogram showing the relationship between Length L, Height H for walls with an assigned shape built until 1970 and (b) bar plots of the shapes of the walls among the selected cases.

The results are shown in Fig. 7.9 by means of a bar plot. Each bar represents the number of cases assigned specifically to one of the selected facades (Fig. 7.7).

The analysis reveals that the selected facades mimic the geometry of about 59% of the entire population of 20 million walls. Facades with an L/H ratio higher than 3, *i.e.*, "FB" and "FH" are the ones associated with the lowest number of cases compared to the other facades. In general, facades with high L and low H values are not common in the dataset Figure 7.8. Nevertheless, the inclusion of facades with high L/H ratios represents a conservative choice for the numerical analyses, as they are expected to be vulnerable to settlement damage compared with facades with low L/H ratios (the reader is further referred to the conclusions of Chapter 5).

Similarly, facades "FC" and "FF" are also observed to be associated with a low number of cases. This is explained by the fact that the above-mentioned facades represent twin- and single-gable geometries, which are less recurrent in the 20 million cases (Fig. 7.8b).

The limited number of selected geometries reflects the variability within the entire population of walls. To achieve a more precise representation of the population, additional models are needed.

However, it is outside the goal of this study to select a sufficient number of facades to

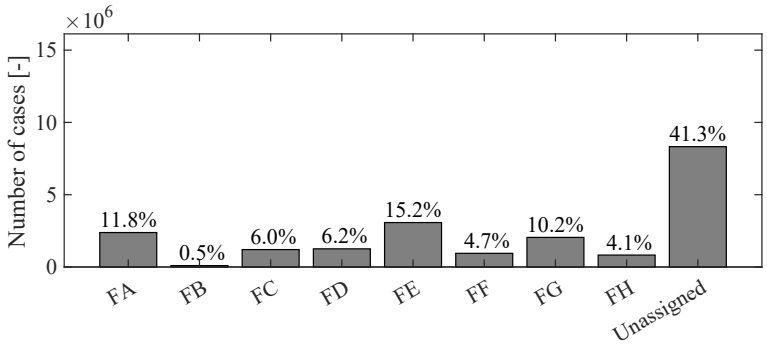

Figure 7.9: Number of walls from buildings with assigned shape and built until 1970, divided by the most similar case among selected facades (Fig. 7.7). The percentage of cases assigned to each facade compared to the total of 20 million is shown.

reflect the distribution of the entire population of walls and their features. Instead, the analysis herein presented proves that the selected geometries represent realistic facades.

In other words, from the analysis presented in this section, it can be concluded that the shape and dimensions of the selected facades represent realistic scenarios for Dutch walls. Thus, the selected facades are used in the following sections for the numerical analyses.

7.3. SET-UP OF THE FINITE ELEMENT MODELS

This section describes the features of the numerical models adopted in **Steps 1** and **2** of the methodology (see section 7.1) adopted in this study. The models are built with the software Diana 10.8 [11]. The 2D FE models adopt the strategy presented in Chapters 5 and further refined in 6, and are detailed in the following.

7.3.1. THE INCLUSION OF THE EFFECT OF THE TRANSVERSAL WALLS

The models include the effect in terms of stiffness and weight of the transversal walls by means of the approach presented in Chapter 6 (Fig. 7.10). The analytical approach proposed in Chapter 6 to compute the length used to represent the influence of the building's transversal walls is herein further detailed. For clarity, the approach adopted in this Chapter is equivalent to the one used in Chapter 6, however, Figure 7.10 further distinguishes more general situations to be considered in the analytical formulation.

The Dutch standard [12] proposes a method to compute the length of the effective flange width as the sum of two areas: the normal compressive force is provided by the part of the building wall located next to the cooperating flange width.

The length of the cooperating flanges corresponds to the sum of two contributions (C1, C2 in Figure 7.10):

- The first contribution ("C1" in Figure 7.10) is computed by considering the minimum of the following transverse wall properties: i) a fifth of the building height ($H_{tot}/5$), ii) half of the internal distance between party walls (Ls/2) iii) half of the wall height (h/2) iv) six times the wall thickness (t), as described in [13];
- The second contribution ("C2" in Figure 7.10), corresponds to the contribution to the normal compression given by the flange, as described in [12]. Two cases are distinguished for this calculation, based on the geometry of the transversal wall;

The parameters shown in Figure 7.10 referred to the parameters of the selected facades reported in Table 7.1.

7.3.2. SELECTED FOUNDATION SYSTEMS

Two strip foundation systems are selected for the analyses:

- An unreinforced masonry foundation in Fig. 7.11a;
- A reinforced concrete (RC) strip below a masonry beam in Fig. 7.11b. The portion of masonry represents an extension of the wall which lies above the ground surface.

The ground surface is assumed to correspond to the top edge of the two selected foundation systems. The selected foundation systems represent two realistic recurring scenarios of shallow foundations found in the Netherlands.

Regarding the reinforced concrete foundation, the non-linear behaviour of the material is included (see section 7.3.4). Therefore, the longitudinal (i.e. along the façade) rebar system of the reinforced concrete foundation is modelled as line reinforcement and

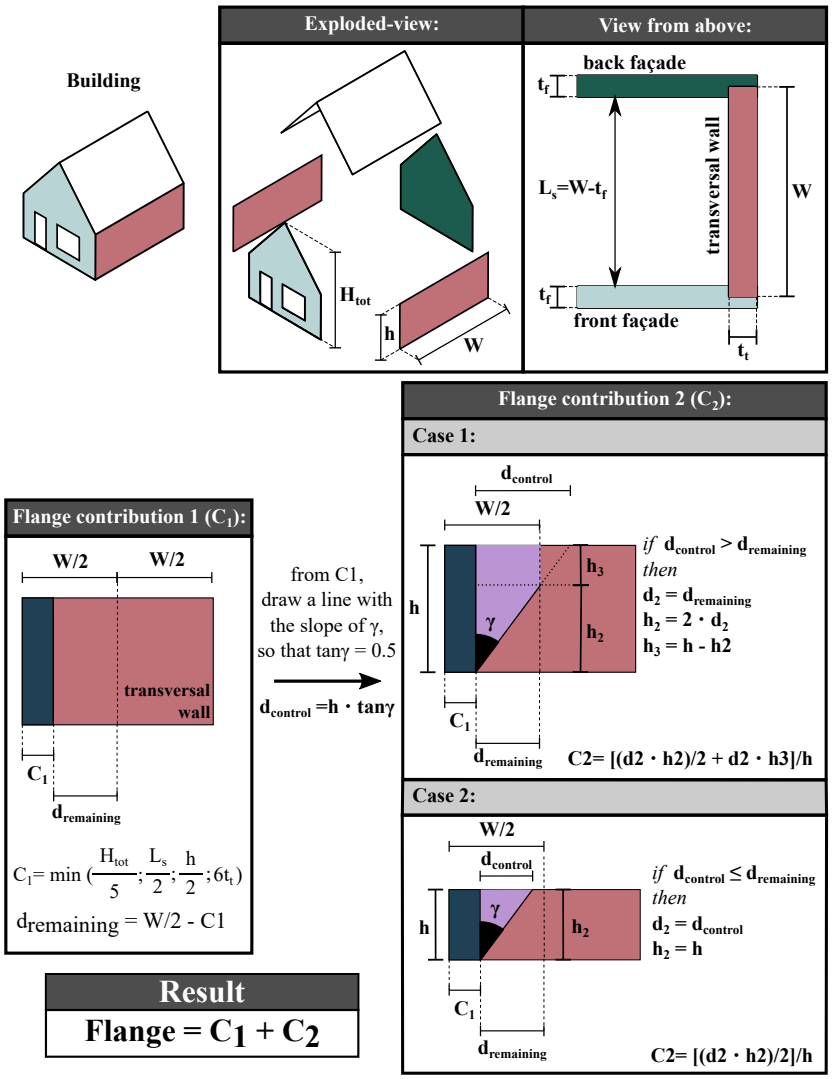

Figure 7.10: The calculation of the effective flange width of the transversal walls adopted in the FE models.

considered fully embedded in the concrete and no slipping behaviour was considered. The cross-section of the rebar is set to represent 4 ϕ 16 both at the top and bottom.
It should be noted, however, that in real situations the dimensions of the foundation, as well as the adopted construction material, are carefully designed considering the type of structure and the characteristics of the subsoil and thus vary from case to case. The two selected foundation scenarios herein adopted may thus represent only approximate idealizations of the foundation which would be otherwise adopted for each of the selected facades. This aspect represents a limitation of the analyses.

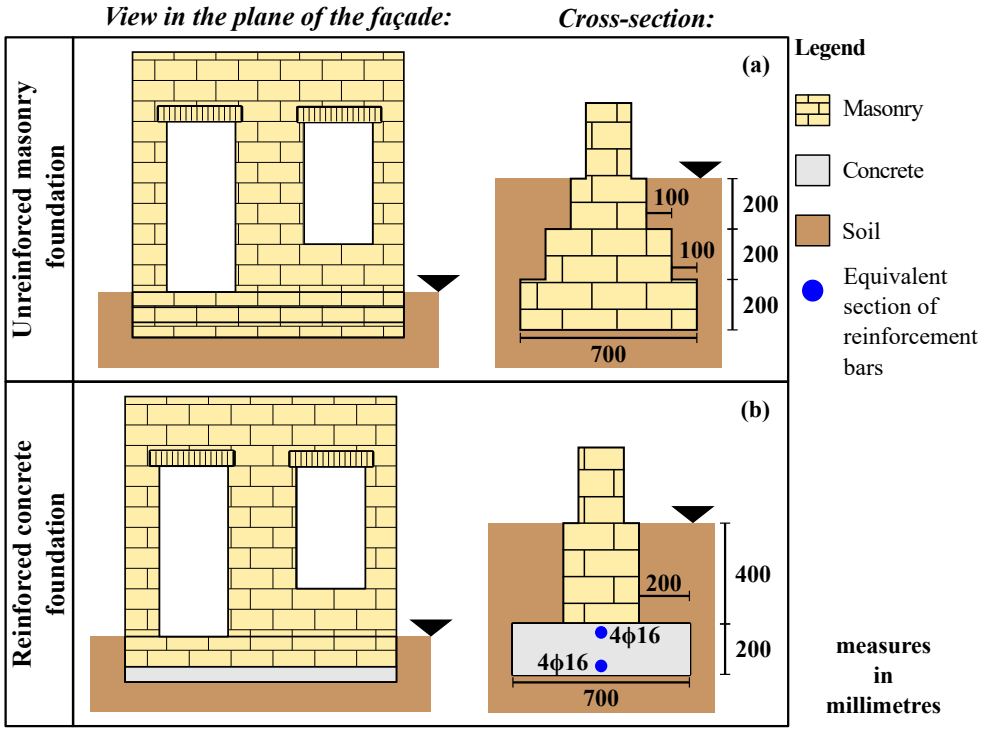

Figure 7.11: The strip foundation systems adopted in the numerical models. In the FE models, the soil volume is not modelled explicitly, and it is represented in the image to illustrate the intended depth of the foundation.

7.3.3. MASONRY MATERIALS

Similarly to the analyses presented in Chapters 5 and 6, the non-linear cracking behaviour of the masonry material is modelled employing an orthotropic, smeared crack/ slip/ crush constitutive law, *i.e.*, the Engineering Masonry Model [14], [15].
The parameters of the adopted constitutive law correspond to the material properties of the clay brick masonry (Table 6.1) [14], [16], [17]. In particular, three material property sets are adopted and correspond to a "Standard" material, a "Weak" material, in which the properties of the standard material are reduced, and a "Strong" material, in which the properties are increased.

The Engineering Masonry Model was adopted for the façade, the lintels and the foundation. The head-joint failure (representing vertical cracking) is based on friction, so a higher vertical pre-compression reduces crack formation. The minimum head-joint strength (as no pre-compression is present) is set to 1.5 times the bed-joint tensile strength. The crack bandwidth is determined by Govindjee's projection method [11].

For the lateral elements placed at the side of the facades to simulate the effect of the transversal walls, the Total Strain Rotating Crack model is adopted for the masonry material, as the Engineering Masonry Model is not available for beam elements.

Table 7.2: Material properties adopted in the FE models. The properties are schematically illustrated in Fig. 7.12.

Material Properties	Symbol	Unit of measure	Weak	Standard	Strong
Young's modulus vertical direction	E_y	[MPa]	2500	5000	7500
Young's modulus horizontal direction	E_x	[MPa]	1250	2500	3750
Shear Modulus	G_{xy}	[MPa]	1000	2000	3000
Bed joint tensile strength	f_{ty}	[MPa]	0.050	0.100	0.15
Minimum strength head-joint	$f_{tx,\,min}$	[MPa]	0.075	0.15	0.225
Fracture energy in tension	$G_{t,I}$	[N/m]	2.6	10.0	22.4
Angle between stepped crack and bed-joint	α	[rad]	0.5	0.5	0.5
Compressive strength	f_c	[MPa]	4.25	8.50	12.75
Fracture energy in compression	G_c	[N/mm]	16.76	18.39	19.90
Friction angle	φ	[rad]	0.64	0.64	0.64
Cohesion	c	[MPa]	0.075	0.150	0.225
Fracture energy in shear	G_s	[N/mm]	0.025	0.100	0.224
Mass Density	ρ	[Kg/m^3]	1900	1900	1900

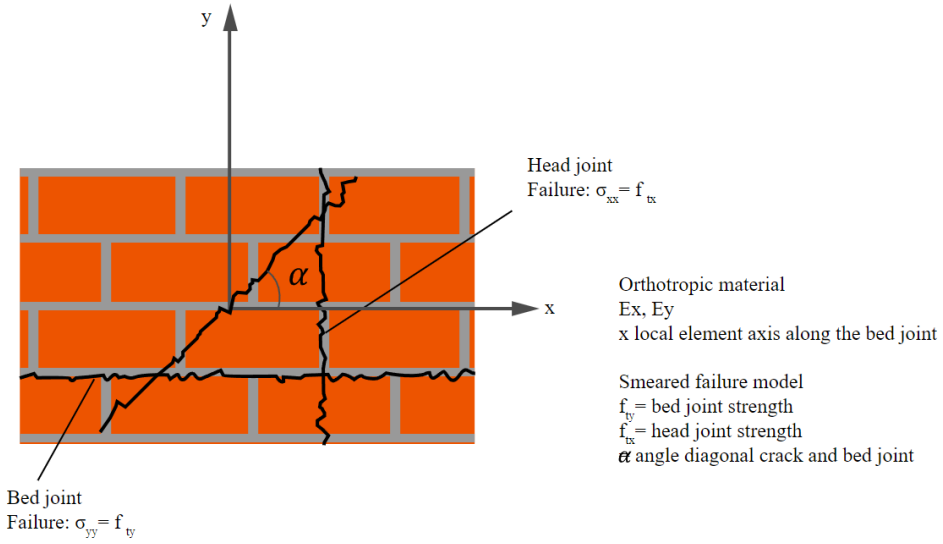

Figure 7.12: General characteristics of Engineering Masonry model. Retrieved from [11].

7.3.4. CONCRETE, STEEL AND TIMBER

For the variations with reinforced concrete foundation, the non-linearity of concrete was explicitly modelled with the Total Strain Rotating Crack Model. The Von Mises Plasticity model was employed for the steel material of the rebar in the RC foundations. A summary of such material properties is shown in Table 5.2 in Chapter 5.

Both the steel and timber materials adopted for the lintels are modelled using linear elasticity. The timber has Young's modulus equal to 11000 MPa, Poisson's ratio equal to 0.35 and a mass density equal to 450 kg/m^3. The steel material used for the lintel has Young's modulus equal to 61204 MPa, Poisson's ratio equal to 0.35 and a mass density equal to 1120 kg/m^3.

It should be noted that the properties of the steel material for the lintel have been chosen to ensure that the equivalent bending stiffness "EI" modelled as a rectangular section in the model corresponds to the "EI" of a steel beam with an IPE200 section.

The steel used for the rebars in the case of reinforced concrete foundations has Young's modulus equal to 210000 MPa and yield stress equal to 235 MPa.

7.3.5. SOIL MATERIALS

Two soil materials are considered in the analyses:

- **Sand**, characterized by a shear modulus of 35 MPa, the Poisson's ratio equal to 0.3 and a friction angle of 30°;
- **Clay**, characterized by a shear modulus of 10 MPa, the Poisson's ratio equal to 0.45 and a friction angle of 15°;

The soil properties are used in the modelling of the soil-structure boundary interfaces, described in detail in section 7.3.6.

7.3.6. BOUNDARY CONDITIONS AND INTERFACE ELEMENTS

SOIL-FOUNDATION CONTACT INTERACTION AND SUPPORTS

At the bottom edge of the strip foundation, interfaces are used to model the soil-foundation interaction, similarly to the methodology discussed in Ch. 6. Vertical and horizontal supports are thus applied at the bottom of the interface elements.

Two corner springs below the transversal walls are placed to support the additional weight of the lateral beam element, representing the soil-structure connection of the transversal walls. The interface uses the Coulomb-friction behaviour, whereas the values of the vertical and horizontal stiffness are determined for each soil material with the formulation reported by [18]–[20] and already adopted in Chapters 5 and 6:

$$K_n = \frac{GL}{1-\nu}\left[0.73 + 1.54 \cdot \left(\frac{B}{L}\right)^{0.75}\right] \tag{7.1}$$

$$K_t = GL\left\{\frac{1}{2-\nu}\left[2 + 2.5 \cdot \left(\frac{B}{L}\right)^{0.85}\right] - \frac{0.2}{2(0.75-\nu)}\left[1 - \frac{B}{L}\right]\right\} \tag{7.2}$$

Where K_n, and K_t from equations (7.1) and (7.2) represent the normal and tangential (*i.e.*, in the plane of the façade) directions to the soil surface. "B" represents the width of the base of the foundation, while "L" is the foundation length (equal to the length of the façade). "G" and "ν" are the shear modulus and the Poisson ratio of the soil material.

The values of K_n, and K_t are then divided by "B" and "L" to obtain smeared values of the normal and shear linear stiffness. For instance, the final smeared values for the facade "FA" on the clay soil are equal 0.026 N/mm^3 and 0.017 N/mm^3 for the normal and shear stiffness.

STEEL LINTEL-MASONRY INTERFACE

Interface elements are also used to simulate the contact behaviour between the masonry facade and steel lintels. In this specific case, Coulomb-friction interfaces with gapping are used. The normal and tangential stiffness values, *i.e.*, $k_{n,steel-masonry(interf.)}$ and $k_{t,steel-masonry(interf.)}$ respectively, of the lintel-masonry interface are computed using the equation reported in equations 7.3 and 7.4 reported in [21], [22]:

$$k_{n,steel-masonry(interf.)} = \frac{E_{steel}E_{y,masonry}}{h_m(E_{steel} - E_{y,masonry})} \tag{7.3}$$

$$k_{t,steel-masonry(interf.)} = \frac{G_{steel}G_{masonry}}{h_m(G_{steel} - G_{masonry})} \tag{7.4}$$

E_{steel} and $E_{y,masonry}$ in equations 7.3 and 7.4 represent Young's moduli of the steel and the masonry material respectively, whereas G_{steel} and $G_{masonry}$ the shear moduli. h_m represents the thickness of the mortar, assumed to be equal to 10 mm. The normal and shear stiffness values, for the standard masonry material, computed with equations 7.3 and 7.4 are equal to 544 and 218 N/mm^3 respectively. The adopted friction angle is equal 16.7°, the dilation angle is 0° whereas the cohesion and the tensile strength are equal to the ones of the masonry materials.

7.3.7. FINITE ELEMENT DISCRETIZATION

Plane stress elements with an average mesh size of 200 x 200 mm are used for the facade, foundation and lintels. Accordingly, 8-node quadrilateral elements with a 3 × 3 Gaussian integration scheme and 6-node triangular elements with 4 Gaussian points are used. An example of the adopted mesh is shown in Fig. 7.13.

Class-III Mindlin beam elements [11] were placed at the sides of the façade and foundation to model the effect of the transverse walls and foundations, following the approach implemented in Chapters 5 and 6.

The line interface elements use 3+3 node elements and the Newton-Cotes (5 points) integration scheme [11]. The corner interfaces make use of 1+1 node elements.

7.3.8. IMPOSED SETTLEMENT ACTIONS

This section describes how the settlement deformation adopted in the numerical analyses is computed, further detailing the approach already adopted in Chapters 5 and 6.

The settlements are modelled as vertical displacements imposed at the base of the interface. The displacements imposed at the interface at the base of the foundation are conformed to a Gaussian curve and were computed using equation 7.5:

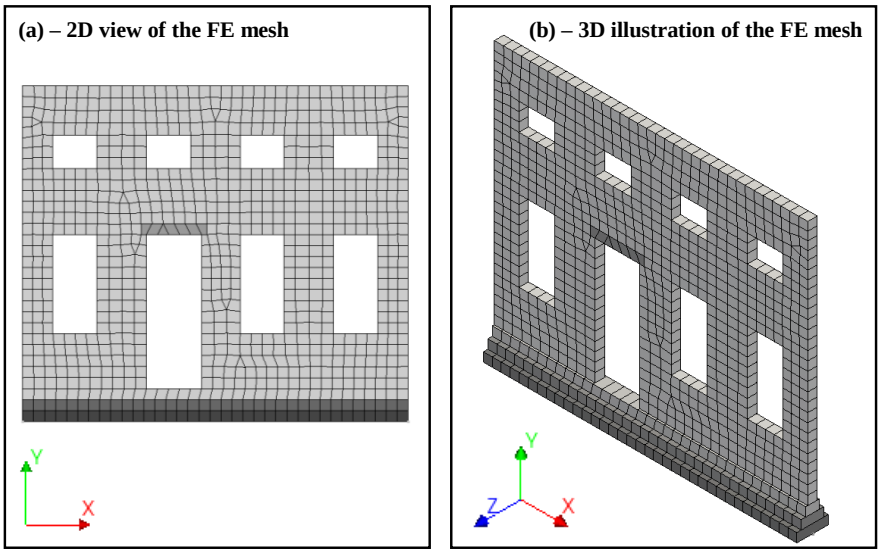

Figure 7.13: An example of the adopted FE mesh for facade "FA" with an unreinforced masonry foundation: (a) screenshot of the mesh from the numerical models and (b) 3D illustration of the FE including the thickness of the elements. The transversal walls and foundations are not included in the illustration.

$$S(x) = (-1)^{\iota} \left\{ e^{\left[\frac{-(x-D_x)^2}{2x_i^2} \right]} \right\} \tag{7.5}$$

Where S(x) is the vertical displacement along the direction "x", parallel to the facade. The influence of the parameters of the equation 7.5 is shown in Fig. 7.14 for a building of unitary length, and discussed in the following:

- "D_x" is the horizontal distance between the symmetry axis of the Gaussian curve and the edge of the building;
- "x_i" is the distance from the symmetry axis of the curve to the point of inflexion;
- "ι" is a term that enables controlling the convexity of the Gaussian curve.

Arbitrary defined intervals of D_x, x_i and ι are used to generate 72 settlement shapes, to idealize and include the variability of ground deformations that could affect buildings, as shown in Fig. 7.15.

All the selected settlement patterns are generated ensuring that the maximum angular distortion is equal to 1/300. Accordingly, an algorithm is used to generate the settlement deformations and entails the following steps:

1. Equation 7.5 is used to generate the settlement deformation S(x) for a building of a unitary length (thus x ranges from 0 to 1); This step results in settlement shapes in Fig. 7.15 defined by two coordinates, *i.e.*, the x-coordinate along the building and the y-coordinate, which refers to the vertical displacement;

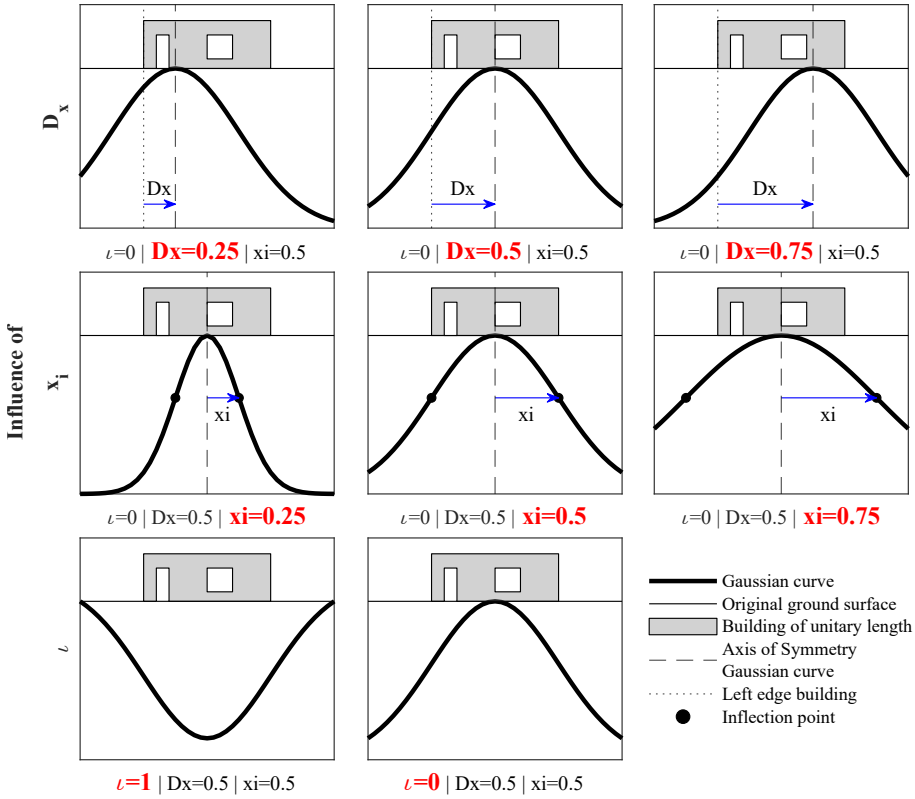

Figure 7.14: Schematic illustration of the interpretation of the parameters of the Gaussian formulation adopted to idealise the settlement shapes.

2. The maximum value of S(x) is subtracted from all the z-coordinates. This step is required to make sure the S(x) values range between negative values and "0", where "0" corresponds to the bottom edge of the foundation;

3. The x-coordinate values are multiplied by the desired length, *i.e.*, the length "L" of the selected facade. In other words, the unitary length is transformed into the desired length (thus x ranges between 0 and "L");

4. Finally, the maximum settlement of S(x) is set so that the maximum angular distortion along the profile is equal to 1/300.

This approach is consistent with the one adopted in Chapters 5 and 6 to generate vertical settlement deformations, purposely neglecting horizontal displacements. The settlement shapes used in Chapters 5 and 6 are also herein included (see Fig. 7.15).

7.3.9. LOADS OF ROOF, FLOORS AND VENEER

Depending on the selected facade, vertical loads are applied in the models to include the weight of the roof, floors and veneer (in the case of cavity walls for facade "FC" and

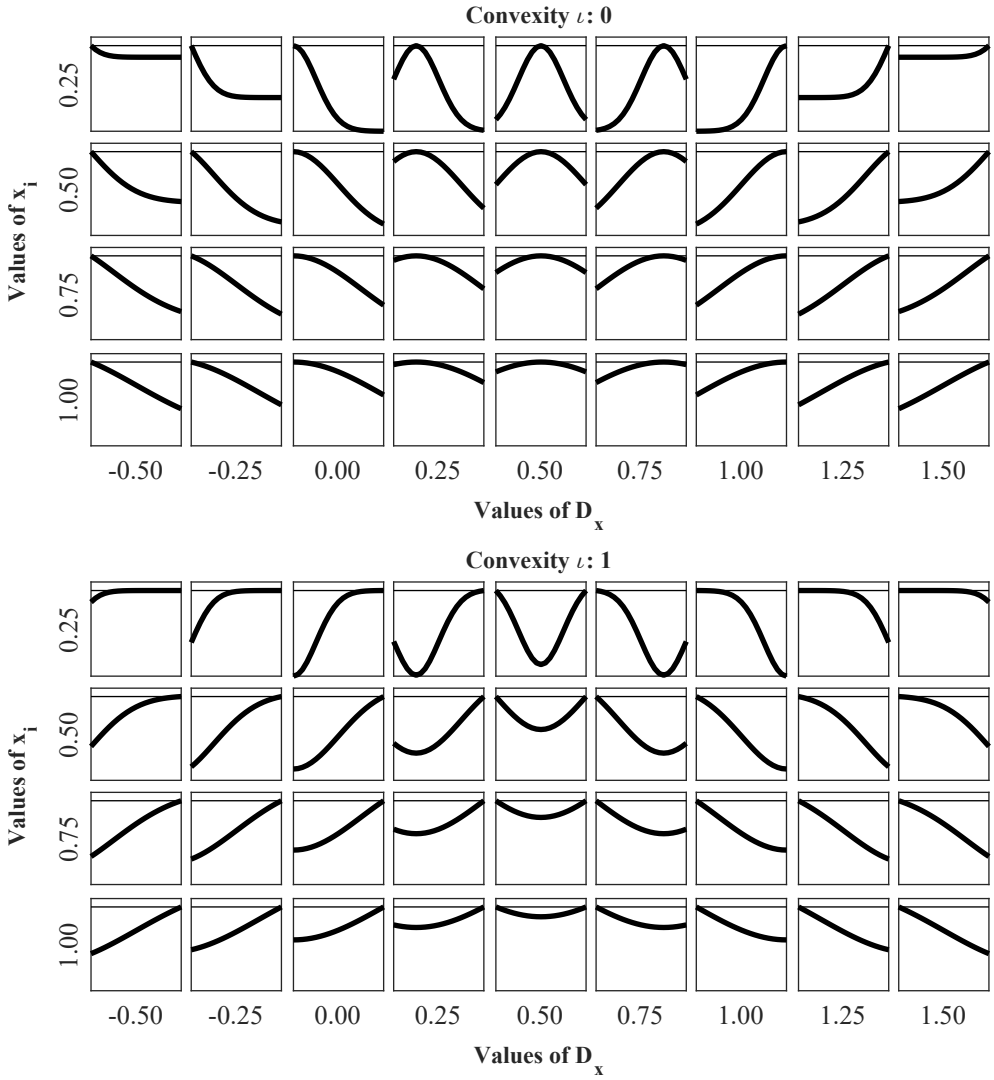

Figure 7.15: The derived settlement shapes adopted in the numerical analyses are based on arbitrary intervals of the parameters D_x, x_i and ι.

"FH"). The way the vertical loads are applied in the model is illustrated schematically in Fig. 7.17, whereas the values of each load for each facade are reported in Tab. 7.3.

7.3.10. LOADING SCHEME AND ITERATION PROCEDURE

The FE analyses make use of a two-step procedure:

- First, gravity was applied to the structure to compute the stress states due to the self-weight and weight of floors/roof (reported in Table 7.3). The two actions are applied separately with 10 steps respectively. After these 20 steps, the resulting

displacement field of the façade was then cleared to keep track of the displacement field from the settlement loading only. The gravity and overburden loads were applied in multiple steps because it is possible that some non-linearities, and thus cracking, could occur in the building during the application of these loads.

- Then, the settlement profiles were applied as prescribed nodal displacements at the bottom of the interface elements that simulate the soil-foundation interaction.

The number of steps used for the application of the settlements differs per shape. Each settlement pattern is applied progressively increasing the displacement with a load step equal to 0.2 mm/step. In this way, the angular distortion was progressively increased from 0 (in the first step after the application of the gravity load) up to 1/300. Figure 7.16 shows an example of the relationship between the imposed increasing displacement and the applied angular distortion for one of the analyses.

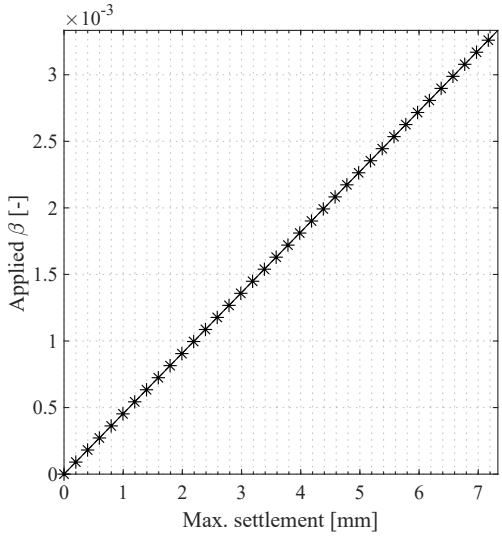

Figure 7.16: The linear relationship between the maximum settlement, progressively increased with a load step equal to 0.2 mm/step, and the applied angular distortion β for facade "FA" and for the settlement shape with ι = 1, D_x=0.5 and x_i=0.5.

The numerical iteration procedure makes use of the Quasi-Newton (Secant) method [11]. The line-search option for the iteration method is activated, which is an option that stabilizes the convergence behaviour and aids the convergence speed. The maximum number of iterations is set to 500 for the gravity load and overburden, whereas it is 200 for the settlement pattern. Force and displacement (with a convergence tolerance equal to 10^{-2}) and the Energy (convergence tolerance equal to 10^{-4}) norms are employed for gravity and overburden, whereas only the Energy norm (with a convergence tolerance equal to 10^{-4}) is used during the application of the settlements. The analyses stop if divergence occurs, *i.e.,* the out-of-balance of the energy norm is higher than 1 x 10^7. Non-convergent steps, *i.e.,* out-of-balance of the energy norm between 1 x 10^4 up to 1 x 10^7, are allowed. Non-convergent steps are accepted as long as convergence is recovered

in the following steps of the analyses. In the FE analyses, cracking of brittle materials, such as masonry, is associated with the occurrence of strong nonlinearity which affects the solution iteration procedure (for instance, due to multiple cracks opening in one step, or if a big crack suddenly opens). Thus, it may be challenging to ensure convergence at each step of the analysis, and even more so for a high number of models and analyses, as in the case of this study.

All the analyses are run in single-core.

Table 7.3: The loads adopted in the finite element analyses of each facade, according to the loading scheme shown in Fig. 7.17.

Façade	Distributed loads			Point loads			
	q_{floor}	q_{roof}	q_{veneer}	$Q_{trans.\ floor,\ left}$	$Q_{trans.\ floor,\ right}$	$Q_{trans.\ veneer,\ left}$	$Q_{trans.\ veneer,\ right}$
	kN/m			kN			
FA	0.00	0.00	0.00	8.86	8.86	0.00	0.00
FB	0.62	4.46	0.00	0.00	16.50	0.00	0.00
FC	0.00	1.77	7.91	7.53	7.53	7.55	7.55
FD	0.00	0.41	0.00	5.50	5.50	0.00	0.00
FE	0.00	2.85	0.00	5.43	5.43	0.00	0.00
FF	0.00	0.00	0.00	4.19	9.42	0.00	0.00
FG	0.00	4.19	0.00	2.89	2.89	0.00	0.00
FH	0.00	5.33	5.08	0.00	0.00	8.76	8.76

7.3.11. "APPLIED" AND "MEASURED" DISTORTIONS

A distinction is made in this study between the applied displacements, herein labelled as "applied", representing the loss of support underneath the foundation, and the resulting displacements at the bottom of the façade, identified as "retrieved" similarly to Chapters 5 and 6. Thus, the angular distortion imposed at the interface level is labelled as "applied β", whereas "measured β" is computed from the measured displacements.

Figure 7.18 schematically illustrates the difference between applied and measured displacements.

7.4. PRELIMINARY SENSITIVITY ANALYSES OF THE NUMERICAL FEATURES

This section refers to the results of **Step 1** of the adopted methodology (Fig. 7.1).

The first part of this section demonstrates how the damage is obtained from the numerical analyses, and how the relationship with the applied angular distortion is retrieved. The results of one of the selected facades are presented and discussed in detail.

The second part of this section illustrates the sensitivity analyses carried out to investigate the role of different aspects of the numerical models on the results. While the analyses presented in Chapter 5 showed the influence of different building and soil features, the role of the mesh size, the iteration norms and the load steps which concern the numerical analyses are herein evaluated and discussed. Finally, the influence of the numerical settings is quantified.

7.4.1. RELATIONSHIP BETWEEN THE MAX. CRACK WIDTH AND THE DAMAGE PARAMETER Ψ

In this section, the results of the facade labelled as "FA" are detailed (Fig. 7.7). The selected facade model referred to in the following as the "reference case" is resting on the unreinforced masonry foundation (as shown in Fig. 7.13) on "Clay" soil, and the analysis considers the "Standard" masonry material.

The analysis considers the reference case subjected to one hogging[2] settlement pattern, obtained with the use of equation 7.5 ($D_x = 0.5$, $x_i = 0.5$, $\iota = 0$, see Fig. 7.15) and the maximum angular distortion is equal to 1/300. Accordingly, the maximum settlement of the considered profile is equal to about 8 millimetres and it is applied to the model in 38 steps after 20 steps of the gravity and overburden load (the reader is referred to section 7.3.10). Additionally, Appendix C reports the results of the same analyses for the other selected facades.

Figure 7.19 shows the results of the selected reference case in terms of crack pattern, and principal stresses as tensor plots. The facade subjected to the symmetric hogging pattern exhibits the development of a crack that starts from the top edge and progressively develops toward the bottom. The tensor plots confirm that the highest tensile stresses are observed where the cracks are developing. However, the interpretation of the principal stresses should be approached with caution, as they may be misleading when analyzing the response of non-linear structures.

Figure 7.20 illustrates how the applied angular distortion is progressively applied in the numerical analysis. Accordingly, Fig. 7.20b and c show how both the maximum crack width and the damage parameters Ψ increase with the progression of the settlement. In the graphs, the degree of damage associated with the visible damage, based on the classification proposed by [23], is shown for both the maximum crack width and Ψ [24]. Moreover, the relationship between the maximum crack width and Ψ is shown in Figure 7.20c. Accordingly, the dashed line shows the relationship between the width of one

[2] In Appendix C, the results of the same analysis for a "sagging" settlement profile are reported.

crack and its corresponding Ψ values [24]. The results of the reference case show a good agreement with the theoretical line, as only the main crack is developing on the facade, as shown in Fig. 7.19. Moreover, the difference with the theoretical trend can be explained by the presence of other small cracks developing on the facade (Fig. 7.19), which are included in the computation of Ψ. Overall, compared to using crack width alone, the damage parameter Ψ directly reflects the increase in damage by comparing its values at two different stages. For example, if the maximum crack width remains the same at two different stages, but new cracks appear, these will be accounted for in the calculation of Ψ. This is significant because varying the imposed settlement patterns can lead to different crack patterns, with multiple cracks potentially developing on the facades.

7.4.2. THE INFLUENCE OF THE ANALYSES SETTINGS

In this section, the influence of different numerical settings on the results is evaluated. The analyses consider variations of the following parameters:

- **Mesh size**: the mesh size of the reference case is 200 x 200 mm, as described in section 7.3. Two variations are studied considering mesh sizes equal to 100 x 100 and 300 x 300 mm (Fig. 7.21).
- **Step size**: the settlement is applied at the bottom of the facade progressively considering 0.2 mm for each step of the numerical analysis. In this section, two load steps equal to 0.1 and 0.05 mm are considered.
- **Convergence norms**: during the settlement application, the considered convergence criterion is the Energy norm. In this section, an additional analysis is carried out considering the Force, Displacement and Energy norms simultaneously to evaluate their effect (Tab. 7.4)

Table 7.4: The adopted convergence norms.

Adopted convergence norms in each phase of the analysis			
Model	**Self-weight**	**Overburden**	**Settlement**
Reference	Force & Displacement & Energy	Force & Displacement & Energy	Energy
Variation for sensitivity analysis			Force & Displacement & Energy

The results of the sensitivity analysis are summarised in Figure 7.22[3]. The plots show a good agreement for small Ψ values, *i.e.*, Ψ smaller than 1.5 - 2.0, and thus the models are initially insensitive to the different selected settings. However, the differences progressively increase for Ψ values higher than 2.0, both in terms of applied and measured angular distortion (Fig. 7.22a and b respectively).

Figure 7.23 and 7.24 shows the crack patterns of all the selected model variations and the corresponding Ψ values for applied angular distortion values equal to 1/1000 (or 1.00 ‰) and 1/500 (or 2.00 ‰).

[3] In addition to this Figure, the results of all the selected facades are reported in Appendix C.

The crack patterns and the Ψ values are almost the same for an angular distortion equal to 1/1000 (Fig. 7.23), whereas differences with the progression of the settlement and damage occur in Fig. 7.24. Due to the application of the symmetric hogging settlement, it is expected that cracks would occur at the top of the facade, which is consistent with what is observed in the reference case (Fig. 7.24a). The crack pattern of the reference case (Fig. 7.24a) is similar to the models with a different mesh size (Fig. 7.24b and c) and with the model that makes use of the load step 0.05 mm/step (Fig. 7.24d). Nevertheless, the models with a load step of 0.10 mm/step and the energy-force-displacement norms (Fig. 7.24e and f) exhibit slightly different crack patterns in which the top vertical crack does not open and cracking localizes at window corners at first floor as horizontal cracks.

The differences between the results of models are not unexpected, as non-linear FE analyses of masonry structures are pathologically affected by issues related to the damage localization which is influenced by the chosen analysis settings, influencing the iteration procedure, and the finite element discretization, *i.e.*, type of FE elements, mesh size and number of integration points. In general, the occurrence of non-convergence steps, influenced by the chosen parameters for the numerical analyses, could be a source of difference between the crack patterns. Figure 7.25 shows the convergence behaviour of all the selected models: The reference case (Fig. 7.25a) exhibits 7 % of non-convergent steps, the model with mesh 100x100 mm (Fig. 7.25b) and 300x300 mm (Fig. 7.25c) 24 % and 9 % steps respectively, the model with a load step equal to 0.10 mm/step exhibits 10 % (Fig. 7.25e), whereas the model with 0.05 mm/step 15 % (Fig. 7.25d). The models that consider force- energy- and displacement- norms (Fig. 7.25f) exhibit 37 % of non-convergent steps.

However, it is important to notice that most of non-convergent steps are observed when the facade models exhibit Ψ values higher than 3. This observation is supported by the results present in Figures 7.22, 7.23 and 7.24. Therefore, it is expected that the difference in the crack patterns can be explained by the occurrence of non-convergent steps for Ψ values higher than 3, for which strong non-linearities develop in the model.
Nevertheless, the analyses presented in this thesis always focus on "light damage", which is attained for Ψ values lower than 3.

In the following analyses, the values of applied and measured angular distortion associated with Ψ values higher than 3 are not included. The values of both applied and measured angular distortion for different Ψ are reported in Table 7.5, based on the results shown in Figure 7.22. Accordingly, it is possible to quantify the variation between the values of the angular distortion of the reference model, the maximum and the minimum values for Ψ values lower than 3. The results indicate that, depending on the selected numerical settings, the values of angular distortion vary between -26 % and 14 % from the reference case. Considering the susceptibility of all non-linear analyses to the specific settings employed, it is not unexpected to observe such variations.

THE INFLUENCE OF THE SETTLEMENT SHAPE: SAGGING VS HOGGING

In addition to the results of the sensitivity analyses for the facade "FA" presented previously subjected to a hogging settlement, in this section the results are presented with reference to a different settlement pattern.

Table 7.5: Variation of the applied and measured angular distortion for different values of Ψ for the reference case subjected to hogging. A colour scheme is applied to distinguish between the lowest (dark cells) and the highest (light cells) values.

Damage Ψ	Applied angular distortion β							
	Reference	Mesh 100x100 mm	Mesh 300x300 mm	Load step 0.05 mm/step	Load step 0.10 mm/step	Energy – Force - Displacement norms	Variation between Reference and Max. value	Variation between Reference and Min. value
0.5	$5.4x10^{-4}$	$4.8x10^{-4}$	$6.0x10^{-4}$	$5.4x10^{-4}$	$5.4x10^{-4}$	$5.4x10^{-4}$	12%	-12%
1	$9.0x10^{-4}$	$7.8x10^{-4}$	$9.8x10^{-4}$	$9.1x10^{-4}$	$9.1x10^{-4}$	$9.0x10^{-4}$	9%	-14%
1.5	$1.3x10^{-3}$	$1.1x10^{-3}$	$1.3x10^{-3}$	$1.2x10^{-3}$	$1.3x10^{-3}$	$1.2x10^{-3}$	4%	-12%
2	$1.5x10^{-3}$	$1.5x10^{-3}$	$1.4x10^{-3}$	$1.3x10^{-3}$	$1.5x10^{-3}$	$1.5x10^{-3}$	0%	-18%
2.5	$1.6x10^{-3}$	$1.7x10^{-3}$	$1.4x10^{-3}$	$1.3x10^{-3}$	$1.6x10^{-3}$	$1.6x10^{-3}$	6%	-20%
3	$1.8x10^{-3}$	$1.8x10^{-3}$	$1.5x10^{-3}$	$1.3x10^{-3}$	$1.8x10^{-3}$	$1.7x10^{-3}$	2%	-26%
Damage Ψ	**Measured angular distortion β**							
	Reference	**Mesh 100x100 mm**	**Mesh 300x300 mm**	**Load step 0.05 mm/step**	**Load step 0.10 mm/step**	**Energy - Force - Displacement norms**	**Variation between Reference and Max. value**	**Variation between Reference and Min. value**
0.5	$7.5x10^{-5}$	$6.6x10^{-5}$	$8.6x10^{-5}$	$7.5x10^{-5}$	$7.1x10^{-5}$	$7.1x10^{-5}$	14%	-12%
1	$1.3x10^{-4}$	$1.1x10^{-4}$	$1.5x10^{-4}$	$1.4x10^{-4}$	$1.3x10^{-4}$	$1.2x10^{-4}$	13%	-16%
1.5	$2.1x10^{-4}$	$1.8x10^{-4}$	$2.2x10^{-4}$	$2.1x10^{-4}$	$2.1x10^{-4}$	$2.0x10^{-4}$	2%	-17%
2	$3.2x10^{-4}$	$3.0x10^{-4}$	$2.7x10^{-4}$	$2.3x10^{-4}$	$2.8x10^{-4}$	$2.7x10^{-4}$	0%	-28%
2.5	$3.5x10^{-4}$	$4.0x10^{-4}$	$3.2x10^{-4}$	$2.7x10^{-4}$	$3.2x10^{-4}$	$3.3x10^{-4}$	14%	-23%
3	$4.3x10^{-4}$	$4.9x10^{-4}$	$4.2x10^{-4}$	$3.4x10^{-4}$	$4.6x10^{-4}$	$4.0x10^{-4}$	14%	-21%

In particular, a sagging settlement pattern is considered, obtained with the use of equation 7.5 ($D_x = 0.5$, $x_i = 0.5$, $\iota = 1$, see Fig. 7.15) and the maximum angular distortion is equal to 1/300. The sagging profile mirrors the hogging profile used in the sensitivity analyses presented previously.
Differently from the results presented in Figure 7.22, Figure 7.26 shows smaller discrepancies among the models with varying settings. Specifically, differences are observed only in the model utilizing a coarser mesh size (300 x 300 mm), compared to the other models. However, the overall damage mechanism is coherent between the different models, as shown by the crack patterns in Figure 7.27 for an applied angular distortion equal to 1/500 (or 2.00 ‰). In addition, it is noticeable how the sagging settlement pattern represents a less critical condition for the facade model, as the final Ψ values range between 3.3 and 4.0 (Figure 7.26a), whereas in hogging between 4.4 and 6.8 (Figure 7.22a). The findings are confirmed by the results reported in Appendix C for the other facade geometries.

THE INFLUENCE OF THE FACADE GEOMETRY

This section shows the results of the sensitivity analyses carried out for facade "FB" subjected to hogging, in addition to the results of "FA" presented previously.
Interestingly, the results of the very long facade "FB" in Figure 7.28 show no significant variation between the results of the different models. This result indicates that certain models due to the combination of geometry, lintels, gravity and overburden loads, may be more prone to non-linearities and variations in damage due to changes in the settings of the numerical analyses than others. This observation is supported by the results reported in Appendix C for the other facade geometries.

7.5. DISCUSSION

In addition to the limitation already discussed in Chapters 5 and 6 regarding the modelling approaches, the sensitivity analyses herein carried out reveal that the use of different numerical settings (mesh size, load step size, convergence norms) could result in a difference of even ± 30% of the final results. This, however, represents a limitation for any analyses that consider brittle materials, such as masonry and concrete, and has to be considered as a source of epistemic uncertainties.

The adopted models, like any numerical model, idealize reality in a simplified fashion. Additional studies and comparisons against experimental benchmarks and existing structures loaded by differential settlement are recommended to further validate the modelling assumption. This step was not possible in this study, as the number of cases available in the literature for such validation campaigns is quite limited or not well documented.

The models depict the behaviour of eight facades that idealize typical geometries of the Dutch low-rise masonry buildings built before 1970, which represent the focus of this study.

Preliminary analyses were carried out to evaluate how well the selected geometries, previously adopted in experimental tests or based on existing buildings, could be representative of the exterior walls of buildings located in the Netherlands and built before 1970. A comparison was thus carried out considering multi-sources data of about 20 million walls in the Netherlands, entailing the geometry and dimension of each wall.

The analyses reveal that the selected facades could be considered representative of a good portion (59%) of about 20 million walls. Considering the variability of each wall of each building, due to its unique combination of shape and dimensions, the analyses are considered satisfactory. However, it was not possible to make any conclusion regarding other relevant features which could also influence the response of the facade, such as for example the opening ratio, *i.e.*, amount and locations of windows and doors. It is thus assumed, but not validated, that the selected facade would also represent realistic scenarios for features such as opening ratio, type of lintels, and floor and roof loads. Similarly, two soil materials and two foundation systems are selected for the analyses, based on the engineering judgment.

7.6. CONCLUSIONS

In this Chapter, it has been observed that:

- The selected facades represent realistic types of masonry facades for buildings in the Netherlands.
- The relationship between the maximum crack width, typically used to evaluate damage due to settlements in numerical analyses, and the damage parameter Ψ is in good agreement with their theoretical relationship. The difference can be explained by the number of cracks and their lengths, which are included in the calculation of Ψ.
- Compared to the maximum crack width, using the damage parameter Ψ allows for a better characterization of the relationship between settlement and light damage.
- Variations in the settings of the numerical analyses (mesh size, load step size, convergence norms) have been observed to influence the relationship between the imposed deformation, the distortions of the buildings and the induced damage. In the worst case (hogging), these differences have been observed to range between -28 and +14 % compared to the results of the settings of the reference model, before the models exceeded light damage ($\Psi < 3$), which represents the focus of this study. However, for larger Ψ these differences increase. Moreover, the variation of the results strongly depends on both the geometry of the facade and the shape of the applied settlements.

Given the differences observed between the models with varying settings, it is not possible to determine the optimal combination of mesh size, load step, and the convergence norms to be used during the application of the settlement load. Nevertheless, the results of the models with the "reference settings", *i.e.*, mesh size of 200 x 200 mm, load step equal to 0.02 mm/step using only energy norm for the settlement phase, have been observed to produce on average the best results for all other models in all cases (reported both in this Chapter and Appendix C). Therefore, these settings are used in the following for the development of numerical fragility curves.

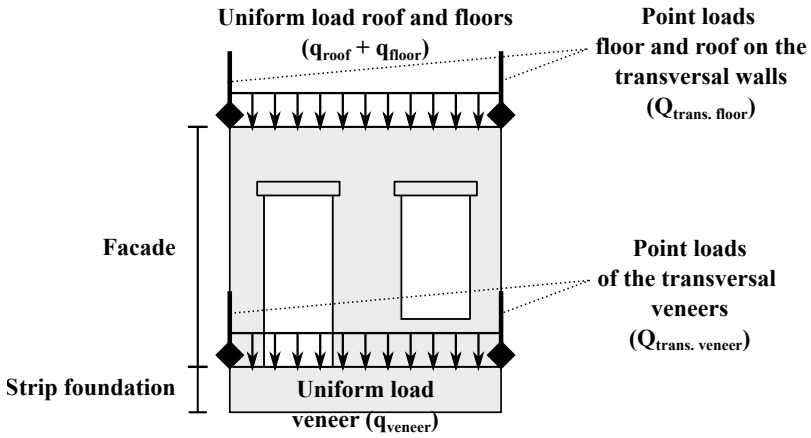

Figure 7.17: Schematic illustration of the location and types of loads applied to the selected facades.

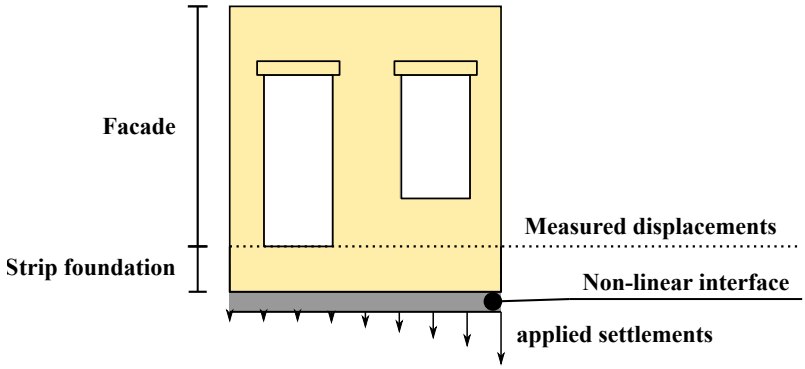

Figure 7.18: Schematic illustration of the location of "applied" and "measured" displacements in the adopted FE models. Applied displacements (and their relative angular distortion β) refer to the settlement pattern imposed in the bottom at the bottom of the interface elements. Measured displacement (and the measured angular distortion β) are retrieved at the bottom of the facade (top edge of the foundation).

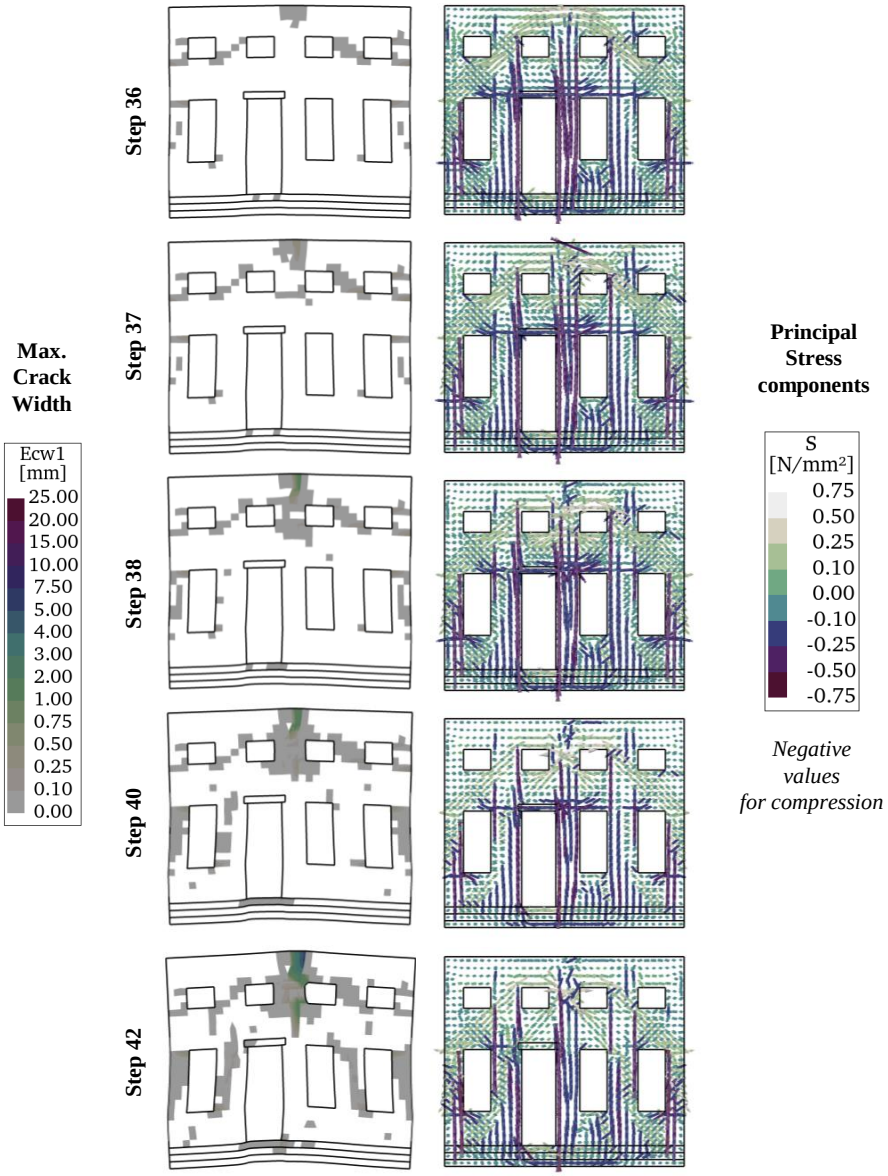

Figure 7.19: Results of the reference model subjected to symmetric hogging: (a) contour plots of the max. crack width (with a magnification factor of the deformations equal to 100) and (b) principal stresses.

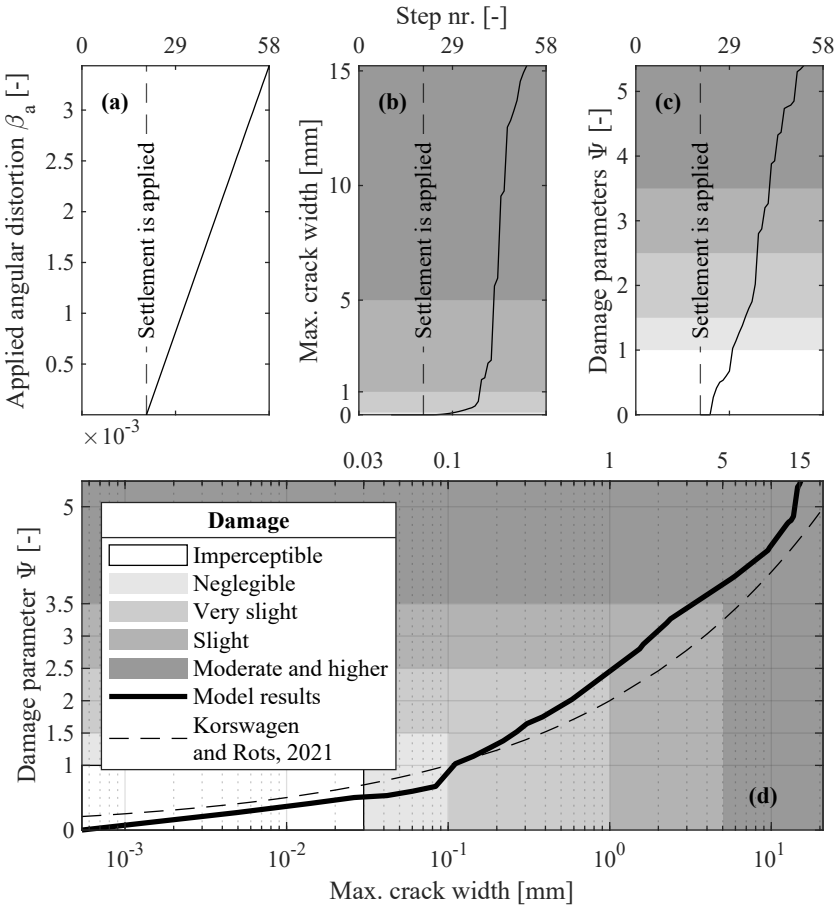

Figure 7.20: Results in the reference case in hogging: (a) Applied angular distortion β_a for each step of the analysis, (b) step number against the max. crack width, (c) step number against Ψ and (d) Max. crack width against Ψ. The dashed line represents the trend for one individual crack [24].

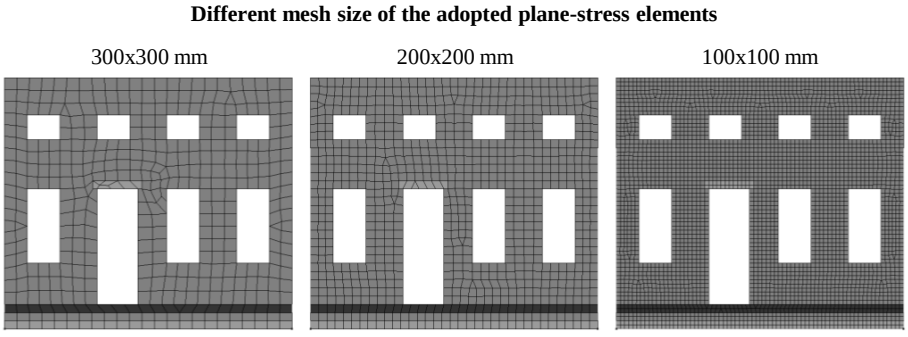

Figure 7.21: The different mesh sizes selected for the sensitivity analyses.

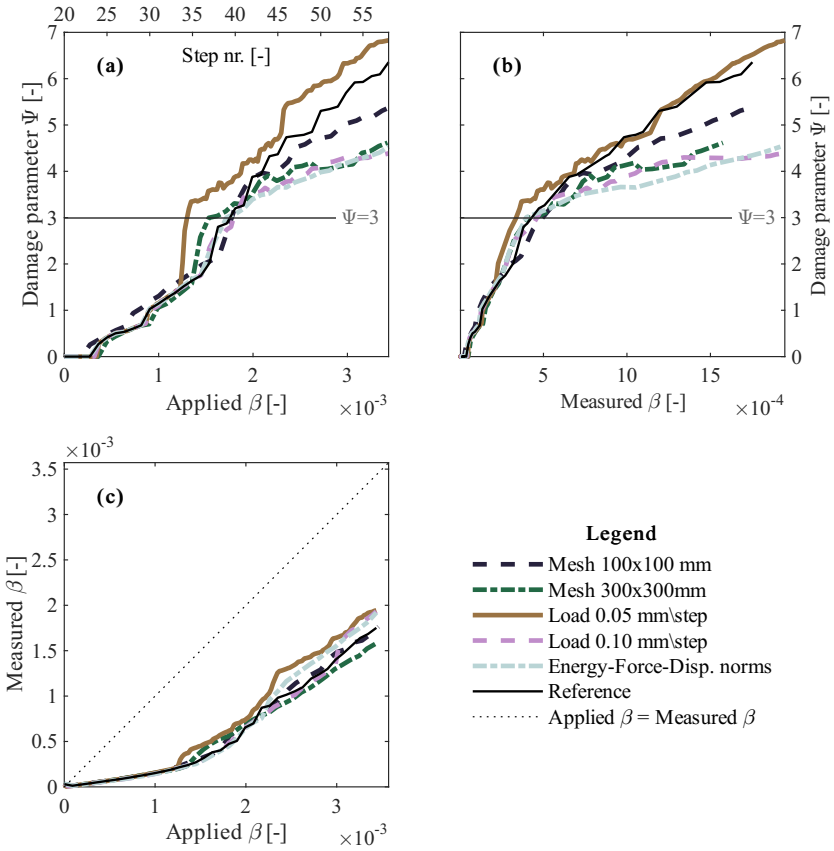

Figure 7.22: Results of the sensitivity analyses for the reference case in hogging in terms of applied and measured angular distortion against the damage parameter Ψ.

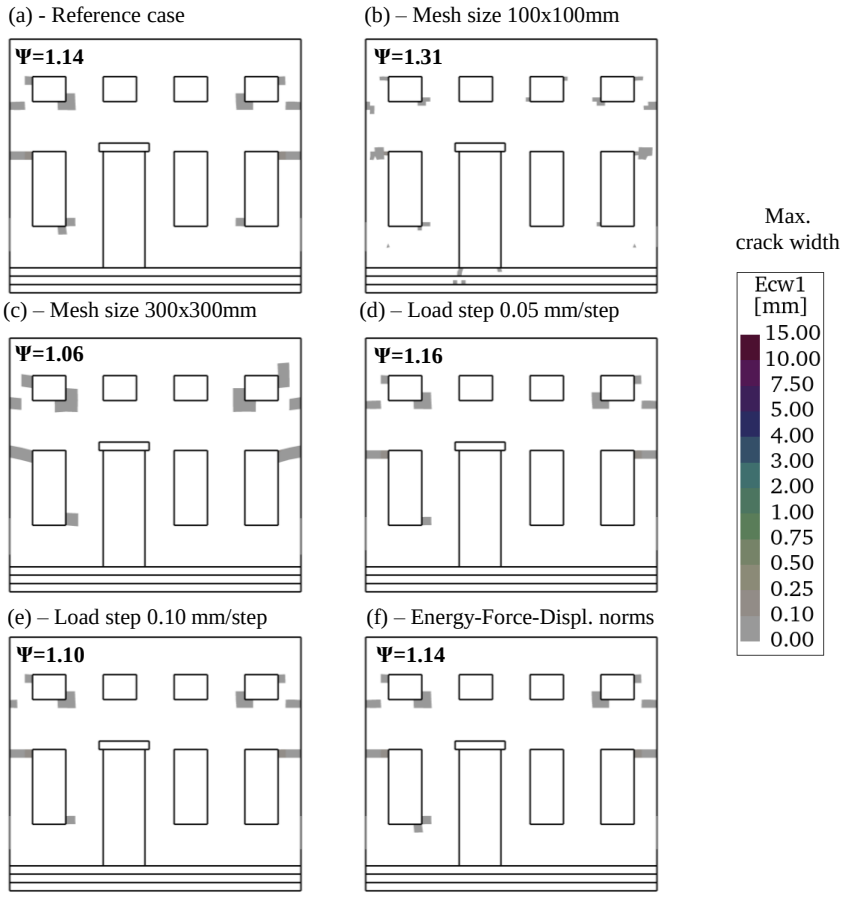

Figure 7.23: Crack patterns of all the models adopted in the sensitivity analyses for an applied angular distortion equal to 1/1000 (or 1.00 ‰) in hogging. The contour plots show the max. crack width. Deformations are not shown.

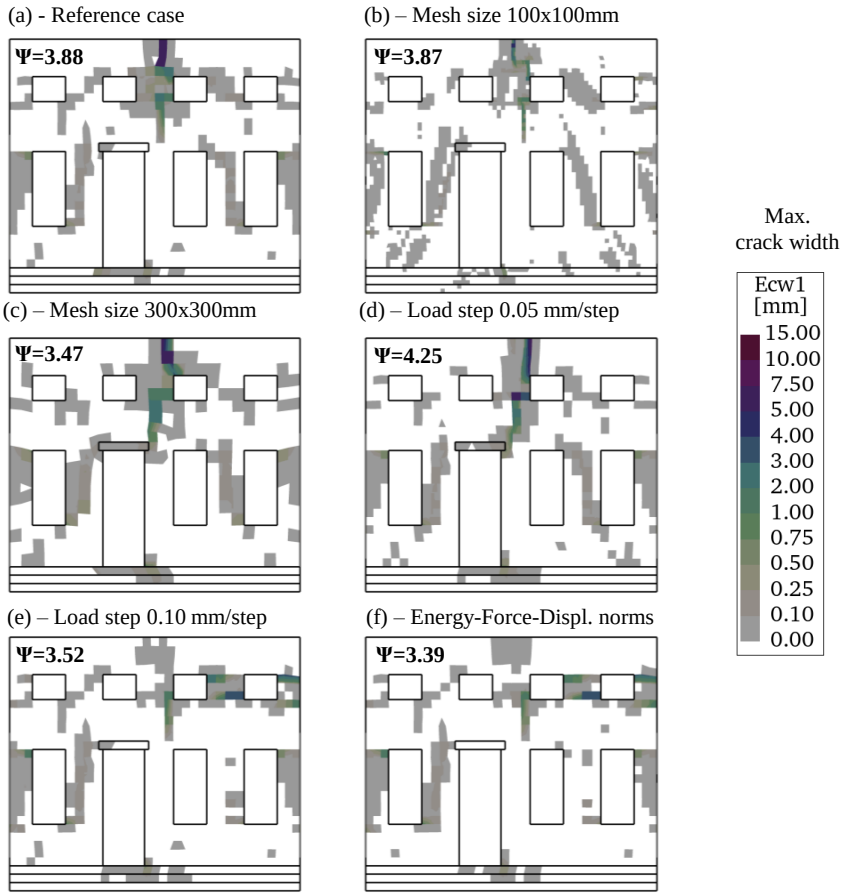

Figure 7.24: Crack patterns of all the models adopted in the sensitivity analyses for an applied angular distortion equal to 1/500 (or 2.00 ‰) in hogging. The contour plots show the max. crack width. Deformations are not shown.

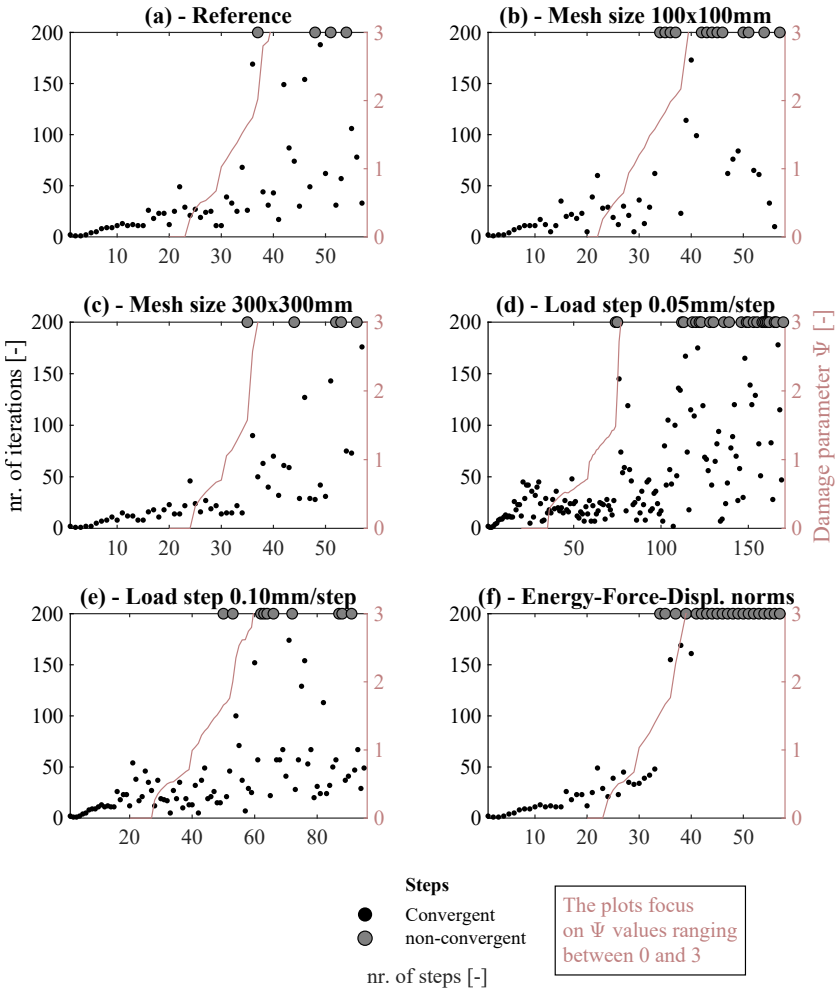

Figure 7.25: Step number against the number of iterations for each of the selected models in hogging. The right y-axis shows the damage parameter Ψ. The plots purposefully focus on Ψ values ranging between 0 and 3. Two colors distinguish the left y-axis (number of iterations, in black) from the right y-axis (Ψ values, in red).

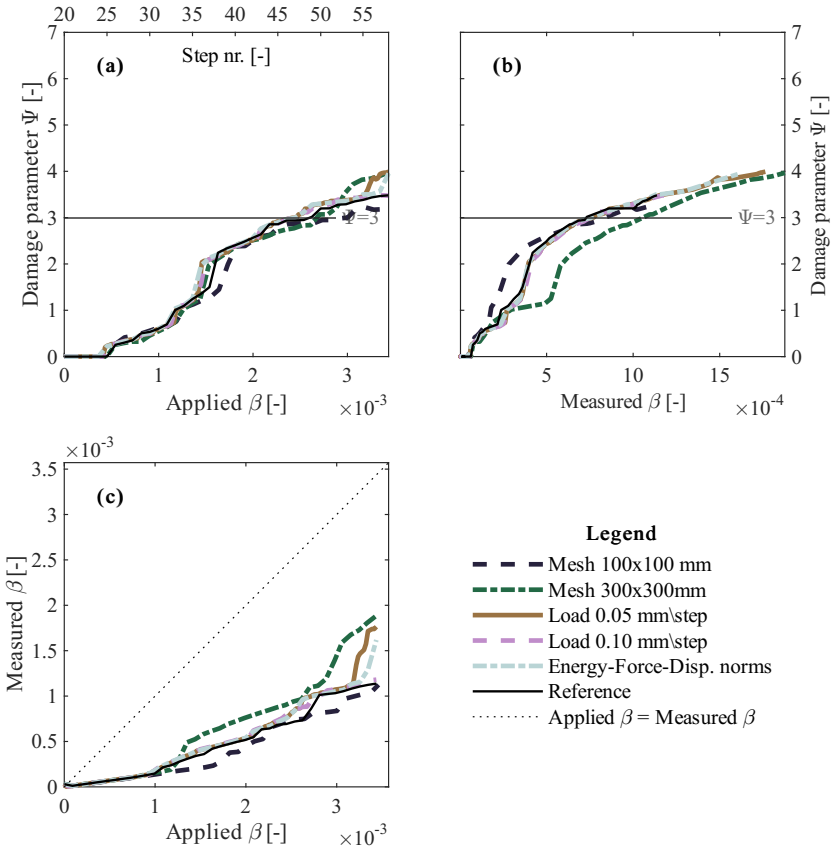

Figure 7.26: Results of the sensitivity analyses for a sagging settlement pattern in terms of applied and measured angular distortion against the damage parameter Ψ.

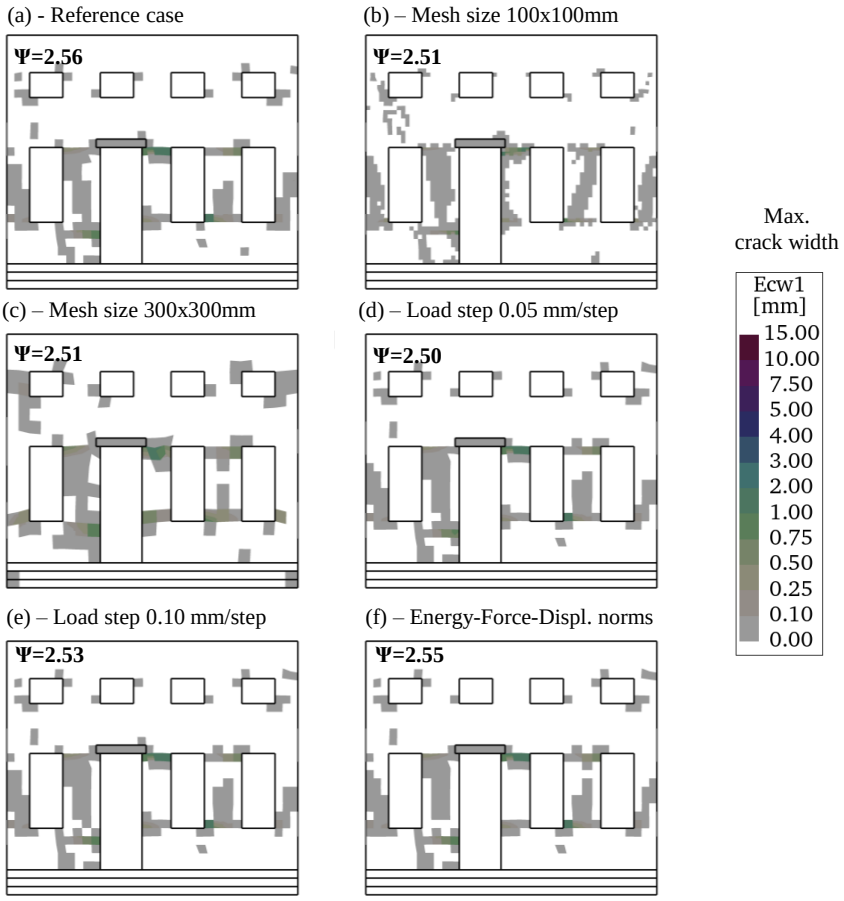

Figure 7.27: Crack patterns of all the models adopted in the sensitivity analyses for an applied angular distortion equal to 1/500 (or 2.00 ‰) in **sagging**. The contour plots show the max. crack width. Deformations are not shown.

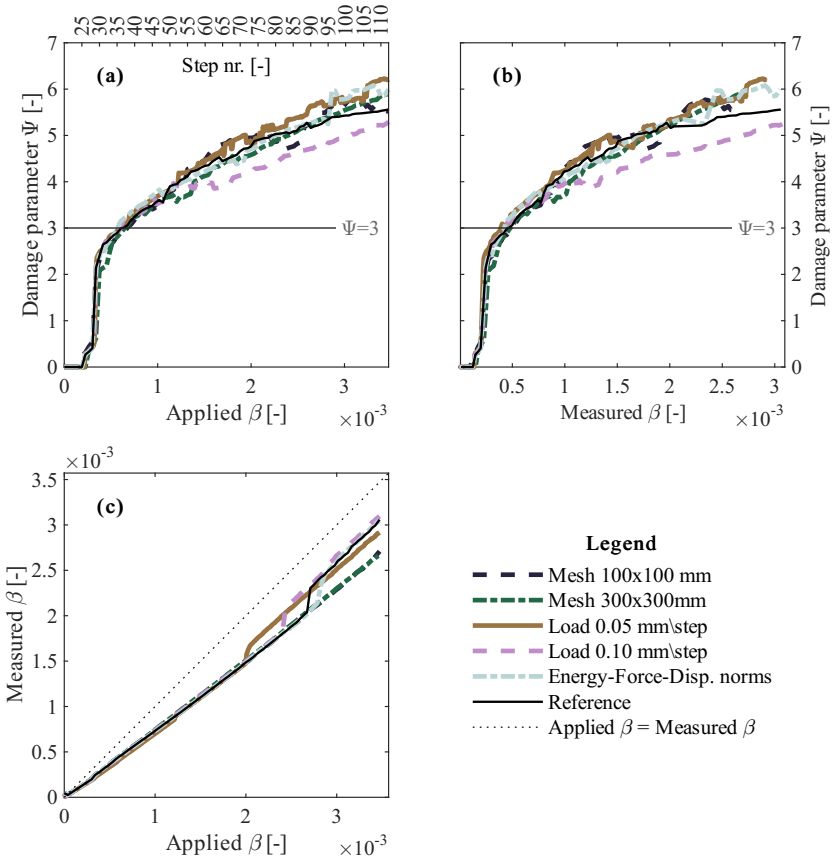

Figure 7.28: Results of the sensitivity analyses for a hogging settlement pattern in terms of applied and measured angular distortion against the damage parameter Ψ for the facade labelled as "FB".

BIBLIOGRAPHY OF CHAPTER 7

[1] P. Korswagen, M. Longo, J. Rots, and A. Prosperi, "Supporting analyses to determine probability of damage and fragility curves due to indirect subsidence effects," *Delft University of Technology. Report*, Final Version 2, October 3, 2022.

[2] P. Korswagen, M. Longo, J. Rots, and A. Prosperi, "Appendixes to supporting analyses to determine probability of damage and fragility curves due to indirect subsidence effects," *Delft University of Technology. Report*, 2022.

[3] R. Peters, B. Dukai, S. Vitalis, J. van Liempt, and J. Stoter, *Automated 3d reconstruction of lod2 and lod1 models for all 10 million buildings of the netherlands*, English, 2022. DOI: 10.14358/PERS.21-00032R2.

[4] "3DBAG - data sources." (2024), [Online]. Available: https://docs.3dbag.nl/en/overview/sources/.

[5] S. Jafari, "Material characterisation of existing masonry: A strategy to determine strength, stiffness and toughness properties for structural analysis," 2021.

[6] F. Messali, R. Esposito, S. Jafari, G. Ravenshorst, P. Korswagen, and J. G. Rots, "A multiscale experimental characterisation of dutch unreinforced masonry buildings," in *16th European Conference on Earthquake Engineering*, Springer, Thessaloniki, Greece, 2018, pp. 18–21.

[7] "Praktijkhandleiding bag - handleiding bij de catalogus van de basisregistratie adressen en gebouwen." (2024), [Online]. Available: https://imbag.github.io/praktijkhandleiding.

[8] J. Rots, P. Korswagen, and M. Longo, "Computational modelling checks of masonry building damage due to deep subsidence," *Delft University of Technology*, 2021.

[9] P. Korswagen, M. Longo, E. Meulman, and C. Van Hoogdalem, "Damage sensitivity of groningen masonry structures–experimental and computational studies," *Delft University of Technology. Report*, no. C31B69WP0-12, 2017.

[10] P. Van Staalduinen, J. Rots, and K. Terwel, "Onderzoek naar de oorzaken van bouwkundige schade in groningen: Methodologie en case studies ter duiding vande oorzaken," 2019.

[11] DIANA FEA, "Finite element analysis user's manual - release 10.8.," Report, 2024.

[12] NPR 9096-1-1:2012 nl, "Steenconstructies - eenvoudige ontwerpregels, gebaseerd op nen-en 1996-1-1+c1 (masonry structures - simple design rules, based on nen-en 1996-1-1+c1)," 2012.

[13] B. Standard, "Eurocode 6—design of masonry structures—," *British Standard Institution. London*, no. 2005, 2005.

[14] G. Schreppers, A. Garofano, F. Messali, and J. Rots, "Diana validation report for masonry modelling," *DIANA FEA report*, 2016.

[15] J. Rots, F. Messali, R. Esposito, S. Jafari, and V. Mariani, "Thematic keynote computational modelling of masonry with a view to groningen induced seismicity," in *Structural Analysis of Historical Constructions: Anamnesis, Diagnosis, Therapy, Controls*, CRC Press, 2016, pp. 227–238.

[16] NPR9998:2020en, *Assessment of structural safety of buildings in case of erection, reconstruction and disapproval - induced earthquakes - basis of design, actions and resistances*, 2021.

[17] P. A. Korswagen Eguren, M. Longo, E. Meulman, and C. van Hoogdalem, "Damage sensitivity of groningen masonry structures–experimental and computational studies: Stream 1," 2017.

[18] G. Gazetas, "Foundation vibrations," in *Foundation engineering handbook*, Springer, 1991, pp. 553–593.

[19] G. Mylonakis, S. Nikolaou, and G. Gazetas, "Footings under seismic loading: Analysis and design issues with emphasis on bridge foundations," *Soil Dynamics and Earthquake Engineering*, vol. 26, no. 9, pp. 824–853, 2006.

[20] NEHRP, "NIST GCR 12-917-21 soil-structure interaction for building structures," 2012.

[21] J. Rots, "Structural masonry: An experimental/numerical basis for practical design rules," 1994.

[22] P. J. B. B. Lourenço, "Computational strategies for masonry structures.," 1997.

[23] J. B. Burland, B. B. Broms, and V. F. De Mello, "Behaviour of foundations and structures," 1978.

[24] P. A. Korswagen, M. Longo, E. Meulman, and J. G. Rots, "Crack initiation and propagation in unreinforced masonry specimens subjected to repeated in-plane loading during light damage," *Bulletin of Earthquake Engineering*, vol. 17, pp. 4651–4687, 2019.

CHAPTER 8

NUMERICALLY-BASED FRAGILITY CURVES FOR MASONRY BUILDINGS ON SHALLOW FOUNDATIONS SUBJECTED TO SUBSIDENCE

CHAPTER 8: TABLE OF CONTENTS

8.1 Numerically-based fragility curves . . . 217
8.1.1 The influence of the number of analyses . . . 219
8.1.2 The influence of the masonry material . . . 221
8.1.3 The effect of hogging and sagging settlement profiles . . . 222
8.1.4 The influence of the foundation system . . . 223
8.1.5 The interface stiffness . . . 225
8.1.6 The effect of the L/H ratio . . . 226
8.1.7 Comparison of the influence of the different parameters . . . 227
8.1.8 The effect of existing damage . . . 231

8.2 Discussion . . . 233
8.2.1 Comparison with numerical fragility curves from previous studies . . . 233
Numerical fragility curves by Korswagen et al., 2022 [4] 233
Numerical fragility curves by Korswagen et al., 2024 [5] 236
8.2.2 Comparison with existing empirical fragility curves . . . 237
Empirical dataset from Zhang and Ng, 2005 [6] . . . 239
Empirically-based fragility curves by Peduto et al., 2019 [7] . . . 241
Empirically-based fragility curves presented in Chapter 4 . . . 242
8.2.3 Comparison with available limit values from codes and standards . . . 243

8.3 Conclusions . . . 248

Bibliography of Chapter 8 . . . 252

In this chapter, the probabilities of damage to masonry buildings exposed to settlements are retrieved by numerically-based fragility curves (hereafter referred to simply as "numerical fragility curves"). This chapter refers to **Step 3** of the methodology presented in section 7.1. The combination of facade geometries, settlement patterns, foundation, soil and masonry material selected and discussed in Chapter 7 are herein used to develop numerical fragility functions.

In particular, considering the 8 selected facade geometries, the 3 masonry materials, the 2 shallow foundation systems, the 2 interface soil materials and the 72 selected variations of possible settlement patterns, a total of 6912 analyses were carried out. The numerical analyses are carried out using the "reference settings" defined in Chapter 7, *i.e.*, mesh size of 200 x 200 mm, load step equal to 0.02 mm/step using only energy norm for the settlement phase (the Reader is further addressed to section 7.3 for details). The results of these analyses were used to construct fragility functions, which are presented herein.

8.1. NUMERICALLY-BASED FRAGILITY CURVES

For each analysis, *i.e.*, 1 specific facade with 1 masonry material, 1 foundation, 1 soil material and 1 settlement, an algorithm summarizes the values of the angular distortion for each Ψ value, similarly to Table 7.5.

In section 7.3.11, a distinction was made between the displacements applied in the model, herein labelled as “applied”, for which the "applied β" is computed, and the resulting displacements at the bottom of the façade, identified as “retrieved”, and the computed “measured β” (the reader is addressed to Fig. 7.18 for further details). Applied and measured β are thus computed for each step of the numerical analyses and used to draw the exceedance curves for all Ψ values which range from 0.5 to 3 with steps of 0.5 Ψ.

In Figure 8.1, the cumulative density functions are shown for all the facade models for all the selected scenarios, corresponding to 864 analyses for each facade. The cumulative density functions express the ratio between the number of analyses that reach or exceed a certain level of damage (expressed by the Ψ values) for a given angular distortion, to the total number of analyses; This is also the definition of fragility functions, which are cumulative distribution functions of the structural capacity for a specific damage state [1].

It is possible to compare the fragility curves of each facade to identify the most vulnerable facades, *i.e.,* the facades that show higher probabilities of each Ψ value for a given applied angular distortion. For instance, the facade labelled as "FC" exhibits probabilities of damage higher than 0 before the application of an angular distortion: this is explained by the fact that for some combination of masonry, soil materials and foundation, the facade exhibits damage due to its gravity loads (self-weight and the overburden) before settlement patterns are applied. These combinations are included to implicitly simulate the effects of settlements on pre-damaged buildings. Additionally, even though the analyses are focused on the effects of settlements, the influence of building loads and material degradation cannot be overlooked in actual structures. Some structures may show damage before any settlements happen, and the curves fictitiously take this condition into account.

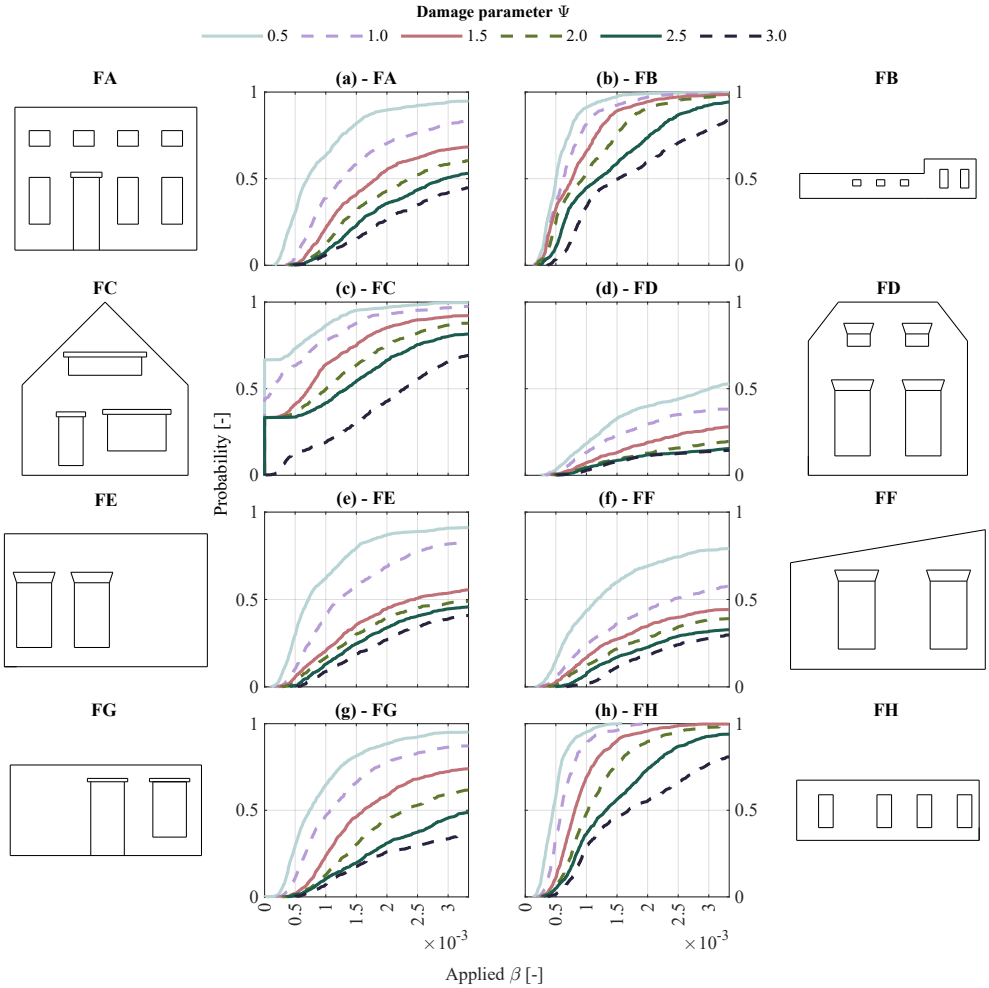

Figure 8.1: The cumulative density curves of all the selected facade geometries. The cumulative density curves describe the probabilities of reaching or exceeding specific levels of damage, expressed by Ψ values, as a function of the applied angular distortion.

Moreover, the facades with the highest L/H ratios, *i.e.*, "FB" and "FH" are the ones which exhibit the highest probabilities of damage for a given angular distortion. The effect of the L/H ratio is detailed in section 8.1.6.

The results of all the selected facades are combined in the cumulative density functions in terms of applied angular distortion in Figure 8.2. Similarly, Figure 8.3 shows the results in terms of measured angular distortion. During the progression of the settlement loads, the values of the applied angular distortion range between 0 and 1/300. However, the values of the measured angular distortion depend on the selected facade and its variations of material, geometry and load. Thus, for each model, the maximum value of the measured angular distortion does not have an upper or a lower bound. For this reason, the curves in 8.3 distinguish the portion in which the outcome of the models is obtained, from the one

extrapolated. For instance, for a measured angular distortion equal to about 1/1000, 90 % of the model exceeded Ψ of 0.5, whereas, 10 % of the models do not show any damage. Higher values of measured angular distortion were not recorded for this specific Ψ value.

The differences between the two sets of curves (Fig. 8.2 and 8.3) are due to the effect of soil-structure interaction. As it is known in the state-of-the-art (see Section 2.5.4 of this thesis), buildings are able to "flatten down" the soil deformation, due to their stiffness and weight, and thus the displacements and distortions measured on buildings are typically lower than what would be measured on the soil in green-field conditions, *i.e.*, in the absence of the building (see section 2.5). In other words, the stiffness and weight of the facade models reduce the imposed deformations, thus, measured distortions are lower than applied ones.

Both sets of curves express the relationship between the (applied or measured) angular distortion and the probability of having or exceeding a certain level of damage, however, they would be suited for different uses: while the curves in terms of applied distortions would be better suited to assess the probability of damage when the soil deformation is known, the curves in terms of measured distortions can be used when the deformations of the buildings are measured.

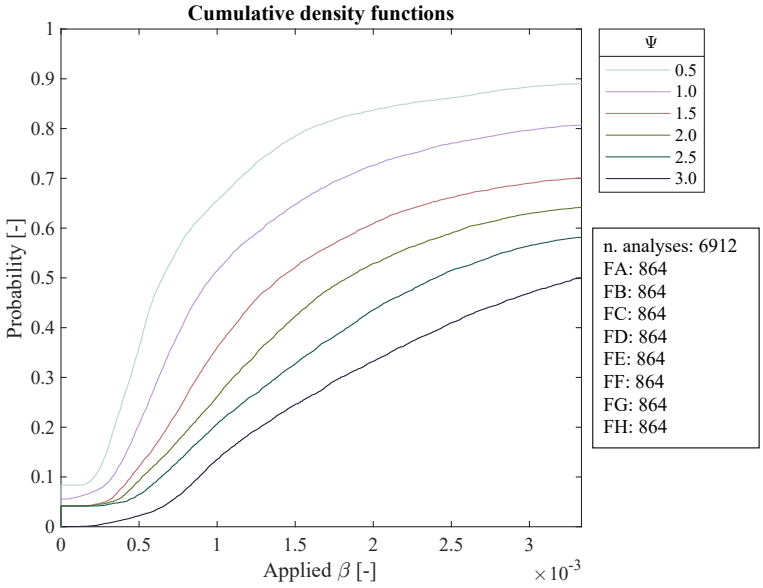

Figure 8.2: The numerical cumulative density curves in terms of **applied** angular distortion against the probability of damage for all the selected facade geometries.

8.1.1. THE INFLUENCE OF THE NUMBER OF ANALYSES

This section explored the influence of the number of analyses adopted in this Chapter. From the total number of combinations equal to 6912, sub-samples are considered a random selection of "n" cases. In particular, Figure 8.4 shows the results obtained

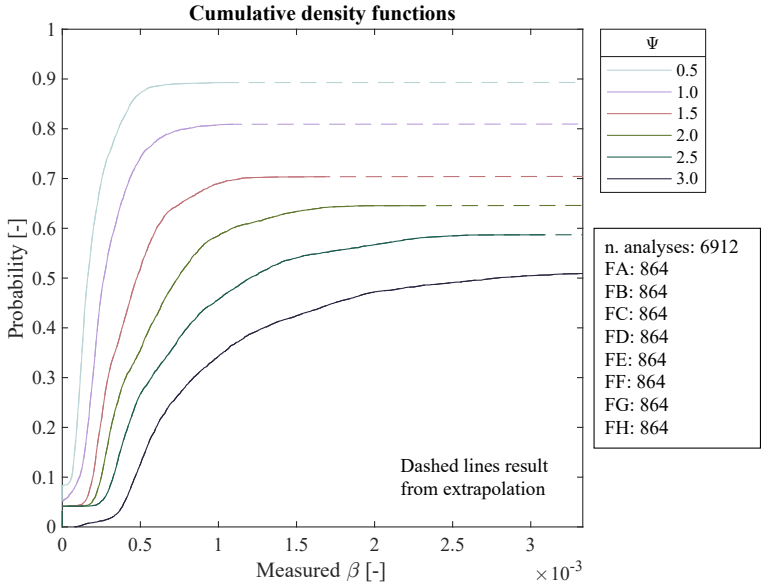

Figure 8.3: The numerical cumulative density curves in terms of **measured** angular distortion against the probability of damage for all the selected facade geometries.

considering subsamples of 100, 500, 1000, 3000 and 5000 analyses (Fig. 8.4a to e), in comparison with the results of the entire samples (Fig. 8.4f). The purpose of this analysis is to investigate how the fragility curves change depending on the selected number of combinations. Additional examples of the influence of the number of analyses are reported in Appendix C.

The curves that consider only 100 analyses in Fig. 8.4a resemble staircase cumulative distributions, whereas increasing the number of analyses from Fig 8.4b to 8.4f makes the curves approximate continuous cumulative distributions. The difference between the curves is in all cases negligible when the number of analyses is higher than 1000.

In this study, a high number of combinations is used to describe the realistic variations of "building-to-building" variability, which leads to the adopted 6912 combinations.

The results shown in Fig. 8.4 suggest that it would have been sufficient to consider a random sample of the analyses to consider the variability of the selected parameters, *i.e.*, material sets, foundation and settlement patterns, (for instance using the Latin hypercube sampling technique, as in [2]), and thus a lower number of analyses.

Nevertheless, due to the high number of combinations herein presented, it is possible to evaluate the effects on the different considered variables separately. In other words, the advantage of a large number of combinations consists in the fact that it is possible to study the influence of each variable on the exceedance curves. Accordingly, fragility curves are segregated based on each selected variable in the following sections.

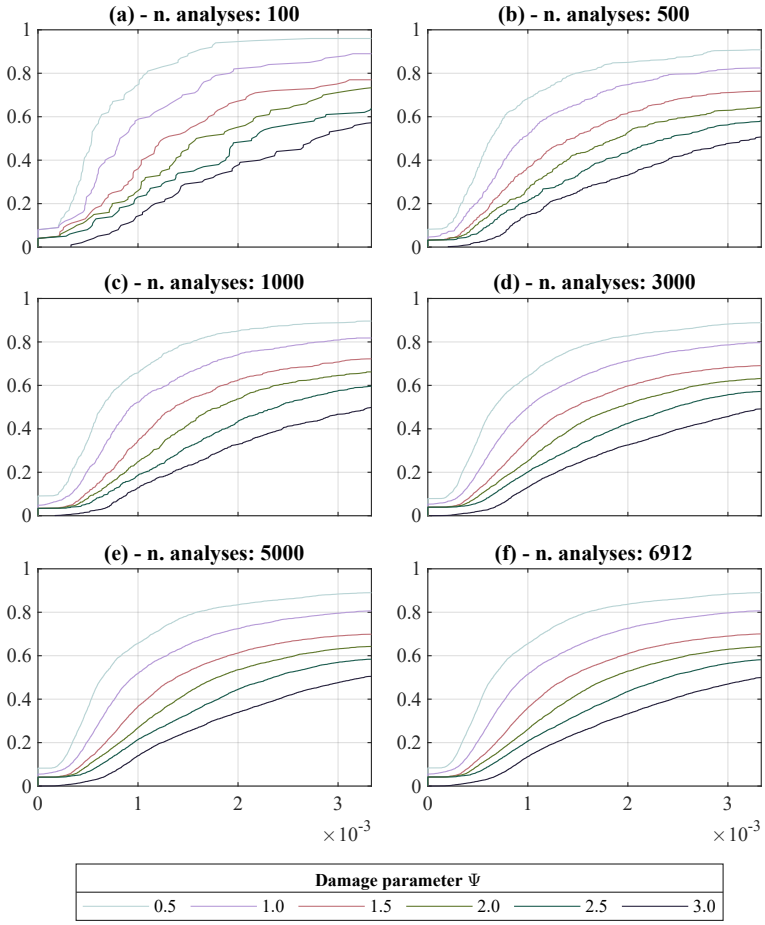

Figure 8.4: Cumulative density functions for different numbers of analyses. In each plot, the analyses are randomly selected from all the 6912 combinations.

8.1.2. THE INFLUENCE OF THE MASONRY MATERIAL

The effect of the selected masonry material properties on the fragility curves is shown in Figure 8.5. The results in terms of measured angular distortion are reported in Appendix C. As expected, the curves confirm that a stronger masonry material makes the building less vulnerable to the applied settlement. Thus, slightly more than 20% of the analyses with the strong masonry do not even exhibit Ψ values higher than 0.5 at the end of the settlement application (which is represented by the area above the curve corresponding to Ψ equal to 0.5 in Figure 8.5c). Conversely, this percentage is equal to about 10% for the standard masonry, whereas all the models exhibit Ψ values higher than 0.5 for the weak masonry.

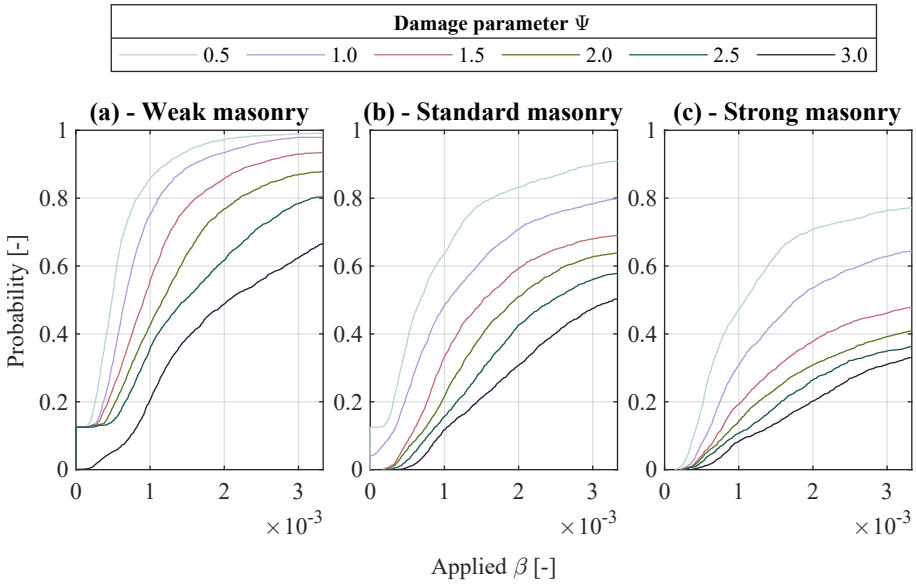

Figure 8.5: Cumulative density functions in terms of applied β for each selected **masonry material**. Each plot presents the outcomes of 2304 analyses.

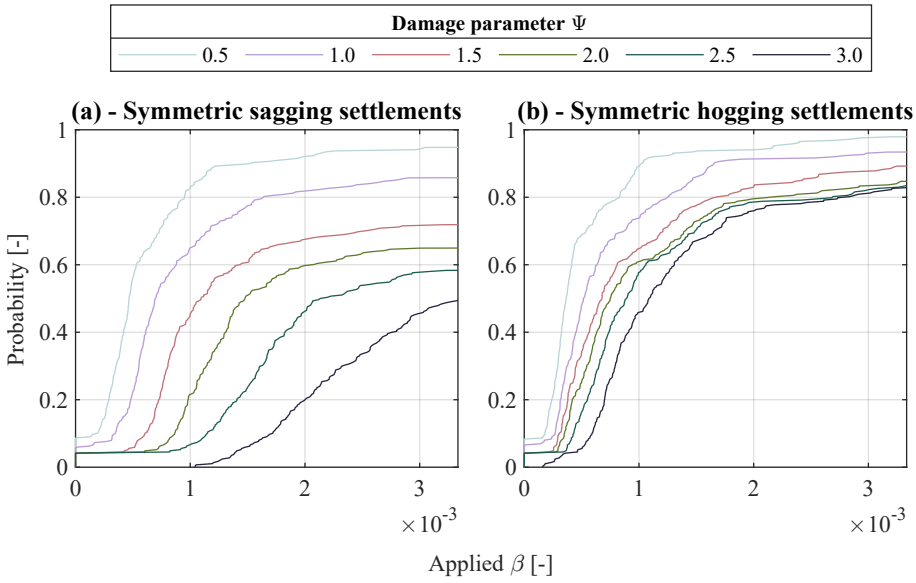

Figure 8.6: Cumulative density functions in terms of applied β for (a) **symmetric sagging** and (b) **symmetric hogging** (b) settlements respectively. Each plot presents the outcomes of 288 analyses.

8.1.3. THE EFFECT OF HOGGING AND SAGGING SETTLEMENT PROFILES

As discussed in section 7.3.8, the settlement actions imposed in the models idealize the variability of ground deformations that could affect buildings. The adopted settlement

profiles include both symmetric and asymmetric profiles conformed to a Gaussian shape. Depending on the location of the point of inflexion ("x_i" in equation 7.5, as shown in Fig. 7.14), the obtained settlements result in hogging or sagging shapes, or a combination of both. To examine the impact of settlement shape on model outcomes, fragility curves are generated by categorizing the results according to symmetric sagging and hogging deformations; Symmetric sagging profiles correspond to the shapes obtained with ι equal to 1, D_x equal to 0.5 and x_i ranging between 0.5 and 1, whereas symmetric hogging profiles are obtained with the same D_x and x_i, but with ι equal to 0. The results are shown in Figure 8.6.

Models exposed to hogging deformations exhibit greater vulnerability to damage compared to those undergoing sagging. Facades subjected to sagging experience tensile stresses concentrated at the bottom, where the foundation helps prevent crack formation. In contrast, during hogging, tensile stresses develop at the top of the facade, leading to more severe damage [3]. This is confirmed by the fragility curves in Fig. 8.6, which illustrate that damage progresses more rapidly in the case of hogging (8.6b), as evidenced by the closer proximity of the curves. The probabilities of damage in the case of symmetric hogging are thus higher than the ones obtained in sagging.

8.1.4. THE INFLUENCE OF THE FOUNDATION SYSTEM

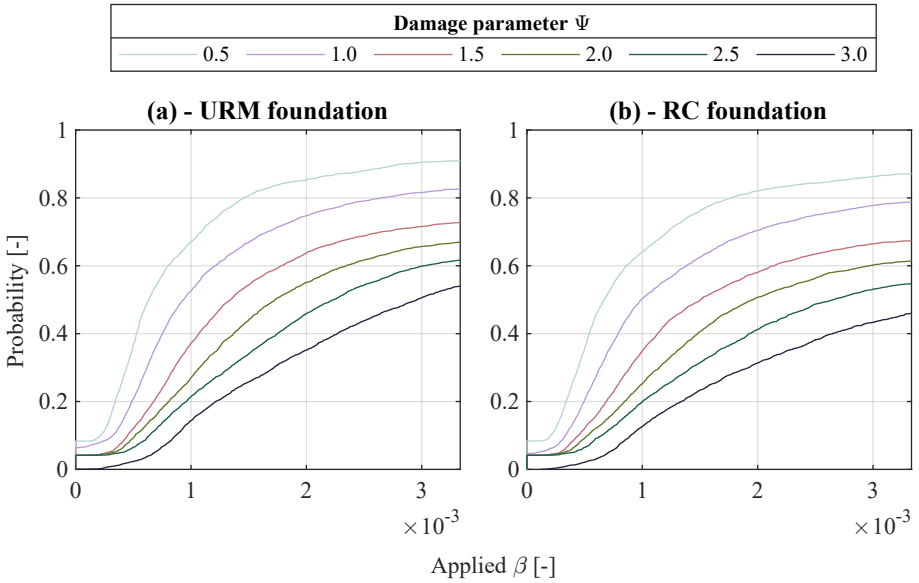

Figure 8.7: Cumulative density functions in terms of applied β for each **foundation system**. Each plot presents the outcomes of 3456 analyses.

The effect of the selected foundation systems on the fragility curves is shown in Figure 8.7. The results in terms of measured angular distortion are reported in Appendix C.

The differences between the fragility curves for RC and URM foundations do not appear

immediately noticeable. However, RC foundations show slightly lower probabilities of damage for a given value of applied angular distortion. For instance, for an applied angular distortion equal to 1/300, the probabilities of reaching or exceeding Ψ values equal to 3 are equal to about 53 % and 46 % for URM and RC foundations respectively, where for Ψ values equal to 0.5, the probabilities are 90 % and 87 %.

The similarity between the two sets of curves is related to the foundation systems selected for the analyses (detailed in Fig. 7.11 and further shown in this Chapter in Figure 8.8b): Two similar RC and URM foundations (Fig. 8.8b) have also been used in the sensitivity analyses presented in Chapter 5 and the results are presented in Fig. 5.11. The results in Fig. 5.11 show that the RC foundation (labelled in Chapter 5 as "RC strip with masonry layer" in Fig. 5.4) had only minor differences with the URM foundation, whereas the T-shaped RC foundation (Fig. 5.4d) has been observed to increase the stiffness of the building significantly, preventing the occurrence of damage higher than Ψ equal to 1.0 (Figure 5.11). Therefore, a major role can be attributed to the RC cross-section and thus the distance between the top and bottom reinforcement bars.

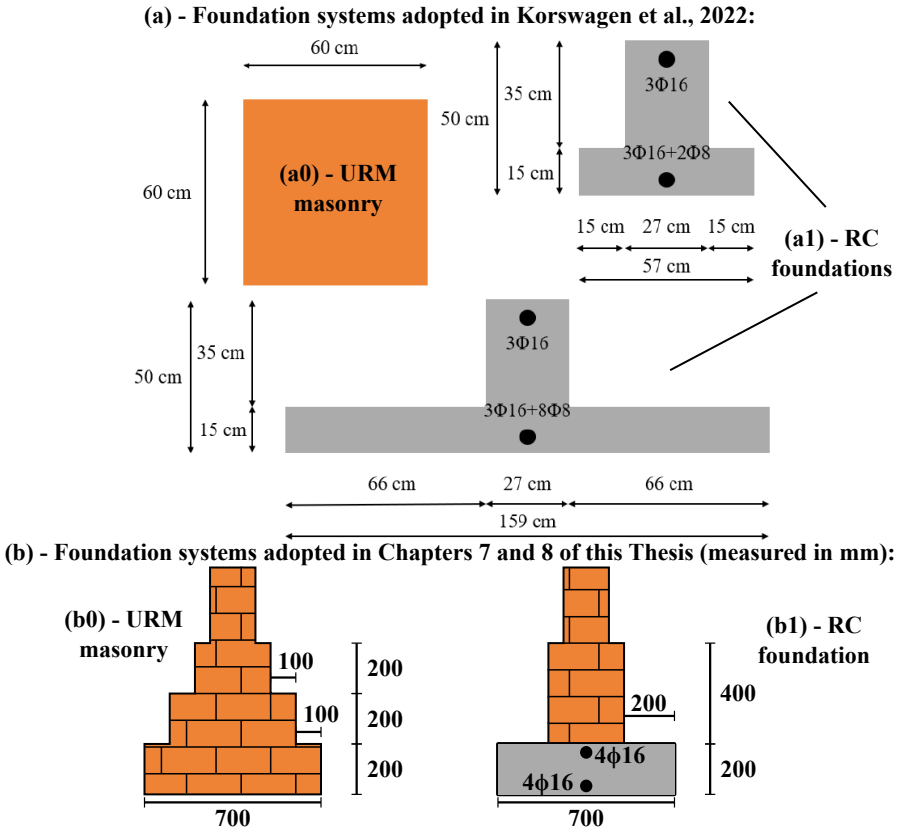

Figure 8.8: The different sets of foundation systems used in: (a) Fragility curves by Korswagen et al., 2022 [4] and (b) Chapters 7 and 8 of this thesis. The foundation systems in (b) are further detailed in Fig. 7.11 in section 7.3.2.

The relative influence of the RC foundation with T-shaped sections (for instance Fig. 5.4d) against URM foundations has been quantified in [4], in which it is stated: *"with distortions of 1/500 leading to a 20% probability of damage for clay brick walls on unreinforced (masonry) foundations or 8% for calcium-silicate walls on reinforced (concrete) foundations"*, with reference to a Ψ equal to 2.5 and for geometries with an L/H between 1 and 2. In this Chapter, an applied angular distortion equal to 1/500 leads to a 46 % probability of damage for URM foundations and 41 % for RC foundations. The differences can be therefore attributed to the different selected masonry materials, i.e., herein only clay-baked masonry is considered whereas in [4] calcium silicate masonry is included, the considered range of L/H and the selected foundation systems (Fig. 8.8). A comparison between the results of this Chapter against the fragility curves presented in [4] is further detailed in section 8.2.1.

To further examine the influence of the selected foundation systems, fragility curves are shown in Figure 8.9 for both URM and RC foundations subjected either to symmetric sagging or hogging profiles, similarly to section 8.1.3. The results highlight that the two foundation system show a similar response when subjected to symmetric hogging settlements (8.9b and d), whereas RC foundations are associated with lower probabilities of damage in sagging (8.9a and c). When the building experiences symmetric sagging profiles, tensile stresses become concentrated at the bottom of the facade. In such scenarios, the reinforcement bars in the concrete foundations can counteract these tensile stresses, thus opposing damage. Such beneficial effect is limited when the building undergoes hogging, as tensile stresses arise at the top of the facade.

8.1.5. THE INTERFACE STIFFNESS

The effect of the selected soil materials on the fragility curves in terms of applied angular distortion is shown in Figure 8.10; The results in terms of measured angular distortion are reported in Appendix C.

The selected soil properties affect the computed normal and tangential interface stiffness values at the bottom edge of the foundation system.

The results clearly show the influence of the stiffness of the building relative to the one of the interfaces, which represents the contact interaction and the behaviour of the soil: when the soil is "weak", i.e., clay soil, the facade model acts stiffer than in the case of the "strong" soil; Thus, the models are able to better withstand the imposed distortions on clay soil rather than on sand.

It should be noted, however, that in reality, high displacements and, in turn, distortions, are more likely to occur in compressible soils, such as clay, rather than sands. Thus, although a stiffer interface, which results from sand soil, represents the worst case for the numerical simulations herein presented, it is also unlikely that high values of distortion, such as imposed herein in the analyses, would occur due to settlements. Nevertheless, the inclusion of a stiffer interface results in conservative estimates, which are thus included in the analyses.

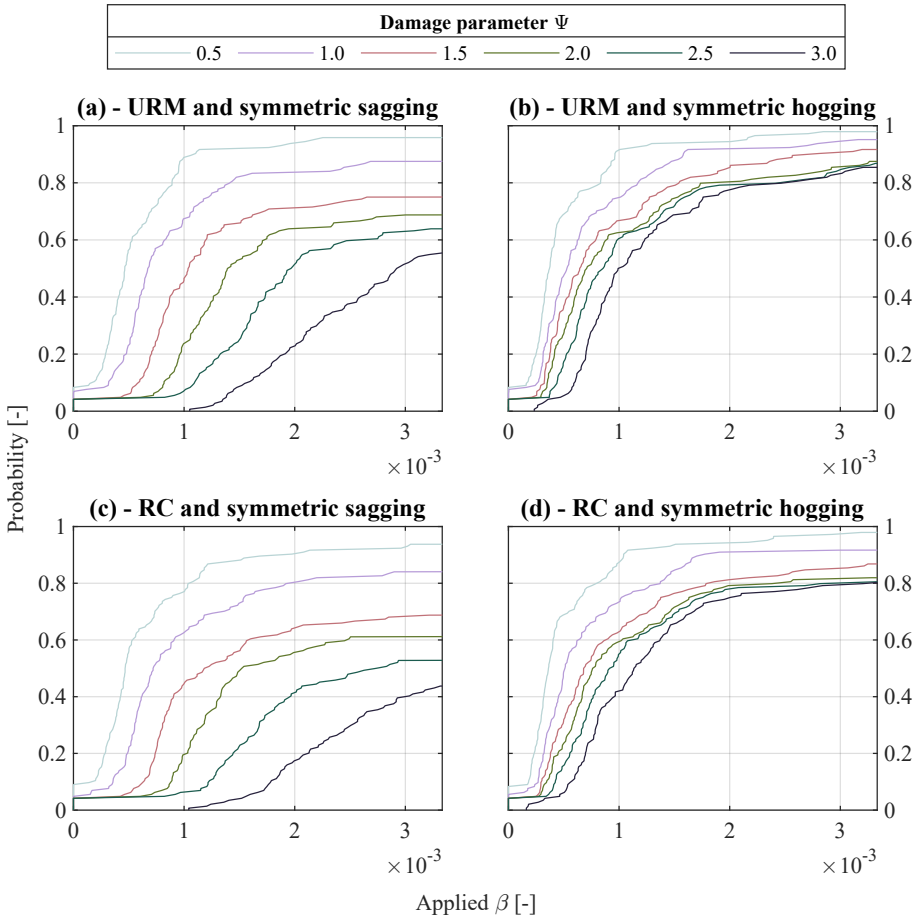

Figure 8.9: Cumulative density functions in terms of applied β for each **foundation system** subjected either to symmetric sagging and hogging settlements. Each plot presents the outcomes of 144 analyses.

8.1.6. THE EFFECT OF THE L/H RATIO

The effect of the different ranges of the length over height L/H ratio on the fragility curves is shown in Figure 8.11. The results in terms of measured angular distortion are reported in Appendix C.

In particular, the facades are divided according to L/H values into four ranges (thus, two facades in each category, see Table 7.1):

- L/H < 1.0 in Fig. 8.11a;
- 1.0 < L/H < 1.5 in Fig. 8.11b;
- 1.5 < L/H < 2.5 in Fig. 8.11c;
- L/H > 2.5 up to 4.5 in Fig. 8.11d;

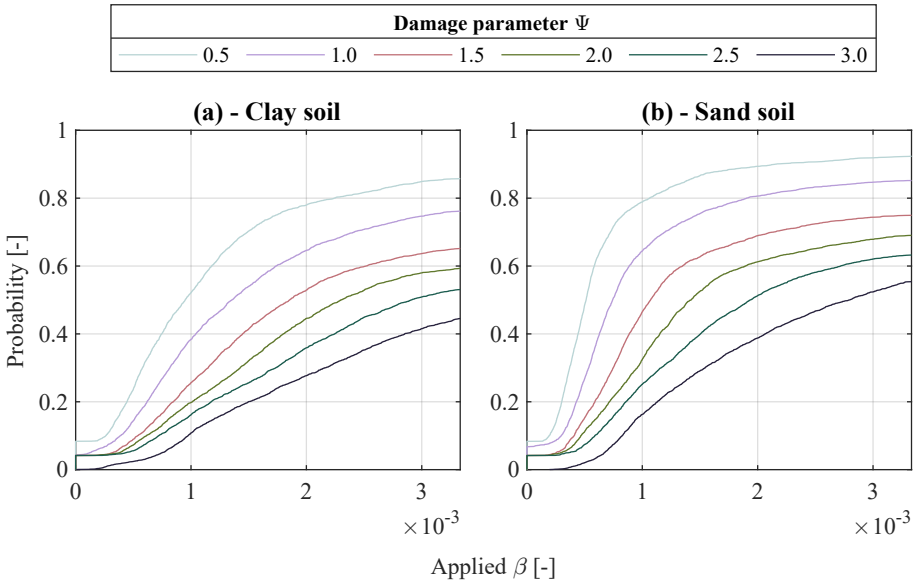

Figure 8.10: Cumulative density functions in terms of applied β for **each selected soil**. Each plot presents the outcomes of 3456 analyses.

It is possible to observe that at that for the maximum value of applied angular distortion equal to 1/300, the facades with the smallest L/H equal 1.0 (Fig. 8.11a) are the ones with the highest number of models that do not exhibit any significant damage (*i.e.*, the part of the graph above the curve Ψ equal to 0.5), progressively followed by L/H between 1.0 and 1.5 (Fig. 8.11b), L/H between 1.5 and 2.5 (Fig. 8.11c) and finally L/H higher than 2.5 (up to 4.5) in Fig. 8.11d.

Thus, the curves shown in Figure 8.11 confirm the results presented in Chapter 5, as short facades are less vulnerable than long facades. Therefore, in general, shorter facades exhibit lower probabilities of a given damage level for a given intensity of the angular distortion.

8.1.7. COMPARISON OF THE INFLUENCE OF THE DIFFERENT PARAMETERS

In Fig. 8.12, box plots are used to represent the median (black dot inside a white circle), the interquartile range (the bottom and top of each box correspond to the 25th and 75th percentiles of the sample, respectively), and the upper and lower bounds (whiskers) of the imposed angular distortion required to exhibit a Ψ value equal to 0.5. The figure focuses on the damage initiation stage (Ψ equal to 0.5), as not all models exhibit higher damage severity. The results are categorized according to the different parameters considered, providing further insight into their relative influence.

For instance, it is possible to observe that the "Weak Masonry" material is characterized by the lowest median and the smallest spread, quantified by the interquartile range, among all the masonry materials considered in the analysis. This indicates that damage initiation for the models with weak masonry occurs, on average, at lower values of applied angular

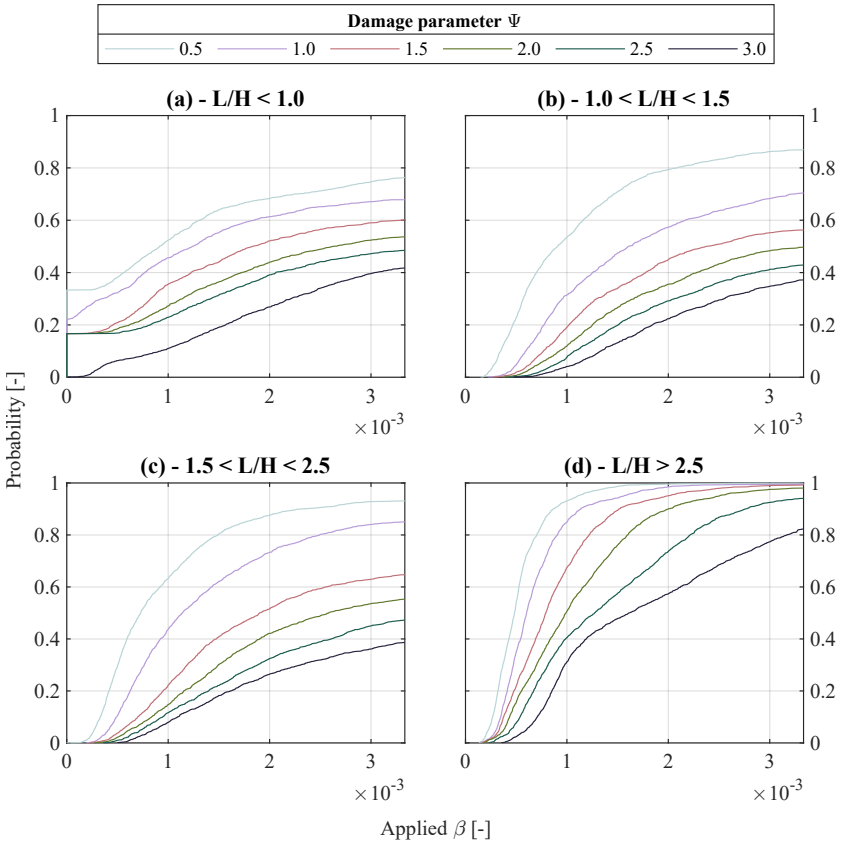

Figure 8.11: Cumulative density functions in terms of applied β for **different L/H ranges**. Each plot presents the outcomes of 1728 analyses.

distortion compared to models with "Standard" or "Strong" masonry. Additionally, the angular distortion values for "Weak" masonry are less variable compared to those for standard and strong materials. The lower variability in the results for "Weak" masonry could indicate that the behaviour of the models is strongly influenced by the weak material properties. In contrast, as the characteristics of the masonry improve with the standard and strong materials, the behaviour of the models becomes less influenced by the masonry and more influenced by other parameters. In other words, when masonry is classified as "Weak" the material itself plays a major role in causing damage, and typically, Ψ equals 0.5 for angular distortions that are closer to the median compared to "Standard" or "Strong" masonry. On the other hand, when masonry is "Strong," the variability in the occurrence of Ψ equal to 0.5 is more influenced by other factors.

A similar effect is observed for the two considered soil materials, where models on clay soil require higher values of applied angular distortion to exhibit visible damage, consistent with the results discussed in section 8.1.5.

The two selected foundation systems show similar results; however, the results are slightly better in the case of the RC foundation, as presented in section 8.1.4. Although it may

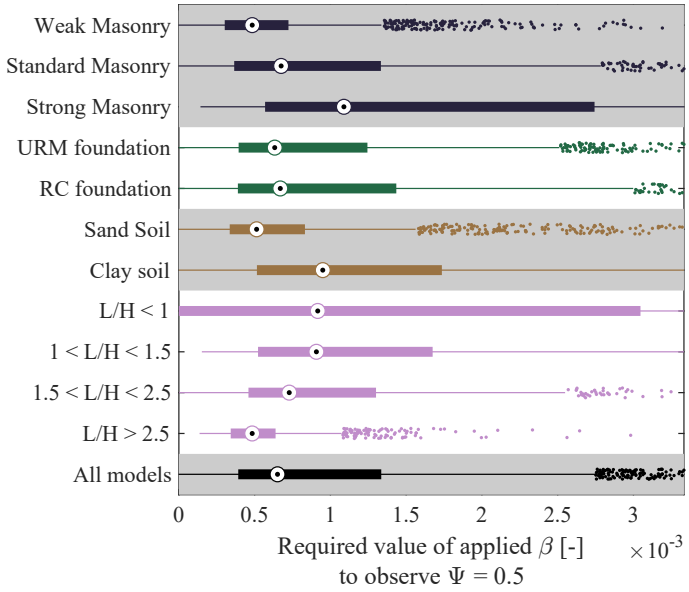

Figure 8.12: Box plot of applied angular distortion for all the models at Ψ equal to 0.5, segregated by the different selected parameters. Each box plot shows the median of each subsample as a black dot inside a white circle, and the interquartile range as a thick bar. The lines that go from the interquartile range to the left and right of each box plot represent the whiskers, which extend to the most extreme data points not considered outliers. The whisker length is equal to 1.5 times the interquartile range. Outliers are represented as dots. A wide bar conveys a large variability.

be expected that RC foundations enhance building stiffness and better prevent crack formation compared to URM foundations, the selected RC foundation has a small cross-section, offering limited structural benefit. A T-shaped RC cross-section would likely provide greater stiffness, but such designs are less recurrent in the old masonry buildings that are the focus of this analysis.

The facade models characterized by an L/H < 1 are associated with the highest median and the greatest spread of applied angular distortion values, followed by models with an L/H between 1 and 1.5, then L/H between 1.5 and 2.5, and finally L/H > 2.5. This observation confirms that squat facades, with low L/H ratios, are less vulnerable to damage than flexible facades with high L/H values.

The box plot for all models is also shown, which indirectly reflects the influence of all the 72 settlement shapes considered in the analyses.

Overall, the results shown in Fig. 8.12 align with those presented in the previous sections of this chapter.

However, it is also possible to evaluate which parameters have the greatest influence on the results. Based on the spread of the box plots, the most influential parameter is the L/H ratio, followed by the masonry material, and then the soil type, foundation, and settlement shape (indirectly shown in the box plot labelled as "All models").

The results confirm the observations regarding the influence of different building and soil features discussed in chapter 5 (section 5.3.6) of this thesis. Chapter 5 presented a

parametric study that demonstrated the impact of individual building and soil features on the models, in contrast to the probabilistic approach used in this chapter. In Chapter 5, the L/H ratio was also found to be the most influential parameter, followed by the shape of the imposed settlement, the masonry material, and then the soil and foundation. The difference in the relative influence of the settlement shape between Chapter 5 and this chapter can be explained by the fact that this chapter considers additional settlement shapes in the analysis, increasing their variability. In contrast, the settlement shapes in Chapter 5 represent only a few scenarios, which may correspond to extreme conditions for the building. Furthermore, the sensitivity analyses conducted in Chapter 5 compared the relative influence of each parameter to one reference model, whereas Fig. 8.12 compares the relative impact of each building and soil feature considering all 6912 numerical analyses. For this reason, the influence of the difference parameters is further evaluated in Figure 8.13. In this figure, the model "FA" which features "Standard Masonry," the "URM" foundation and "Sand" soil is used as the "reference case". Each boxplot in Fig. 8.13 shows the effect of the variation of a single parameter while keeping the other parameters fixed at the reference case:

- the boxplot "Settlement" considers only the variation of the 72 settlement shapes (see Fig. 7.15) of the reference model ;
- the boxplot "L/H" considers the results of the 72 settlement shapes for all the selected facades (see Fig. 7.7 and Table 7.1);
- the boxplot "Masonry" considers the results of the 72 settlement shapes for the reference model considering the three masonry materials ("Weak", "Standard" and "Strong");
- the boxplot "Foundation" considers the results of the 72 settlement shapes for the reference model and the two foundation systems ("URM" and "RC");
- the boxplot "Soil" considers the results of the 72 settlement shapes for the reference model and the two soils ("Sand" and "Clay");

Interestingly, the soil material is observed to have a similar influence on the result compared to the L/H. However, it is important to highlight that the number of analyses included in the soil material boxplot is considerably smaller than that of the L/H, which could result in a wider spread due to the limited sample size. The differences observed between the relative influence of the selected parameters compared to the results presented in Chapter 5 can be attributed both to the differences in sample size and the scenarios considered: for example, in Chapter 5, calcium silicate masonry was included among the masonry materials, whereas in this chapter, only baked-clay masonry is analyzed. Similarly, Chapter 5 considered four foundation systems and only 8 settlement shapes, while this chapter examines two foundation systems and 72 settlement shapes. Despite these differences, the results in Figures 8.12 and 8.13 consistently demonstrate that the L/H ratio is the most influential parameter.

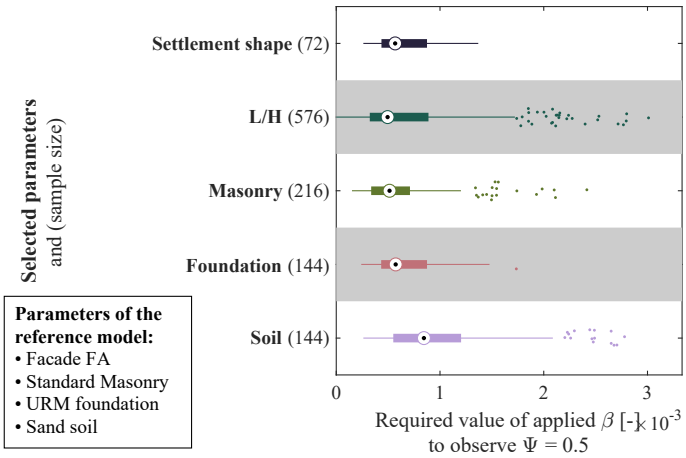

Figure 8.13: Box plot of applied angular distortion required for model FA to exhibit Ψ equal to 0.5. Each boxplot in Fig. 8.13 shows the effect of the variation of a single parameter while keeping the other parameters fixed at the reference case (Facade "FA", "Standard" Masonry, "URM" foundation and "Sand" soil). Each box plot shows the median of each subsample as a black dot inside a white circle, and the interquartile range as a black bar. The lines that go from the interquartile range to the left and right of each box plot represent the whiskers, which extend to the most extreme data points not considered outliers. The whisker length is equal to 1.5 times the interquartile range. Outliers are represented as dots.

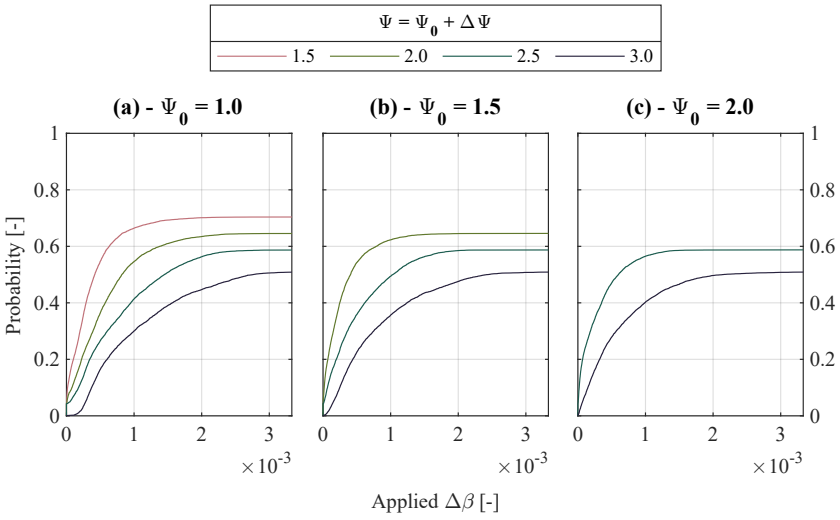

Figure 8.14: Fragility curves in terms of applied angular distortion for models with different values of initial damage Ψ_0: (a) $\Psi_0 = 1.0$, (b) $\Psi_0 = 1.5$ and (c) $\Psi_0 = 2.0$.

8.1.8. THE EFFECT OF EXISTING DAMAGE

As discussed at the beginning of section 8.1, from the results of the numerical analyses it is possible to obtain the values of the angular distortion and Ψ values for each step of the analyses. Therefore, it is possible to draw fragility curves which consider settlements imposed on facades with varying degrees of initial damage. However, the following curves

pertain specifically to damage caused solely by settlement and may not be applicable in cases where pre-existing damage results from other factors.

In Figure 8.14, fragility curves are proposed for values of the initial damage Ψ_0 which varies between 1.0 and 2.0. Therefore, the curves provide the probability of reaching a damage level Ψ, due to a damage increase $\Delta\Psi$, which is given by the increase applied angular distortion $\Delta\beta$, which is summed to the angular distortion that the model exhibits for the initial damage value Ψ_0. In other words, the curves quantify the probability of damage given an additional $\Delta\beta$ which is required to increase the damage from Ψ_0 to Ψ.

It is possible to observe that increasing the initial values Ψ_0 is associated with an increase in the probabilities of damage for a given value of $\Delta\beta$: for instance, for a $\Delta\beta$ equal to 1 ‰(1/1000), the probabilities of Ψ equal to 2.5 increase from about 40 % for Ψ_0 equal to 1.0 up to 60 % for Ψ_0 equal to 2.0.

8.2. DISCUSSION

In addition to the characteristic of the numerical analyses, discussed in section 7.5, in the analyses presented in this Chapter, each facade is subjected to vertical loads (gravity and overburden) and then 72 settlement patterns, to consider different possible combinations of the unpredictable settlements to which a building could be exposed. Accordingly, all the possible combinations of the selected material, foundation, and soil are considered. It should be noted, however, that in reality, some combinations may be less recurrent than others. For instance, the "standard" masonry material, which is retrieved from the Dutch standard, could be more recurrent than the considered variations labelled as "weak" or "strong". This points toward the development of weighted fragility curves, where weights modify the count of the models to reflect probabilistic distributions of the combination of structural and soil parameters that appear in real buildings. However, the exact distribution of such features for all the buildings in the Netherlands is unknown, and thus no hypothesis can be formulated without inevitably including uncertainties related to the subjectiveness.

6912 analyses are performed in total and used to generate numerical fragility functions. The advantage of such a large number of analyses consists in the fact that it was also possible to segregate the fragility curves based on the different selected features, to further explore the role of each parameter.

Some models already exhibit cracks before the soil distortion is applied. This is because of the gravity load and overburden which leads to some stresses in the masonry due to its low tensile strength, and thus cracking; at this stage, the flexibility of the soil also plays a role since it allows the masonry to deform under the gravity loads. This is the case in particular for the facade herein labelled as "FC". However, the analyses that exhibit cracking before the settlement phase could be fictitiously representative of pre-damaged buildings; The existing damage could be the result of shrinkage, previous settlement deformations, thermal expansion, or, as in this case, gravity loads, making walls more vulnerable.

In the following, the numerical fragility curves herein proposed are compared against the results of previous numerical and empirical studies available in the literature.

8.2.1. COMPARISON WITH NUMERICAL FRAGILITY CURVES FROM PREVIOUS STUDIES

NUMERICAL FRAGILITY CURVES BY KORSWAGEN ET AL., 2022 [4]

Previous research was carried out with numerical models to estimate the probability of damage for Dutch masonry façades subjected to settlement profiles underneath their foundations. In the study by Korswagen et al., 2022 [4], numerical fragility curves for clay facades resting on shallow foundations are proposed. Almost three thousand façade models are used for clay-brick masonry walls, including variations of the settlement patterns, soil and masonry material, similar to this study. Additionally, the selected facade geometries include variations of the opening percentage and typology. Moreover, it should be noted that the study by Korswagen et al., 2022 [4] includes the effect of transversal

walls modelled including linear elastic beams with the cross-section of one brick at the side of the facade models, similar to Chapter 5 of this thesis.

The results of the comparison are reported in figures 8.15 and 8.16 for applied and measured angular distortion values respectively.

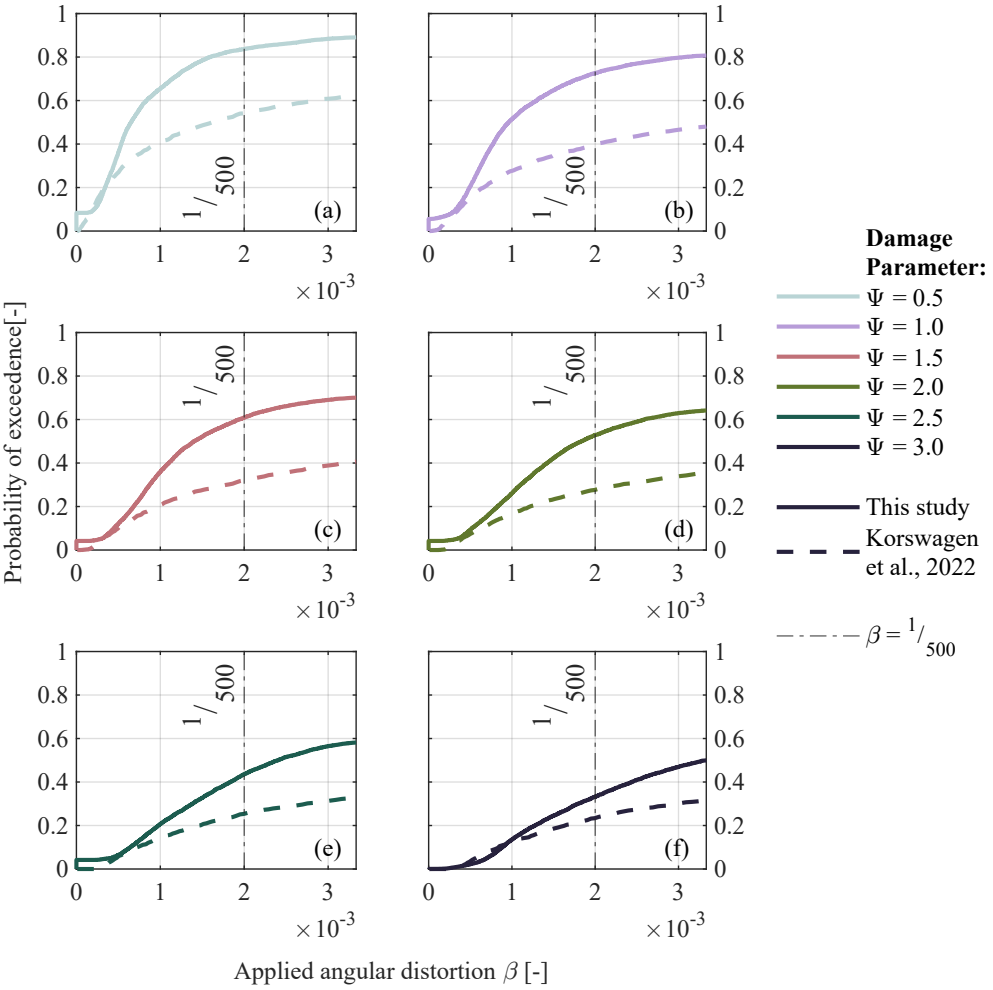

Figure 8.15: Comparison of the fragility curves in terms of **applied angular distortion** between the results of this study and the one by Korswagen et al., 2022 [4].

Interestingly, the curves proposed by [4] show lower values of the probability of damage for applied angular distortion values (Fig. 8.15), whereas higher ones for curves in terms of measured angular distortion (Fig. 8.16). Moreover, while the differences decrease with the progression of the damage in the case of applied distortions, they increase for measured distortions. The observed difference can be explained by the following factors:

- The analyses presented in [4] focus on different combinations of geometry, material

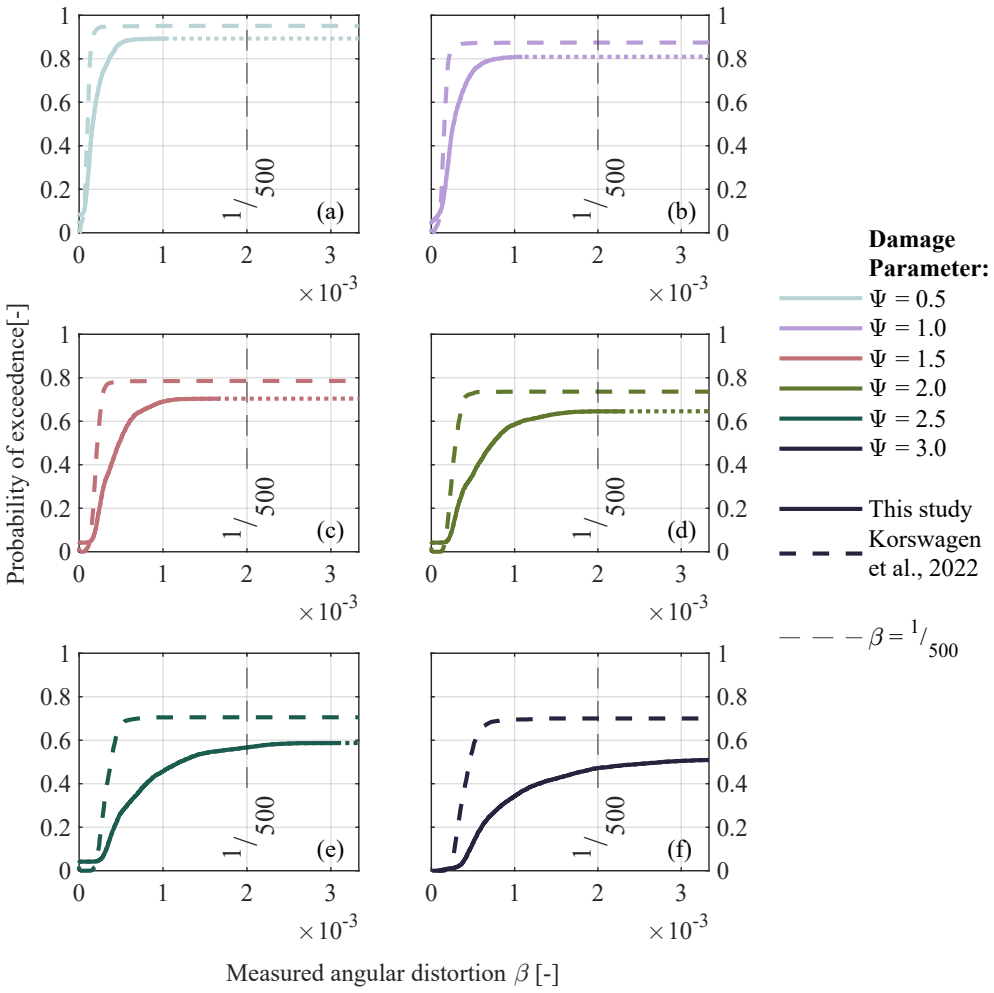

Figure 8.16: Comparison of the fragility curves in terms of **measured angular distortion** between the results of this study and the one by Korswagen et al., 2022 [4].

and settlement patterns than the analyses presented in this Chapter. In particular, the facade geometries in [4] were chosen to be representative specifically of masonry walls located predominantly in the north of the Netherlands.

- The ratio between the imposed deformation and the measured one is different due to the different modelling approaches: The analyses presented in Chapter 6 prove how the ratio between imposed and measured distortions is governed by the modelling technique. Accordingly, models that include transversal walls as lateral elements with one-brick sections, as for the analyses of [4], show lower ratios between imposed and measured distortions than the modelling approach presented herein. Incorporating the effect of transversal walls into the models, as demonstrated in Chapters 6 and 7, adds an additional influence from the weight

and stiffness of these elements.

- In the analyses conducted by [4], small variations in the measured angular distortion are required to achieve big variation in the Ψ values. Consequently, the discrepancies between the measured angular distortion values for all Ψ values are smaller compared to the curves presented in this chapter. Indeed, the curves by [4] exhibit a faster rate of progression than those proposed here.

Thus, the models by [4] require higher angular distortions to exhibit a given Ψ value, predominately due to the different scenarios and modelling techniques; Additionally, the facades by [4] exhibit a stiffer behaviour than the models presented herein, thus high variations in applied angular distortions are required to observe small variations in the measured angular distortion. While it might appear that increasing the cross-section of the transversal walls with the approach outlined in Chapters 6 and 7 and adopted here would only enhance the stiffness of the facade, it also significantly increases the weight of the lateral elements, adding extra loads to the facade and consequently affecting the deformations and cracking damage.

It should be noted, that for very low values of both applied and measured angular distortions, the curves are in good agreement, whereas increasing differences are observed up to 30% for an angular distortion equal to 1/300.

NUMERICAL FRAGILITY CURVES BY KORSWAGEN ET AL., 2024 [5]

The study reported in [5] investigates the combined effect of horizontal soil strains and angular distortions using numerical analyses for Dutch masonry facades.

The numerical models adopted in [5] are built considering the coupling between the soil and the structure. Thus, 3D models including both the soil surface and the structure are adopted, as shown in Figure 8.17. The 3D models also include the effect of transversal walls. Displacements are applied at the bottom of the soil volume, whereas horizontal strains are applied at the sides.
The results of the 3D models are used to develop fragility curves for different values of horizontal strains, which idealize their different possible scenarios. Figure 8.18 show the comparison with the fragility curves proposed in this Chapter. A good agreement is observed, as the curves are not observed to differ for more than 10 %.
The agreement of the curves from the two studies consolidates the conclusions of Chapter 6: the 2D modelling strategy employed in the numerical approach can accurately replicate the outcomes of more complex 3D analyses. Additionally, applying the settlements at the non-linear interface at the foundation's base in semi-coupled models serves as a valid alternative to more complex coupled analyses.

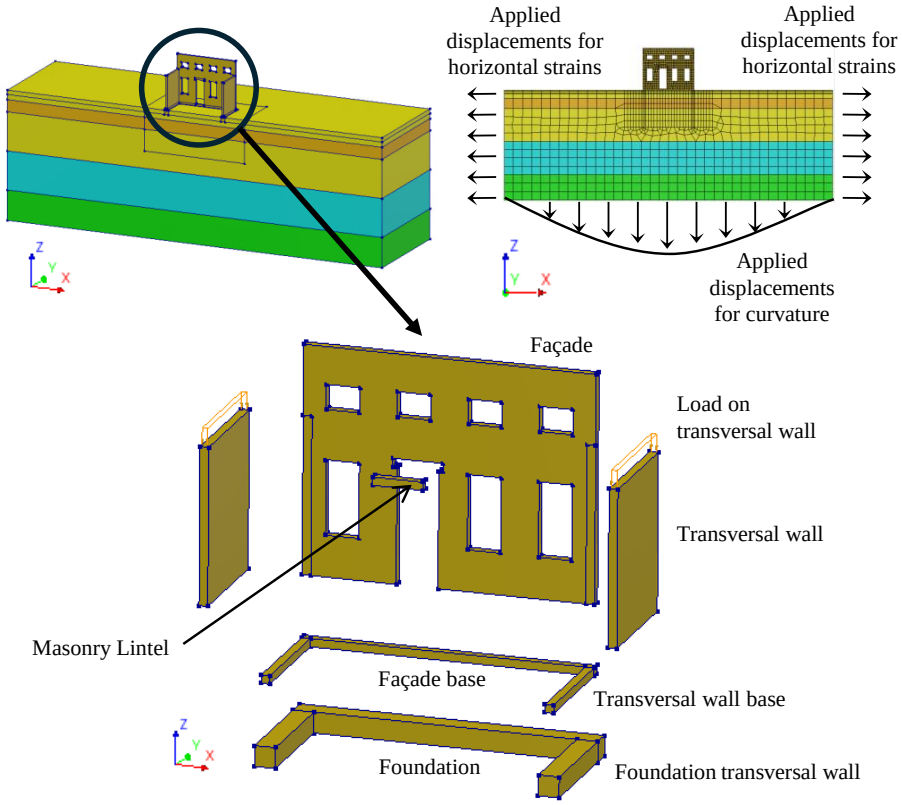

Figure 8.17: An example of the 3D coupled models adopted in Korswagen et al., 2024 [5]. Displacements are applied at the bottom of the soil volume, and their intensity is quantified by the angular distortion. Horizontal strains are applied at the side of the soil volume. The models make use of symmetry, and thus half of the domain is represented.

8.2.2. COMPARISON WITH EXISTING EMPIRICAL FRAGILITY CURVES

The proposed fragility functions obtained from the numerical analyses herein presented are compared with curves obtained from the observation of existing structures from different sources.

It should be noted that neither the curves from empirical studies, based only on a few selected buildings nor the models should be regarded as portraying reality best. When comparing the results from models with empirical observations, a few aspects should be considered as sources of differences and uncertainties:

- Measuring the distortion from real walls may lead to higher displacements and distortions since points are gathered at fixed, limited intervals; this may cause overestimation of the values of the distortion for which damage appears. This effect enhances the difference between empirical curves and numerical ones.

- The location or height of the walls where the measurements are taken could influ-

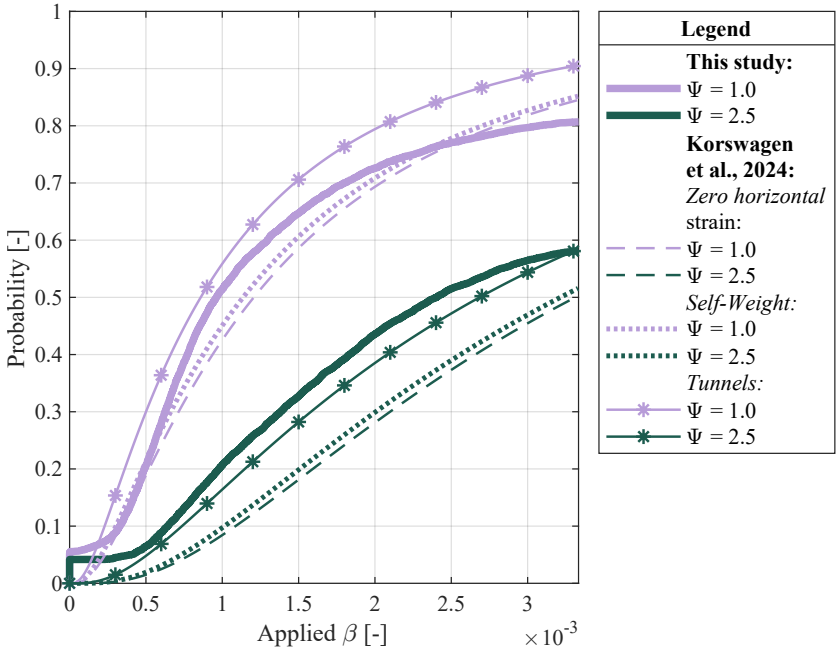

Figure 8.18: Comparison of the fragility curves in terms of **applied angular distortion** between the results of this study and the one by Korswagen et al., 2024 [5]. The fragility curves by [5] are segregated by increasing values of horizontal strains corresponding to different settlement-scenarios.

ence the values of the distortions.

- Empirical datasets may represent convenience samples rather than random samples. This is related to the fact that detailed information on both the displacements and the damage to buildings are not typically available for a large number of cases, and thus, the samples necessarily contain the cases readily available to the researchers which are not necessarily randomly sampled.

- Moreover, empirical datasets of tens or hundreds of cases may have a limited capability to represent the behaviour of the entire population of an area or a country (typically millions of buildings).

- Related to the sampling technique, empirical datasets may be biased since the inspections have been carried out on buildings that displayed damage, but other buildings, exhibiting high distortion values but no damage, for example, may not have been not reported.

- Time may play a huge contribution in the development of damage on buildings: deformations may take place slowly over the span of decades and the (masonry) buildings may be able to accommodate the ground deformations without displaying cracks due to creep effects. Moreover, some cracks could seal due to autogenous healing phenomena of the cement or lime in the mortar.

- In existing structures, various drivers can exert simultaneous effects on buildings. Therefore, damage could also be caused by other actions, such as thermal or chemical actions, accidental loads, storms and more, as outlined in section 2.2.2.

- Ground movements caused by subsidence that impact existing structures can be characterized not only by vertical components but also by horizontal ones. These induced horizontal strains could consequently affect the response of the structures.

- Time effects are not included in the numerical analyses herein proposed, due to a lack of available detailed information in the state-of-the-art. Therefore, material creep and relaxation could allow the models to accommodate higher distortions before damage initiate. This effect would, in turn, reduce the differences between empirical and numerical curves.

- In the numerical analyses, material properties have not been calibrated against large and old masonry samples which could exhibit a more flexible overall behaviour than what has been modelled. This would also shift the measured distortion closer to the applied soil distortions (thus, to higher values).

- The numerical analyses herein presented use the facades as a proxy for the buildings: this approach assumes that the damage assessed in the 2D model describes the damage severity of the entire building. However, in real structures, settlement patterns may cause damage localized in specific walls or parts of the structure. Consequently, the overall damage to the structures may be less severe than what is observed in models. This effect would lead to lower probabilities of damage for a given settlement in empirical datasets compared to numerical analyses.

Moreover, It should be noted that some literature sources refer to settlements and distortions of buildings without clarifying if they were measured on the buildings or the surrounding soil.

EMPIRICAL DATASET FROM ZHANG AND NG, 2005 [6]

A dataset of a sample of 300 buildings has been collected by [6]. The dataset included different building typologies, such as offices, office blocks, flats, hotels and hospitals, and mill types, such as warehouses and factories, and their deformation. Both steel and reinforced concrete frame structures and structures with load-bearing walls were considered by the authors, resting on either sand, clay or alluvium. The authors distinguished the buildings into shallow and deep foundations. The subset of buildings on shallow foundations for which it was possible to retrieve the angular distortion contains 153 cases. The data of the angular distortion available in [6] are shown in Table 8.1.
The Authors distinguished "tolerable" and "intolerable" cases, without clarifying what damage states these two terms refer to. Based on other literature sources, the "intolerable" cases refer to displacements and distortion affecting the functionality/safety and appearance of buildings [7], [8]. In some cases, the "intolerable" curves have been compared to damage cases involving the complete damage of the structure, which may not be repairable for economical or practical purposes [8], [9].

Table 8.1: Summary of the angular distortion for buildings on shallow foundations, retrieved from [6].

Angular distortion		0 – 0.001	0.0011 – 0.002	0.0021 – 0.003	0.0031 – 0.004	0.0041 – 0.005	0.0051 – 0.006	0.0061 – 0.008	0.0081 – 0.010	0.011 – 0.050	0.051 – 0.100
Shallow foundation	Tolerable Cases	18	21	14	7	2	1	1	0	0	0
	Intolerable cases	0	4	7	17	6	7	9	19	18	2

Similarly, the "tolerable" limit is compared with fragility curves that refer to crack widths of 1.0 mm [8], corresponding to Ψ values ranging between 1.5 and 2.5 in this study. In the "Conclusions" section of [6], it is stated that "The probability distribution of the limiting tolerable displacement can also be implemented directly in a fully reliability-based serviceability criterion". Thus, "tolerable" cases could have been used to determine the limits for "serviceability" damage, corresponding to cracks wider than 5 mm [10].

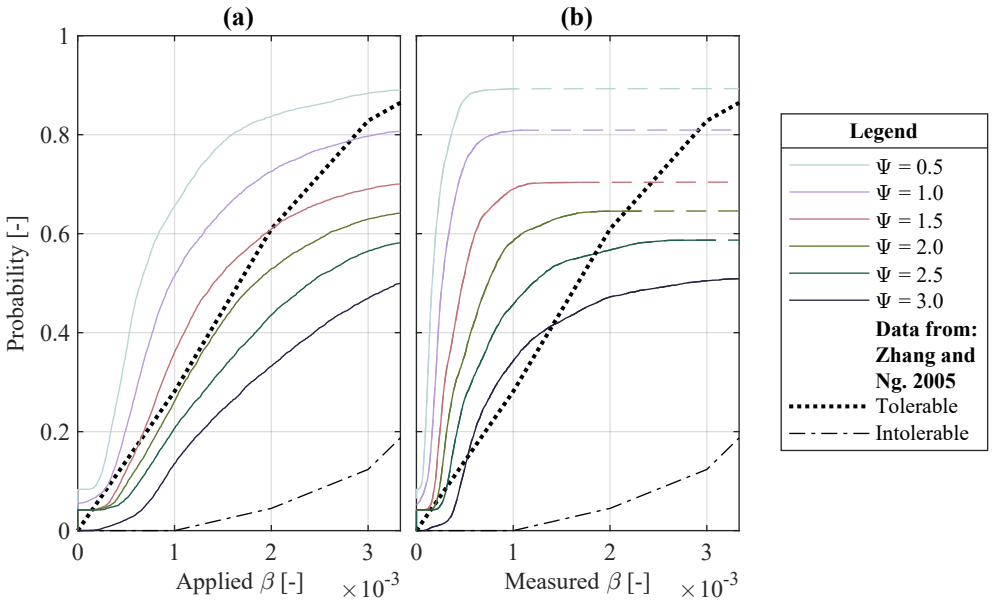

Figure 8.19: Comparison of the proposed fragility curves in terms of (a) applied and (b) measured angular distortion with the ones of Zhang and Ng, 2005 [6].

Due to the subjectiveness of the interpretation of the "tolerable" and "intolerable" curves, in this study, they are regarded as "light damage" (corresponding to $\Psi < 3$) and "moderate to severe damage" (corresponding to $\Psi > 3$) for simplicity. The data reported in Table 8.1 are herein used to retrieve the cumulative density functions for each distribution individually (*i.e.*, "tolerable" or "intolerable") and the curves are shown in Figure 8.19 against the numerical curves proposed in this Chapter. It is not clear if the distortion values reported were measured on the structures in all cases or derived from soil measures.

Therefore, Figure 8.19 show the comparison for both applied and measured distortions computed from this study.

Thus, a good match is observed between the "tolerable" function based on the data from [6] and the curves proposed in this study. The curve of "intolerable" cases has a slower growth rate, which can be explained by the fact that it may refer to cases for which the equivalent Ψ would be way higher than 3.

Compared to the empirical curves, the numerical fragility functions herein proposed are capable of assessing the probability of damage even for low values of the angular distortion, which are difficult to observe and measure in real structures.

Considering the variety of building typologies and structural layouts in the data from [6], the comparison shown in Figure 8.19 is considered adequate.

EMPIRICALLY-BASED FRAGILITY CURVES BY PEDUTO ET AL., 2019 [7]

When the tilt of the building is low, the values of the rotation θ may not be dissimilar from the ones of the angular distortion β. The correlation between the rotation θ and the angular distortion β is also confirmed in the literature (*i.e.* [11]). For this reason, it is possible to compare the numerical fragility curves in terms of measured β proposed in this study with empirically-based curves in terms of θ proposed by [7], based on a sample of 180 Dutch masonry buildings on shallow foundations. Moreover, the curves from [7] refer to distortion values computed from space-borne measurements over an interval of 5 years; Thus, it is unlikely that high tilt values will be measured over such a short time interval.

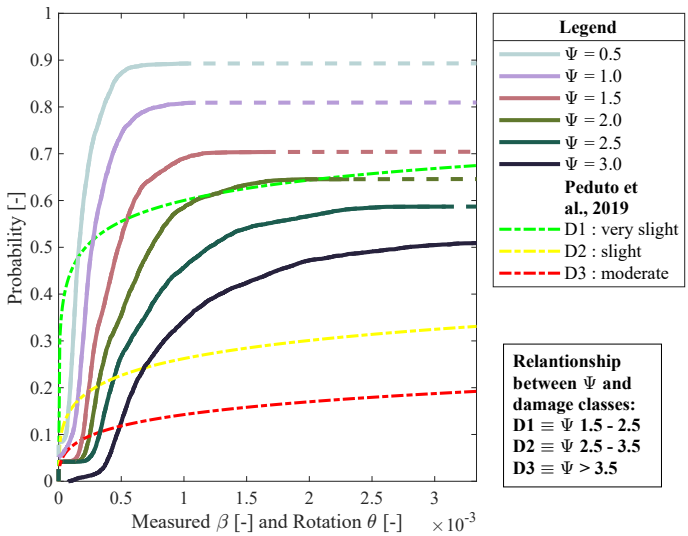

Figure 8.20: Comparison of the proposed fragility curves in terms of measured angular distortion with the ones of Peduto et al., 2019 [7].

The comparison is shown in Figure 8.20. In particular, the relationship between damage

classes adopted by [7] and the Ψ values is the following:

- D1 = very slight, crack width up to 1 mm; corresponding Ψ values between 1.5 and 2.5;
- D2 = slight, crack width up to 5 mm; corresponding Ψ values between 2.5 and 3.5;
- D3 = moderate, crack width up to 15 mm; corresponding Ψ > 3.5;

As acknowledged by the Authors, the shapes of the curves in terms of θ tend to be convex upward (*i.e.*, the existence of an inflection point cannot be clearly recognized), mainly develop horizontally, and the probability of reaching or exceeding a given damage severity level can attain the unit value for unrealistic values of θ [7]; Such limitations may be a consequence of the method used to develop the curves. Moreover, the space-borne acquisitions only cover a period of about 5 years, whereas the damage to the houses may have accumulated over much longer periods, which translates to an overestimation of the damage related to the measured parameter.

Nevertheless, the comparison between the two sets of curves shows a good agreement for each damage class and the considered range of Ψ values. For instance, for measured angular distortion values higher than 1/1000, the curves "D1" and Ψ = 2.0 are in good agreement, whereas "D2" and "D3" show lower probabilities as they reflect damage states worse than the ones considered in this study, which is limited to "light damage", *i.e.*, Ψ values lower than 3.

EMPIRICALLY-BASED FRAGILITY CURVES PRESENTED IN CHAPTER 4

Figure 8.21 shows the comparison between the numerical fragility curves herein proposed and the empirical curves from Chapter 4 of this thesis. Big differences are observed between the two sets of curves. Many of the reasons for such big differences are introduced at the beginning of the section 8.2.2. Among the most significant factors expected to accentuate the differences between the curves are:

- facade models are used as a proxy for the behaviour of the entire building in the numerical analyses, whereas the damage of the entire building could be lower due to 3D effects;
- The time-dependency of both the development of the settlements and the visco-elastic response of the masonry structure is not depicted in the model.
- Moreover, the sample presented in chapter 4 may not be random and thus, lack statistical significance.
- The classification of damage in empirical cases is performed using a subjective approach that differs from the more objective method used in the numerical analyses in this chapter. Consequently, the subjectivity of the assessment and the detectability of the damage could play a significant role in increasing the differences.

Table 8.2 uniforms the damage classification systems adopted for the empirical cases (Chapter 4) and for the numerical analyses (Chapters 5, 6, 7 and 8) of this thesis. To

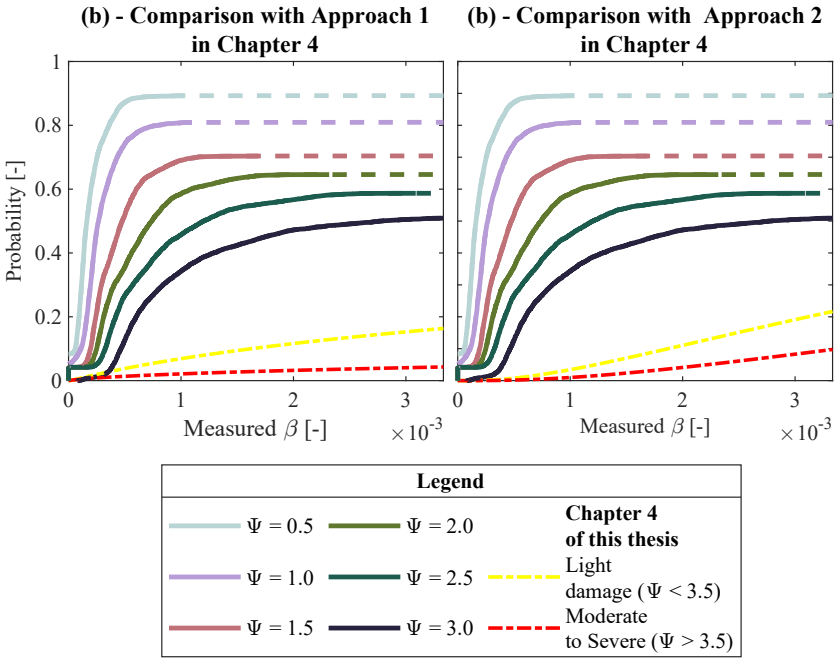

Figure 8.21: Comparison of the proposed fragility curves in terms of measured angular distortion with the proposed in Chapter 4 of this thesis.

further compare the two classifications, the numerical fragility curves can be redrawn using the damage classification adopted in Chapter 4. Specifically, cases with Ψ values between 1.5 and 3.0 can be categorized as "light damage" (Table 8.2). Accordingly, Fig. 8.22 shows the numerical fragility curves grouped as "light damage" compared against the empirical curves from Chapter 4. The differences between the curves in terms of "light damage" are smaller than in the case of the curves segregated by Ψ (Fig. 8.21). Nevertheless, the differences are still significant. An additional curve is plotted as a black dashed line, showing the only results for facade "FD", which was observed to be the least vulnerable to the imposed settlement deformations (Figure 8.1), as it is characterized by the lowest L/H ratio. Interestingly, the curve of the facade "FD" shows a better agreement with the empirical curves. This observation indicates that the numerical fragility curves herein proposed yield more conservative estimates of the probability of damage than the empirical curves.

8.2.3. COMPARISON WITH AVAILABLE LIMIT VALUES FROM CODES AND STANDARDS

In Chapter 5, it was briefly discussed how the limiting values of the angular distortion available in (inter)national codes could be too optimistic compared to the results of the FE analyses. This section further explores this topic.
As discussed in section 8.2.2, the numerical fragility curves tend to be conservative compared to empirically-based curves, *i.e.*, higher probability of damage for a given β; However, the comparison with other literature sources suggest that the difference may

Table 8.2: Damage scale with different classifications of visible damage based on ease of repair and the crack width adopted in this thesis: Category of damage (polka dotted) retrieved from [12]; Damage classification system (white background) from [13], [14]; Damage group from Chapter (dark grey filling and white text) 4; Damage levels and parameter of damage from [15].

Category of damage	Damage classification system:			Chapter 4 of this thesis:	Chapter 5, 6, 7 and 8 of this thesis:	
	Damage class	Approximate crack width	Description of typical damage (and ease of repair)	Damage group:	Damage Level	Parameter of damage
Aesthetic damage	No Damage	Imperceptible cracks	-	No Damage	DL0	$\Psi < 1$
	Negligible	up to 0.1 mm	Hairline cracks of less then about 0.1 mm are classed as negligible		DL1	$1 \leq \Psi < 1.5$
	Very slight	up to 1 mm	Fine cracks which can easily be treated during normal decoration.	Light Damage	DL2	$1.5 \leq \Psi < 2.5$
	Slight	up to 5 mm	Cracks easily filled. Re-decoration probably required. Some re-pointing may be required.		DL3	$2.5 \leq \Psi < 3.5$
Functional damage, affecting serviceability	Moderate	5 to 15 mm	The cracks require some opening up and can be patched by a mason. Re-current cracks can be masked by suitable linings. Repointing of external brickwork and possibly a small amount of brickwork to be replaced.	Moderate to severe damage	DL4 and above	$\Psi \geq 3.5$
	Severe	15 to 25 mm	Extensive repair work involving breaking-out and replacing sections of walls, especially over doors and windows.			
Structural damage, affecting stability	Very Severe	Higher than 25 mm	This requires a major repair job involving partial or complete re-building.			

be limited. Thus, it is possible to retrieve the probability of damage of each Ψ value for different limit values of the measured angular distortion available in the literature [14], [16], [17]. The computed probabilities are reported in Table 8.3 and 8.4 for applied and measured distortion respectively.

The results indicate that all the limit values correspond to probabilities of $\Psi = 1.5$ (thus the occurrence of visible damage with cracks wider than 0.1 mm) ranging between 5 and 70 % for applied β and 21 and 70 % for measured β. Additionally, the probabilities for $\Psi = 3.0$ (cracks up to 5 mm) range between 0 and 50 for applied β whereas 1 and 51 % for measured β.

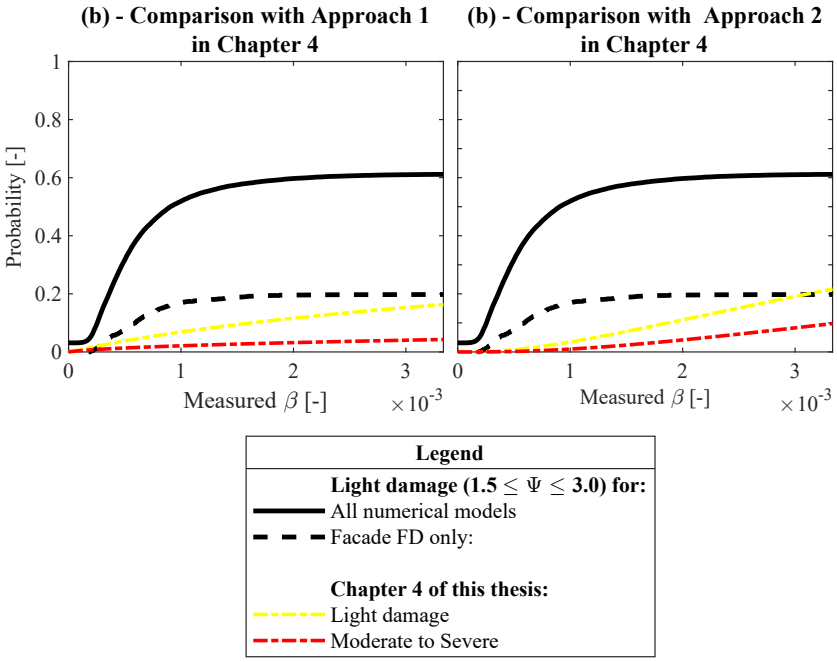

Figure 8.22: Comparison of the fragility curves grouped as "light damage" in terms of measured angular distortion with the curves proposed in Chapter 4 of this thesis.

In general, only the lower limits reported in the Eurocode for both sagging and hogging (1/2000 and 1/4000) prevent the occurrence of cracks up to 5 mm according to the results of this study. Nevertheless, when the measured distortion on the building is equal to 1/4000 (lower limit for hogging), a probability of 21 % of $\Psi = 1.5$ is observed. This could be an indication that some buildings would exhibit visible damage even for very low values of angular distortions. Given the wide variability of buildings and their features, none of the considered limit values seem to exclude the occurrence of visible damage (cracks between 0.1 - 1.0 mm) if they are intended to refer to the distortion measured on the building.

In the Eurocode [16] it is reported that "*A maximum relative rotation of 1/500 is acceptable for many structures*". In this study, a measured angular distortion equal to 1/500 corresponds to a probability of $\Psi = 3.0$ (cracks up to 5 mm) equal to 47 %. Thus, one building out of two may exhibit damage which may require repointing works, or even replacing some bricks, depending on the number of cracks and their location [18]. Nevertheless, at this damage intensity, such cracks in structural walls may remain without compromising the safety of the structure, granting some validity to the threshold proposed by the guidelines.

It should be pointed out, however, that visible damage may be unpreventable in existing structures, given the fact that it seems to occur at very low values of measured angular distortion, which could not only result from settlements, but also from other factors, such as the thermal expansion of the buildings, or vertical and horizontal loads. This observation also points out that it may be difficult to accurately depict the causality

Table 8.3: Overview of the available literature limit values and their corresponding probability of damage for each Ψ value, based on the numerical fragility curves in terms of **applied β presented in this Chapter.**

Reference	Values [‰]	Ratio [1/$\beta_{appl.}^{-1}$]	Description	Probability [%] retrieved from the numerical fragility curves presented in this thesis for each value of Ψ					
				Ψ = 0.5	Ψ = 1.0	Ψ = 1.5	Ψ = 2.0	Ψ = 2.5	Ψ = 3.0
Eurocode* and Dutch norm**	0.5 to 3.3	1/2000 to 1/300	Sagging (serviceability limit state)	36	21	12	10	6	2
				88	80	70	64	58	50
	0.25 to 1.7	1/4000 to 1/600	Hogging (serviceability limit state)	12	8	5	5	4	0
				81	68	56	47	37	28
Boscardin and Cording, 1989***	1.0	1/1000	Very slight damage (self weight)	65	51	36	26	21	14
	1.5	1/667	Slight damage (self weight)	79	65	52	43	33	25
	3.3	1/300	Moderate to severe damage (self weight)	88	80	70	64	58	50

* Eurocode [16]

** Dutch norm [17]

*** Boscardin and Cording, 1989 [14]

between subsidence and damage to buildings, as low distortions may be difficult to measure and could be the symptom of different actions.

Table 8.4: Overview of the available literature limit values and their corresponding probability of damage for each Ψ value, based on the numerical fragility curves in terms of **measured β presented in this Chapter.**

Reference	Values [‰]	Ratio [1/$\beta_{meas.}^{-1}$]	Description	Probability [%] retrieved from the numerical fragility curves presented in this thesis for each value of Ψ					
				Ψ = 0.5	Ψ = 1.0	Ψ = 1.5	Ψ = 2.0	Ψ = 2.5	Ψ = 3.0
Eurocode* and Dutch norm**	0.5 to 3.3	1/2000 to 1/300	Sagging (serviceability limit state)	87	74	51	35	27	12
				90	80	70	65	58	51
	0.25 to 1.7	1/4000 to 1/600	Hogging (serviceability limit state)	70	47	21	10	5	1
				90	80	70	64	55	44
Boscardin and Cording, 1989***	1.0	1/1000	Very slight damage (self weight)	89	80	69	58	46	35
	1.5	1/667	Slight damage (self weight)	90	80	70	63	54	43
	3.3	1/300	Moderate to severe damage (self weight)	90	80	70	65	58	51

* Eurocode [16]

** Dutch norm [17]

*** Boscardin and Cording, 1989 [14]

8.3. CONCLUSIONS

In this Chapter, numerical analyses are used to develop fragility curves for baked clay masonry buildings on shallow foundations built before 1970.

Based on the results of all 6912 numerical simulations, which include 8 variations of the facade geometry, 2 foundation systems, 3 masonry and 2 soil materials and imposed 72 settlement shapes, it was possible to observe the relative influence of the difference considered parameters. Accordingly:

- The results of the models show how the parameters that influence the most the damage initiation of the model is the length over height (L/H) ratio of the selected facades, followed by the masonry material, the soil, foundation systems and the shape of the imposed settlement actions.

Two sets of fragility curves are produced, with the goal of damage assessment over wide areas:

- Curves in terms of **applied angular distortion**, which may be suitable to assess and predict the damage to buildings when only the ground deformations are known, for instance via modelling of measurements.

- Curves in terms of **measured angular distortion**, for damage assessment procedures in which the deformations of buildings are known.

The curves, which focus on the occurrence of light damage, are compared against previous studies. Thus, it is observed that:

- Differences are observed between the results of models and empirical cases. This points toward the urgent necessity of experimental campaigns, empirical observation and monitoring data to validate and calibrate future numerical analyses.

- For the purpose of additional studies that include realistic scenarios of the existing buildings' features, openly accessible datasets containing information on the number of openings and their location on walls, the construction material building and the type of foundation of each building are required.

- Based on the results of the finite element models, the limit values available in the state-of-the-art are not observed to prevent the occurrence of visible damage, *i.e.*, cracks between 0.1 - 1 mm.

- For a value of the angular distortion measured on the building equal to 2 ‰(or 1/500), the analyses indicated that 1 out of 2 facades might exhibit cracks up to 5 mm.

- In some cases, low values of the angular distortions could be measured on the buildings due to actions different than settlements, such as vertical loads; The buildings, in turn, may already exhibit light damage.

- Based on the outcome of the numerical analyses, it can be pointed out that the occurrence of light damage to existing structures due to settlements may not be prevented, as damage could occur even for low values of angular distortions, due to possible combinations of poor construction materials or weak soil, which enhance the probability of damage.

BIBLIOGRAPHY OF CHAPTER 8

[1] B. Huang, S. Chen, W. Lu, and K. M. Mosalam, "Seismic demand and experimental evaluation of the nonstructural building curtain wall: A review," *Soil Dynamics and Earthquake Engineering*, vol. 100, pp. 16–33, 2017.

[2] D. N. Grant, J. Dennis, R. Sturt, *et al.*, "Explicit modelling of collapse for dutch unreinforced masonry building typology fragility functions," *Bulletin of Earthquake Engineering*, vol. 19, pp. 6497–6519, 2021.

[3] J. B. Burland and C. Wroth, "Settlement of buildings and associated damage," Tech. Rep., 1975.

[4] P. Korswagen, M. Longo, J. Rots, and A. Prosperi, "Supporting analyses to determine probability of damage and fragility curves due to indirect subsidence effects," *Delft University of Technology. Report*, Final Version 2, October 3, 2022.

[5] P. Korswagen, M. Longo, and J. Rots, "Research into the combined effects of soil strains, soil curvatures and earthquake vibrations from multiple mining activities on damage in masonry," *Delft University of Technology. Report*, 2024.

[6] L. Zhang and A. Ng, "Probabilistic limiting tolerable displacements for serviceability limit state design of foundations," *Geotechnique*, vol. 55, no. 2, pp. 151–161, 2005.

[7] D. Peduto, M. Korff, G. Nicodemo, A. Marchese, and S. Ferlisi, "Empirical fragility curves for settlement-affected buildings: Analysis of different intensity parameters for seven hundred masonry buildings in the netherlands," *Soils and Foundations*, vol. 59, no. 2, pp. 380–397, 2019.

[8] O. Mavrouli, S. Fotopoulou, K. Pitilakis, *et al.*, "Vulnerability assessment for reinforced concrete buildings exposed to landslides," *Bulletin of Engineering Geology and the Environment*, vol. 73, pp. 265–289, 2014.

[9] C. Negulescu and E. Foerster, "Parametric studies and quantitative assessment of the vulnerability of a rc frame building exposed to differential settlements," *Natural Hazards and Earth System Sciences*, vol. 10, no. 9, pp. 1781–1792, 2010.

[10] W. Rankin, "Ground movements resulting from urban tunnelling: Predictions and effects," *Geological Society, London, Engineering Geology Special Publications*, vol. 5, no. 1, pp. 79–92, 1988.

[11] P. Wikby, E. Haaf, A. Abed, L. Rosén, J. Sundell, and M. Karstunen, "A grid-based methodology for the assessment of time-dependent building damage at large scale," *Tunnelling and Underground Space Technology*, vol. 149, p. 105 788, 2024.

[12] G. Giardina, "Modelling of settlement induced building damage," 2013.

[13] J. B. Burland, B. B. Broms, and V. F. De Mello, "Behaviour of foundations and structures," 1978.

[14] M. D. Boscardin and E. J. Cording, "Building response to excavation-induced settlement," *Journal of Geotechnical Engineering*, vol. 115, no. 1, pp. 1–21, 1989.

[15] P. A. Korswagen, M. Longo, E. Meulman, and J. G. Rots, "Crack initiation and propagation in unreinforced masonry specimens subjected to repeated in-plane loading during light damage," *Bulletin of Earthquake Engineering*, vol. 17, pp. 4651–4687, 2019.

[16] B. EN *et al.*, "Eurocode 7: Geotechnical design-part 1: General rules," *British Standards Institution*, 2004.

[17] NEN9997-1:2023Ontw.nl, *Geotechnisch ontwerp van constructies - deel 1: Algemene regels (geotechnical design of structures - part 1: General rules)*, 2023.

[18] J. B. Burland, B. B. Broms, and V. F. De Mello, "Behaviour of foundations and structures," 1978.

CHAPTER 9
CONCLUSIONS AND OUTLOOK

CHAPTER 9: TABLE OF CONTENTS

9.1 Conclusions 255
9.1.1 Returning to the research questions 255

9.2 Relevance and contributions 259
9.2.1 Scientific contributions 259
9.2.2 Societal relevance 259
9.2.3 Utilisation: Integrating the results into a Systematic Regional Scale Damage Assessment 260

9.3 Recommendations for Further research 263
9.3.1 Soil heterogeneity: combining the lithological heterogeneity with the spatial variability of the material properties . 263
9.3.2 The influence of the horizontal soil strains 264
9.3.3 Time-dependent behaviour of masonry 264
9.3.4 Scale effect on the engineering properties of masonry . . 264
9.3.5 Integrating of laboratory tests, monitoring data, measurements and numerical analyses 265
9.3.6 Modelling approaches, numerical robustness and constitutive models 265
9.3.7 Cyclic ground movements: settlement and uplift 266
9.3.8 The effect of existing damage and simultaneous actions . 267

Bibliography of Chapter 9 272

This thesis aims to contribute to the insight required for risk assessment analyses at different scales (*i.e.*, single structure, city, region, country). The analyses combined geotechnical and structural engineering into empirical and numerical analyses.

This final Chapter gathers the main findings of the PhD research presented in this thesis, discussing their implications and limitations, while recommending possible future research directions.

This Chapter begins with section 9.1, which consolidates the findings presented in detail in the previous Chapters while answering the research questions. Section 9.2 reflects on the scientific and societal relevance of this PhD research, whereas a discussion of how the results of this study contribute to systematic regional assessments of damage to buildings exposed to subsidence is presented in section 9.2.3. Finally, directions for future research are suggested in section 9.3.

9.1. CONCLUSIONS

9.1.1. RETURNING TO THE RESEARCH QUESTIONS

In Section 1.3 the principal aim has been decomposed into sub-questions. In the following, each sub-question is addressed:

- ***What is the influence of the variability of the soil on the occurrence of differential settlements at the building scale?***

  The influence of soil variability on the occurrence of differential settlements at the building scale has been evaluated through numerical simulations. The analyses employed high-resolution models to analyze in-situ lithological heterogeneity and compare results with national-resolution models. The analyses included the influence of various loading and hydrostatic conditions.

  A good agreement is observed between the results of the two independent datasets at high (in-situ level) and low (country level) resolution. In particular, the distribution of the settlements computed using the models based on the two datasets agree in terms of mean, spread and shape.

  Furthermore, the analyses reveal that the spatial variability of the lithological variations in the soil stratigraphy is observed to have the same order of magnitude as the one reported in previous studies for the material properties of soil layers. The values of the correlation length range between about 1 and 10 meters, matching the extension of typical structures, *e.g.*, houses, roads and embankments. Therefore, soil heterogeneity could contribute with the same relevance in augmenting the differential settlements at the scale of structures.

  Overall, the findings highlight the importance of accurately capturing the effects of lithological heterogeneity on ground movements. These insights provide a foundational understanding for further assessments aimed at evaluating the combined impact of lithological variability and other uncertainties on buildings in subsiding regions.

Thus, the influence of soil lithological heterogeneity, measured by the scale of fluctuation in soil strata thicknesses, can:

(i) Lead to significant variation in the thickness of soil strata across the footprint of structures, as observed in the case study analyses.

(ii) Affect the spatial distribution of settlement, contributing to increased differential settlements at the structural scale.

- ***How can empirical insights into existing structures exposed to ground settlement and their damage be utilized to assess the probability of damage?***

  Empirical information from buildings affected by ground settlement provides valuable insights for assessing damage likelihood and contributes essential data for numerical analyses. A sample of nearly 400 buildings in the Netherlands, resting on either shallow or piled foundations, was collected in this research to gather empirical data.

  From these observations, recurrent wall deformations were identified and used as the basis for defining settlement patterns in numerical analyses. The results indicate that asymmetric settlement patterns are more recurrent than symmetric shapes. Moreover, the observed hogging and sagging settlement shapes conformed to Gaussian probability distributions, similar to settlements due to specific drivers, such as tunnelling, mining and excavations.

  The analyses evaluated the predictive effectiveness of various settlement intensity metrics commonly used in the state-of-the-art. Receiving Operating Characteristic (ROC) analyses revealed that "rotation" and "angular distortion" were the most effective predictors of building damage, followed by "deflection ratio" and "differential settlement."

  In addition, empirical fragility functions were obtained to characterize the probabilistic relationship between settlement measurements and the observed damage in the sampled buildings. These empirically-based fragility curves offer insights into the behaviour of existing structures, differentiating between buildings supported by piles and those with shallow foundations. The proposed curves serve as a basis for risk analyses related to land subsidence.

  The fragility curves underwent a comparison with the outcomes of the numerical simulations, enriching the analysis and providing further insight.

- ***What structural and geotechnical parameters (i.e., geometry, foundation, material properties and soil) influence the relationship between imposed soil settlements and the resulting damage to buildings?***

  To investigate the influence of various structural and geotechnical parameters on the relationship between settlements and building damage, exploratory non-linear finite element analyses were conducted. The models were built using an established

technique incorporating the masonry façade, the underlying strip foundation, and a non-linear interface at the foundation base that accounts for soil-structure interaction. Different settlement profiles have been applied to the non-linear interface at the base of the model, to simulate the loss of support given by ground displacements.

Non-linear tensile cracking and softening of the masonry material were included through smeared cracking in the model, enabling assessment of damage by observing induced wall cracking. The sensitivity analyses considered variations in building features such as masonry type, length-to-height (L/H) ratio, wall thickness, number and size of openings, and types of strip foundations (reinforced concrete and unreinforced). Additionally, the influence of soil-structure interaction was examined.

The analyses were indirectly validated by comparing both the deformations of the model and the resulting damage with findings from previous studies and international standards guidelines.

The results indicate that building damage is significantly influenced by façade geometry in terms of length over height (L/H) ratio, masonry material properties and the shape of the settlement, soil-structure interaction influenced by both the soil and the foundation system. The analyses also suggest that as damage increases, modelled façades tend to exhibit greater flexibility, thus better accommodating imposed settlement deformations.

- ***What are the best modelling strategies to evaluate the response of structures subjected to subsidence?***

  To select the most suitable modelling strategy for buildings on strip foundations exposed to subsidence, state-of-the-art 2D and 3D finite element modelling approaches have been used to simulate the structural response in terms of damage. Both types of analyses included the non-linear behaviour of the building and soil-structure interaction. Comparing the results from these 2D and 3D models highlights the significant impact of including transversal walls on damage prediction.

  In an enhanced 2D modelling approach, transversal walls are represented by adding lateral elements, which account for the additional stiffness and weight. This method reduces modelling effort and computational burden compared to more detailed 3D analyses, while still effectively addressing masonry cracking and soil-structure interaction. The proposed 2D model provides results consistent with those from the 3D analyses in terms of displacements and damage.

  While 3D analyses are effective in incorporating complex three-dimensional structural effects and assessing the impact of 3D settlement patterns, the proposed 2D model is selected in this research as the most suitable approach for analyzing masonry façades on strip foundations subjected to subsidence. This choice is based on the 2D model's lower computational burden and its effectiveness in predicting façade damage, which is the focus of this study.

- ***How can numerical analyses be used to develop probabilistic relationships between subsidence and the damage to existing masonry structures?***

  Nearly seven thousand numerical analyses were conducted using the enhanced 2D modelling approach developed in this thesis, which includes the effect of transversal walls on damage prediction. The analyses include realistic scenarios involving façade geometry, material variations, foundation systems, soil-structure interaction, and settlement patterns.

  The outcomes of these 2D analyses have been used to establish probabilistic relationships between the intensity of ground settlements, measured by their angular distortion, and the resulting damage to masonry façades.

  Fragility curves were derived and categorized based on factors such as length-to-height (L/H) ratio, foundation and soil type, and masonry material. This segmentation allows for evaluating the influence of these parameters on the probability of damage.

  The analyses show that long façades and those on unreinforced masonry foundations are twice as likely to experience 5 mm cracks from settlement damage compared to short façades or those with reinforced concrete foundations, under an angular distortion of 2 ‰(or 1/500).

  Overall, the analyses indicated that for a value of the angular distortion measured on the building equal to 1/500, one out of two buildings could exhibit cracks up to 5 millimetres.

  The findings from this research can contribute to a systematic assessment of building damage. Moreover, the adopted framework is open to the inclusion of empirical and monitoring data to calibrate the models and further numerical results to improve the probabilistic prediction.

9.2. RELEVANCE AND CONTRIBUTIONS

The following sections address the scientific contributions and societal relevance of this thesis. Additionally, the use of the findings and knowledge presented in this work is further explored.

The research presented in this thesis was conducted alongside other akin projects at TU Delft, which focused on the impact of deep subsidence in the Groningen area as a cause of building damage, *i.e.*, [1]), and the combined effects of soil deformation and vibrations from multiple mining activities on masonry damage [2]. The interaction between these projects fostered a productive collaboration, resulting in mutual benefits and enriched outcomes for all involved.

9.2.1. SCIENTIFIC CONTRIBUTIONS

This research offered several scientific contributions, summarized as follows:

- *Effect of variations in the stratigraphy of soil layers:* Whereas previous research focused on the effect of the heterogeneity of the soil properties (such as permeability of compressibility) within a soil stratum, this study shows the effects of variations of the thickness of the soil layer in the settlement occurrence. The proposed model can be applied to different case studies and demonstrate potential for upscaling over regional scales.

- *Empirical data of structures exposed to subsidence:* Empirical observations of structures undergoing differential settlements are key to developing a better understanding of how damage to buildings occurs. This research provided valuable data that filled gaps left by limited or unavailable data from previous studies.

- *Numerical models of structures exposed to subsidence:* Advancements have been proposed to improve existing modelling strategies. The adopted 2D and 3D finite element models offer tools to study the response of structures undergoing settlements. As a major advantage, the proposed modelling strategies provide an objective characterization of the damage.

- *Parametric study into the effect of soil and structural features:* The interpretation of the numerical results from the sensitivity study offered insight into the effect of different structural aspects, such as foundation typology, building geometry, construction material and soil-structure interaction scenarios which are to be essential for the study of the structural response and thus for the damage assessment.

- *Relationships between settlement and damage:* Probabilistic relationships between the intensity of the differential settlements and the damage have been proposed as tools for the damage assessment of buildings subjected to soil subsidence.

9.2.2. SOCIETAL RELEVANCE

The Netherlands has experienced significant societal and economic unrest due to ongoing land subsidence. Climate change and the current land use have led to tipping points in

land subsidence [3], posing challenges in finding solutions for mitigation and adaptation. While municipalities and governmental institutions usually bear the costs of maintaining and repairing infrastructure systems, damage to buildings can directly burden homeowners. Moreover, given the adjacency of the existing structures, implementing solutions will unavoidably influence the surrounding buildings. These aspects raise several questions:

- Given that subsidence is caused by a combination of natural and anthropogenic drivers, sometimes linked to state policy, who is responsible for the damage to buildings?
- In areas prone to subsidence, should the government fund assistance for managing costs or should homeowners bear the costs of building damage themselves?
- Are there acceptable subsidence scenarios that minimise the probability of damage to buildings?

This study only partially helps to answer these questions. This thesis forms part of the research project *Living on Soft Soils (LOSS): Subsidence and Society* (grantnr.: NWA.1160.18.259) [3], as outlined in section 1.6 of this thesis. The results of this PhD research provide insight into the probabilities of damage due to settlements. This quantitative knowledge is expected to contribute to cost-benefit analyses which, in turn, are needed to address proper mitigation and adaptation strategies.

9.2.3. UTILISATION: INTEGRATING THE RESULTS INTO A SYSTEMATIC REGIONAL SCALE DAMAGE ASSESSMENT

This PhD research aimed to provide inputs and tools for regional scale damage assessment for areas exposed to subsidence. In addition to the discussion provided in the previous Chapters on how to use the findings of this study, this section explores how the results can be integrated into damage assessment procedures and which aspects still require further attention and research effort.

Figure 9.1 shows how the results of this research can be used to evaluate damage both at the scale of individual structures and over wide areas, thereby illustrating the connection between these scales.

The analyses presented in this thesis focused on the relationship between ground settlements and damage (angular distortion $\beta \rightarrow$ damage parameter Ψ in Fig. 9.1), and on the effect of the stratigraphical variability of the soil layers that characterizes soil heterogeneity (correlation length θ in Fig. 9.1). Nevertheless, establishing the relationship between soil heterogeneity and the differential settlements (quantified by correlation length $\theta \rightarrow$ angular distortion β) has not currently been achieved due to time limitations and requires further research efforts.

Although the analyses presented in this thesis provide evidence of the relationship of the effect of soil heterogeneity at different scales (correlation length $\theta \leftrightarrow$ soil heterogeneity over wide areas Θ) in Fig. 9.1), it should be acknowledged that additional studies are required to support the findings.

Additional analyses are also needed to include the effect of soil heterogeneity on subsidence prediction at regional scales (correlation length Θ → subsidence rates δ').

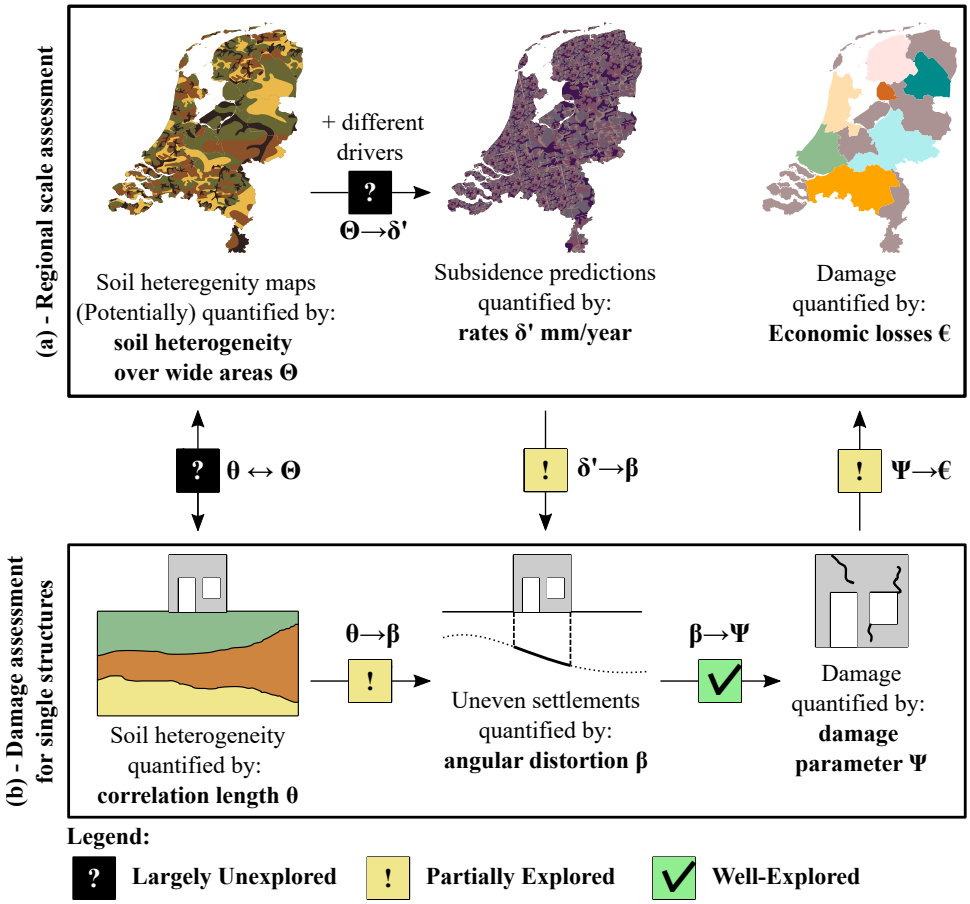

Figure 9.1: Schematic illustration of the links between different soil heterogeneity, the differential settlement and the damage to buildings: (a) regional assessments and (b) at the scale of single structures. The links between the different aspects relevant to damage assessment analyses are indicated.

Moreover, subsidence over wide areas is often measured by subsidence rates (δ'), whereas the assessment of damage to structures requires the determination of differential settlements in a specific time over multiple points at the scale of the buildings (subsidence rates δ' → angular distortion β). This thesis also proves the importance of computing settlement parameters which quantify the distortion experienced by buildings, for which it is necessary to retrieve the displacements in at least three points of the buildings (the reader is addressed to the definitions of the settlement parameters in section 2.5.3 of this Thesis). Previous studies, however, assume and adopt simplified relationships between subsidence rates and damage to structures (such as in [4]). Assuming that (differential) settlement rates can be directly retrieved from settlement rates with a simplified relation-

ship could overestimate the distortion and deformation of buildings, and, in turn, the damage.

Moreover, the damage to masonry structure is assessed with a classification system which considers the ease of repair [5] and can be thus converted into losses [6] (damage $\Psi \rightarrow$ losses e), in practice this is feasible for individual structures, but further studies should evaluate how to upscale such relationships to entire regions.

9.3. RECOMMENDATIONS FOR FURTHER RESEARCH

Different aspects would be worth further investigation, but time limitations did not allow doing so. In the following sections, the suggestions and recommendations for future research are formulated.

9.3.1. SOIL HETEROGENEITY: COMBINING THE LITHOLOGICAL HETEROGENEITY WITH THE SPATIAL VARIABILITY OF THE MATERIAL PROPERTIES

As discussed in chapter 3, soil heterogeneity is typically distinguished in: i) **inherent spatial soil variability**, which describes the variability of the soil properties, such as the compressibility or permeability, from one point to another within a layer, and ii) **lithological heterogeneity**, which refers to the variation of the stratigraphical information, such as lithology, unit thickness and the slope of the soil strata.

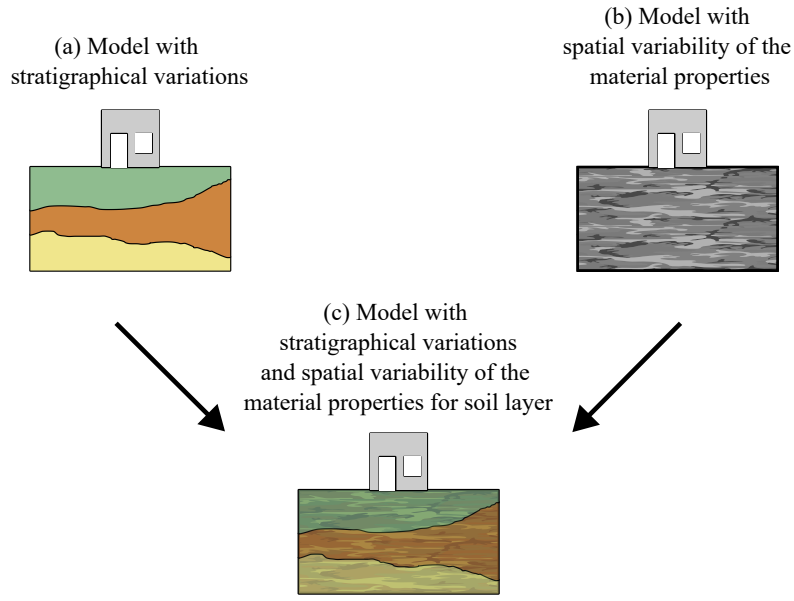

Figure 9.2: Schematic illustration of numerical models including (a) lithological soil heterogeneity, (b) the variability of the soil properties and (c) the combination of the two effects. Similar models could be used to explore the link between soil heterogeneity and damage to structures.

Figure 9.2 schematically illustrates how the two typologies of soil heterogeneity could be combined in one model, which could in turn be used to explore the response of structures. Of course, one challenge is represented by the in-situ investigations required to accurately depict soil heterogeneity at the scale of one building.

Whereas chapter 3 of this thesis focused on exploring the effect of stratigraphical variations, further research could address the combined effect of stratigraphical variations and the spatial variability of the soil properties within each layer. Additionally, the role

of heterogeneous loading conditions could be explored. These aspects have not been explored in this thesis due to time limitations.

9.3.2. THE INFLUENCE OF THE HORIZONTAL SOIL STRAINS

The ground surface may experience not only vertical movements but also horizontal displacements. While the magnitude of the vertical distortions is quantified using the settlement parameters introduced in section 2.5.3 (namely "differential settlement", "rotation", "deflection ratio" and "angular distortion") the intensity of horizontal ground displacements is typically measured by "horizontal strain" (or "lateral distortion"), which is defined as the average strain between two reference points due to relative horizontal movement [7]. Horizontal strains generate horizontal stresses, which can lead to tensile or compressive damage to the building [8].

Significant horizontal components have been associated with ground movements related to specific sources of settlements, such as mining, tunnelling and open excavation, in contrast to cases where buildings settle under their own weight [7]. As a structure experiences increasing lateral strains, its tolerance to differential settlement decreases [7].

While horizontal strains are a key factor in building damage, monitoring data on horizontal ground movements from settlement sources other than mining, tunnelling, and excavations is currently unavailable. Therefore, further research is needed to assess horizontal displacements in subsiding areas and their effects on building damage.

In this context, an ongoing project [2] at TU Delft is examining the combined effects of soil distortion and horizontal strains on building damage.

9.3.3. TIME-DEPENDENT BEHAVIOUR OF MASONRY

Creep identifies the change of dimensions of a material subject to constant actions. The viscoelastic properties of masonry depend on time and the intensity of the actions applied to the material [9].

It is well-known that long-term settlements are affected by the effects of creep and relaxation of the construction material. Settlements due to land subsidence can develop gradually over an extended period (e.g., decades). If these settlements progress slowly enough, creep and relaxation can significantly influence stress redistribution within the building, potentially allowing the structure to adapt to ground movements and reducing the risk of damage [10].

However, in the state-of-the-art, only a limited number of studies consider the combined effects of long-term settlements and material creep. This highlights the necessity for the characterization of the viscoelastic property of masonry not only at the material level but also at the scale of the entire structure.

9.3.4. SCALE EFFECT ON THE ENGINEERING PROPERTIES OF MASONRY

The engineering properties of masonry are frequently measured through laboratory tests on small samples, such as drill cores, couplets, triplets, and window banks. This method is commonly used as an alternative to in-situ mechanical characterization since both

destructive and non-destructive tests can still be invasive and more expensive to conduct for many structures.

Nevertheless, at different scales, masonry exhibits varying mechanical responses due to factors such as material heterogeneity, imperfections, defects, and existing damage. As a result, laboratory tests on small samples may not accurately reflect the behaviour of full-scale structures. Therefore, understanding the scale effect is essential for accurate modelling and prediction of masonry behaviour.

9.3.5. INTEGRATING OF LABORATORY TESTS, MONITORING DATA, MEASUREMENTS AND NUMERICAL ANALYSES

This research emphasized the critical need to integrate laboratory tests, monitoring data, observations, measurements of existing structures, and numerical analyses to enhance our understanding of damage in structures affected by subsidence.

Despite this necessity, only a few prior laboratory tests have specifically examined damage to masonry structures resulting from settlements. This gap underscores the need for additional experimental campaigns.

Additionally, observational data on existing structures are often limited or unavailable, and when present, they vary significantly in quality and quantity depending on the source. It is also essential to gather and make accessible cadastral data related to existing structures, including details about foundation systems, materials, and openings, for scientific research purposes.

Monitoring data can offer valuable insights into the progression of ground settlements, building displacements, and damage.

Finally, while numerical analyses contribute to understanding, incorporating the aforementioned knowledge into these analyses would significantly enhance insights into how subsidence affects building damage.

9.3.6. MODELLING APPROACHES, NUMERICAL ROBUSTNESS AND CONSTITUTIVE MODELS

In this thesis, semi-coupled non-linear finite element analyses have been used to model the response of masonry structures on strip foundations, including the soil-structure interaction.

In semi-coupled analyses, the structural response is assessed without explicitly including the soil volume but with soil-structure interactions represented by interfaces that account for bedding, gapping, and friction, as outlined in section 2.6. In contrast, 3D fully-coupled coupled models integrate the structure with the soil volume, allowing settlements to be triggered by various soil actions. These coupled models could provide valuable insights into building damage resulting from factors such as fluctuations in groundwater levels or the oxidation of organic matter. Moreover, coupled models can enhance our understanding of the effects of simultaneous actions, improving the representation of buildings and incorporating 3D effects.

Attention should be directed toward refining the constitutive relationships of the masonry material utilized in finite element analyses to more accurately depict damage. In this thesis, the Engineering Masonry Model has been employed for the non-linear representation of masonry. Although this model adequately includes orthotropy, tensile, shear and compressive failures, limitations have been observed in capturing the localization of damage and requires further improvements [11]. Finally, future research could explore alternative solution methods for non-linear finite element analyses, enhancing the reliability of results and the robustness of the analyses. In incremental-iterative non-linear finite element analyses, materials characterized by brittle failure, such as masonry and concrete, often encounter convergence issues that lead to inaccurate outcomes [12]. When masonry structures experience settlements, cracks may initiate, gradually propagate, and then suddenly snap to a free surface; thus, the final fracture becomes localized and is often highly brittle [12]–[14].

A promising alternative to traditional incremental-iterative non-linear finite element analyses is the Sequentially Linear Analysis (SLA) procedure. This method simulates damage in quasi-brittle materials by allowing for one damage event at a time, identifying a critical integration point in the finite element model with the maximum stress. The strength and stiffness of this critical point are then reduced according to a discretized step-wise constitutive relation known as the saw-tooth law [12], [14], [15]. This procedure has demonstrated greater robustness compared to the traditional incremental-iterative solutions used in the finite element method [12], [13], [15], [16], and could be further improved for non-proportional and cyclic loading.

9.3.7. CYCLIC GROUND MOVEMENTS: SETTLEMENT AND UPLIFT

Structures are subject to more than just downward displacement. Seasonal factors, such as the shrinkage and swelling of clay layers, fluctuations in groundwater levels driven by droughts or heavy rains, and the periodic extraction of underground resources, subject structures to alternating cycles of sinking and uplifting.

In order to illustrate the possible effects of the alternation of sinking and uplifting of the building, an exploratory numerical analysis is presented in the following.

One façade model already adopted in Chapter 7 is used herein: For simplicity, the model employs the same features described in Chapter 7, and readers are referred there for further details. The façade is subjected to settlement and uplift. The shape of the ground movements is obtained with equation 7.5 ($D_x = 0.5$, $x_i = 0.5$, $\iota = 1$) and the maximum angular distortion is equal to 1/300.

The loading scheme is applied with the following steps (see Fig. 9.3):

- **Step 1**: downward movements are applied. This step simulates the initial sinking of the building;
- **Step 2**: The imposed movement is reversed, and the displacements are gradually reduced. In this manner, the building is unloaded.
- **Step 3**: The façade is subjected to uplift by applying upward displacements.

- **Step 4**: The façade is unloaded again;
- **Step 3**: The downward movements are applied for the second time.

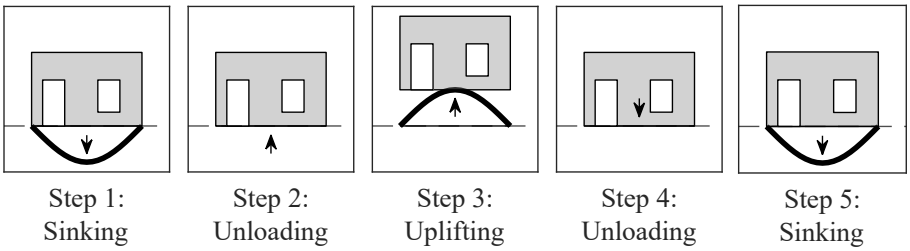

Figure 9.3: Loading scheme for the model that explores the effect of shrinkage and swelling alternation.

The results of the analysis are shown in Fig. 9.4. The cracks that open at the end of the first step (sinking) seal almost completely when the façade is unloaded (step 2). New cracks open due to the application of uplifting displacements (step 3), and the damage severity is higher than in the case of sinking. The cracks that open due to uplift do not seal when the façade is unloaded (step 4). Moreover, when sinking is applied again in step 5, the damage severity is higher than in the case of the first sinking stage (step 1).

Although the intensity of the applied sinking displacements, quantified by the angular distortion, is the same in steps 1 and 5, the damage at the end of the analysis is higher due to the damage accumulation: due to the "pre-existing" damage, herein fictitiously simulated with steps 1 to 4, the damage at the end of step 5 is higher than in step 1, and the crack patterns are also different. The results demonstrate how damage accumulates over time.

For the purpose of simplicity, the analysis assumes that the intensity of the distortions in sinking and uplift is the same. However, this example proves that cyclic settlement deformations could lead to the accumulation and aggravation of the damage with every sink-and-uplift cycle.

9.3.8. THE EFFECT OF EXISTING DAMAGE AND SIMULTANEOUS ACTIONS

In addition to the effect of cyclic settlements, section 9.3.7 indirectly shows the effect of the existing damage in the assessment of the response of the structure. For instance, in section 9.3.7 the façade is initially undamaged before the application of the settlements. Step 1 to Step 5 (Fig. 9.4) represent the results of different cycles of settlement and uplift. However, in reality settlements could arise when the buildings has already experienced some damage due to previous settlements along the perimeter of the buildings or due to the effect of previous or simultaneous actions, such as thermal or chemical actions and vibrations. Therefore, Step 1, for instance, could represent the condition of a building with existing damage before settlement occurs.

In this section, the same model adopted in section 9.3.7 is used to further demonstrate the effect of the existing damage. Two analyses are compared: one, in which the façade

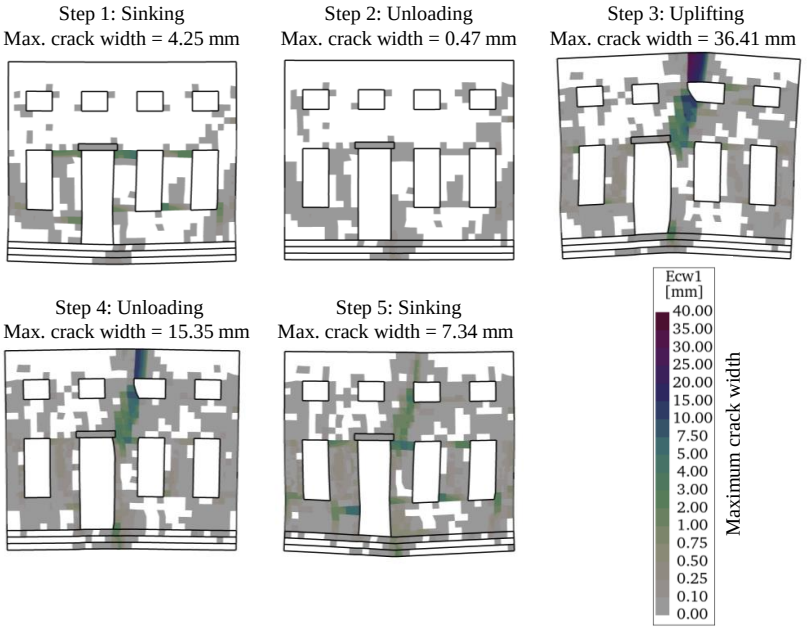

Figure 9.4: Crack pattern obtained at the end of each loading step. The contour plot refers to the maximum crack width. The absolute deformation of the façade is shown with a magnification factor equal to 30.

does not show any damage before the application of the settlement, is compared with another analysis in which an initial crack pattern is considered. The results are shown in Figure 9.5.

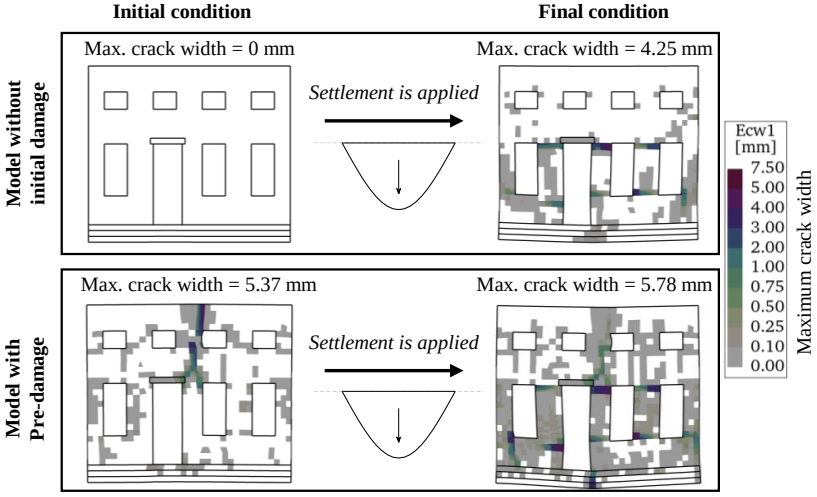

Figure 9.5: The crack patterns of two models after the application of the settlement load: one model without initial damage and another with an imposed pre-damage. The absolute deformation of the façade is shown with a magnification factor equal to 30.

Compared to the model without any initial damage, the pre-damage model exhibits higher damage at the end of the settlement application, both in terms of the number of cracks and their width. However, the damage in the pre-damage model is more severe already before the application of the settlement. Therefore, for a consistent approach, the two models should be compared in terms of damage aggravation, *i.e.*, the difference between the initial damage and the final one. This can be achieved by comparing the difference between the initial and the final damage parameter Ψ, obtaining the damage aggravation $\Delta\Psi$, similarly to section 8.1.8 of this thesis.

To achieve this, the increase in damage is determined by the difference between the initial and final maximum crack widths. Specifically, for the model without initial damage, this difference equals the final crack width (4.25 mm), while for the pre-damaged model, the difference is 0.41 mm. Therefore, even though the final damage is greater in the pre-damaged model, the increase in damage is lower.

BIBLIOGRAPHY OF CHAPTER 9

[1] P. Korswagen, M. Longo, J. Rots, and A. Prosperi, "Supporting analyses to determine probability of damage and fragility curves due to indirect subsidence effects," *Delft University of Technology. Report*, Final Version 2, October 3, 2022.

[2] P. Korswagen, M. Longo, and J. Rots, "Research into the combined effects of soil strains, soil curvatures and earthquake vibrations from multiple mining activities on damage in masonry," *Delft University of Technology. Report*, 2024.

[3] E. Stouthamer, G. Erkens, K. Cohen, *et al.*, "Dutch national scientific research program on land subsidence: Living on soft soils–subsidence and society," *Proceedings of the International Association of Hydrological Sciences*, vol. 382, pp. 815–819, 2020.

[4] Deltares, "Technische toelichting risicokaarten funderingen," Report, Apr. 2021.

[5] J. B. Burland, B. B. Broms, and V. F. De Mello, "Behaviour of foundations and structures," 1978.

[6] A. L. Costa, S. Kok, and M. Korff, "Systematic assessment of damage to buildings due to groundwater lowering-induced subsidence: Methodology for large scale application in the netherlands," *Proceedings of the International Association of Hydrological Sciences*, vol. 382, pp. 577–582, 2020.

[7] M. D. Boscardin and E. J. Cording, "Building response to excavation-induced settlement," *Journal of Geotechnical Engineering*, vol. 115, no. 1, pp. 1–21, 1989.

[8] X. Liu and L. Xu, "Soil-building interaction under surface horizontal strain induced by underground mining," *Advances in Civil Engineering*, vol. 2022, no. 1, p. 2 425 936, 2022.

[9] A. Taliercio *et al.*, "An overview of masonry creep," *Structural Studies, Repairs and Maintenance of Heritage Architecture XI*, vol. 109, p. 197, 2009.

[10] H. D. Netzel, "Building response due to ground movements," 2009.

[11] M. Sousamli, "Orthotropic cyclic continuum constitutive model for masonry structures and comparative studies," 2024.

[12] M. Pari, M. Hendriks, and J. Rots, "Sequentially linear analysis on masonry walls – a new crack closure algorithm," Jun. 2017.

[13] J. Rots, M. Boonpichetvong, B. Belletti, and S. Invernizzi, "An application of sequentially linear analysis to settlement damage prediction for masonry façades," *Fracture mechanics of concrete and concrete structure. High-performance concrete, brick-masonry and environmental aspects*, vol. 3, pp. 1653–1660, 2007.

[14] M. Pari, J. Rots, and M. Hendriks, "Recent advancements in sequentially linear analysis (sla) type solution procedures," in *Computational Modelling of Concrete and Concrete Structures*, CRC Press, 2022, pp. 432–442.

[15] M. Pari, A. Van de Graaf, M. A. Hendriks, and J. Rots, "A multi-surface interface model for sequentially linear methods to analyse masonry structures," *Engineering Structures*, vol. 238, p. 112 123, 2021.

[16] N. W. KOSTENSE, Y. YANG, M. HENDRIKS, and J. ROTS, "A comparative study of implicit and explicit solution procedures for computational modeling of reinforced concrete structures,"

LIST OF PUBLICATIONS

JOURNAL ARTICLES

- **D. Peduto, A. Prosperi, G. Nicodemo M. Korff,** *District-scale numerical analysis of settlements related to groundwater lowering in variable soil conditions.* Canadian Geotechnical Journal, 59(6), 978-993 (2022).
- **A. Prosperi, P. A. Korswagen, M. Korff, R. Schipper, J. G. Rots**, *Empirical fragility and ROC curves for masonry buildings subjected to settlements.* Journal of Building Engineering, 68, 106094 (2023).
- **A. Prosperi, M. Longo, P. A. Korswagen, M. Korff, J. G. Rots**, *Sensitivity modelling with objective damage assessment of unreinforced masonry façades undergoing different subsidence settlement patterns.* Engineering Structures, 286, 116113 (2023).
- **A. Prosperi, M. Longo, P. A. Korswagen, M. Korff, J. G. Rots**, *2D and 3D Modelling Strategies to Reproduce the Response of Historical Masonry Buildings Subjected to Settlements.* International Journal of Architectural Heritage (2024).
- **A. Prosperi, T. de Gast, P. A. Korswagen, M. Korff, J. G. Rots**, *The effect of lithological heterogeneity on soil settlements at the building scale.* Under Review. (2024).
- **A. Prosperi, M. Longo, P. A. Korswagen, M. Korff, J. G. Rots**, *Comparison of coupled and uncoupled 3D finite element models for soil-structure interactions in masonry structures with strip foundations undergoing subsidence.* Under Review. (2024).

CONFERENCE CONTRIBUTIONS

- **A. Prosperi, G. Nicodemo, M. Korff, D. Peduto**, *Multi-source monitoring data and numerical analyses for the assessment of settlements affecting built-up areas in variable soil conditions.* In 11th International Symposium on Field Monitoring in Geomechanics (ISFMG2022). ISSMGE.
- **A. Prosperi, M. Longo, P. A. Korswagen, M. Korff, J. G. Rots**, *Shape matters: Influence of varying settlement profiles due to multicausal subsidence when modelling damage in a masonry façade.* In Tenth International Symposium on Land Subsidence (2023).
- **A. Prosperi, M. Longo, P. A. Korswagen, M. Korff, J. G. Rots**, *Accurate and Efficient 2D Modelling of Historical Masonry Buildings Subjected to Settlements in Comparison to 3D Approaches.* In International Conference on Structural Analysis of Historical Constructions (pp. 232-244) (2023).
- **P. A. Korswagen, M. Longo, A. Prosperi, J. G. Rots, K. C. Terwel**, *Modelling of Damage in Historical Masonry Façades Subjected to a Combination of Ground Settlement and Vibrations.* In International Conference on Structural Analysis of Historical Constructions (pp. 904-917) (2023).

- **A. Prosperi, M. Longo, P. A. Korswagen, M. Korff, J. G. Rots**, *Comparative analysis of coupled and uncoupled 3D Finite Elements models for masonry structures subjected to settlements.* In: 18th International Brick and Block Masonry Conference (2024).
- **P. A. Korswagen, M. Longo, A. Prosperi, J. G. Rots** , *Analysing Damage from Quasi-static and Dynamic Ground Movements on Dutch Masonry Buildings via Numerical Models.* submitted to 15th Canadian Masonry Symposium (2025).
- **A. Prosperi, M. Longo, P. A. Korswagen, M. Korff, J. G. Rots**, *Damage from ups and downs: investigating cracking in unreinforced masonry structures exposed to settlement and uplift cycles using finite element analyses.* submitted to 15th Canadian Masonry Symposium (2025).

REPORTS

- **P. A. Korswagen, M. Longo, J. G. Rots, A. Prosperi**, *Supporting analyses to determine probability of damage and fragility curves due to indirect subsidence effects. Delft University of Technology. Final Version October 3, 2022.*
- **Straathof, R., Prosperi, A., Korswagen, P. A.** (2024). *Data verification for "Empirical fragility and ROC curves for masonry buildings subjected to settlements". Delft University of Technology.*

APPENDIX A

Appendix to Chapter 4

A.1. DIFFERENCES FROM THE RESULTS PUBLISHED IN [1]

This section briefly illustrates the differences between the data used in [2] and available within 4TU.ResearchData [1], and the one used in the Chapter 4 of this Dissertation.

The data collection and analyses were originally carried out between 2020 and 2021, while the final version was published in 2023 [2]. During the writing of this thesis, a revision was undertaken to enhance the quality of the results. This data verification has been published [3], further detailing the existing dataset.

A verification was carried out to ensure that the input information was accurately collected from the various hard copies. A native Dutch speaker conducted the verification of the quality of the collected documentary information. This step was conducted to identify and correct any typos or errors that might have affected the manually gathered data. The details of this activity are provided in section A.1.1.

In the published paper, a MATLAB algorithm was employed to automatically calculate the SRI parameters (i.e., differential settlement, rotation, angular distortion, and deflection ratio) for all the surveyed walls. Enhancements were made to the algorithm, improving the code and resolving bugs and technical glitches, resulting in slightly different values for the computed SRI. Moreover, the calculations of the settlement parameters adopted in the original publication were also checked during the data verification.

It is important to emphasize that both checks were conducted independently of the Authors of the published articles to ensure an unbiased and independent process. However, the Authors provided the original data and supported the initiative to verify both the data and calculations, ensuring the quality and accuracy of the dataset.

A.1.1. CORRECTIONS TO THE DATASET

The bed-joint levelling measurements of 615 walls were collected into a digital Database. The procedure involved collecting the coordinates of the surveyed points along the walls from hardcopies and from technical drawings, and manually typing it into the MATLAB dataset [2].

After closer inspection of the dataset, a few typos were found. In order for the reader to quickly and efficiently identify the cases with typos, it should be noticed that:

- Each dataset item includes an "ID", which corresponds to a label intended just to differentiate the cases;
- Each dataset item includes a field called "Wall", which is a MATLAB structure that contains the x- (*i.e.*, the coordinate along each surveyed wall, in meters) and z- (*i.e.*, the recorded vertical displacement, in millimetres) coordinates;

Accordingly, Table A.1 reports a list of the cases, walls, and detected typos.
The data verification has not revealed any major issues with the information stored dataset, although typos or mistakes could be present, they are not expected to have a major impact on the results and/or conclusion of the published manuscript [3]. No inconsistencies were detected in the collected data regarding foundation typology, year of construction, or structural typology.

Table A.1: Overview of the typos found among the levelling measurements stored in the dataset [1], [3].

Case	Wall	Coordinate	Mistake	Correction
B16	1	Z	[−115, −10, −135, −105]	[−115, −120, −135, −105]
B28	4	Z	[−20, 20, −28, −94]	[−20, −20, −28, −94]
B31	4	Z	[−114, −89, −84, −14]	[−114, −89, −84, −114]
B63	3	X	[0, 3.8, 8.4, 13.1, 17.2, 22.1, 16.7, 30.4]	[0, 3.8, 8.4, 13.1, 17.2, 22.1, 26.7, 30.4]
B40	3	X	[0, 2.9, 5.8, 9.1]	[0, 2.9, 6.2, 9.1]
B104	6	Z	[-1.71, -0.40, -0.97, 0, -0.31]	[-17.10, -4.00, -9.70, 0,-3.10]
B121	1	X	[0, 3.69, 8.80, 12.45, 16.10, 25.35, 285.44, ... 34.11, 38.70, 46.08, 50.87, 59.90, 66.10, 72.49]	[0, 3.69, 8.80, 12.45, 16.10, 25.35, 28.54, ... 34.11, 38.70, 46.08, 50.87, 59.90, 66.10, 72.49]
B212	1	X	[0, 5.27, 11.99, 18.29, 24.73, 31.62, 37.14, ... 3.97, 50.19, 57, 63.36, 60.61, 75.96, 82.6, 88.8]	[0, 5.27, 11.99, 18.29, 24.73, 31.62, 37.14, ... 3.97, 50.19, 57, 60.61, 63.36, 75.96, 82.6, 88.8]
B245	1	Z	[250, 237, 228, 223, 254, 271, 238]	[250, 237, 228, 223, 254, 271, 283]
B256	1	Z	[−8, −9, 0]	[−8, 9, 0]
B376	1	X	[0, 1, 20, , 7.02, 14.49, 21.20, 28.31, 35.50]	[0, 7.02, 14.49, 21.20, 28.31, 35.50]
	1	Z	[0, 1, 218.68, 38.63, 27.64, 19.48, 9.93, 0]	[21.87, 38.63, 27.64, 19.48, 9.93, 0]

A.2. DIFFERENCES BETWEEN THE FRAGILITY CURVES

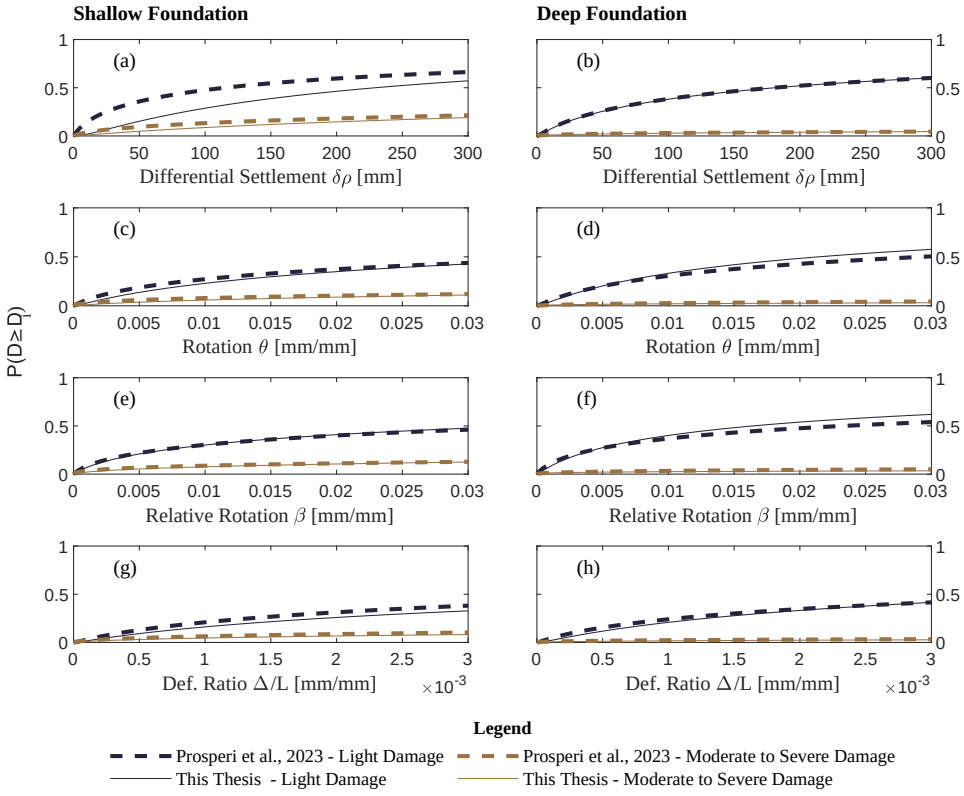

Figure A.1: Differences between the Fragility Curves presented in [2] (dashed lines) and the ones proposed in this Dissertation in Chapter 4 (solid lines).

The calculations of the settlement parameters were verified with hand calculations and using an algorithm. This step did not reveal any issues [3].

Figure A.1 shows the difference between the fragility curves published in [2] and the ones proposed in this chapter 4 of this thesis, obtained with the "Approach 1" detailed in section 4.2.5. The differences between the results, due to the corrections, are negligible and do not affect the main conclusions.

BIBLIOGRAPHY OF APPENDIX A

[1] A. Prosperi, P. A. Korswagen, M. Korff, R. Schipper, and J. G. Rots, *Supporting data for: Empirical fragility and roc curves for masonry buildings subjected to settlements*, 2023. DOI: 10.4121/18279155.V1. [Online]. Available: https://data.4tu.nl/articles/_/18279155/1.

[2] A. Prosperi, P. A. Korswagen, M. Korff, R. Schipper, and J. G. Rots, "Empirical fragility and roc curves for masonry buildings subjected to settlements," *Journal of Building Engineering*, vol. 68, p. 106 094, 2023.

[3] R. Straathof, P. Korswagen, and A. Prosperi, "Data verification for" empirical fragility and roc curves for masonry buildings subjected to settlements" report,"

APPENDIX B

Appendix to Chapter 5

B.1. An example of the calculation of the relative bending stiffness for the reference model in Ch. 5

This section reports an example of the calculation of the relative bending stiffness ρ, described in section 5.3.7 of Chapter 5, for the reference modelling case. The relative information of the model assumed as the reference case is the following:

- Masonry Material: M2, Young's Modulus = 5000 MPa (Tab. 5.1);
- Foundation: Unreinforced Masonry (Fig. 5.4a), Base of the foundation B = 610 millimetres, height of the foundation equals to 600 millimetres;
- Double wythe (i.e., 210 mm) facade with a length and height of 8 and 7 meters respectively. The opening ratio is 0.27 (Fig. 5.3f).
- Soil A (Tab. 5.4), with a shear modulus G equal to 35 MPa and a Poisson's ratio ν of 0.30.

First, the Young's modulus of the soil is obtained as:

$$E = 2 * G(1 + \nu)$$

Which results in the E_{soil} being equal to 91 MPa for the selected soil.
The inertia of the foundation is computed as:

$$I_{foundation} = \frac{(0.6\,[m])^3 * 0.61\,[m]}{12} = 1.10 * 10^{-2}\,[m^4]$$

The inertia of the facade is computed considering the different positions of the neutral axis in sagging and hogging respectively, accordingly:

$$I_{facade,sagging} = \frac{(7\,[m])^3 * 0.21\,[m]}{12} = 6.00\,[m^4]$$

$$I_{facade,hogging} = \frac{(7\,[m])^3 * 0.21\,[m]}{3} = 24.01\,[m^4]$$

Accordingly, the values of the building bending stiffness EI of the facade are computed with equation 5.7 considering a reduction factor α_r o equals to 0.1 (Opening 27% with L<2H, Tab. 5.6). Thus, the following values are obtained:

$$EI_{sagging} = 3.06 * 10^6\,[kN * m^2]$$

$$EI_{hogging} = 1.21 * 10^7\,[kN * m^2]$$

From which the values of relative bending stiffness ρ are computed with equation 5.6:

$$\rho_{sagging} = \frac{3.06 * 10^6 \left[kN * m^2\right]}{91 \left[N/mm^2\right] * 1000 \left(to\ convert\ in\ kN/m^2\right) * (8\,[m])^3 * (0.21\,[m])} = 0.11\,[-]$$

$$\rho_{hogging} = \frac{1.21 * 10^7 \left[kN * m^2\right]}{91 \left[N/mm^2\right] * 1000 \left(to\ convert\ in\ kN/m^2\right) * (8\,[m])^3 * (0.21\,[m])} = 0.42\,[-]$$

APPENDIX C

Appendix to Chapters 7 and 8

C.1. GEOMETRIES OF THE MODELS ADOPTED IN CHAPTERS 7 AND 8

In this section, the geometries of the facades adopted in the numerical analyses in Chapters 7 and 8 are detailed:

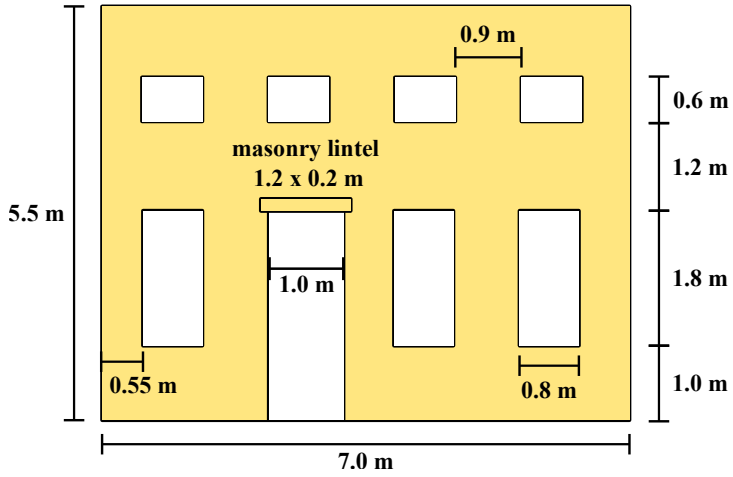

Figure C.1: Sizes of the facade labelled as "FA" used in the analyses presented in Chapters 7 and 8. The illustration is not in scale.

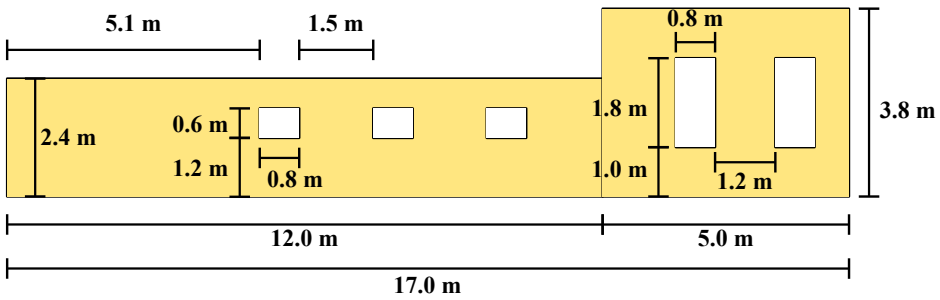

Figure C.2: Sizes of the facade labelled as "FB" used in the analyses presented in Chapters 7 and 8. The illustration is not in scale.

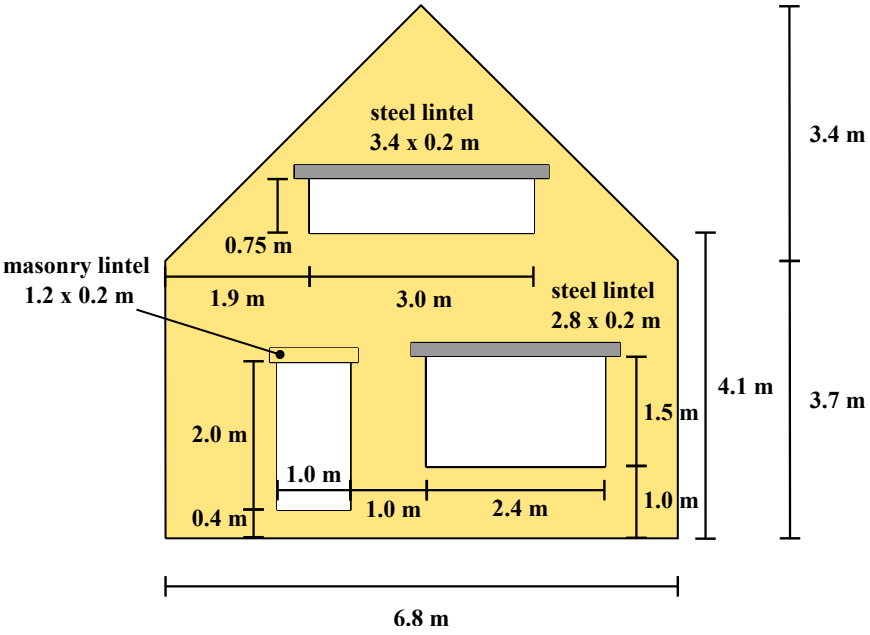

Figure C.3: Sizes of the facade labelled as "FC" used in the analyses presented in Chapters 7 and 8. The illustration is not in scale.

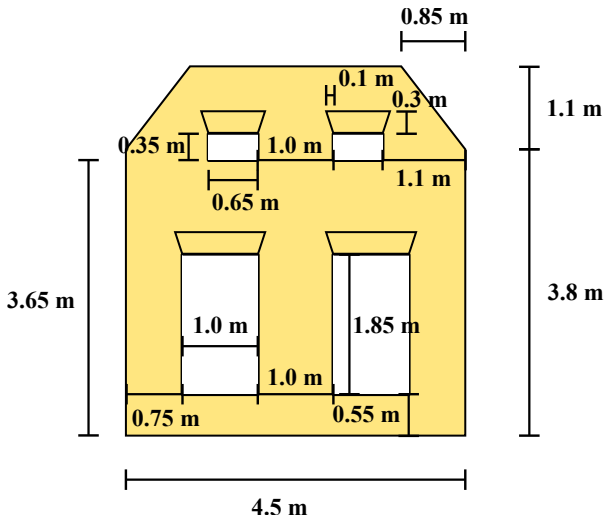

Figure C.4: Sizes of the facade labelled as "FD" used in the analyses presented in Chapters 7 and 8. The illustration is not in scale.

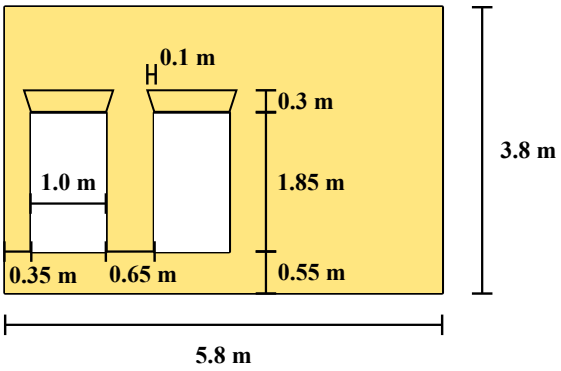

Figure C.5: Sizes of the facade labelled as "FE" used in the analyses presented in Chapters 7 and 8. The illustration is not in scale.

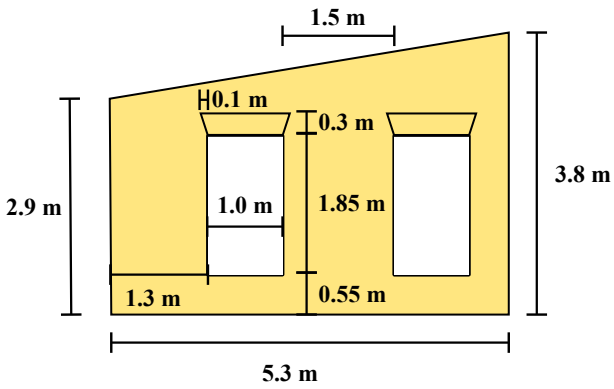

Figure C.6: Sizes of the facade labelled as "FF" used in the analyses presented in Chapters 7 and 8. The illustration is not in scale.

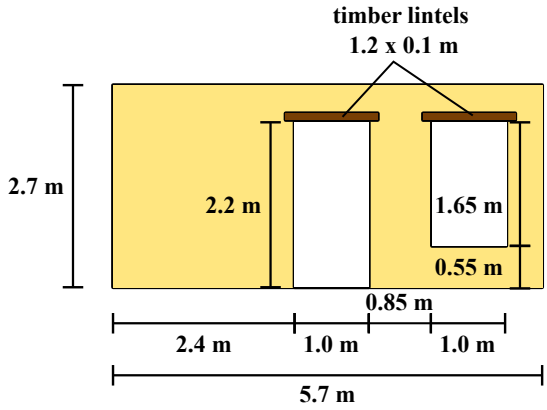

Figure C.7: Sizes of the facade labelled as "FG" used in the analyses presented in Chapters 7 and 8. The illustration is not in scale.

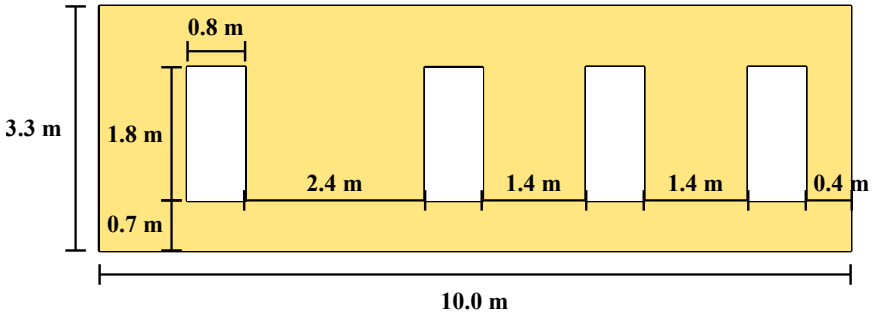

Figure C.8: Sizes of the facade labelled as "FH" used in the analyses presented in Chapters 7 and 8. The illustration is not in scale.

C.2. RESULTS OF THE SENSITIVITY ANALYSIS FOR ALL THE SELECTED FACADES

C.2.1. RESULTS FOR HOGGING

In this section, the results of the sensitivity analyses presented in Chapter 7 are shown with reference to all the selected facades, whereas Chapter 8 focused on the models labelled as "FA" and "FB".

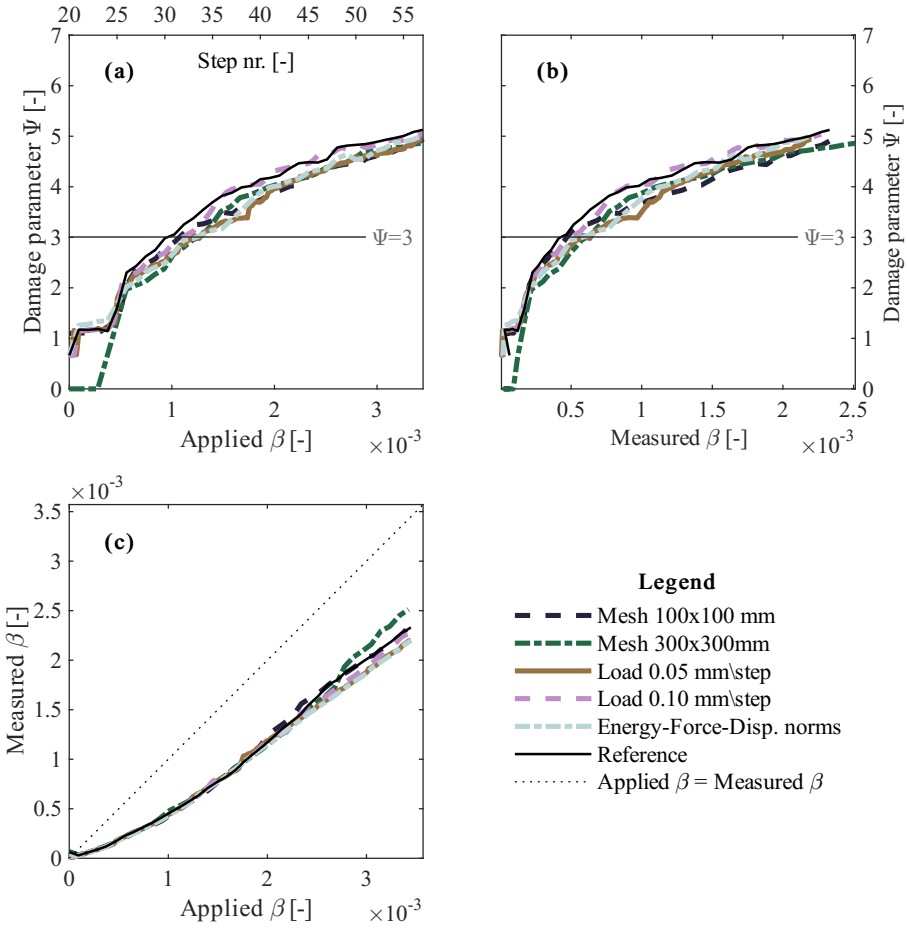

Figure C.9: Results of the sensitivity analyses for a hogging settlement pattern in terms of applied and measured angular distortion against the damage parameter Ψ for the facade labelled as "FC".

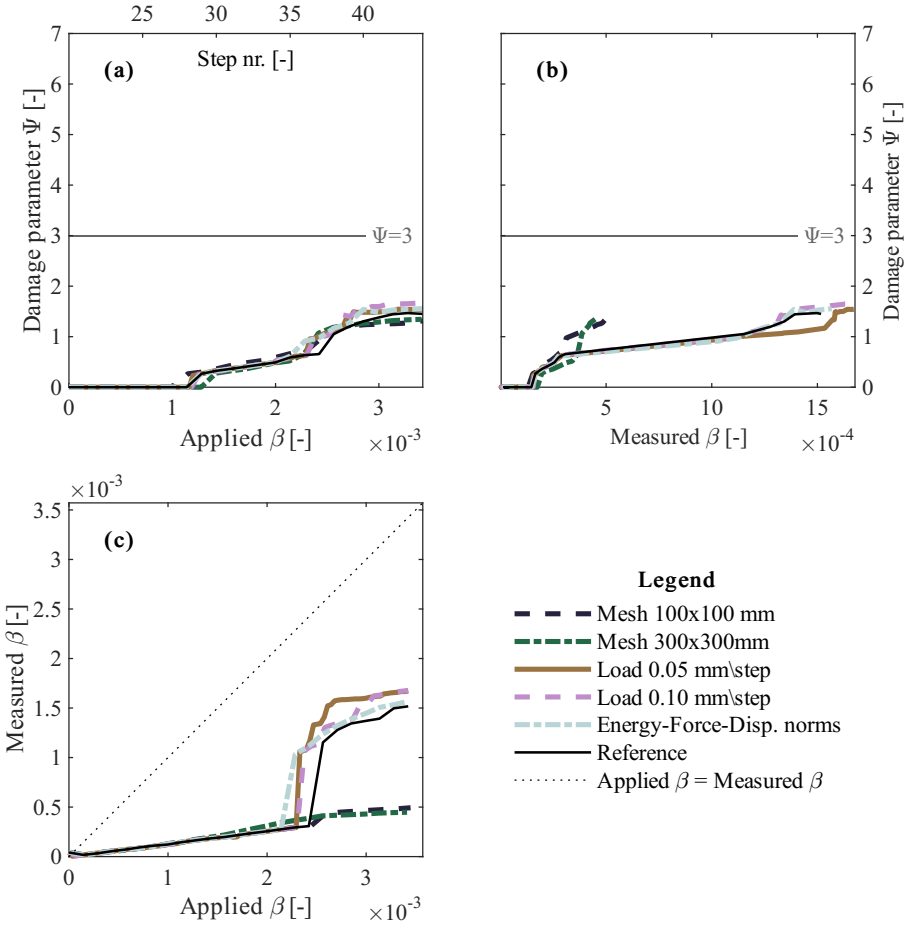

Figure C.10: Results of the sensitivity analyses for a hogging settlement pattern in terms of applied and measured angular distortion against the damage parameter Ψ for the facade labelled as "FD".

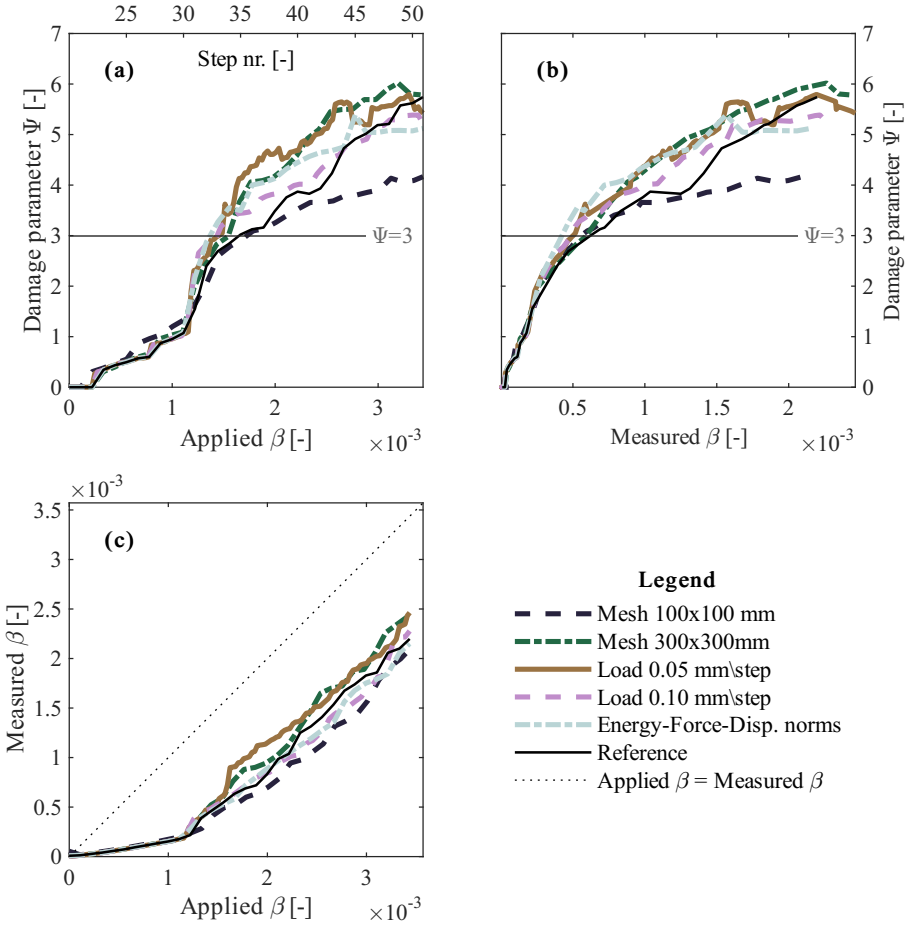

Figure C.11: Results of the sensitivity analyses for a hogging settlement pattern in terms of applied and measured angular distortion against the damage parameter Ψ for the facade labelled as "FE".

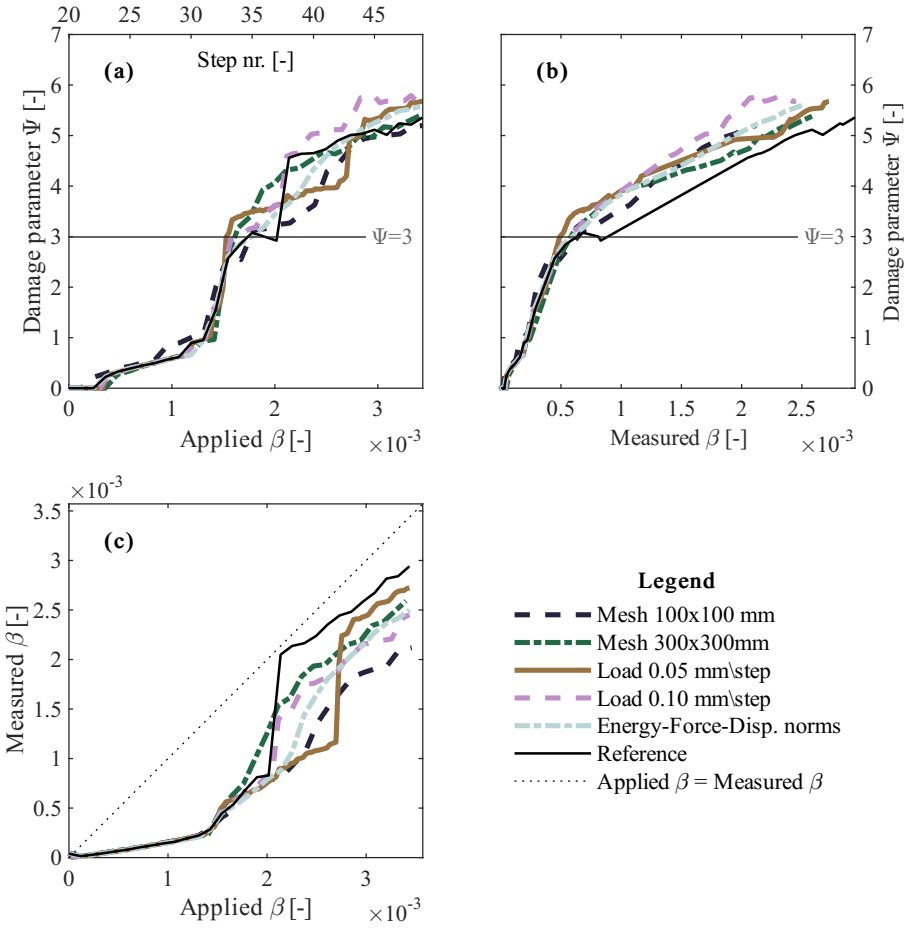

Figure C.12: Results of the sensitivity analyses for a hogging settlement pattern in terms of applied and measured angular distortion against the damage parameter Ψ for the facade labelled as "FF".

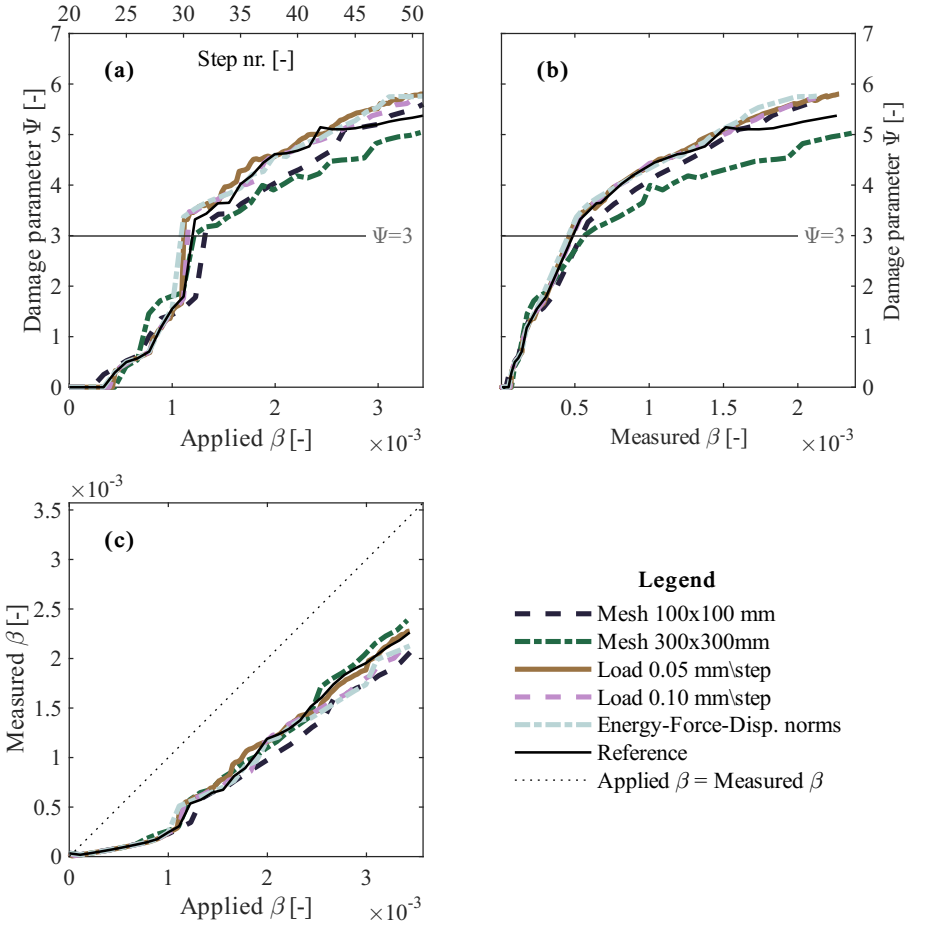

Figure C.13: Results of the sensitivity analyses for a hogging settlement pattern in terms of applied and measured angular distortion against the damage parameter Ψ for the facade labelled as "FG".

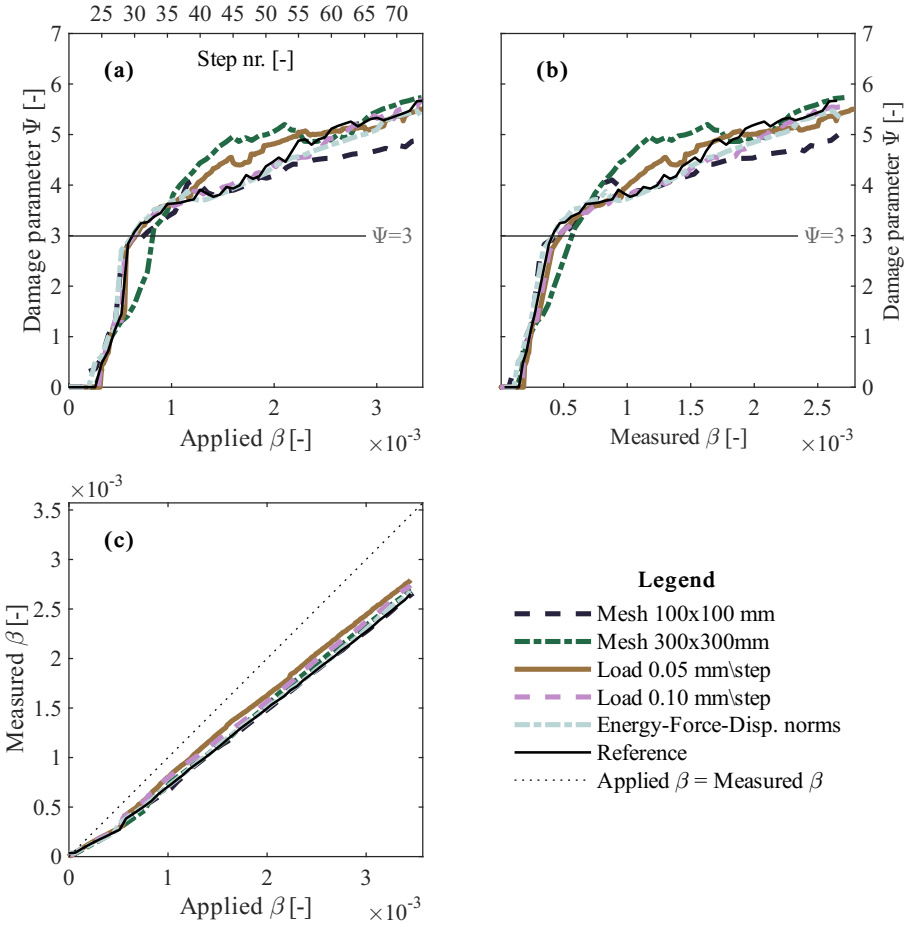

Figure C.14: Results of the sensitivity analyses for a hogging settlement pattern in terms of applied and measured angular distortion against the damage parameter Ψ for the facade labelled as "FH".

C.2.2. RESULTS FOR SAGGING

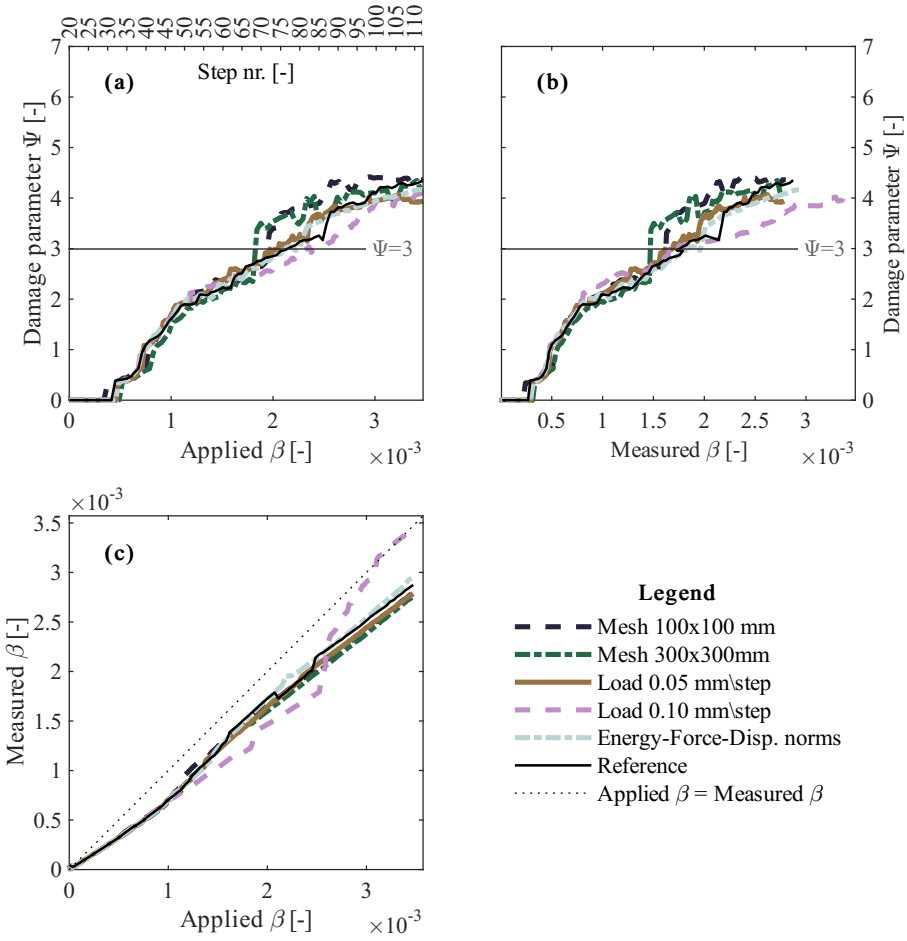

Figure C.15: Results of the sensitivity analyses for a sagging settlement pattern in terms of applied and measured angular distortion against the damage parameter Ψ for the facade labelled as "FB".

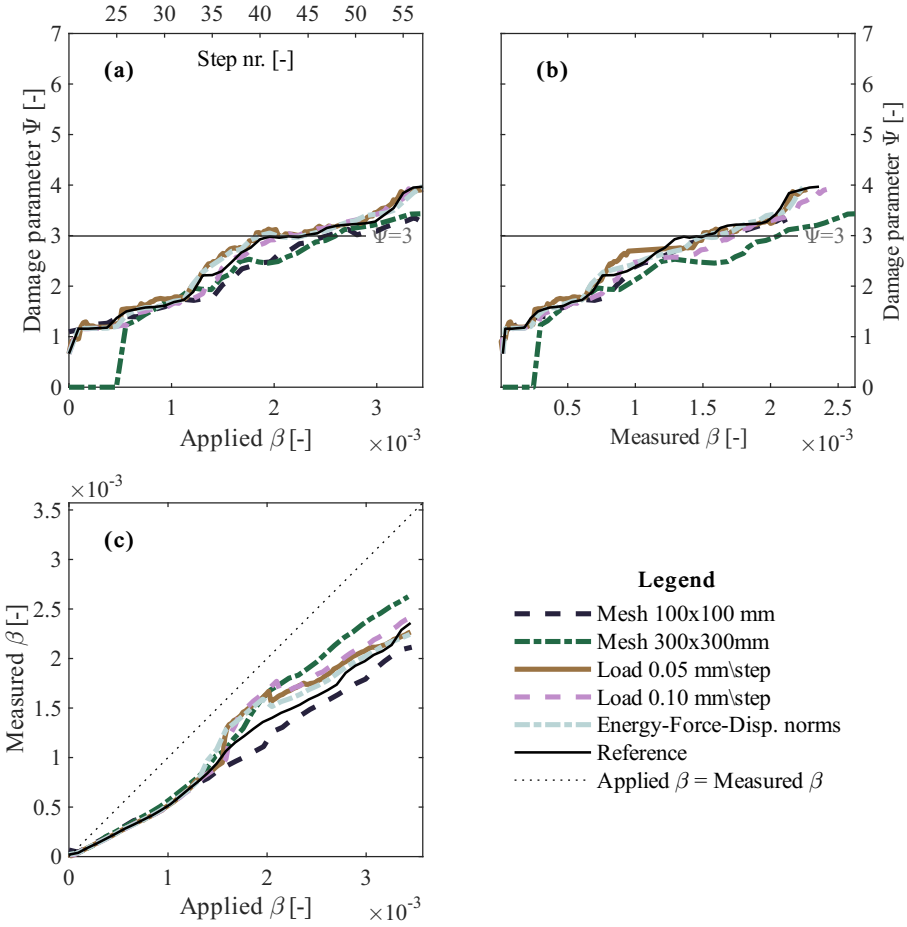

Figure C.16: Results of the sensitivity analyses for a sagging settlement pattern in terms of applied and measured angular distortion against the damage parameter Ψ for the facade labelled as "FC".

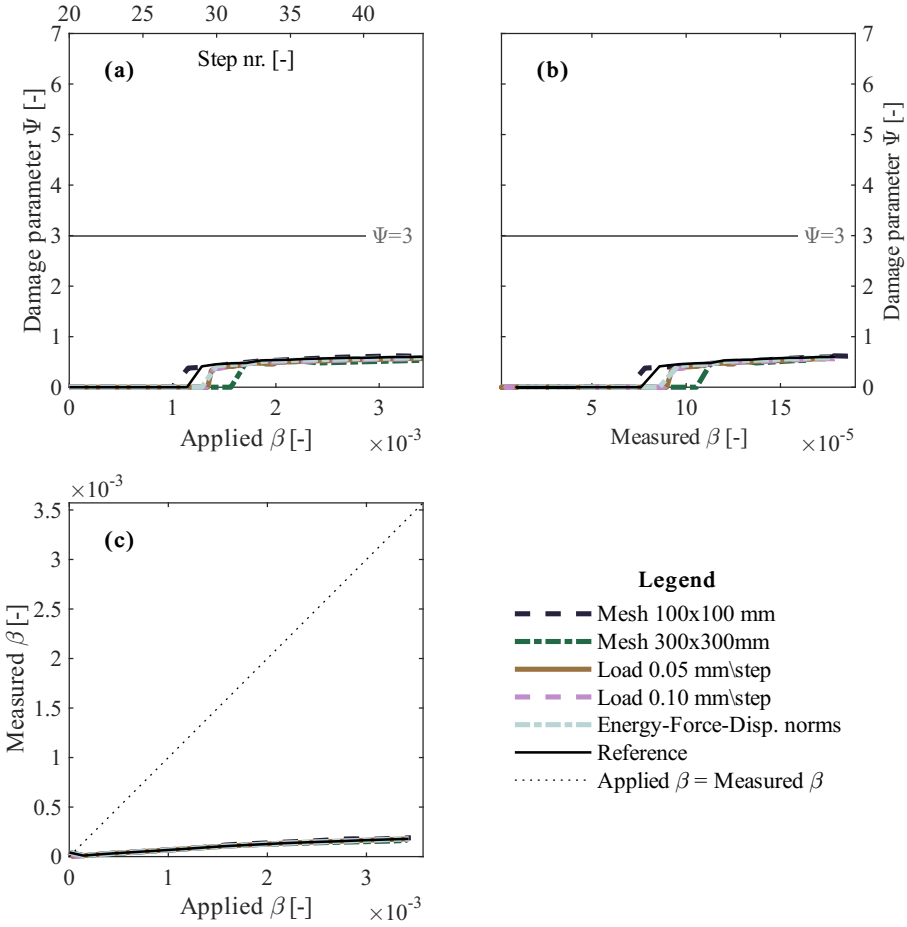

Figure C.17: Results of the sensitivity analyses for a sagging settlement pattern in terms of applied and measured angular distortion against the damage parameter Ψ for the facade labelled as "FD".

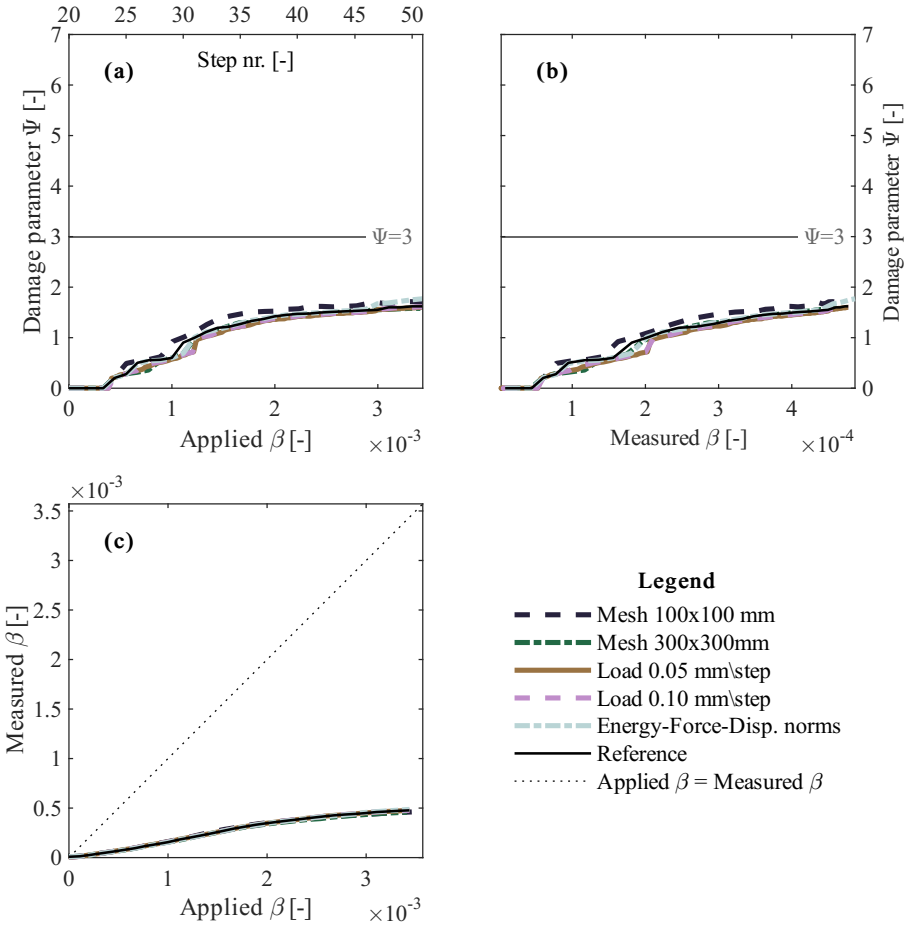

Figure C.18: Results of the sensitivity analyses for a sagging settlement pattern in terms of applied and measured angular distortion against the damage parameter Ψ for the facade labelled as "FE".

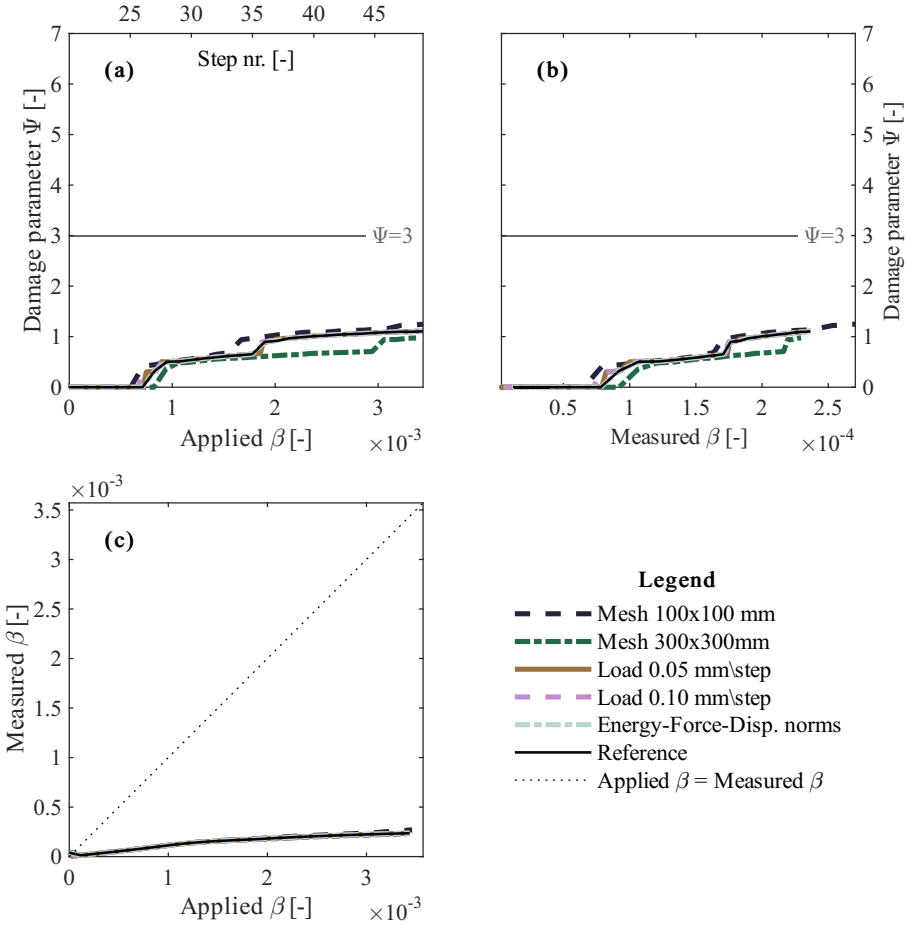

Figure C.19: Results of the sensitivity analyses for a sagging settlement pattern in terms of applied and measured angular distortion against the damage parameter Ψ for the facade labelled as "FF".

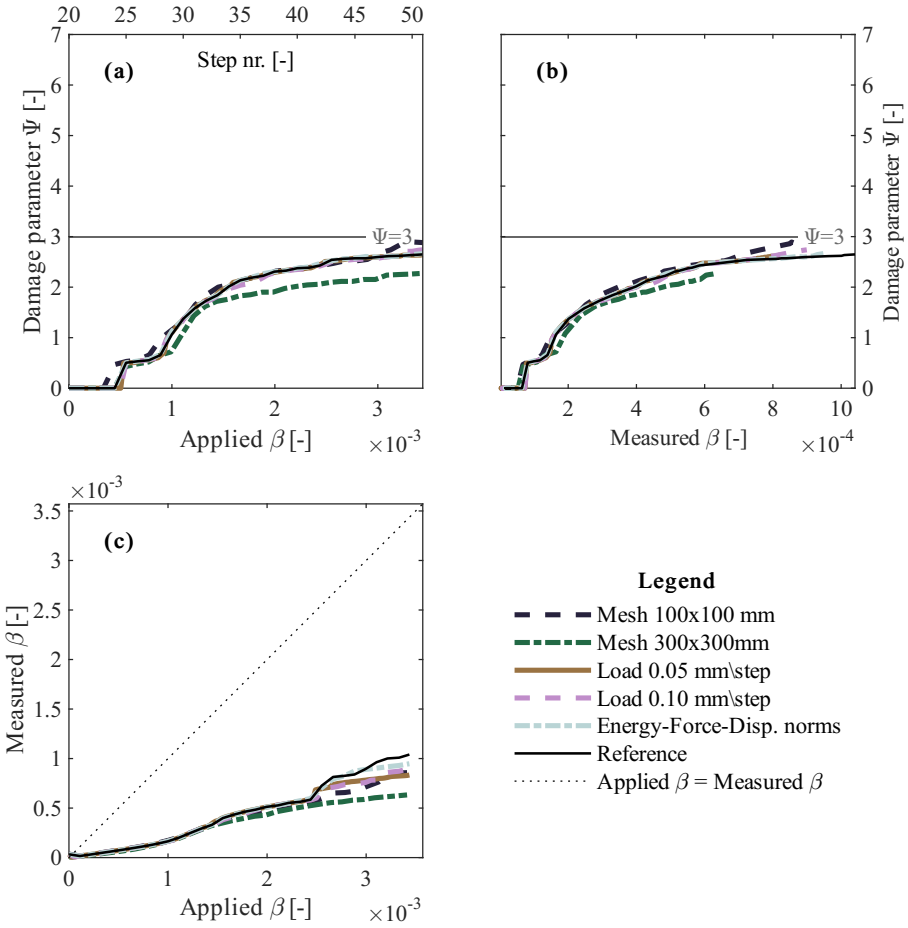

Figure C.20: Results of the sensitivity analyses for a sagging settlement pattern in terms of applied and measured angular distortion against the damage parameter Ψ for the facade labelled as "FG".

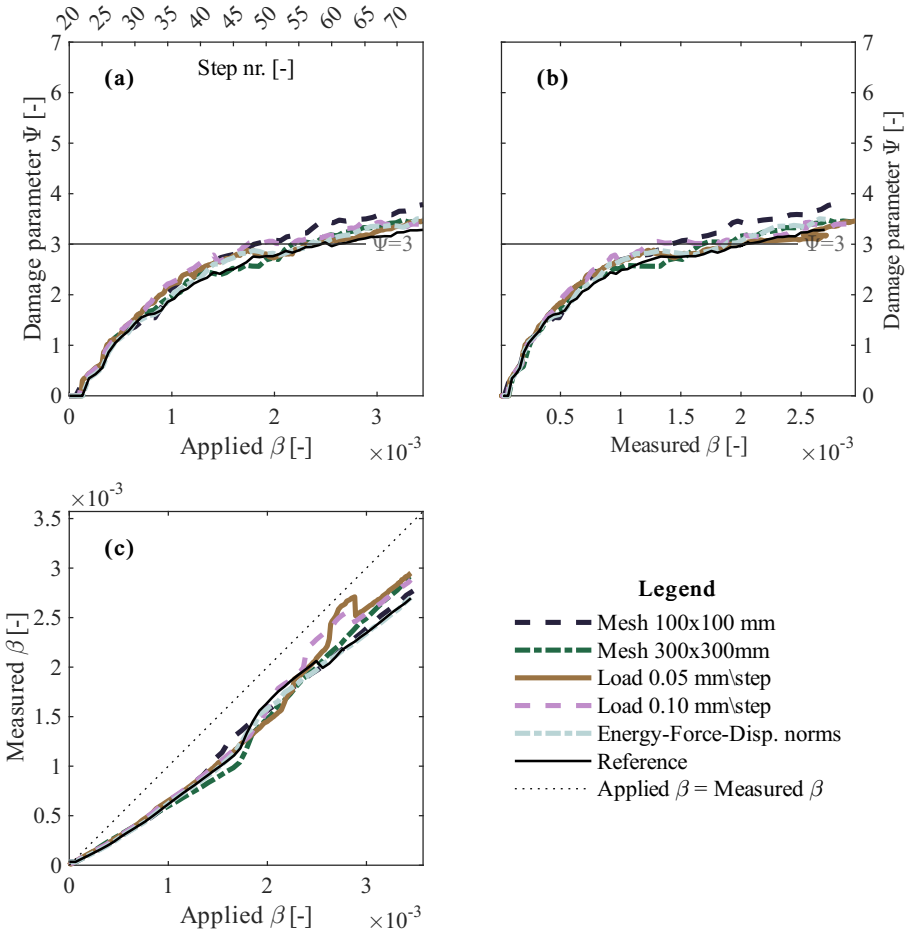

Figure C.21: Results of the sensitivity analyses for a sagging settlement pattern in terms of applied and measured angular distortion against the damage parameter Ψ for the facade labelled as "FH".

C.3. THE INFLUENCE OF THE NUMBER OF ANALYSES

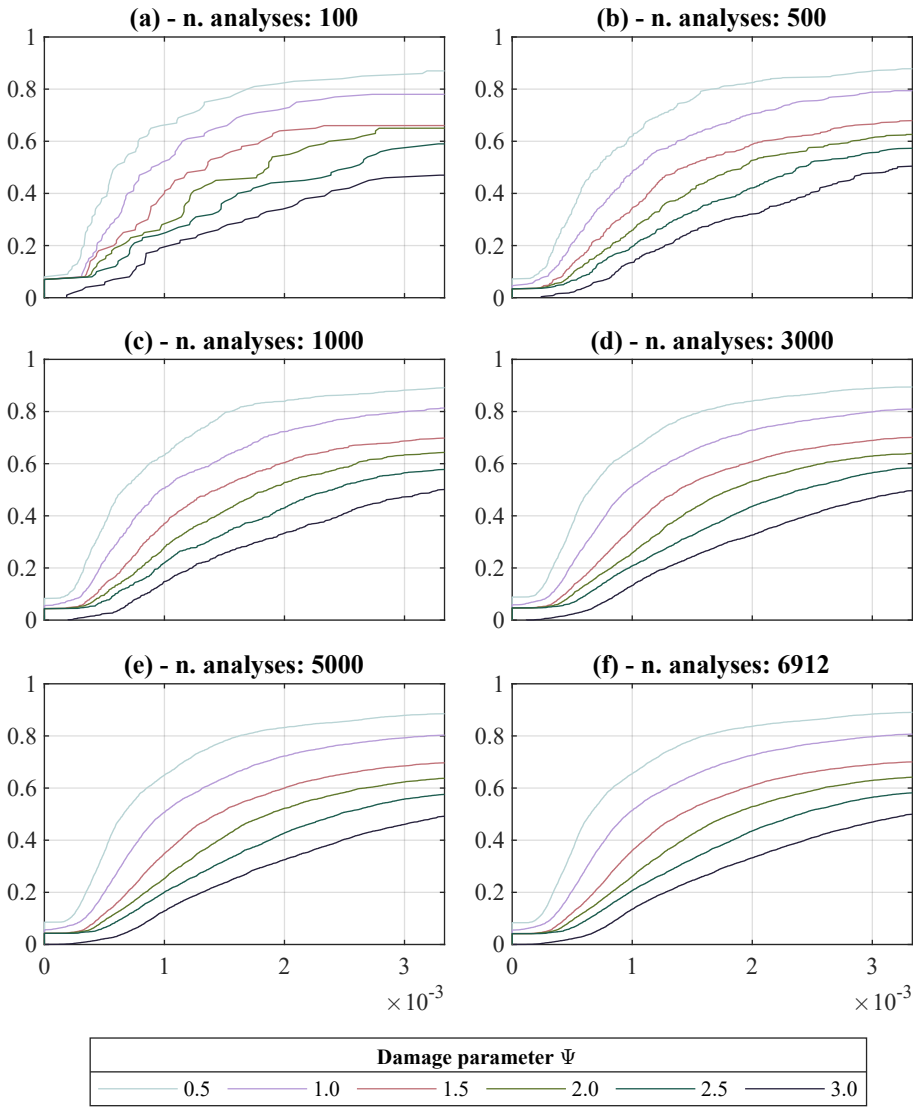

Figure C.22: Additional Example 1: Cumulative density functions for different numbers of analyses. In each plot, the analyses are randomly selected from all the 6912 combinations. This image integrates the results shown in Chapter 8.

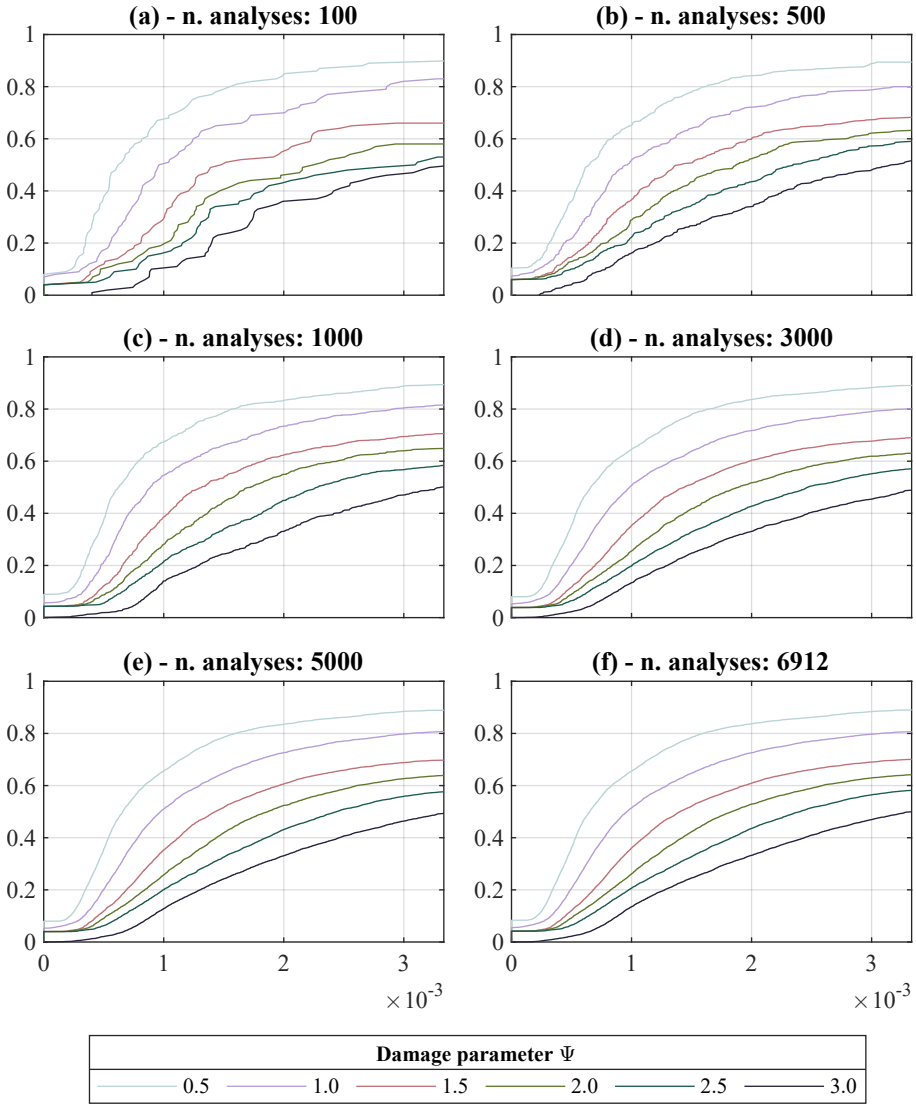

Figure C.23: Additional Example 2: Cumulative density functions for different numbers of analyses. In each plot, the analyses are randomly selected from all the 6912 combinations. This image integrates the results shown in Chapter 8.

C.4. THE INFLUENCE OF THE MASONRY MATERIAL

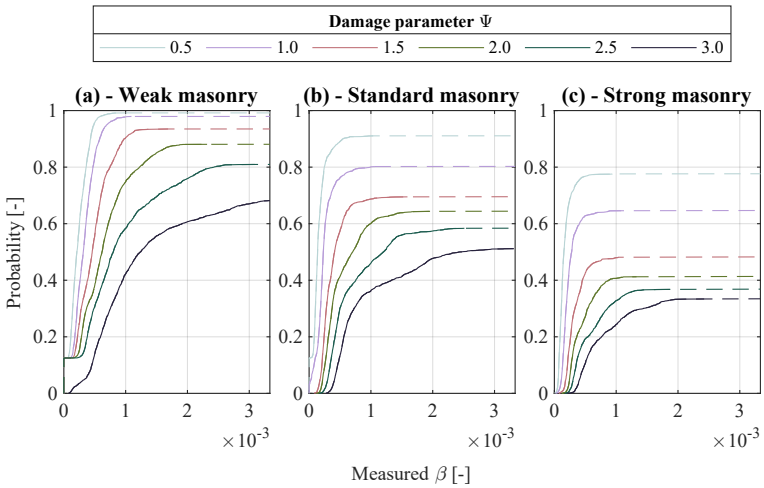

Figure C.24: Cumulative density functions in terms of measured β for each selected masonry material. Dashed lines represent extrapolations.

C.4.1. THE EFFECT OF HOGGING AND SAGGING SETTLEMENT PROFILES

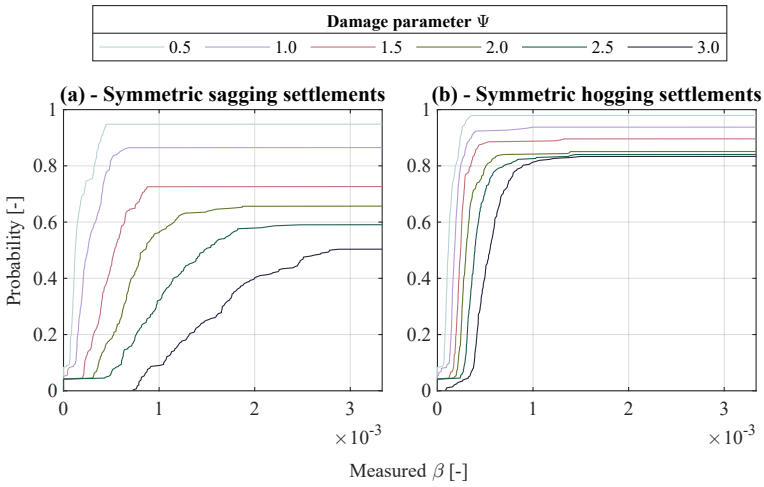

Figure C.25: Cumulative density functions in terms of measured β for (a) **symmetric sagging** and (b) **symmetric hogging** (b) settlements respectively. Each plot presents the outcomes of 288 analyses.

C.5. THE INFLUENCE OF THE FOUNDATION SYSTEM

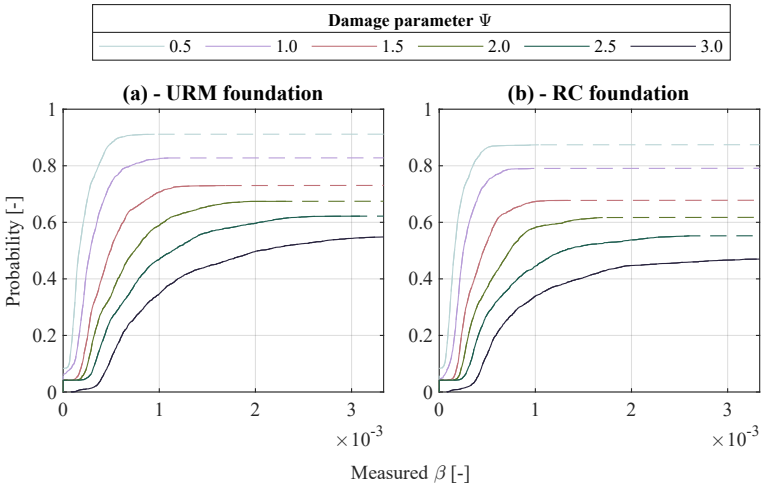

Figure C.26: Cumulative density functions in terms of measured β for each selected foundation system. Dashed lines represent extrapolations.

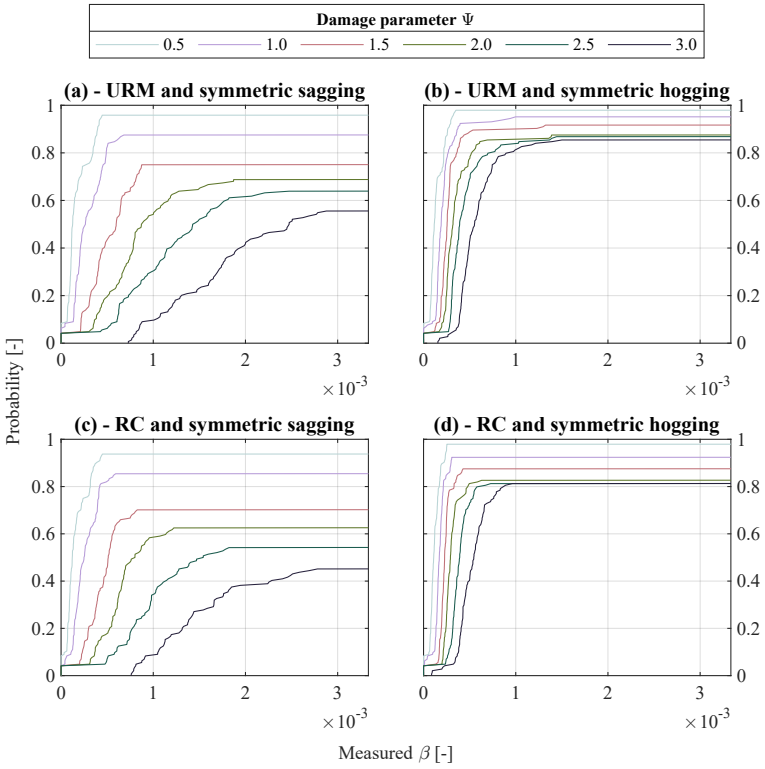

Figure C.27: Cumulative density functions in terms of measured β for each **foundation system** subjected either to symmetric sagging and hogging settlements. Each plot presents the outcomes of 144 analyses.

C.6. THE INTERFACE STIFFNESS

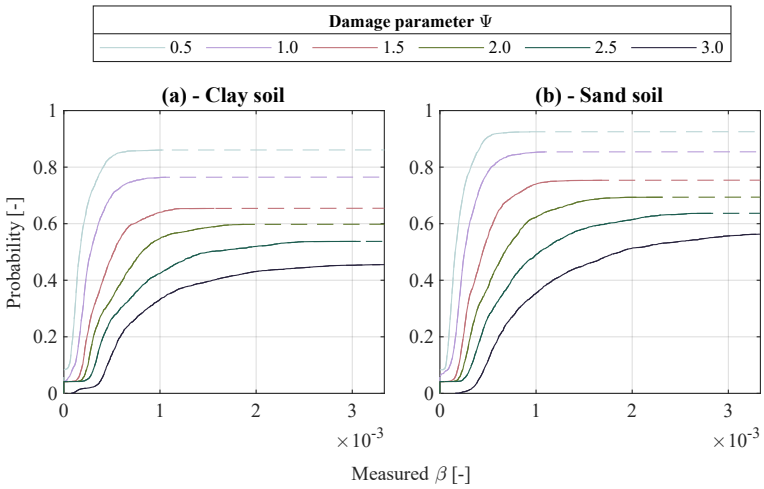

Figure C.28: Cumulative density functions in terms of measured β for each soil material. Dashed lines represent extrapolations.

C.7. THE EFFECT OF EXISTING DAMAGE

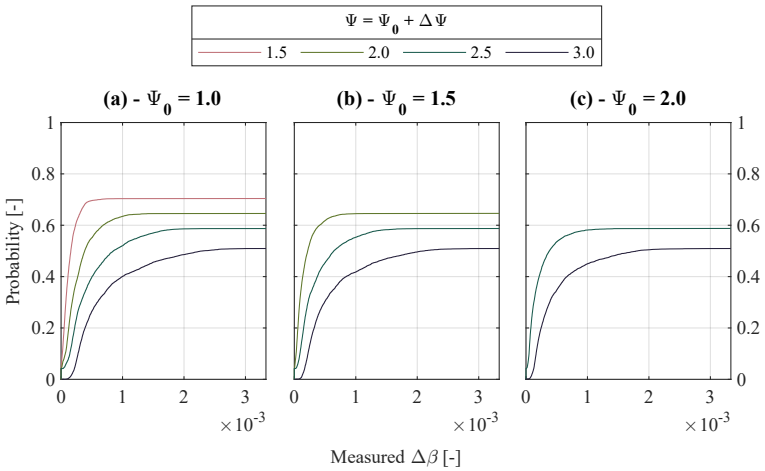

Figure C.29: Fragility curves in terms of measured angular distortion for models with different values of initial damage Ψ_0: (a) $\Psi_0 = 1.0$, (b) $\Psi_0 = 1.5$ and (c) $\Psi_0 = 2.0$.

C.8. THE EFFECT OF THE L/H RATIO

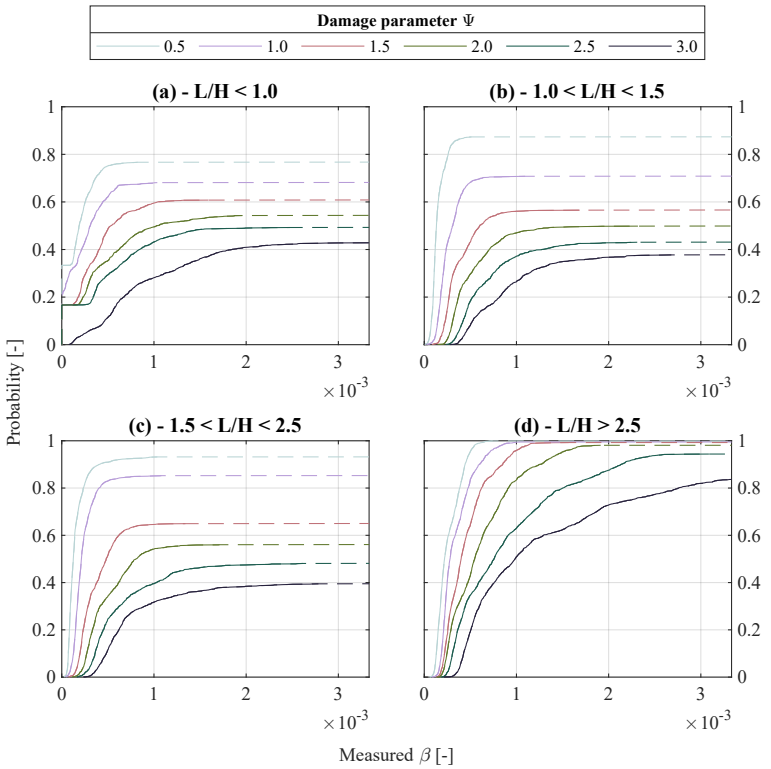

Figure C.30: Cumulative density functions in terms of measured β for different L/H ranges. Dashed lines represent extrapolations.

APPENDIX D
Supervised MSc Projects

This section provides an overview of the MSc projects supervised by the author that are relevant to the topic of this PhD research. In the following, a short abstract that outlines each MSc project is included.

The complete reports are available on the university website repository.tudelft.nl under the section for “education”.

INFLUENCE OF DIFFERENT SUBSIDENCE-RELATED DRIVERS ON DAMAGE TO EXISTING BUILDINGS
Student: Roy P. Meinen

This Thesis provides insight into the relative influence of different subsidence drivers on the damage to existing masonry buildings resting on shallow foundations. Numerical models in PLAXIS 2D are used to compute settlements for various scenarios, including three soil stratigraphies, three building models, and three subsidence drivers. The focus of the modelling is on representing soil settlements rather than accurately depicting the non-linear structural response.

Based on the available literature, two settlement metrics, namely differential settlements and angular distortion, are used to determine the intensity of the computed settlements and, in turn, the damage to the structures.

The findings reveal that the soil scenario had the greatest influence on the induced damage, followed by the subsidence drivers and the building scenarios.

CALIBRATED NUMERICAL MODELS FOR MASONRY BUILDINGS SUBJECTED TO SUBSIDENCE-RELATED GROUND SETTLEMENTS
Student: Javier F. Guadarrama

This study reviews different state-of-the-art empirical, analytical, and numerical assessment methods relevant to evaluating damage in masonry structures experiencing settlements.

Based on the literature review, the selected assessment methods are applied to an existing structure with available levelling measurements and damage information. Therefore, the chosen case study serves as an empirical benchmark to validate the results.

Particular emphasis is given to the numerical methods, that accurately depict the nonlinear cracking behaviour of masonry structures undergoing settlements.

This Thesis assesses the relative effectiveness of different damage assessment methods and identifies their limitations.

APPENDIX E
Datasets

The collected dataset of 386 anonymised buildings used in Chapter 4 is available at:

https://doi.org/10.4121/18279155

The numerical fragility curves developed in Chapter 8, including the ones reported in Appendix C, are available at:

https://doi.org/10.4121/f4ff95cf-5846-45fc-841b-7df7d74e7e5f

A ReadMe file is included in each repository to detail the additional metadata.

List of Figures

1 Relationship between soil strata variability and computed settlements, quantified by correlation length. The results reveal a link between soil variability and superficial settlements at the structural scale. xi

2 Schematic illustration of a 2D non-linear finite element model of a masonry facade on strip foundations subjected to ground settlements, applied progressively at the bottom of the model. Interfaces simulate the contact interaction with the soil. The model includes the effect of transversal walls and foundations, supported by springs. xii

3 An example of the automatic identification of cracks and calculation of Ψ from the results of a facade model subjected to a symmetric hogging settlement. In the legend, the crack width is expressed in μm whereas the crack length is in mm. xiii

4 Fragility curves in terms of measured angular distortions. The curves reveal a probability of cracks up to 5mm (corresponding to Ψ = 3.0) equal to about 47% for an angular distortion measured on the building equal to 2 ‰(or 1/500). xv

5 Relatie tussen de variabiliteit van bodemlagen en de berekende zettingen, gekwantificeerd door de gevonden correlatielengte. De resultaten tonen een verband aan tussen bodemvariabiliteit en maaiveldzettingen op de schaal van gebouwen. xxi

6 Schematische illustratie van een 2D niet-lineair eindige-elementmodel van een metselwerk gevel op strokenfundering, blootgesteld aan zettingen, met toenemende zettingen opgelegd aan de onderkant van het model. Interfaces simuleren de interactie met de ondergrond. Het model omvat het effect van dwarswanden en funderingen, ondersteund in de vorm van veren. xxiii

7 Voorbeeld van de automatische identificatie van scheuren en berekening van Ψ op basis van de resultaten van een gevelmodel blootgesteld aan een symmetrische hogging-zetting. In de legenda wordt de scheurwijdte uitgedrukt in μm en de scheurlengte in mm. xxiv

8 Kwetsbaarheidscurves op basis van gemeten hoekverdraaiing. De curves tonen eenkans op scheuren tot 5 mm (corresponderend met $\Psi = 3.0$) van ongeveer 47% voor een hoekverdraaiing gemeten op het gebouw gelijk aan 2 ‰(of 1/500). xxvi

1.1 (a) Cumulative subsidence prediction map for the period 2020-2050, including the effect of climate change and (b) Risk of differential settlements for buildings on shallow foundations. Data retrieved from klimaateffectatlas.nl [23], [24]. 4

1.2 Outline of the dissertation. In the flowchart, schematic illustrations are included as graphical abstracts for each chapter. 9

1.3 LOSS research program structure, retrieved from [13]. 11

2.1 Mind map that connects the sections of this Chapter. 20

2.2 Examples of masonry buildings located in Delft, the Netherlands. Photographs taken by the Author. 23

2.3 Schematic illustration of the housing typologies in the Netherlands. . . 24

2.4 The relationship between the age of masonry buildings and the types of walls and masonry used in the Netherlands. Retrieved from [15]. 25

2.5 Schematic illustration of some examples of shallow and piled foundations common in the Netherlands. 26

2.6 The cumulative thickness of Holocene deposits in the Netherlands, retrieved from [24]. 27

2.7 Schematic illustration of the different possible subsidence drivers and mechanisms, retrieved from [28]. Natural and human-induced drivers are distinguished, as well as the depth at which they occur. 28

2.8 Illustration of the possible sagging and hogging settlement patterns, with reference to the ground movements. The response of the building and how the displacements are transferred from the soil to the structures is influenced by the soil-structure interaction, see section 2.5.4. 30

2.9 Illustration of the settlement parameters, according to the definition proposed by [34]. Measurements collected with manual surveys are typically collected only for a limited number of levelling points, providing a limited picture. Straight segments are typically used to connect the measurements. 32

2.10 Modification factors from field data versus relative bending stiffness according to [40], [42], [44]. Image retrieved from [7]. The field data confirms the design envelopes by [40], based on numerical analyses. . 36

2.11 Crack patterns due to different settlement shapes modes [47]. Retrieved from [7]. 37

2.12 Relationship of damage to angular distortion and horizontal extension strain, retrieved from [37]. 39

2.13 Schematization of the LTSM approach after [34], [37]. Retrieved from [61], [62]. This illustration shows the application of the method in the case of tunnelling-induced settlements. 41

2.14 Scheme of coupled and semi-coupled modelling techniques for building subjected to settlements. 43

2.15 Examples of local failure mechanisms of the masonry material: (a) joint tensile failure, (b) joint shear failure, (c) brick and mortar tensile failure, (d) diagonal masonry failure and (e) masonry crushing, splitting and spalling under compression. Image retrieved from [84], and published in [85], originally adapted from [86] 45

2.16 Modelling strategies for the masonry material [87]–[89]. While the micro models distinguish the brick and mortar joints, macro models describe the material via anisotropic continuum elements. 45

2.17 Schematic illustration of the components required for damage assessment in the Netherlands. The maps are not based on actual data and are used only for illustration purposes. 46

3.1 Flowchart of the adopted procedure. 62

3.2 Location of the study area and the available cone penetration tests (CPTs). (a) show the location of the study area, plot (b) shows the elevation maps, (c) shows the selected cross-sections over the study area and (d) shows the stratigraphy at each location based on the interpretation of the CPT data [15]. 64

3.3 The voxel columns from the available GeoTOP model: (a) the location of the voxel columns, (b) and (c) the 100 equiprobable realizations for columns 1 and 2 respectively. 66

3.4 Schematic illustration of the relationship between (a) the computed soil lithoclass from the GeoTOP model and (b) the assigned soil type for each voxel column realization. 67

3.5 Schematic illustration of the adopted FE models. The directions x and y represent the local axis of the models. z is the vertical axis along the depth direction. The lower boundary at the bottom of the models is schematically illustrated. 68

3.6 Schematic illustration of the three load scenarios for the 1D, 2D and 3D models. In the models with a double load (b), the load is applied by doubling the mass of the sand material rather than using 2 meters of sand. The decision to double the mass rather than the sand thickness was guided by the structure of the Python code used to generate the models, as it allowed for a more straightforward implementation. . . . 69

3.7 Maps obtained via linear interpolation and box plots of the soil layer thickness and the computed correlation length: (a) and (f) for Dyke material, (b) and (d) for peat, (c) and (g) for organic clay and (d) and (h) for silty clay. The bottom plots, from (i) to (l), show the results of fitting the autocorrelation function described in Eq. (3) through the points of the empirical autocorrelation function, Eq. (1), for each soil material. . 71

3.8 An example of the results of one of the 1D models subjected to the reference load: (a) the CPT interpretation and the groundwater level, (b) the development of the excess pore water pressure and (c) the computed settlements against the time. 73

3.9 The settlement maps derived from the linear interpolation of the final (*i.e.*, 5000 years) settlement computed at each CPT location via the numerical models of the reference load (see Fig. 3.6). 74

3.10 Values of the correlation length of the computed settlement of each soil stata for each loading condition. The values correspond to the mean and the standard deviation of θs considering the five time steps, *i.e.*, 1, 10, 50, 500 and 5000 years for: (a) reference load, (b) double load and (c) no groundwater (see Fig. 3.6). 75

3.11 Empirical distribution functions of the total settlement computed for all the loading conditions and the numerical models, described in section 3.2.2, for the selected time steps. The distributions show the results at the 100 CPTs locations (Fig. 3.2) and the 100 realizations for two voxel columns (Fig. 3.3). The darker and lighter areas in the plots separate the results for the CPTs and the voxel columns, respectively. The red cross (+) markers show the mean of each distribution. 76

4.1 Flowchart of the adopted procedure. The definition of the settlement-related intensity parameters are detailed in Fig. 4.2. 86

4.2 Typical building damage for sagging and hogging profiles and the definitions of the settlement parameters: maximum settlement ρ_{max}, minimum settlement ρ_{min}, differential settlement $\delta\rho_{max}$, rotation θ, relative rotation (or angular distortion) β, deflection Δ, deflection ratio Δ/L and tilt ω. 87

4.3 The selected settlement shapes, conformed to a Gaussian distribution that idealizes the most recurrent bed joint levelling measurement shapes, based on the visual observation: (a), (c), (e) and (g) idealize four settlement profiles while (b), (d), (f) and (h) the hogging ones. All the profiles are computed by means of equation 4.1 by varying the position of the wall x and the distance of the inflection point xi. 89

4.4 Explanatory illustration of ROC curve: (a) distribution of undamaged and damaged cases as a function of the settlement-related parameter; (b) conceptual ROC curve, the optimized threshold value is determined using the closest-to-(0,1) criterion [16], which identifies the sensitivity pair that is at the minimum distance (d_{min}) from the perfect classifier (0,1). 91

4.5 A schematic illustration of the selected building typologies based on the structural features and the adjacency with other structures: (a) Unit House (UH), (b) Block Unit Single (UBHS), (c) Block Unit Multiple (UBHM), and (d) Others (OTH). 94

4.6 An example of the levelling measurements, pictures of damage and technical notes for one of the buildings in the collected dataset. 96

4.7 Box plot of damage level vs. settlement-related intensity parameters for (a), (c), (e) and (g) for shallow and b), d), f) and h) for deep foundations. The damage level generally increases as the selected SRI parameters increase. 97

4.8 Non-dimensional sagging settlement profiles of the considered surveyed buildings: from (a0) to (d0) Proposed settlement profiles (Figure 4.3a,c,e and g); Settlement profile for: from (a1) to (d1) for buildings on shallow foundations, and from (a2) to (d2) for buildings on deep foundations. The number of cases for each foundation system is indicated on top of each bin from (a3) to (d3). 99

4.9 Non-dimensional hogging settlement profiles of the considered surveyed buildings: from (a0) to (d0) Proposed settlement profiles (Figure 4.3b,d,f and h); Settlement profile for: from (a1) to (d1) for buildings on shallow foundations, and from (a2) to (d2) for buildings on deep foundations. The number of cases for each foundation system is indicated on top of each bin from (a3) to (d3). 100

4.10 ROC curves for the selected SRI parameters (a), (c), (e) and (g) for shallow and b), (d), (f) and (h) deep foundations. Each SRI parameter varies between 0 and the maximum recorded value. The black dot shows the best sensitivity-pair. The shaded area represents the Area Under the Curve (AUC). 102

4.11 Fragility curves of buildings resting on shallow and deep foundations for all the SRI parameters obtained with "Approach 1" (section 4.2.5). . 103

4.12 Fragility curves of buildings resting on shallow and deep foundations for all the SRI parameters obtained with "Approach 2" (section 4.2.6). . 105

5.1 Flowchart of the adopted procedure. 118

5.2 Illustration of the intended mechanical model and the adopted FE modelling approach, the features included and the variations investigated. Number of variations per parameter indicated in parenthesis (N). The foundation systems adopted in the model are shown in detail in Figure 5.4, while the settlement profiles applied at the bottom edge of the interface are shown in Figure 5.5. 118

5.3 Reference geometries for the masonry facade. The geometries from a1) to e2) are characterized by an opening ratio ($A_{opening}/A_{facade}$) of 0.27. The model f) represents the reference case. The height of the openings of f) is modified arbitrarily for the geometries g) and h) to obtain the two selected opening percentages (*i.e.*, 0.10 and 0.20 respectively). The foundation systems adopted in the model are shown in detail in Figure 5.4. Not to scale. Measures in meters. 120

5.4 Sketch of the recurrent strip foundation systems in the Netherlands: (a) URM foundation, (b) RC block foundation, (c) RC strip with masonry layer on top and (d) RC strip with stiffening RC beam. The level of the ground surface and the view in the plane of the façade are shown for each foundation system. Upper and lower reinforcement bars are represented as equivalent embedded bars. The equivalent section of each bar was based on the design values of existing structures. Measures in millimetres. 121

5.5 The applied settlement profiles, that reproduce a loss of support underneath the strip foundation, computed from a Gaussian shape for a façade of 8 meters and an angular distortion β equal to 1/10 (illustrated as a shaded area), defined according to the definition proposed by [7]: a) SAG1, b) HOG1, c) SAG2, d) HOG2, e) SAG3, f) HOG3, g) SAG4 and h) HOG4. All profiles were obtained by considering different positions of the façade over the displacement distributions, as schematically indicated in the centre pictures. The settlement shapes are applied in the numerical model with increasing amplitude as illustrated in i). 124

5.6 Crack patterns of the masonry façade for all the settlement profiles at step 60 (maximum applied settlement equals to about 11 mm) of the numerical model: a) HOG1, b) HOG2, c) HOG3, d) HOG,4 e) SAG1, f) SAG2, g) SAG3 and h) SAG4. Note that for a given numerical step the applied settlement configurations are not characterized by the same value of the angular distortion, due to the variable load step, as discussed in section 5.2. The cracks' width in the plots is exaggerated. 128

5.7 Influence of the settlement configuration on the applied vs. retrieved settlement parameters for each level of damage for: angular distortion for a) hogging and b) sagging, rotation for c) hogging and d) sagging, deflection ratio for e) hogging and f) sagging, differential settlement for g) hogging and h) sagging. The shapes of the settlement profiles (not to scale) are shown for clarity. Plots in the logarithmic scale. 129

5.8 Differences of the applied vs. retrieved angular distortion for each level of damage for the variation of the: a) material typology, b) variation of the elastic parameters. The secondary x- and y- axes (on top and the right of the plots) show the values of the angular distortion as $1/\beta^{-1}$, as typically adopted in the literature. 130

5.9 Influence of the length over height (L/H) ratio on the difference between applied vs. retrieved angular distortion. The secondary x- and y- axes (on top and on the right of the plots) show the values of the angular distortion as $1/\beta^{-1}$, as typically adopted in the literature. 131

5.10 Differences of the applied vs. retrieved angular distortion for each level of damage for the variation of the: a) mass density, b) opening percentage and c) presence of the transverse walls. The secondary x- and y- axes (on top and on the right of the plots) show the values of the angular distortion as $1/\beta^{-1}$, as typically adopted in the literature. 132

5.11 Differences of the applied vs. retrieved angular distortion for each level of damage for the variation of the foundation typology. The secondary x- and y- axes (on top and on the right of the plots) show the values of the angular distortion as $1/\beta^{-1}$, as typically adopted in the literature. . 133

5.12 Differences of the applied vs. retrieved angular distortion for each level of damage for the variation of the: a) interface stiffness, b) interface model, c) soil type. The secondary x- and y- axes (on top and on the right of the plots) show the values of the angular distortion as $1/\beta^{-1}$, as typically adopted in the literature. 133

5.13 Sensitivity chart of the results of all the numerical models. The x-axis in the logarithmic scale shows the ratio between the mean applied angular distortion β_a and the one of the reference model. The results are categorized by the number of models used to study the influence of each parameter by a dashed line. 134

5.14 Modification factors for the deflection ratio with relative bending stiffness for all Ψ values. Design curves from [37]. The results refer to all the façade models and all the settlement profiles. 136

5.15 Cumulative density function for all the Ψ values for the retrieved: (a) angular distortion β_r, (b) rotation θ_r, (c) deflection ratio Δ/L_r and (d) differential settlement $\delta\rho_r$. The secondary x-axes (on top of the plots of the (a) angular distortion, (b) rotation and (c) deflection ratio) show the values of the parameters as $1/x^{-1}$, as typically adopted in the literature. 137

6.1 The six modelling approaches selected from the state-of-the-art: (a) 2D FAçade model (2DFA); (b) 2D façade with lateral Short Flanges (2DSF); (c) 2D façade with lateral Long Flanges (2DLF); (d) 3D FAçade model (3DFA); (e) 3D BOX model (3DBOX); (f) 3D FULL model (3DFULL). Measures in meters. 149

6.2 The calculation of the cross-section of the lateral beam elements used in the model 2DLF (Figure 6.1c). Measures in meters. 151

6.3 The two settlement shapes imposed at the base of the interfaces in the finite element models: (a) Hogging and (b) Sagging. The settlement profiles are conformed to a Gaussian curve. Their angular distortion is equal to 1/300. Measures in meters. 154

6.4 An example of the progression of the damage for model 2DLF (Figure 6.1c) and 3DFULL (Figure 6.1f) for the imposed hogging settlement (Figure 6.3a) for different values of imposed distortion βa. The principal crack width (Ecw1) is shown. 3DFULL depicts half the model. 155

6.5 Applied and Retrieved angular distortion β against the resulting damage parameter Ψ for all the FE models for both hogging and sagging. The results of the models 2DFA and 3DFA overlap in all the plots. 156

6.6 Resulting crack patterns for all the FE models at an applied angular distortion of 2 ‰(or 1/500). The principal crack width (Ecw1) is shown. The damage parameter Ψ is reported for every model. (e1), (f1), (e2) and (f2) depict half the model. 157

6.7 The resulting vertical displacements (TDtZ in the Legend) for all the FE models at an applied angular distortion of 2 ‰(or 1/500). Deformations are exaggerated (The magnification factor is equal to 500). The damage parameter Ψ is reported for every model. (e1), (f1), (e2) and (f2) depict half the model. 158

6.8 Out-of-plane (OOP) displacements (TDtY in the Legend) for all the FE models 3DBOX and 3DFULL at an applied angular distortion of 2 ‰(or 1/500) for both hogging and sagging. Deformations are shown and exaggerated along the direction of the transverse walls (The magnification factor is equal to 5000). The plots depict half the models. 159

6.9 Normal (*i.e.*, direction of gravity) interface stresses for hogging and sagging, with applied angular distortion of 2 ‰(or 1/500). Positive values represent tension, and negative ones, compression. (e1), (f1), (e2) and (f2) depict half the model. 160

7.1 Flowchart of the adopted methodology. Steps 1 and 2 are detailed in Chapter 7, whereas Step 3 is in Chapter 8. 172

7.2 Aerial view of the ground and 3D view of city centre of Delft. From the website 3DBAG.nl [4]. 175

7.3 An example of the unfolded geometry of two buildings showing the individual walls' length and height: (a) the 3D visualization of the building and (b) the identified facades. 176

7.4 Histogram of the year of construction for existing buildings in the Netherlands available in the BAG 3D database [1], [2]. The data refers to the buildings identified as "in use" ("*pand in gebruik*", in Dutch [7]). The data for buildings that have been demolished is not available. 177

7.5 Recurrent shapes of the walls distinguished in found macro-categories. Each wall is automatically assigned to one of the categories. 178

7.6 Histograms of the walls' length (a) and height (b). (c) shows the length-over-height ratio. 179

7.7 The selected facades adopted in the numerical models. Each facade is associated with an ID which is only used to further reference them. . . 181

7.8 (a) Bivariate histogram showing the relationship between Length L, Height H for walls with an assigned shape built until 1970 and (b) bar plots of the shapes of the walls among the selected cases. 183

7.9 Number of walls from buildings with assigned shape and built until 1970, divided by the most similar case among selected facades (Fig. 7.7). The percentage of cases assigned to each facade compared to the total of 20 million is shown. 184

7.10 The calculation of the effective flange width of the transversal walls adopted in the FE models. 186

7.11 The strip foundation systems adopted in the numerical models. In the FE models, the soil volume is not modelled explicitly, and it is represented in the image to illustrate the intended depth of the foundation. 187

7.12 General characteristics of Engineering Masonry model. Retrieved from [11]. 188

7.13 An example of the adopted FE mesh for facade "FA" with an unreinforced masonry foundation: (a) screenshot of the mesh from the numerical models and (b) 3D illustration of the FE including the thickness of the elements. The transversal walls and foundations are not included in the illustration. 191

7.14 Schematic illustration of the interpretation of the parameters of the Gaussian formulation adopted to idealise the settlement shapes. . . . 192

7.15 The derived settlement shapes adopted in the numerical analyses are based on arbitrary intervals of the parameters D_x, x_i and ι. 193

7.16 The linear relationship between the maximum settlement, progressively increased with a load step equal to 0.2 mm/step, and the applied angular distortion β for facade "FA" and for the settlement shape with ι = 1, D_x=0.5 and x_i=0.5. 194

7.17 Schematic illustration of the location and types of loads applied to the selected facades. 202

7.18 Schematic illustration of the location of "applied" and "measured" displacements in the adopted FE models. Applied displacements (and their relative angular distortion β) refer to the settlement pattern imposed in the bottom at the bottom of the interface elements. Measured displacement (and the measured angular distortion β) are retrieved at the bottom of the facade (top edge of the foundation). 202

7.19 Results of the reference model subjected to symmetric hogging: (a) contour plots of the max. crack width (with a magnification factor of the deformations equal to 100) and (b) principal stresses. 203

7.20 Results in the reference case in hogging: (a) Applied angular distortion β_a for each step of the analysis, (b) step number against the max. crack width, (c) step number against Ψ and (d) Max. crack width against Ψ. The dashed line represents the trend for one individual crack [24]. . . . 204

7.21 The different mesh sizes selected for the sensitivity analyses. 204

7.22 Results of the sensitivity analyses for the reference case in hogging in terms of applied and measured angular distortion against the damage parameter Ψ. 205

7.23 Crack patterns of all the models adopted in the sensitivity analyses for an applied angular distortion equal to 1/1000 (or 1.00 ‰) in hogging. The contour plots show the max. crack width. Deformations are not shown. 206

7.24 Crack patterns of all the models adopted in the sensitivity analyses for an applied angular distortion equal to 1/500 (or 2.00 ‰) in hogging. The contour plots show the max. crack width. Deformations are not shown. 207

7.25 Step number against the number of iterations for each of the selected models in hogging. The right y-axis shows the damage parameter Ψ. The plots purposefully focus on Ψ values ranging between 0 and 3. Two colors distinguish the left y-axis (number of iterations, in black) from the right y-axis (Ψ values, in red). 208

7.26 Results of the sensitivity analyses for a sagging settlement pattern in terms of applied and measured angular distortion against the damage parameter Ψ. 209

7.27 Crack patterns of all the models adopted in the sensitivity analyses for an applied angular distortion equal to 1/500 (or 2.00 ‰) in **sagging**. The contour plots show the max. crack width. Deformations are not shown. 210

7.28 Results of the sensitivity analyses for a hogging settlement pattern in terms of applied and measured angular distortion against the damage parameter Ψ for the facade labelled as "FB". 211

8.1 The cumulative density curves of all the selected facade geometries. The cumulative density curves describe the probabilities of reaching or exceeding specific levels of damage, expressed by Ψ values, as a function of the applied angular distortion. 218

8.2 The numerical cumulative density curves in terms of **applied** angular distortion against the probability of damage for all the selected facade geometries. 219

8.3 The numerical cumulative density curves in terms of **measured** angular distortion against the probability of damage for all the selected facade geometries. 220

8.4 Cumulative density functions for different numbers of analyses. In each plot, the analyses are randomly selected from all the 6912 combinations. 221

8.5 Cumulative density functions in terms of applied β for each selected **masonry material**. Each plot presents the outcomes of 2304 analyses. 222

8.6 Cumulative density functions in terms of applied β for (a) **symmetric sagging** and (b) **symmetric hogging** (b) settlements respectively. Each plot presents the outcomes of 288 analyses. 222

8.7 Cumulative density functions in terms of applied β for each **foundation system**. Each plot presents the outcomes of 3456 analyses. 223

8.8 The different sets of foundation systems used in: (a) Fragility curves by Korswagen et al., 2022 [4] and (b) Chapters 7 and 8 of this thesis. The foundation systems in (b) are further detailed in Fig. 7.11 in section 7.3.2. 224

8.9 Cumulative density functions in terms of applied β for each **foundation system** subjected either to symmetric sagging and hogging settlements. Each plot presents the outcomes of 144 analyses. 226

8.10 Cumulative density functions in terms of applied β for **each selected soil**. Each plot presents the outcomes of 3456 analyses. 227

8.11 Cumulative density functions in terms of applied β for **different L/H ranges**. Each plot presents the outcomes of 1728 analyses. 228

8.12 Box plot of applied angular distortion for all the models at Ψ equal to 0.5, segregated by the different selected parameters. Each box plot shows the median of each subsample as a black dot inside a white circle, and the interquartile range as a thick bar. The lines that go from the interquartile range to the left and right of each box plot represent the whiskers, which extend to the most extreme data points not considered outliers. The whisker length is equal to 1.5 times the interquartile range. Outliers are represented as dots. A wide bar conveys a large variability. 229

8.13 Box plot of applied angular distortion required for model FA to exhibit Ψ equal to 0.5. Each boxplot in Fig. 8.13 shows the effect of the variation of a single parameter while keeping the other parameters fixed at the reference case (Facade "FA", "Standard" Masonry, "URM" foundation and "Sand" soil). Each box plot shows the median of each subsample as a black dot inside a white circle, and the interquartile range as a black bar. The lines that go from the interquartile range to the left and right of each box plot represent the whiskers, which extend to the most extreme data points not considered outliers. The whisker length is equal to 1.5 times the interquartile range. Outliers are represented as dots. 231

8.14 Fragility curves in terms of applied angular distortion for models with different values of initial damage Ψ_0: (a) $\Psi_0 = 1.0$, (b) $\Psi_0 = 1.5$ and (c) $\Psi_0 = 2.0$. 231

8.15 Comparison of the fragility curves in terms of **applied angular distortion** between the results of this study and the one by Korswagen et al., 2022 [4]. 234

8.16 Comparison of the fragility curves in terms of **measured angular distortion** between the results of this study and the one by Korswagen et al., 2022 [4]. 235

8.17 An example of the 3D coupled models adopted in Korswagen et al., 2024 [5]. Displacements are applied at the bottom of the soil volume, and their intensity is quantified by the angular distortion. Horizontal strains are applied at the side of the soil volume. The models make use of symmetry, and thus half of the domain is represented. 237

8.18 Comparison of the fragility curves in terms of **applied angular distortion** between the results of this study and the one by Korswagen et al., 2024 [5]. The fragility curves by [5] are segregated by increasing values of horizontal strains corresponding to different settlement-scenarios. . . 238

8.19 Comparison of the proposed fragility curves in terms of (a) applied and (b) measured angular distortion with the ones of Zhang and Ng, 2005 [6]. 240

8.20 Comparison of the proposed fragility curves in terms of measured angular distortion with the ones of Peduto et al., 2019 [7]. 241

8.21 Comparison of the proposed fragility curves in terms of measured angular distortion with the proposed in Chapter 4 of this thesis. 243

8.22 Comparison of the fragility curves grouped as "light damage" in terms of measured angular distortion with the curves proposed in Chapter 4 of this thesis. 245

9.1 Schematic illustration of the links between different soil heterogeneity, the differential settlement and the damage to buildings: (a) regional assessments and (b) at the scale of single structures. The links between the different aspects relevant to damage assessment analyses are indicated. 261

9.2 Schematic illustration of numerical models including (a) lithological soil heterogeneity, (b) the variability of the soil properties and (c) the combination of the two effects. Similar models could be used to explore the link between soil heterogeneity and damage to structures. 263

9.3 Loading scheme for the model that explores the effect of shrinkage and swelling alternation. 267

9.4 Crack pattern obtained at the end of each loading step. The contour plot refers to the maximum crack width. The absolute deformation of the façade is shown with a magnification factor equal to 30. 268

9.5 The crack patterns of two models after the application of the settlement load: one model without initial damage and another with an imposed pre-damage. The absolute deformation of the façade is shown with a magnification factor equal to 30. 268

A.1 Differences between the Fragility Curves presented in [2] (dashed lines) and the ones proposed in this Dissertation in Chapter 4 (solid lines). . 277

C.1 Sizes of the facade labelled as "FA" used in the analyses presented in Chapters 7 and 8. The illustration is not in scale. 286

C.2 Sizes of the facade labelled as "FB" used in the analyses presented in Chapters 7 and 8. The illustration is not in scale. 286

C.3 Sizes of the facade labelled as "FC" used in the analyses presented in Chapters 7 and 8. The illustration is not in scale. 287

C.4 Sizes of the facade labelled as "FD" used in the analyses presented in Chapters 7 and 8. The illustration is not in scale. 287

C.5 Sizes of the facade labelled as "FE" used in the analyses presented in Chapters 7 and 8. The illustration is not in scale. 288

C.6 Sizes of the facade labelled as "FF" used in the analyses presented in Chapters 7 and 8. The illustration is not in scale. 288

C.7 Sizes of the facade labelled as "FG" used in the analyses presented in Chapters 7 and 8. The illustration is not in scale. 289

C.8 Sizes of the facade labelled as "FH" used in the analyses presented in Chapters 7 and 8. The illustration is not in scale. 289

C.9 Results of the sensitivity analyses for a hogging settlement pattern in terms of applied and measured angular distortion against the damage parameter Ψ for the facade labelled as "FC". 290

C.10 Results of the sensitivity analyses for a hogging settlement pattern in terms of applied and measured angular distortion against the damage parameter Ψ for the facade labelled as "FD". 291

C.11 Results of the sensitivity analyses for a hogging settlement pattern in terms of applied and measured angular distortion against the damage parameter Ψ for the facade labelled as "FE". 292

C.12 Results of the sensitivity analyses for a hogging settlement pattern in terms of applied and measured angular distortion against the damage parameter Ψ for the facade labelled as "FF". 293

C.13 Results of the sensitivity analyses for a hogging settlement pattern in terms of applied and measured angular distortion against the damage parameter Ψ for the facade labelled as "FG". 294

C.14 Results of the sensitivity analyses for a hogging settlement pattern in terms of applied and measured angular distortion against the damage parameter Ψ for the facade labelled as "FH". 295

C.15 Results of the sensitivity analyses for a sagging settlement pattern in terms of applied and measured angular distortion against the damage parameter Ψ for the facade labelled as "FB". 296

C.16 Results of the sensitivity analyses for a sagging settlement pattern in terms of applied and measured angular distortion against the damage parameter Ψ for the facade labelled as "FC". 297

C.17 Results of the sensitivity analyses for a sagging settlement pattern in terms of applied and measured angular distortion against the damage parameter Ψ for the facade labelled as "FD". 298

C.18 Results of the sensitivity analyses for a sagging settlement pattern in terms of applied and measured angular distortion against the damage parameter Ψ for the facade labelled as "FE". 299

C.19 Results of the sensitivity analyses for a sagging settlement pattern in terms of applied and measured angular distortion against the damage parameter Ψ for the facade labelled as "FF". 300

C.20 Results of the sensitivity analyses for a sagging settlement pattern in terms of applied and measured angular distortion against the damage parameter Ψ for the facade labelled as "FG". 301

C.21 Results of the sensitivity analyses for a sagging settlement pattern in terms of applied and measured angular distortion against the damage parameter Ψ for the facade labelled as "FH". 302

C.22 **Additional Example 1**: Cumulative density functions for different numbers of analyses. In each plot, the analyses are randomly selected from all the 6912 combinations. This image integrates the results shown in Chapter 8. 303

C.23 **Additional Example 2**: Cumulative density functions for different numbers of analyses. In each plot, the analyses are randomly selected from all the 6912 combinations. This image integrates the results shown in Chapter 8. 304

C.24 Cumulative density functions in terms of measured β for each selected masonry material. Dashed lines represent extrapolations. 305

C.25 Cumulative density functions in terms of measured β for (a) **symmetric sagging** and (b) **symmetric hogging** (b) settlements respectively. Each plot presents the outcomes of 288 analyses. 305

C.26 Cumulative density functions in terms of measured β for each selected foundation system. Dashed lines represent extrapolations. 306

C.27 Cumulative density functions in terms of measured β for each **foundation system** subjected either to symmetric sagging and hogging settlements. Each plot presents the outcomes of 144 analyses. 306

C.28 Cumulative density functions in terms of measured β for each soil material. Dashed lines represent extrapolations. 307

C.29 Fragility curves in terms of measured angular distortion for models with different values of initial damage Ψ_0: (a) $\Psi_0 = 1.0$, (b) $\Psi_0 = 1.5$ and (c) $\Psi_0 = 2.0$. 308

C.30 Cumulative density functions in terms of measured β for different L/H ranges. Dashed lines represent extrapolations. 309

List of Tables

2.1 Calculated (relative) bending stiffness White House. Retrieved from [7]. 35

2.2 Damage scale with classification of visible damage based on ease of repair and the crack width [48]. The category of damage was later introduced by [37] and refined by [5]. 38

2.3 Bending and shear strains for the equivalent beam model. Retrieved from [7]. The term "t" represents the distance of the neutral axis to the edge of the beam, assumed to be equal to 0.5H in sagging and H in hogging. Δ/L represents the deflection ratio. 41

3.1 Material properties of each soil layer. Sources: 1 - from [15]; 2 - from [20]; 3 - estimated values. 65

3.2 The adopted phased analyses and numerical settings. 67

3.3 Mean (μ) and coefficient of variation (CoV) values of the computed settlement at the surface level for all the numerical analyses and all the loading conditions. A colour scheme is applied to each parameter, *i.e.* μ and CoV, to distinguish the lowest (dark shades) and the highest (light shades) values. 77

4.1 Damage scale with the classification of visible damage based on ease of repair and the crack width (from [7]–[10]). 88

4.2 Parameters adopted in equation 4.1 to generate the settlement shapes. The values of D_x and x_i should be multiplied by the length of the wall, which is unitary for the shapes shown in Figure 4.3. The shapes "SAG4" and "HOG4" correspond to the profiles "SAG3" and "HOG3" respectively, with the high distortion parts of the SAG3 and HOG3 curves mirrored (see fig:fig 4.4). 90

4.3 Contingency table. 91

4.4 Summary of building data for some provinces distinguished by foundation type, building typology and year of construction. 95

4.5 Median $\overline{SRI}_i$ and Standard deviation ζ of the lognormal distribution obtained with Approach 1 (section 4.2.5) for each considered settlement parameter distinguished by foundation type and damage level. 104

4.6 Median $\overline{SRI}_i$ and Standard deviation ζ of the lognormal distribution obtained with Approach 2 (section 4.2.6) for each considered settlement parameter distinguished by foundation type and damage level. 106

5.1 Adopted material properties for the masonry in the numerical models. 122

5.2 Adopted material properties for the reinforced concrete in the numerical models. 123

5.3 Characteristics of the iterative scheme. 125

5.4 Material properties of the soil types considered. 126

5.5 Damage scale with classification of visible damage based on the crack width and discretization of the damage parameter in sub-levels (adapted from [28], and [29]). 127

5.6 Reduction factor of wall bending stiffness EI (from Melis and Ortiz [41]). 136

5.7 Overview of the available literature limit values [7], [14], [43]–[49] with the estimated Ψ values and corresponding probabilities of exceedance. 138

6.1 Material properties adopted in the FE models. 152

6.2 A comparison of the performance of all the adopted models. The values of the proposed modelling approach 2DLF (Figure 6.1c) are shaded. . . 161

7.1 Geometrical parameters of the selected facades shown in 7.7. 182

7.2 Material properties adopted in the FE models. The properties are schematically illustrated in Fig. 7.12. 188

7.3 The loads adopted in the finite element analyses of each facade, according to the loading scheme shown in Fig. 7.17. 195

7.4 The adopted convergence norms. 197

7.5 Variation of the applied and measured angular distortion for different values of Ψ for the reference case subjected to hogging. A colour scheme is applied to distinguish between the lowest (dark cells) and the highest (light cells) values. 199

8.1 Summary of the angular distortion for buildings on shallow foundations, retrieved from [6]. 240

8.2 Damage scale with different classifications of visible damage based on ease of repair and the crack width adopted in this thesis: Category of damage (polka dotted) retrieved from [12]; Damage classification system (white background) from [13], [14]; Damage group from Chapter (dark grey filling and white text) 4; Damage levels and parameter of damage from [15]. 244

8.3 Overview of the available literature limit values and their corresponding probability of damage for each Ψ value, based on the numerical fragility curves in terms of **applied β presented in this Chapter.** 246

8.4 Overview of the available literature limit values and their corresponding probability of damage for each Ψ value, based on the numerical fragility curves in terms of **measured β presented in this Chapter.** 247

A.1 Overview of the typos found among the levelling measurements stored in the dataset [1], [3]. 277

CURRICULUM VITAE

Alfonso PROSPERI

25-10-1994	Born in Nocera Inferiore, Italy.
2013–2017	Bachelor of Science (B.Sc.) in Civil Engineering. *University of Salerno, Italy.*
2016–2017	Curricular Bachelor's Internship. *Transportation System Analysis Laboratory, University of Salerno, Italy.*
2017–2020	Master of Science (M.Sc.) in Civil Engineering. *University of Salerno, Italy.*
2018–2018	Part-time collaboration: Support activities for the administrative offices. *University of Salerno, Italy.*
2020–2020	Master Graduate (thesis) Internship. *Deltares, The Netherlands.*
2020–2024	Doctor of Philosophy (Ph.D.) Candidate. *Delft University of Technology, The Netherlands.*
2024–present	Postdoc Researcher. *Delft University of Technology, The Netherlands.*

ACKNOWLEDGEMENTS

Back in October 2020, I moved to the Netherlands, eager to start a PhD at TU Delft. I remember feeling grateful for the opportunity to pursue my dream of working in research. I felt welcomed by the Dutch landscape, with its picturesque countryside, flat fields, windmills, and charming built heritage. Eventually, the Netherlands became my home, and I've always considered myself fortunate to have the opportunity to contribute to work to contribute to the preservation and study of its beautiful buildings.

Nevertheless, many things happened during my PhD journey. It has been a roller-coaster of both good and bad experiences, and reaching the end would not have been possible without the help and support of many wonderful people, to whom I would like to express my gratitude.

I was introduced to the topics of soil-structure interaction and damage to buildings by my MSc thesis supervisor **Dario Peduto**. He, along with **Enzo Martinelli** and **Gianfranco Nicodemo**, guided and encouraged me. They helped me reach heights I wouldn't have believed possible. During my thesis, I had the opportunity to undertake an internship at Deltares, where I received support from **John Lambert** and **Ana Laura Costa**. Their guidance has been greatly appreciated.

I'd like to extend my gratitude to my promotor, **Jan G. Rots**, and co-promotor, **Mandy Korff**, who also supervised me during my internship at Deltares. They both encouraged, inspired and generously supported me throughout my PhD journey.

Jan has always demonstrated his deep knowledge and passion for many engineering topics. It is hard to not notice his enthusiasm for research and projects, and he also has a great sense of humour. He once asked me "*Does your life always converge?*" Unfortunately, it does not. However, if it hasn't diverged completely, it is also thanks to **Jan**'s support.

Mandy was, in a way, the first person to believe in me, even when I did not. At the beginning of the PhD journey, she told me "*A PhD is not a sprint; it's a marathon*". I adopted that comment as my motto and have tried to stay consistent in my journey, taking one step at a time. However, sometimes one step forward was followed by three steps back, and if I've managed to reach the finishing line, it is also thanks to **Mandy**.

My supervisor, **Paul Korswagen**, deserves my heartfelt thanks for taking on the challenge of guiding me. I have learned many things from him and have always looked up to him as a model for becoming a better researcher. **Paul** introduced me to *coding*, challenged me with complex questions (not always related to work but also to life and philosophy), and shared his passion for books, shows, and games like *Chaquete*, which I eventually came to enjoy as well. I would not have been successful without **Paul**'s guidance.

I had the pleasure and honour of sharing many coffee breaks, drinks, and, most importantly, pleasant memories with a number of great colleagues: **Langzi Chang**, **Marianthi Sousamli**, **Satyadhrik Sharma**, **Rita Esposito**, **Francesco Messali**, **Giovanna Cera**, **Niels**

Kostense, **Pedro Rios**, **Navid Vafa**, **Nikoletta Christidi**, **Ziwei Dai**, and **Abide Ashikoglu**. I enjoyed fun moments outside the office with many of them.

Several people I met at the university quickly became important in my life and also deserve special mention:

Michele Longo has made significant contributions to many of the analyses presented in this thesis. Without his help, I would not have been able to study various topics and carry out numerous projects. His deep knowledge and understanding of finite element analyses are undisputed. I have never heard anyone say anything negative about **Michele**, and for good reason: he is one of the kindest souls I have met.

When I met **Maria Belen Gaggero**, we discovered that we had both lived in and visited the same places, yet we had never crossed paths before sharing the same office. This led me to believe that we were destined to become friends at some point in our lives, and nothing has proven me wrong. She has managed to support me at my worst without ever judging me. Always considerate of those she cares about, **Belen** made me feel safe. And it goes without saying that she is always the life of the party.

Manimaran Pari has been a great buddy. He is always available for emotional support, even when it's not the best time for him. **Mani** was always ready to share some "*tricks*" to ease the PhD journey. I wish him all the best.

I became closer to **Yopi Prabowo Oktiovan** during the SAHC2023 conference in Kyoto. **Yopi** is a great person, a funny buddy, and I believe a skilled researcher. He consistently shows passion and dedication in his work, qualities I truly admire.

Thanks are due to other colleagues who have provided guidance and with whom I had the opportunity to collaborate: **Tom de Gast** for his supervision and expertise in geotechnics and soil heterogeneity. **Roel Schipper** for his experience and insights on building damage, as well as his help with part of the data collection. **Giorgia Giardina** for her guidance as a member of my Go/No Go committee and her previous work on building damage due to settlements.

Among the people I met in Delft, I'd like to mention and thank: **Raffaella Berritto**, who initially moved to the Netherlands under circumstances similar to mine and with whom I quickly became friends. **Davide Moretti** and **Irene Zubin** for helping me with many everyday challenges and always having fun with me. **Thomas**, **Prudence**, and their wonderful family, the "*Achteromers*", for being such amazing people. I should also thank **Robert Baumgartner** for his patience while we were living together and for being a good friend.

A lot of support also came from many dear friends around the world: *mon frère* **Vincenzo Zarra**, with whom I have a band, "*the 2/4*" (read as "*the Two Quarters*"). At some point, **Enzo**, we should publish our album "*Not Even Brothers*". **Raffaele Zarra** and **Salvatore Ferraioli**, my partners in crime; **Antonio Ansalone**, **Aniello Esposito**, **Raffaele Santelia**, **Marco Rizzano**, and **Hasan Doci**, whom I met during my time as a student at the University of Salerno. They are all now great civil engineers, and I am confident they will all be successful (or *chin' 'e sord'*, as we wish each other in Neapolitan dialect). Thanks to **Graziella Quagliozzi** for her support and love throughout these years. Without her presence, this journey would not have been the same.

I would like to extend my gratitude to the **support staff** at the university, including the ICT section, financial division, facility management, and the Secretariat.

I want to thank my **family** for their unwavering patience and support. I am sure they are proud today. They constantly remind me, as I get lost in codes, calculations, and deep thinking, that the truly important things in life are simple and should be appreciated.

It might sound cliché, but I want to thank myself. I haven't always believed in my abilities, but I've kept working regardless. I often thought there might have been a better candidate for this research, but instead of giving up, I worked hard to become that person. In the end, I'm not entirely sure if I became who I hoped to be. Perhaps I became someone different along the way, but I hope that person still deserves this achievement. Ultimately, it's probably fine to be imperfect, and I'm happy with how things turned out in the end.

Finally, if you've come to this last line, dear **Reader**, thank you.